Characterisation and Mechanistic Studies

of the Acylation of Anisole Catalysed by

Zeolite BEA

Matteo L. M. Bonati

A thesis submitted in partial fulfilment of the requirements of the

Nottingham Trent University for the degree of Doctor of Philosophy

February 2006

Abstract

This thesis presents a study on the acylation of anisole catalysed by zeolite BEA. Zeolite BEA samples were prepared by aqueous ion exchange and characterised by XRD, ICP, TPD-MS and FTIR. These samples are shown to possess different amounts of Brønsted and Lewis acid sites. For example, H-BEA has the highest amount of Brønsted acid sites and Na-BEA the lowest. Catalytic activity in the liquid phase acylation of anisole was highest for H-BEA and lowest for Na-BEA. These results indicate that the reaction should be Brønsted catalysed. However, no straightforward correlation was found between Brønsted acidity and catalytic activity when all the ion-exchanged samples were taken into account.

Investigations by TPD-MS and FTIR of the adsorption of acetic anhydride on BEA suggest that most of the acetic anhydride undergoes decomposition to acetic acid and ketene. Adsorption and catalytic data shows that there is an inverse correlation between the initial rate of acylation and the amount of ketene desorbed intact for a number of catalysts. These results have been interpreted as evidence of the involvement of ketene in the acylation reaction and a mechanism was proposed whereby ketene is formed from acetic anhydride interacting with BEA and then ketene attaches onto the aromatic ring of anisole to give p-MAP. However, subsequent catalytic experiments using deuterium-exchanged reagents and NMR to analyse the product, have shown that ketene can not be the species attaching to the aromatic ring of anisole.

The adsorption studies also indicate stronger bonding of acetic acid/acetic anhydride than the product, p-MAP. Further studies on the hydrolysis of acetic anhydride catalysed by BEA also suggest that neither acetic anhydride nor acetic acid deactivate the catalyst. Thus, multiply acylated products may well be the species responsible for the deactivation and ketene might be responsible for their formation.

Further investigations on the nature of the active sites have shown that the acylation reaction is Brønsted catalysed in the case of H-BEA, but Lewis catalysed when Cu-BEA is used.

Acknowledgements

I would like to thank the following people for their contribution to this thesis, by providing knowledge, encouragement and friendship.

Dr. M. Stockenhuber

Prof. R.W. Joyner

Dr. G.S. Paine

Dr. J. Dixon

Prof. J.D. Wallis

Mr. M. Wood

Mr. D. Belton

Mr. G. Burgess

Mr. O. Sonntag

Dr. M.W.E. Van Den Berg

And my parents

Contents

1 Introduction

1.1 Scope of the Thesis

The acylation of aromatic compounds is an important process in the chemical industry for the production of many pharmaceuticals, and also fragrances and dyestuffs. In the past few decades, zeolites have shown great potential in aromatic acylation while at the same time reducing the environmental problems associated with classical Friedel-Crafts acylation. In this context, zeolite BEA has been recently introduced as catalyst in an industrial process for the acylation of anisole.

The scope of this thesis is the characterisation of a series of zeolite BEA samples and the investigation of the mechanism of acylation as catalysed by BEA. The acidic properties of the various zeolite BEA samples prepared by ion-exchange will be related to their catalytic activity. The adsorption of acylating reagents and products on zeolite BEA samples will be investigated by FTIR and TPD-MS in order to probe the reaction mechanism and the deactivation process. Catalytic experiments will be performed with deuterium-exchanged reagents and monitored by NMR in order to investigate the nature of the active species in the acylation reaction. The location and nature of the active sites in the acylation reaction will also be investigated by selectively deactivating either the external surface acidity of zeolite BEA or its Brønsted acid sites.

1.2 Zeolites

Zeolites are silica-aluminate minerals and are both present in nature and can be synthesised. Natural zeolites are generally formed over thousands of years by the interaction of water and volcanic glass under alkaline conditions and at temperatures under about 200 °C [1]. Recently, researchers have also found evidence for the presence of zeolite minerals on the surface of Mars, which could imply the existence at some stages of liquid water on the planet [2].

The Swedish mineralogist Baron Axel Cronstedt was the first to discover and describe zeolites as a mineral group in 1756 [3]. It is their ability to lose water on heating that gave their name, from the Greek words *zeo*: to boil, and *lithos*: stone.

Despite their widespread availability, the naturally occurring zeolites are of limited use because they almost always contain undesired impurities, their chemical composition varies from one deposit to another and even from one stratum to another in the same deposit, and nature did not optimise their properties for catalytic applications [4].

After the Second World War, the fundamental work on the synthesis of zeolites of Barrer [5, 6] and Milton [7, 8] opened the possibility of using zeolites in the chemical industry. For example, Barrer studied the ion-exchange thermodynamics of sodium and calcium ions in zeolites [9] and this led to zeolite A being introduced as an environmentally friendly replacement for phosphates in detergents in the 70's.

The first important application of zeolites in the petrochemical industry was the introduction of synthetic faujasites (i.e. zeolites X and Y) on an industrial scale in fluid catalytic cracking (FCC) of heavy petroleum distillates in 1962 [10], one of the most important chemical processes world-wide. The new zeolitic catalysts were not only far more active than the previously used amorphous silica-alumina catalysts, which enabled drastic process engineering improvements, but they also brought about a significant increase in the yield of gasoline [11], the most valuable product from FCC plants. It has been estimated that this increase in gasoline yield alone resulted in an added value in the order of at least several billion dollars per year [11, 12]. It has further been estimated that the overall cost of petroleum refining world-wide would be higher by at least 10 billion US dollars per year, if zeolite catalysts were not available today [13].

In the petrochemical industry zeolites are also used for the hydrocracking of heavy petroleum distillates [14], octane number enhancement of light gasoline by isomerisation [15], the synthesis of ethylbenzene (the precursor of styrene and polystyrene) from benzene and ethene through the Mobil-Badger process [16], the disproportionation of toluene into benzene and xylenes [17] and the isomerisation of xylenes. Zeolites are also used as drying agents, gas purifiers, in waste-water treatment, as soil improvers and even as animal feed supplements [18].

1.3 Chemical Composition and Framework Structure of Zeolites

Zeolites can be defined as a class of crystalline aluminosilicates with rigid framework structures comprising well-defined channels and cavities with dimensions ranging from ca. 0.2 to 1 nm. Each negative charge on the framework, introduced by the trivalent aluminium being tetrahedrally coordinated to oxygens (i.e. AlO_2^-), is balanced by cations (e.g. NH_4^+, Na^+, Ca^{2+}, Cu^{2+}, etc.) located within the channel structure. The general formula for a zeolite can be written as:

$$M^m_{x/m}[(AlO_2^-)_x (SiO_2)_y] \cdot nH_2O$$
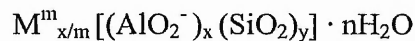
where cations M of valence m neutralise the negative charges on the aluminosilicate framework introduced by AlO_2^-, (x + y) is the number of tetrahedra in each unit cell, and (y / x) is the so-called framework silica to aluminium ratio.

Loewenstein's Rule [19], an empirical observation, limits the maximum amount of aluminium in the framework by stating that the aluminium can only be coordinated, via the oxygens, to silicon atoms in the framework. This is because of the instability of the Al-O-Al bonds due to the proximity of two positively charged atoms. As a consequence of Loewenstein's Rule the lowest possible Si/Al ratio for any zeolites is 1.

The primary building unit of the zeolite structure is a silicon or aluminium atom surrounded by four oxygen atoms in a tetrahedral configuration. This is commonly referred to as a TO_4 unit, the T-atom being either silicon or aluminium. Each tetrahedron shares at least two of its corner oxygen atoms with its neighbours.

Figure 1.3.1 shows the structures of four selected zeolites, together with their structural building units and depictions of the channel systems and pore dimensions. In these commonly used representations, the T-atoms are located at the vertices and the lines connecting them stand for T-O-T bonds.
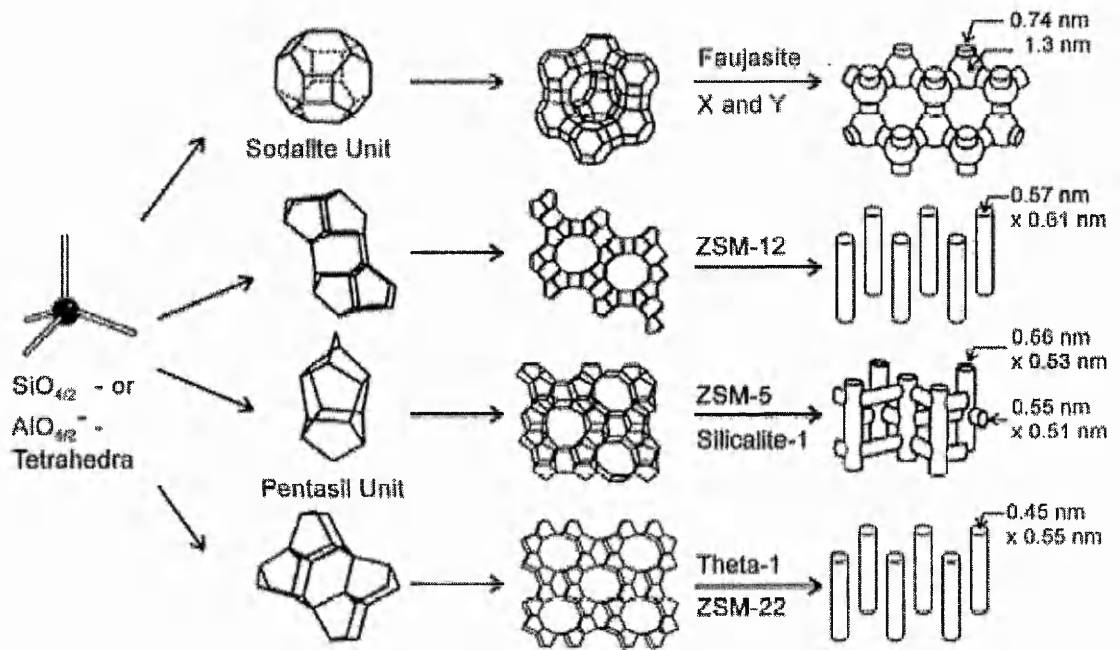
Figure 1.3.1 – Structural building units and framework structures of selected zeolites.
Reproduced from Weitkamp [4]

The sodalite unit or β-cage, shown in the top line of Figure 1.3.1, is formed when 24 tetrahedra are joined together. It is an important secondary building unit from which various zeolite structures derive. If sodalite units are connected via their hexagonal faces, as shown in Figure 1.2.1, the structure of the mineral faujasite results, which is identical to the structures of the synthetic zeolites X and Y. Its pore system is relatively spacious and consists of spherical cages, referred to as supercages, with a diameter of 1.3 nm and connected tetrahedrally with four neighbouring cages through windows with diameters of 0.74 nm.

Zeolite ZSM-12 is an example of a zeolite with a unidimensional channel system, its pores are slightly elliptical with dimensions of 0.57 x 0.61 nm. Zeolite ZSM-5 and its all-silica analogue Silicalite-1 are built from the pentasil unit and are examples of zeolites with an intersecting system of straight and sinusoidal channels. Zeolite Theta-1 (isostructural to ZMS-22) is again a zeolite with a unidimensional channel system, but with pores smaller than ZSM-12.

The large number of possible connecting sequences for the tetrahedra gives rise to the many zeolite structures so far identified. Currently, about 140 different framework structures are known [20]. To each framework type a three-letter code is assigned by the Structure Commission of the International Zeolite Association [21]. The framework

type of a zeolite describes the connectivity of the framework tetrahedral atoms in the highest possible symmetry without reference to chemical composition, and therefore defines the topology of the material with respect to size and shape of the pore openings, the dimensionality of the channel system, the volume and arrangement of the cages, and the type of cation sites available [22].

Zeolites are often characterised by their smallest pore opening named after the number of T-atoms in the rings defining the size of the pore. Small pore zeolites such as zeolite A (framework code LTA) and Sodalite (SOD) have pore openings comprising eight T-atoms, also called an eight-membered ring. Medium pore zeolites, such as ZSM-5 (MFI) have minimum pore openings defined by 10-membered rings, while the pore openings of large pore zeolites such as zeolite Y (FAU), Mordenite (MOR) and Beta (BEA) are defined by 12-membered rings. The largest pore openings reported are for UDT-1 [23] and CIT-5 [24], both zeolites having 14-membered rings.

As a consequence of their small dimensions, zeolites' pores and channels can induce a high level of selectivity on the reactants (e.g. separation of branched and unbranched alkanes), the final product (e.g. very high selectivity towards the para-product) or the transition state for a reaction, as illustrated in Figure 1.3.2. Degnan [25] has reviewed the fundamentals of shape selectivity for the development of catalysts for the petroleum and petrochemical industries.

Molecular modelling techniques can be employed to calculate the kinetic diameter (i.e. the minimum cross sectional width) of the reactant and product molecules [26]. Then the kinetic diameters can be compared with the reported pore diameters of selected zeolites [20] to obtain information on the feasibility of a particular reaction with a particular zeolite. However, this picture is complicated by the fact that the zeolites' pores are actually flexible. For example, Coker et al. [27] demonstrated the sorption at elevated temperatures of 1,3,5-tri-t-butylbenzene and 2,4,6-tribromo-1,3,5-triethylbenzene into zeolite NaX even if these two bulky aromatics have minimum diameters of ca. 0.90 nm and 0.95 nm respectively while the nominal pore diameter of NaX is only 0.74 nm.
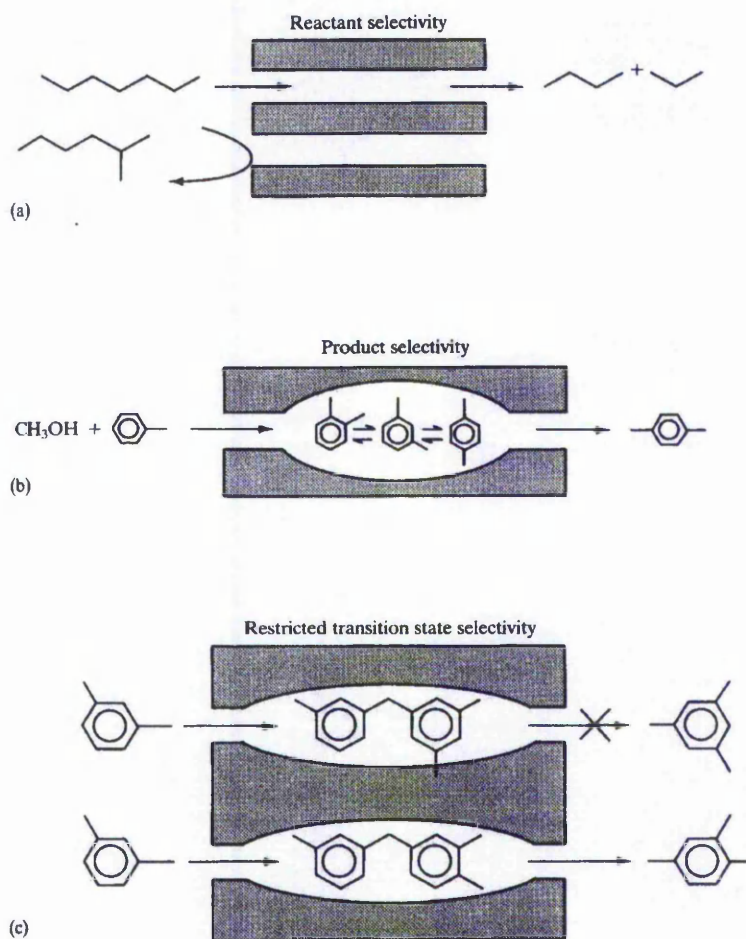
Figure 1.3.2 – Selectivity as induced by the zeolite pores.
Reproduced from Smart and Moore [28]

1.4 Brønsted Acid Sites

In zeolites, a Brønsted acid site is formed by a hydroxyl group bridging between a silicon and an alumium atom (i.e. a Si-OH-Al group). As illustrated in Figure 1.4.1, if a zeolite containing ammonium counter-cations is heated sufficiently, ammonia is released and the framework retains the protons in bridging hydroxyl groups. The aluminium content of the zeolite therefore determines the maximum concentration of the Brønsted acid sites.
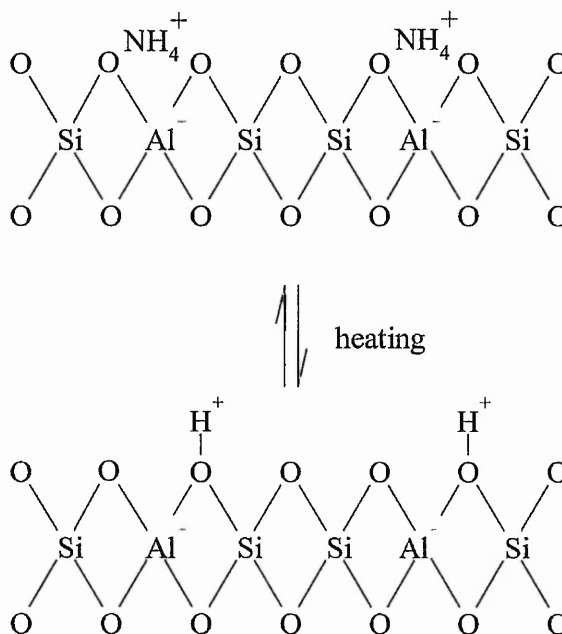
Figure 1.4.1 – The formation of Brønsted acid sites in zeolites

As a consequence of Loewenstein rule [19], each AlO_4 tetrahedron is surrounded by four SiO_4 tetrahedra. Adjacent AlO_4 tetrahedra are referred to as next nearest neighbours (NNN). Various models, reviewed by Barthomeuf [29], relate the acid strength of Brønsted sites to the concentration of NNN Al atoms. The strongest acid sites are observed in the absence of NNN AlO_4 tetrahedra. The site strength decreases as the concentration of NNN AlO_4 tetrahedra increases. Thus, the higher the Si/Al ratio the lower the concentration of Brønsted acid sites and the higher their acid strength.

In addition to the long-range effects of the chemical composition, experiments and theoretical calculations [30] show that short-range effects influence the strength of acid sites. Additionally, other factors such as the lengths of Al–O and Si–O bonds and the corresponding Al–O–Si and Si–O–Si angles [31] and the nature of the metal cations at exchange sites can influence the strength of acid sites [32, 33].

For the zeolites with the highest acid strength (i.e. the ones where there are no aluminium NNN atoms) Brønsted acid sites appear to be identical in strength and catalytic activity. This has been shown for protolytic cracking of n-hexane [34] and the isomerization of m-xylene [35], both being monomolecular reactions under the chosen reaction conditions. For n-hexane and n-hexene cracking this equivalency was shown also for materials with varying aluminum concentration [34].

The Brønsted acid sites can be directly detected by infrared spectroscopy in the region between 3650 and 3550 cm^{-1} for most zeolites. However, it is worth mentioning that the position of the infrared band cannot be used as a direct indication of the acid strength of the Brønsted acid site [36]. ^{1}H magic angle spinning (MAS) NMR spectroscopy can also be used, for most zeolites the Brønsted hydrogens will give a peak at ca 4 ppm [37].

1.5 Lewis Acid Sites

Lewis acid sites are electron pair acceptor sites. For example, a trigonally coordinated aluminium atom is electron deficient and thus behaves as a Lewis acid [38]. The strength of a Lewis acid site is proportional to the ratio between the charge of the metal cation and its size [39] but it can be reduced by limited accessibility (i.e. inability to assume minimum bond distance).

Lewis acid sites in zeolites can be formed when a H-zeolite is heated to high temperature with consequent release of water and formation of trigonally coordinated Al^{3+} ions [38], which can act as strong Lewis acids (see Figure 1.5.1).
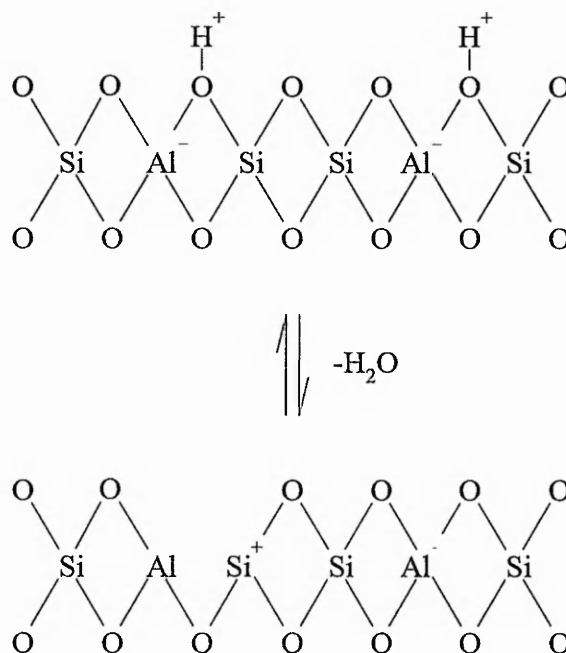
Figure 1.5.1 – The formation of Lewis acid sites in zeolites

Over the years different researchers have identified different possible Lewis acid sites in zeolites. As already mentioned, Lewis acid sites can originate from lattice defects or by degradation of the lattice, and this can also lead to alumina or silica/alumina nanoparticles formed by the extraction from the lattice of aluminium, which can be charged or neutral [40, 41]. Al^{3+} can exist in octahedral and tetrahedral coordination and will have stronger Lewis acid sites than exchangeable metal cations [42]. Another type of aluminium is the extra-framework alumina species (EFAL), which are typically extracted from the zeolite lattice by steam treatment at higher temperatures. EFAL can block active sites by substituting for exchangeable cations, enhance the acidity by interacting with a Brønsted acid site, or block the access to micropores by forming voluminous oligomeric species [43-46]. A third type of Lewis acid site has been recently described as Al^{3+} reversibly and partially extracted from the lattice using a base molecule such as ammonia [47, 48]. The Al^{3+} cation assumes an octahedral coordination under such conditions. The reversibility is broken, however, once Al–O–Al bonds are formed, i.e., when the aluminium oxide species are completely detached from the lattice. Detailed information on such sites is not available, but it can be speculated that the drastic enhancement of catalytic activity for acid-catalysed hydrocarbon conversion after mild steaming is associated with such reversibly detached Lewis acid sites [49].

Lewis acid sites formed by metal cation exchange are weak to moderately strong, because often the exchangeable cation has a low electronegativity (e.g. alkali or alkali earth metals) or is relatively large (e.g. La^{3+}) [39]. Together with the adjacent framework oxygen atoms they act as Lewis acid/base pair and may polarise bonds in reacting molecules. It should be noted here that the interaction of the Lewis acid sites with electron pair donor molecules is very strong. The presence of the acid–base pairs allows the polarisation of reactant molecules, which can potentially enhance their reactivity [50, 51]. Lewis acid sites also act as hydride or anion receptors in a variety of reactions. Their presence seems also to stimulate dehydrogenation of alkanes to some degree.

1.6 Basic Sites

Basic sites in zeolites are proton accepting or electron pair donating oxygen atoms of the lattice. The strength of a given basic site is proportional to the negative charge on the oxygen, which can be estimated calculating the intermediate electronegativity using the Sanderson electronegativity principle [52] or the electronegativity equalization

method (EEM) [30]. The basic strength varies inversely to the intermediate electronegativity, i.e. materials with lower intermediate electronegativity and higher polarity show higher base strength [53, 54]. Like the acid strength discussed in Section 1.4 the base strength of the oxygen atoms in the lattice also depends on T–O–T bond angles and on the local chemical environment. For example, the oxygen atoms in AlO_4 tetrahedra are more basic than in SiO_4 tetrahedra [55]. Additionally, the type of cation influences the polarity of the lattice [56]. Even when all cation exchange sites are exchanged with alkali cations, the overall chemical composition allows for the SiO_2-based materials only a weak base strength. Stronger base sites are therefore linked to clusters of alkaline or alkali-earth oxide hydroxides in the zeolite pores [57, 58]. Very strong basic sites can be created by supporting metallic sodium in the zeolite pores [59], which interact with framework oxygen atoms or react with trace humidity. Loading zeolites with alkali metal oxides utilises the microporous material primarily as support [60]. Such materials show high activity in typical base-catalysed reactions such as alcohol dehydrogenation or toluene side chain alkylation [61]. However, the low rates of base-catalysed reactions make the materials always very susceptible to traces of catalytically more active protons, which then dramatically change the chemical reactivity [61].

1.7 Modification of Zeolites

One of the major factors in the importance of zeolites as catalysts is their ability to accommodate a wide variety of chemical modifications with relative ease while retaining their open structure.

Ion exchange, used in the present study, is one of the routes to achieve modification. During the ion exchange procedure a suspension of the zeolite is in equilibrium with a solution of the cation to be introduced. Generally, the ion-exchanged materials are excellent redox catalysts for gas-phase reactions in environmental applications. For excellent reviews on the materials, see references 62-64. By exchanging copper, for example, or other multivalent cations, it is possible to introduce redox sites in the zeolite [65]. Fe-exchanged-zeolites have recently seen renewed interest due to their ability to catalyse selective reactions in various fields [66-68]. Transition metal cation exchanged materials have seen enormous interest as potential materials for reduction of NOx with hydrocarbons [69, 70]. Most of the materials investigated are based on the MFI structure, and Cu, Co, and Fe are the most studied materials [71].

Redox sites can also be introduced into zeolites by isomorphous substitution of metal ions into framework positions, thus producing materials that can possibly mimic enzyme catalysis. Isomorphous replacement can be attained either as a post-synthesis modification or the zeolite can be synthesised as such. For example, Camblor et al. [72] reported the isomorphous replacement of Si by Ti in the BEA framework by direct synthesis. Other examples of isomorphous substitutions include Ti-silicalite (TS1-1) [73], vanadium silicates with MFI and MEL structures [74], iron-containing MFI zeolites [75]. The uniqueness of these materials lies in the fact that isolated, identical, and stable sites are formed within the framework. This allows the proper adsorption of the reactants and provides sufficient space for the chemical transformations while at the same time the steric constraints of the zeolite channels direct the reaction. Additionally, the materials can be tailored to have the proper hydrophobic/hydrophilic properties [76]. Next to incorporation into the MFI or MEL structure, incorporation of Ti has also been reported, e.g. for BEA (Ti-Beta), MTW (Ti-ZSM-12), and MWW (Ti-MCM-22) [77-79]. Iron-containing ZSM-5 materials are especially remarkable as their catalytic activity differs markedly from that of bulk Fe_2O_3 [75]. Fe-ZSM-5 is unable to activate O_2, but shows high activity for the decomposition of N_2O [80] and utilises the oxygen for selective gas-phase oxidation steps.

Dealumination is another way to modify zeolites and it is typically achieved by acid leaching or steaming at high temperatures, and results in an increase in the silicon to aluminium ratio [81].

1.8 Zeolite Synthesis

The majority of synthetic zeolites are prepared from solutions containing sodium silicates and aluminates, $[Al(OH)_4]^-$, at high pH, obtained by using an alkali metal hydroxide and/or an organic base. A gel forms by a process of co-polymerization of the silicate and aluminate ions. The gel is then heated gently (at 333-373 K) in a closed vessel for about two days, producing a condensed zeolite. The characteristics of the product obtained are determined by the synthesis conditions: temperature, time, pH and pressure are possible reaction variables.

Since zeolite structures are built from SiO_4 and AlO_4 tetrahedra, these primary building blocks must also be present in the synthesis mixture and, because aluminate ions are only stable at high pH values [82], zeolite synthesis takes place in basic solutions.

Zeolite synthesis can be generally divided in 4 steps [83, 84]:

1. Batch preparation (mixing of reaction sources and gel formation)
2. Nucleation
3. Crystallisation
4. Product recovery

Batch preparation takes place at room temperature, nucleation and crystallisation at elevated temperatures (typically 333 – 523 K) and sometimes at elevated pressure [85]. Stainless steel vessels or vessels lined with polymers such as Teflon are preferred, since species found in glass (e.g. Na and silica) can participate in the chemical formation of the zeolite framework [83].

1.9 Zeolite BEA

The main zeolite used in this research is zeolite Beta, framework code BEA. It is a large pore zeolite, which exhibits a strong Brønsted acidity, typical of high-silica zeolites. Examples of successful applications of zeolite BEA include aromatic alkylation [86], aromatic acylation [87], indole synthesis [88], aromatic nitration [89] and aliphatic alkylation [90].

Zeolite Beta was first synthesised at Mobil Oil Corporation by Wadlinger et al. in 1967 [91], and its structure was first described by Treacy et al. [92] and Higgins et al. [93]. Detailed structural determination [94] has shown that it consists of an intergrowth of two distinct, but closely related structures, which respectively have tetragonal and monoclinic symmetry. In both systems, straight 12-membered-ring channels are present in two crystallographic directions perpendicular to [001], while the 12-memberd ring in the third direction, parallel to the c axis, is sinusoidal. The sinusoidal channels have circular openings (5.5 Å), and the straight channels have elliptical openings. The only difference between the two polymorphs is in the pore dimensions of the straight channels. In the tetragonal system, the straight channels have openings of 6.0 x 7.3 Å, whereas in the monoclinic system they are 6.8 x 7.3 Å.

Zeolite BEA has been synthesised with varying Si/Al ratio [95-98], and its acidity can be fine-tuned by the incorporation of several other trivalent elements such as Ti^{3+} [72]. The crystallites of zeolite BEA are usually very rough with a diameter of approximately 50 nm, and thus possess a large external surface area which accounts for approximately 35% of the total surface area [99].

Zeolite BEA has Brønsted acid sites in both the micropores and on the external surface area, while Lewis acid sites are predominantly present in the micropores [94]. Lewis acidity in zeolite BEA has been associated with its high number of defect sites. These are generated when a tertiary building unit is rotated 90° around the c-direction with respect to TBUs in the same layer. The rotated TBU cannot connect properly with adjacent layers, resulting in partially coordinated T-atoms, which can create potential Lewis acid sites [94]. Kuehl et al. [100] observed octahedral aluminium species connected to the framework structure of zeolite BEA, and suggested that these aluminium sites exhibit characteristics of Lewis acid sites. They suggested that such aluminium species are created by partial hydrolysis of framework Si-O-Al bonds. Similarly, Jia et al. [101] and Beck et al. [102] suggest that framework aluminium atoms in a non-tetrahedral coordination may exhibit Lewis acidic properties.
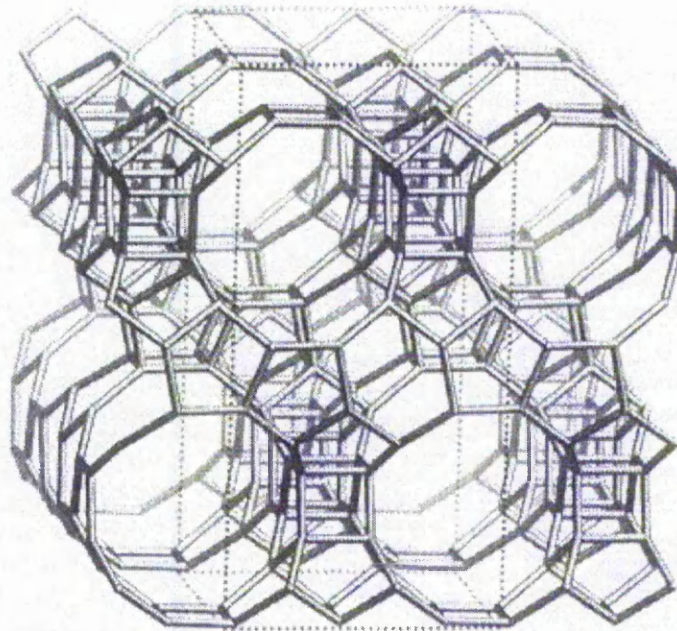
Figure 1.9.1 – Representation of BEA framework viewed along [010].
Reproduced from Baerlocher et al. [20]

Zeolite beta is typically synthesised by hydrothermal treatment from a mixture of:

$$1.97 \, Na_2O : 1.00 \, K_2O : 12.5 \, (TEA)_2O : Al_2O_3 : 50 \, SiO_2 : 750 \, H_2O : 2.9 \, HCl$$

held in an autoclave at 408 K for 15 – 20 hours [103]. The resulting crystallites are generally rather small, and are usually recovered in a centrifuge. Zeolite BEA can also

be synthesised in a wide range of Si/Al ratios in fluoride media, where OH⁻ anions are substituted by fluoride anions, which can also play a mineralising role [104].

1.10 Friedel-Crafts Acylation of Aromatics

The conventional Friedel-Crafts acylation of aromatics involves the reaction of a carboxylic acid chloride (RCOCl) with an aromatic compound, and is generally catalysed either by a Lewis acid catalyst, such as $AlCl_3$ or BF_3, or by mineral acids, such as HF [105].

The reaction proceeds by formation of an acyl group (-COR), which is then attached to the aromatic ring. One example of acylation is the reaction of benzene with acetyl chloride and $AlCl_3$ catalyst to yield acetophenone (see Figure 1.10.1).
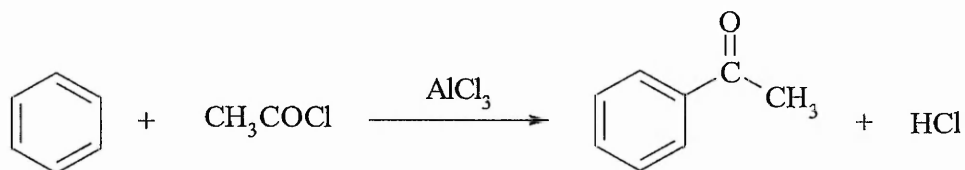
Figure 1.10.1

The reactive intermediate in Friedel-Crafts acylation is an acyl cation ($RC^+=O$), generated by the reaction between the carboxylic acid chloride and $AlCl_3$ [106]. The acyl cation is resonance stabilised by the interaction of the vacant orbital on carbon with a lone pair of electrons on the neighbouring oxygen (see Figure 1.10.2).
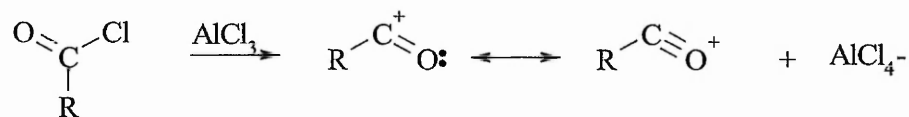
Figure 1.10.2

Once formed, the acyl cation does not rearrange, rather it is attacked by the aromatic ring to give the substitution product [106] (see Figure 1.10.3).
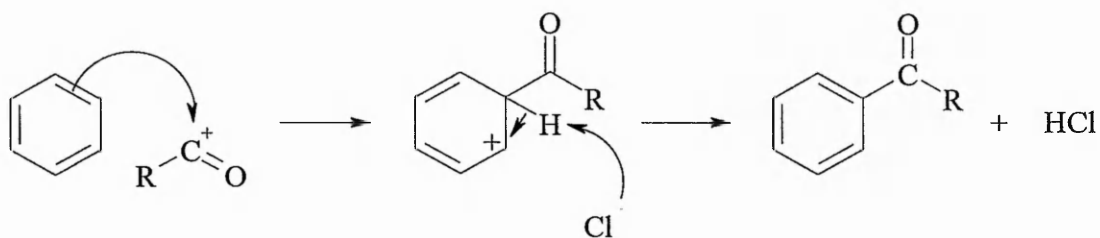
Figure 1.10.3

Friedel-Crafts acylation normally requires more than stoichiometric quantities of catalyst, thus should not be regarded as catalytic. In the case of AlCl₃, the first mole of catalyst coordinates with the oxygen on the acylating reagent [107] (see Figure 1.10.4). The hydrolysis of this complex then leads to the loss of catalyst and the formation of large amounts of inorganic by-products, in particular corrosive hydrochloric acid, which causes considerable environmental problems [108].
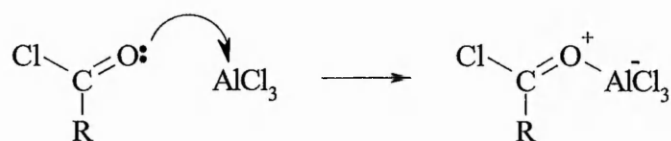
Figure 1.10.4

The acylation of aromatics is of great importance in the manufacture of many pharmaceuticals [109]. For example, the acylation of 2-methoxynaphthalene by aluminium chloride was a step in the first large-scale synthesis of the non-steroidal anti-inflammatory drug naproxene [110], and the acylation of isobutylbenzene with hydrogen fluoride is currently used in the synthesis of ibuprofen [111], another non-steroidal anti-inflammatory drug (see Figure 1.10.5). Also, many synthetic fragrances of the musk type contain an acetyl group [105, 112].

naproxene   ibuprofen
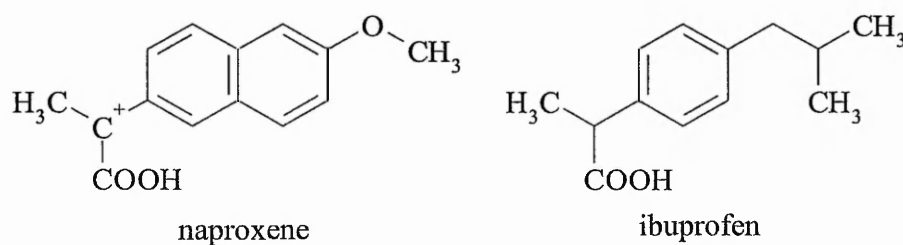
Figure 1.10.5

15

1.11 Zeolites as Catalysts for Aromatic Acylation

The environmental problems associated with classical Friedel Crafts acylation can be overcome by using zeolites as heterogeneous catalysts. The use of zeolites avoids the formation of toxic wastes such as HCl, and the catalyst is reusable. Additionally, selectivity is not only determined by the characteristics of the acid sites but can also be orientated towards the desired product by the zeolite pore system.

Several reviews have been published illustrating a wide variety of organic reactions proceeding in the presence of zeolites [113-116]. In particular, the acylation of aromatics with zeolite catalysts has been extensively studied. Some of the earliest results were published by Chiche et al. [117], who carried out the acylation of toluene and p-xylene with straight-chain carboxylic acids, catalysed by CeNa-Y zeolites in the liquid phase. The authors observed a yield of the para-isomer of at least 94% with all acids studied. For acids of carbon numbers C12 to C20, the maximum yield of acylated p-xylene was found to be dependent on the chain length.

Neves et al. [118] investigated the acylation of phenol with acetic acid over ZSM-5. Phenyl acetate and o-hydroxyacetophenone are the primary products, O-acylation being much faster than C-acylation. At high conversion, part of the o-hydroxyacetophenone results from the acylation of phenol with phenyl acetate. The authors found that the formation of p-hydroxyacetophenone, which is important for the synthesis of paracetamol [115], does not occur through phenol acylation. Instead, it involves the hydrolysis of p-acetoxyacetophenone selectively formed through the auto-acylation of phenyl acetate, a mechanism also known as Fries rearrangement. The ortho-selectivity of phenol acylation can be related to a pronounced stabilization of the transition state while the para-selectivity of phenyl acetate autoacylation could be due to a steric hindrance to the approach of the acetyl group in the ortho-position of phenyl acetate.

The acylation of phenol with acetic acid has also been investigated over zeolite BEA [119, 120]. Rohan et al. [120] found that the rate of hydroxyacetophenone formation depends on the order of introduction of the reactants. A higher rate of reaction was obtained when phenol was added to a zeolite previously impregnated with phenyl acetate. The authors also investigated the loss of activity of the catalyst with time and found that the catalyst was rapidly deactivated. This deactivation was attributed to the strong adsorption of phenols (reactant and products) inhibiting the access of phenyl acetate to the inner acid sites [120].

As already mentioned, the Fries rearrangement of phenyl acetate may be regarded as an intramolecular acylation reaction proceeding by migration of the acyl group to the ortho- or para-position of the aromatic ring to give o-hydroxyacetophenone and/or p-hydroxyacetophenone (see Figure 1.11.1).

phenyl acetate

and/or

o-hydroxyacetophenone

p-hydroxyacetophenone
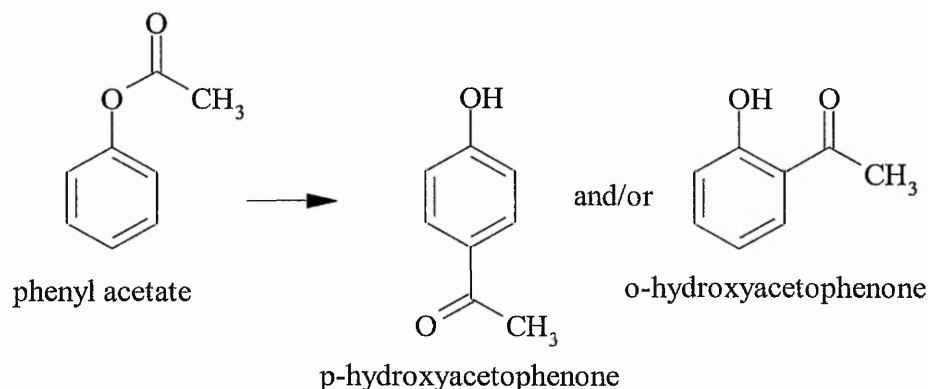
Figure 1.11.1 – Fries rearrangement of phenyl acetate

The Fries rearrangement of phenyl acetate was extensively studied in the gas phase using zeolite BEA [121, 122], Y [123, 124] and ZSM-5 [118, 123, 125, 126] to improve the yield of p-hydroxyacetophenone. In general, the expected ortho- and para-hydroxyacetophenones were minor components and phenol was the main product. The deactivation (i.e. loss of catalytic activity) of the zeolite catalyst with time was a common feature in all the investigations. Some authors explained the rapid deactivation as a consequence of the condensation of formed ketene [124, 127]. Ketene would be a decomposition product at high temperatures of the acylium ion and could play an important role in the gas phase reaction [127, 128]

The acylation of toluene with acid chlorides was investigated over La-Y [129] while the acylation of toluene and butyl-benzene with carboxylic acids and anhydrides was investigated over BEA [130].

The activity of various cation-exchanged Y zeolites was investigated in the acylation of toluene with octanoic acid [131]. The reaction yielded 75% of acylated product and the selectivity for the para-isomer was 94%. The most efficient catalysts were the rare-earth exchanged zeolites. The following order of activity was observed: Cr^{3+}, $Zr^{4+} < Mg^{2+}$, Cu^{2+}, $Co^{2+} \ll H^+ \ll Pr^{3+}$, La^{3+}, Gd^{3+}, Yb^{3+}, Ce^{3+}. A parallel drawn between the acylation reaction and the cyclohexanol dehydration suggested that the active centres were Brønsted acid sites.

Singh et al. [132] reported on zeolite catalysed formation of acetophenone by the reaction of benzene with acetic acid over various zeolites. ZSM-5 showed higher catalytic activity and selectivity than Mordenite for the vapour phase acylation of benzene by acetic acid. The authors suggested that the excellent activity and selectivity of ZSM-5 compared to Mordenite are due to both the stronger acid sites and to its narrow pore structure. Increased reaction temperature and molar ratios of benzene/acetic acid lead to increase in acetic acid conversion. In contrast, acetic acid conversion decreased with the increase in reaction time, degree of sodium-exchange in H-ZSM-5, and Si/Al ratio.

The acylation of naphthalene and its derivatives requires large pore zeolites as catalysts. For example, the liquid-phase benzoylation of naphthalene with benzoyl chloride has been shown to proceed with BEA but not with narrow pores zeolites such as ZSM-5 and ZSM-12 [133].

Many studies have been devoted to the investigation of BEA zeolites as catalysts in the acylation of 2-methoxynaphthalene (see Figure 1.11.2), an important step in the production of the drug naproxene [134-140]. A new type of zeolite, Al-ITQ-7, was found to be as active as BEA in the acylation of 2-methoxynaphthalene but with better selectivity [141]. This zeolite has a three-dimensional channel system, with 12-membered ring pores with a slightly smaller diameter than the pores in BEA. Thus, the better selectivity of Al-ITQ-7 may be due to differences in the relative diffusion coefficients of the isomeric products.

2-methoxynaphthalene → acylating agent / zeolite → 2-acetyl-6-methoxynaphthalene

Figure 1.11.2

The acylation of heterocyclic compounds is another important reaction for the production of pharmaceuticals, such as amiodarone and cordarone [142-144].

The acylation of thiophene by butyryl chloride was investigated by Isaev et al. [145] in the presence of twelve zeolite catalysts with different structures, varying numbers of Brønsted and Lewis acid sites, and various amounts of extraframework aluminium species. The authors claimed that there is a correlation between the initial rates of

reaction and the number of Lewis acid sites, however they found no correlation between initial rates and Brønsted acidity.

The acylation of benzofuran and of 2-methylbenzofuran by acetic anhydride was investigated over zeolite Y in a dynamic flow reactor at 333 K, under atmospheric pressure [146]. Deactivation was significant for benzofuran, but much less so for 2-methylbenzofuran, with which high yields (95%) of 3-acetyl-2-methylbenzofuran could be obtained. 2-Methylbenzofuran was about twice as reactive as benzofuran, the position 3 in 2-methylbenzofuran being at least two orders of magnitude more reactive than the position 3 in benzofuran. Deactivation of the catalyst was more pronounced with benzofuran than 2-methylbenzofuran. The loss of activity with time was exponential with benzofuran but essentially linear with 2-methylbenzofuran. The differences in the deactivation behaviour between benzofuran and 2-methylbenzofuran were attributed to a greater tendency for benzofuran to form the heavier polymeric species responsible for the deactivation of the catalyst [146].

1.12 Acylation of Anisole

The first commercial process for the acylation of anisole with acetic anhydride using zeolite BEA (see Figure 1.12.1) was developed by researchers at Rhône Poulenc [147].

Figure 1.12.1

Harvey et al. [148] investigated the acylation of anisole with acetic anhydride and consistently found BEA to be the most active catalyst for acylation reactions compared with USY and ZSM-5. Similarly, Freese et al. [149] found zeolite BEA to be the most active catalyst for the acylation of anisole with acetic anhydride, as compared to zeolite Y and ZSM-5. In both the above studies the reactions were carried out in the liquid phase in a batch reactor.

Rohan et al. [150] studied the acylation of anisole with acetic anhydride over zeolite H-BEA, and determined its deactivation behaviour in the gas and liquid phase. The authors

showed that the product p-methoxyacetophenone (p-MAP) is selectively and rapidly formed over the fresh catalyst. However, rapid deactivation of BEA occurred and this was attributed both to the product being strongly retained in the large mesopore volume of BEA and to multiply acylated derivatives of anisole becoming trapped in the micropores, causing pore blockage. The authors showed that the use of an anisole-rich mixture (anisole/anhydride molar ratio of 5) enhanced catalyst stability by limiting both the retention of the highly polar p-methoxyacetophenone and the formation of multiply acylated products.

In the literature, the acylation of anisole was investigated using different acylating reagents, such as phenylacetyl chloride [121, 151], phenylpropionyl chloride [151], acetyl chloride [152], acetic anhydride [121, 152, 153], and phenylacetic and phenylpropionic acids [151].

The acylation of anisole was also investigated with various zeolites, such as BEA [149, 150, 152, 154-156], MFI [149, 155], FAU [149, 155] and La-Y [152].

1.13 The Mechanism of Aromatic Acylation over Zeolite Catalysts

In the early days of research on catalysis by zeolites, Boreskova et al. [157] assumed that the acylation reaction took place on Lewis sites. Subsequently, Corma et al. [151] suggested the intervention of Brønsted acidity on the basis of the activity of partially sodium-exchanged HY zeolites. Successive studies confirmed a Brønsted catalysed process in the acylation of aromatics [148, 153, 158, 159]. Molecular mechanics and DFT calculations also appear to confirm a Brønsted catalysed process in the acylation of aromatics over zeolites [160].

Pandey et al. [161] investigated the acylation of benzene, toluene, xylenes, mesitylene, isopropylbenzene and N,N-dimethylaniline with acetic acid or acetyl chloride using medium- and large-pore zeolites. ZSM-5 and BEA were found to exhibit the higher turnover rate with both acetic and acetyl chloride as acylating agents. The results also showed that the reactivity of the aromatic substrate in the acylation increases with the number of methyl substituents in the benzene ring. When reactions were carried out at the same conditions with acetyl chloride and H-BEA the following order of reactivities resulted: N,N-dimethylaniline = mesitylene > o-xylene = m-xylene = p-xylene. The authors proposed that the mechanism of acylation involves the reaction of the acylating

agent (either acetic acid or acetyl chloride) with a Brønsted acid site, which polarises the acylating agent and in turn produces an electrophile (CH_3CO^+). Then the generated electrophilic species would attack the aromatic ring resulting in the formation of the corresponding ketone.

Freese et al. [149] investigated the acylation of anisole with acetic anhydride over a series of zeolites, including BEA. The authors proposed that the acylation reaction proceeds through an acylium intermediate, which is formed via an attack of the proton of the Brønsted acid site on the nucleophilic carbonyl group of acetic anhydride (see Figure 1.13.1). The acylium ion would then react with anisole to give a Wheland type intermediate. The size of the intermediate is larger than the intersection of the channels in ZSM-5 but smaller than in BEA, so this would explain the much higher activity of BEA in the acylation reaction as compared to ZSM-5. The constrained environment should also determine the preferential formation of p-MAP. In the final step p-MAP desorbs and the Brønsted acid site is restored.
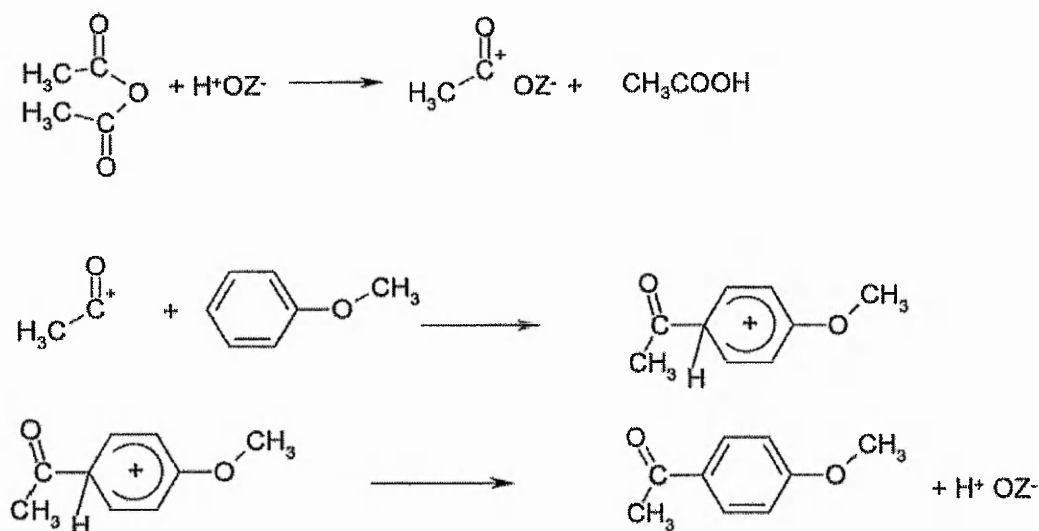
Figure 1.13.1 – Reaction scheme for the formation of p-MAP on zeolite.
Reproduced from Freese et al. [149]

Kim et al. [162] investigated the acylation of 2-methoxynaphthalene (2-MN) with acetic anhydride over a series of different zeolites, and found that only BEA was highly selective towards the desired product 2-acetyl-6-methoxynaphthalene (2,6-AMN). The authors proposed that the acylation over H-BEA involves the formation of an electrophilic complex between acetic anhydride and a Brønsted acid site in the zeolite. First, acetic anhydride is coordinated to a Brønsted acid site to form an electrophilic

complex (see Figure 1.13.2). Then, the complex attacks an incoming 2-MN molecule to produce aromatic ketones and another electrophilic complex. This other complex gives acetic acid as by-product and the Brønsted acid site is recovered. Among aromatic ketones, only 1,2-AMN and 2,6-AMN are major products. They are produced in different ratios depending on the geometric restrictions imposed on the catalytic sites. Less stable 1,2-AMN undergoes further reactions of de-acylation to 2-MN and isomerisation to 2,6-AMN. These reactions may proceed in two steps. First, 1,2-AMN is easily de-acylated to 2-MN, and gives acylium ions on the sites. In the next step, the attached acylium ion attacks the less sterically hindered 6-position of 2-MN to produce 2,6-AMN.
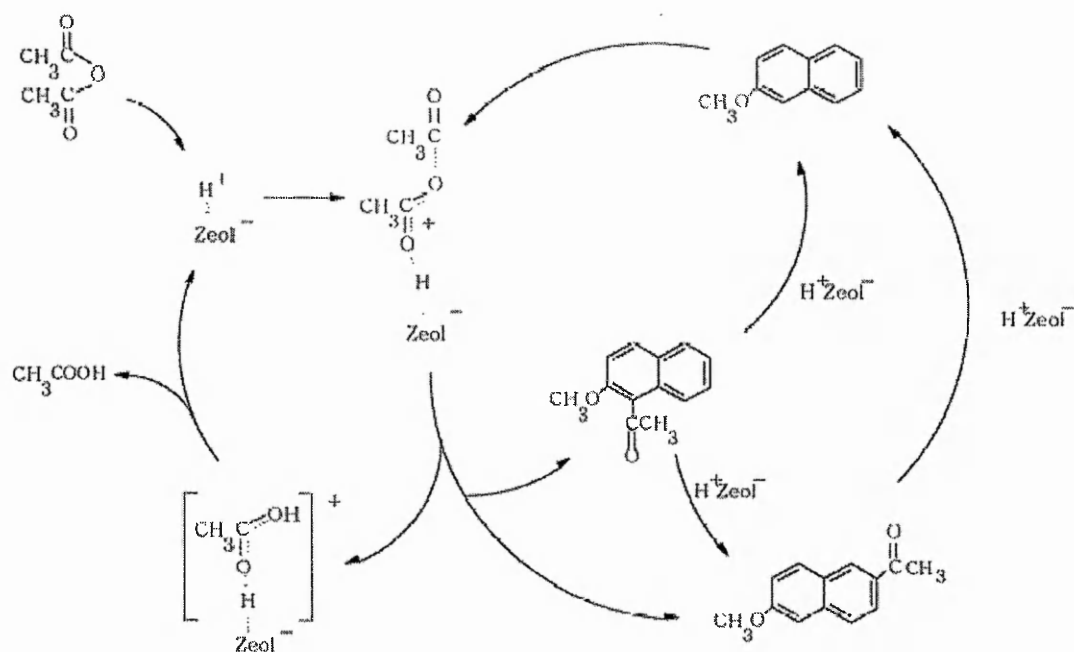
Figure 1.13.2 – reaction scheme for the formation of 2-acetyl-6-methoxynaphthalene over zeolite. Reproduced from Kim et al. [162]

Bosacek et al. [163] used ^{13}C NMR spectroscopy to investigate the adsorption of the acylating agent acetyl chloride on metal-exchanged zeolites X, Y and ZSM-5. Two species were observed upon adsorption: acetyl chloride bound to the lattice oxygen of the zeolite and acetyl chloride complexed with counter-cations in the zeolite lattice. In a few cases, a third species was found and identified as "free" acylium ions stabilised on the surface of the zeolite. Experiments in which toluene was adsorbed on a zeolite pre-treated with acetyl chloride showed the preferential participation of the cation

coordination complex of acetyl chloride in the acylation of toluene. This observation is in agreement with the known role of donor-acceptor complexes, formed between acylium ion precursors and Lewis acids, as acylating agents in the Friedel Crafts acylation of aromatic compounds [164].

More recently, Kresnawahjuesa et al. [165] investigated the adsorption of acetic acid, acetic anhydride and acetyl chloride on ZSM-5. Acetic acid formed a hydrogen-bonded complex with the Brønsted acid sites, while the interaction of both acetic anhydride and acetyl chloride with Brønsted acid sites resulted in the formation of an acylium-ion-like acetyl-zeolite intermediate. In contrast with Freese et al. [149], the authors suggest that H-ZSM-5 is often not an effective catalyst for the acylation reaction because various other intermediates are formed, such as ketones and olefins. These compounds are known to produce coke in the zeolite and thus deactivate the sites.

In contrast to the previous research, Ma et al. [166] studied the acylation of anisole with carboxylic acids, anhydrides, and substituted benzoic acids over a number of zeolite catalysts and concluded that Lewis acid sites were more active and selective than Brønsted acid sites when using carboxylic acids. The mechanism of the reaction was found to be similar to the case of homogeneous catalysis, i.e. the electrophilic intermediate formed from the acylating agent over zeolite acid sites attacked at the aromatic ring of anisole. However, the structure of the electrophilic intermediate depended upon the acylating agent and the nature of zeolite acid sites. The electrophilic intermediate formed from a carboxylic anhydride would be the acylium cation; while when a carboxylic acid was used as acylating agent, the carboxylic acid protonated by the Brønsted acid sites or coordinated on the Lewis acid sites of the zeolite catalyst would react directly with the aromatic ring. The protonated form would be less reactive than the coordinated one for the attack at the aromatic ring, but more reactive for the acylation at the oxygen atom of anisole. The protonated carboxylic acid would preferentially attack at the oxygen atom of anisole and give phenyl carboxylic ester, while the coordinated carboxylic acid and the acylium cation would predominantly react with the aromatic ring, leading to the acylation product p-methoxyacetophenone [166].

Similarly, Isaev et al. [145] studied the acylation of thiophene by butyryl chloride over a series of different zeolites and determined the numbers of Brønsted and Lewis acid sites by FT-IR of chemisorbed ammonia. They concluded that there is a correlation between the initial rates of reaction and the number of Lewis acid sites while there is no correlation between the initial rates and the number of Brønsted acid sites.

Kouwenhoven et al. [167] suggested that Lewis acid catalysts were preferred when using acid chlorides as acylating agents, and Brønsted acid catalysts when using acid anhydrides or carboxylic acids.

Haouas et al. [168] studied the effect of flexible lattice aluminium in zeolite BEA during the nitration of toluene with nitric acid and acetic anhydride. A flexible lattice aluminium species is described as a framework aluminium atom that can reversibly transform its coordination geometry from tetrahedral to octahedral upon interaction with molecules such as acetic anhydride. The authors concluded that surface bonded acetyl nitrate was the active nitrating species, and that acetyl nitrate coordinates to lattice aluminium forming an adsorption complex of distorted octahedral geometry, depicted in Figure 1.13.3. The formation of this adsorption complex was possible because of the flexible framework aluminium species [169], which are abundantly available in BEA zeolite [170].
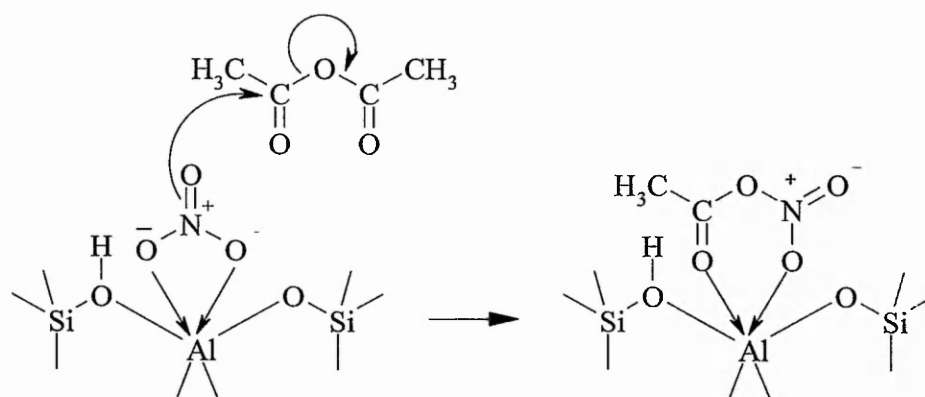
Figure 1.13.3–The formation of acetyl nitrate coordinated to framework Al in zeolite BEA [168]

Paine [171] studied the acylation of anisole with acetic anhydride over a series of zeolite BETA samples modified by thermal and hydrothermal treatments, chemical modification and ion exchange. Catalytic activity was found to be related to the concentration of framework tetrahedral aluminium, and to its partial positive charge. Furthermore, the coordination environment of aluminium in active zeolite BEA samples was found to change from framework tetrahedral to framework octahedral symmetry upon the adsorption of acetic anhydride; while only limited transformation was observed on the inactive Na-BEA. The mechanism proposed involves a molecule of acetic anhydride interacting with framework tetrahedral aluminium, forming a framework octahedral complex, which polarises the anhydride molecule, forming the

acylium cation intermediate. Following an Eley-Rideal type mechanism, a molecule of aromatic substrate (anisole) impinges from the liquid phase, reacting with the polarised anhydride molecule and forming a Wheland type intermediate. The decomposition of the Wheland intermediate to p-MAP and acetic acid completes the process, see Figure 1.13.4.
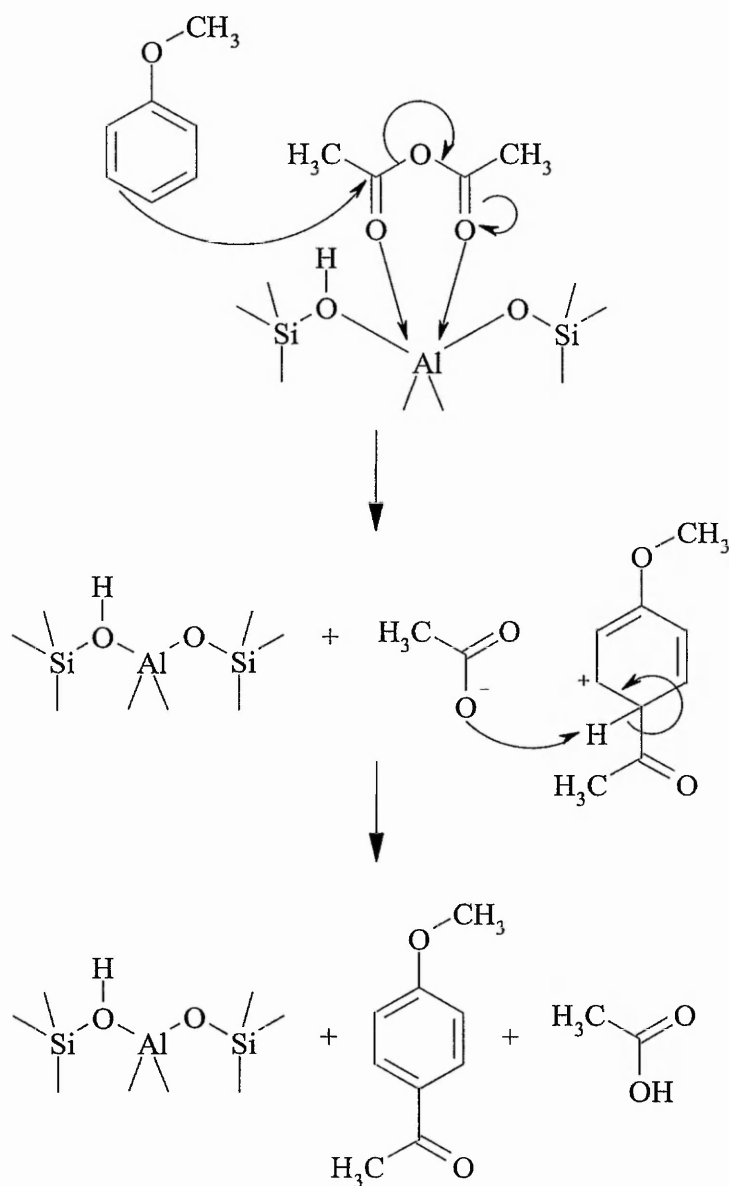
Figure 1.13.4 – Mechanism of acylation of anisole with acetic anhydride over zeolite BEA, as proposed by Paine [171]

1.14 Objectives

The main objective of this thesis is to gain a better understanding of the mechanism of reaction in the acylation of anisole catalysed by zeolite BEA. As shown in the previous section, there are only a few studies directly concerning this subject and their results do not appear in agreement with each other.

The main objective of this thesis can be broken down into several separate tasks. The first one is to prepare a series of ion-exchanged zeolite BEA samples and to characterise them together with the parent zeolite BEA by using techniques such as XRD, ICP, TPD-MS and FTIR. Then the catalytic activity of each BEA sample will be investigated in the liquid-phase acylation of anisole. Subsequently, the interaction of acylating reagents (i.e. acetic acid, acetic anhydride and anisole) and product (i.e. p-MAP) with the various zeolite BEA samples will be studied by TPD-MS and FTIR. This step will allow investigating the formation of species upon the interaction between these chemicals and the zeolite BEA samples. Then, the data from the adsorption experiments will be combined with the catalytic data to try to identify a reaction mechanism. Once a possible reaction pathway has been identified, deuterium-exchanged reagents (i.e. acetic anhydride-d_6, anisole-d_8) will be used to test this hypothesis.

Additional goals of this work are the investigation of the type (i.e. Brønsted or Lewis acid sites) and location (i.e. micropores or external surface) of the active sites in zeolite BEA that are responsible for the acylation of anisole with acetic anhydride.

1.15 References

1.   R.L. Hay, R.A. Sheppard, *Natural Zeolites: Occurrence, Properties, Applications*, Mineralogical Society of America, Washington DC, p. 217

2.   S.W. Ruff, *Icarus*, 2004, **168**, 131

3.   Dyer, *An Introduction to Zeolite Molecular Sieves,* Wiley, Chichester, 1988

4.   J. Weitkamp, *Solid State Ionics*, 2000, **131**, 175

5.   R.M. Barrer, *Journal of the Chemical Society*, 1948, 127

6.   R.M. Barrer, *Journal of the Chemical Society*, 1948, 2158

7.   R.M. Milton, *US Patent 2882243*, 1959

8.   R.M. Milton, *US Patent 2882244*, 1959

9.   R.M. Barrer, L.V.C. Rees, D.J. Ward, *Proceedings of the Royal Society of London, series A*, 1963, 180

10.   E.C. Luckenbach, et al., *Petroleum Processing Handbook*, J.J. McKetta (Ed.), Marcel Dekker, New York, 1992, p. 417

11.   P.B. Venuto, E.T. Habib, *Fluid Catalytic Cracking with Zeolite Catalysts*, Marcel Dekker, New York, 1979, p. 156

12.   R. von Ballmoos, D.H. Harris, J.S. Magee, in *Handbook of Heterogeneous Catalysis, vol. 4*, G. Ertl, H. Knoezinger, J. Weitkamp (Eds.), Wiley-VCH, Weinheim, 1997, p. 1955

13.   J.E Naber, et al., *Studies Surface Science and Catalysis*, 1994, **84**, 2197

14.   J. Scherzer, A.J. Gruia, *Hydrocracking Science and Technology*, Marcel Dekker, New York, 1996, p. 305

15.   S.T. Sie, in *Handbook of Heterogeneous Catalysis, vol. 4*, G. Ertl, H. Knoezinger, J. Weitkamp (Eds.), Wiley-VCH, Weinheim, 1997, p. 1998

16.   F.G. Dwyer, in *Catalysis of Organic Reactions*, W.R. Moser (Ed.), Marcel Dekker, New York, 1981, p. 39

17.   N.Y. Chen, W.E. Garwood, F.G. Dwyer, *Shape Selective Catalysis in Industrial Applications*, Marcel Dekker, New York, 1989, p. 203

18.   L. Moscou, *Introduction to Zeolite Science and Practice*, H. van Bekkum, E.M. Flanigen, J.C. Jansen (Eds.), Elsevier, Amsterdam, 1991

19.   W. Loewentein, *American Mineralogist*, 1954, **39**, 92

20. C.H. Baerlocher, W.M. Meier, D.H. Olson, *Atlas of Zeolite Framework Types, 5ᵗʰ ed.*, Elsevier, Amsterdam, 2001

21. www.iza-structure.org/databases

22. L.B. McCusker, C. Baerlocher, in *Introduction to Zeolite Science and Practice*, H. van Bekkum, et al. Eds., Elsevier, Amsterdam, 2001

23. C.C. Freyhardt, et al., *Nature*, 1996, **381** (6580), 295

24. P. Wagner, et al., *Journal of the Chemical Society Chemical Communications*, 1997, **21**, 2179

25. T.F. Degnan, *Journal of Catalysis*, 2003, **216**, 32

26. A. Chatterjee, R. Vetrivel, *Journal of the Chemical Society Faraday Transactions*, 1995, **91**, 4313

27. E.N. Coker, et al., *Micropourous Mesoporous Materials*, 1998, **22**, 261

28. L. Smart, E. Moore, *Solid State Chemistry: an Introduction*, Chapman & Hall, London, 1992

29. D. Barthomeuf, *Studies in Surface Science and Catalysis*, 1991, **65**, 157

30. W.J. Mortier, S.K. Ghosh, S. Shankar, *Journal of the American Chemical Society*, 1986, **108**, 4315

31. R.A. van Santen, *Catalysis Today*, 1997, **38**, 377

32. J.F. Haw, *Physical Chemistry Chemical Physics*, 2002, **4**, 5431

33. J.W. Mortier, *Journal of Catalysis*, 1978, **55**, 138

34. R.M. Lago, et al., *Studies in Surface Science and Catalysis*, 1986, **28**, 677

35. G. Mirth, J. Cejka, J.A. Lercher, *Journal of Catalysis*, 1993, **139**, 24

36. A. Jentys, J.A. Lercher, *Introduction to Zeolite Science and Practice*, H. van Bekkum, et al. (Eds.), Elsevier, Amsterdam, 2001, p. 370

37. H. Pfeifer, D. Freude, M. Hunger, *Zeolites*, 1985, **5**, 274

38. B.C. Gates, *Catalytic Chemistry*, Wiley, Chichester, 1992, p. 270

39. R.G. Pearson, *Chemical Hardness*, Wiley-VCH, Weinheim, 1997

40. A.C.L. Gomes, et al., *Applied Catalysis A*, 1997, **148**, 373

41. A. Gola, et al., *Microporous Mesoporous Materials*, 2000, **40**, 73

42. J.A. Martens, et al., in *Handbook of Heterogeneous Catalysis, vol. 1*, G. Ertl, H. Knoezinger, J. Weitkamp (Eds.), Wiley-VCH, Weinheim, 1997, p. 324–365

43. T.F Narbeshuber, et al., *Applied Catalysis A*, 1996, **146**, 119

44. J. Abbot, F.N. Guerzoni, *Applied Catalysis A*, 1992, **85**, 173

45. H. Foerster, et al., *Journal of Molecular Catalysis A*, 1995, **95**, 267

46. E.A. Lombardo, W.K. Hall, *Journal of Catalysis*, 1988, **112**, 565

47. M. Haouas, A. Kogelbauer, R. Prins, *Catalysis Letters*, 2000, **70**, 61

48. Y. Oumi, et al., *Materials Chemistry and Physics*, 2003, **78**, 551

49. T. Sano, et al., *Microporous Mesoporous Materials*, 2000, **34**, 348

50. F. Lonyi, J.H. Lunsford, *Journal of Catalysis*, 1992, **136**, 566

51. R. Carvajal, P.J. Chu, J.H. Lunsford, *Jornal of Catalysis*, 1990, **125**, 123

52. R.T. Sanderson, *Chemical Bonds and Bond Energy*, Academic Press, New York, 1976

53. D. Barthomeuf, *Journal of Physical Chemistry*, 1984, **88**, 42

54. D. Barthomeuf, A. De Mallmann, *Studies in Surface Science and Catalysis*, 1988, **37**, 365

55. D. Barthomeuf, *Catalysis Review: Science and Engineering*, 1996, **38**, 521

56. M. Rep, et al., *Journal of Physical Chemistry B*, 2000, **104**, 8624

57. Y. Wang, et al., *Microporous Mesoporous Materials*, 1998, **26**, 175

58. K. Arishtirova, P. Kovacheva, S. Vassilev, *Applied Catalysis A*, 2001, **213**, 197

59. L.R.M. Martens, et al., *Studies in Surface Science and Catalysis*, 1987, **31**, 531

60. P.E. Hathaway, M.E. Davis, *Journal of Catalysis*, 1989, **116**, 263

61. Y. Ono, T. Baba, *Catalysis Today*, 1997, **38**, 321

62. R.A. Sheldon, I. Arends, H.E.B. Lempers, *Collection of Czechoslovak Chemical Communications*, 1998, **63**, 1724

63. J.S. Rafelt, J.H. Clark, *Catalysis Today*, 2000, **57**, 33

64. B. Wichterlova, Z. Sobalik, J. Dedecek, *Applied Catalysis B*, 2003, **41**, 97

65. J. Sarkany, W.M.H. Sachtler, *Zeolites*, 1994, **14**, 7

66. M. Mauvezin, et al., *Journal of Physical Chemistry B*, 2001, **105**, 928

67. R.W. Joyner, M. Stockenhuber, *Journal of Physical Chemistry B*, 1999, **103**, 5963

68. X. Feng. W.K. Hall, *Catalysis Letters*, 1996, **41**, 45

69. Y. Traa, B. Burger, J. Weitkamp, *Microporous Mesoporous Materials*, 1999, **30**, 3

70. J.N. Armor, *Catalysis Today*, 1995, **26**, 99

71. Z. Sobalik, et al., *Microporous Mesoporous Materials*, 1998, **21**, 525

72. M.A. Camblor, A. Corma, J. Perez-Pariente, *Zeolites*, 1993, **13**, 82

73. V. Bolis, et al., *Langmuir*, 1999, **15**, 5753

74. P.R. Rao, A.V. Ramaswamy, *Applied Catalysis A*, 1993, **93**, 113

75. G.I. Panov, et al., *Catalysis Today*, 1998, **41**, 365

76. J.M. Thomas, et al., *Chemistry: a European Journal*, 2001, **7**, 2973

77. P. Wu, et al., *Journal of Catalysis*, 2001, **202**, 245

78. D.T. On, et al., *Microporous Mesoporous Materials*, 2003, **57**, 169

79. A. Brait, M.E. Davis, *Applied Catalysis A*, 2000, **204**, 117

80. N.S. Ovanesyan, et al., *Kinetics and Catalysis*, 1998, **39**, 792

81. M. Muller, G. Harvey, R. Prins, *Microporous Mesoporous Materials*, 2000, **34**, 135

82. D.F. Shriver, P.W. Atkins, *Inorganic Chemistry, 3rd ed.*, Oxford University Press, Oxford, 1999, p. 367

83. H. Robson, K.P. Lillerud, *Verified Synthesis of Zeolitic Materials, 2nd ed.*, Elsevier, Amsterdam, 2001

84. S. Elliot, *The Chemistry and Physics of Solids*, Chicester, 1997

85. D.W. Breck, *Zeolite Molecular Sieves: Structure, Chemistry and Use*, Wiley-Interscience, London, 1974

86. G. Bellussi, et al., *Journal of Catalysis*, 1995, **157**, 227

87. A.J. Hoefnagel, H. van Bekkum, *Applied Catalysis A*, 1993, **97**, 87

88. M. Rigutto, et al., *Studies Surface Science and Catalysis*, 1993, **78**, 661

89. K. Smith, A. Musson, G.A. DeBoos, *Journal of the Chemical Society Chemical Communications*, 1996, 469

90. K.P. de Jong, et al., *Chemical Engineering Science*, 1996, **51**, 2053

91. R.L. Wadlinger, G.T. Kerr, E.J. Rosanisky, *US Patent 3308069*, 1967

92. M.M.J. Treacy, J.M. Newsam, *Nature*, 1988, **332**, 249

93. J.B. Higgins, et al., *Zeolites*, 1986, **8**, 446

94. J.C. Jansen, et al., *Catalysis Today*, 1997, **38**, 205

95. A.E. Bond, et al., US Pat. No. 3793385, 1974

96. H.E. Robson, *US Pat. No. 4560542*, 1985

97. M.K. Rubin, *Eur. Pat. Appl. EP 159846*, 1985

98. J. Perez-Pariente, et al., *Zeolites*, 1988, **8**, 46

99. G. Harvey, G. Binder, R. Prins, *Studies Surface Science Catalysis*, 1995, **94**, 397

100. G.H. Kuehl, H.K.C. Timken, *Microporous Mesoporous Materials*, 2000, **35-36**, 521

101. C. Jia, P. Massiani, D. Bartholomeuw, *Journal of the Chemical Society Faraday Transactions I*, 1993, **89**, 3659

102. L. Beck, J.F. Haw, *Journal of Physical Chemistry*, 1995, **99**, 1076

103. H. Robson, K.P. Lillerud, *Verified Syntheses of Zeolitic Materials, 2nd ed.*, Elsevier, Amsterdam, 2001, p. 115

104. M.A. Camblor, A. Corma, S. Valencia, *Journal of Materials Chemistry*, 1998, **8**, 2137

105. G.A. Olah, *Friedel-Crafts Chemistry*, Wiley, London, 1973

106. J. McMurry, *Organic Chemistry, 4th ed.*, Brooks/Cole, London, 2000

107. J. March, *Advanced Organic Chemistry, 4th ed.*, and p?

108. K. Tanabe, W.F. Holderich, *Applied Catalysis A*, 1999, 181, 399

109. H.G. Franck, J.W. Stadelhofer, *Industrial Aromatic Chemistry*, Springer-Verlag, Berlin/Heidelberg, 1987

110. P.J. Harrington, E. Lodewijk, *Organic Process Research & Development*, 1997, **1**, 72

111. R.A. Sheldon, *Chemistry & Industry*, 1992, **23**, 903

112. H. van Bekkum, et al, *Studies in Surface Science and Catalysis*, 1994, **83**, 379

113. P.B. Venuto, *Microporous Materials*, 1994, **2**, 29

114. J.H. Clark, D.J. Macquarrie, *Organic Process Research & Development*, 1997, **1**, 149

115. M.E. Davis, *Microporous and Mesoporous Materials*, 1998, **21**, 173

116. W.F. Hoelderich, et al., *Catalysis Today*, 1997, **37**, 353

117. B. Chiche, et al., *Journal of Organic Chemistry*, 1986, **51**, 2128

118. I. Neves, et al., *Journal of Molecular Catalysis*, 1994, **93**, 169

119. E.V. Sobrinho, et al, *Proceedings 12th International Zeolite Conference*, Baltimore, 1998, p. 1463

120. D. Rohan, et al., *Journal of Molecular Catalysis A*, 1998, **129**, 69

121. G. Harvey, et al., *Proceedings of the 9th International Zeolite Conference*, Montreal, 1992, p. 363

122. H. van Bekkum, et al., *Studies in Surface Science and Catalysis*, 1994, **83**, 379

123. Y. Pouilloux, et al., *Journal of Molecular Catalysis*, 1987, **40**, 231

124. I. Neves, et al., *Proceedings of the 9th International Zeolite Conference*, Montreal 1992, p. 543

125. C.S. Cundy, et al., *Tetrahedron Letters*, 1989, **30**, 2281

126. A. Vogt, H.W. Kouwenhoven, R. Prins, *Applied Catalysis A*, 1995, **123**, 37

127. Y. Pouilloux, et al., *Studies in Surface Science and Catalysis*, 1991, **59**, 513

128. M. Sasidharan, R. Kumar, *Studies in Surface Science and Catalysis*, 1997, **105**, 1197

129. D.E. Akporiaye, et al., *Studies in Surface Science and Catalysis*, 1993, **78**, 521

130. E.A. Gunnewegh, R.S. Dawning, H. van Bekkum, *Studies in Surface Science and Catalysis*, 1995, **97**, 447

131. C. Gauthier, et al., *Journal of Molecular Catalysis*, 1989, **50**, 219

132. A.P. Sing, A.K. Pandey, *Journal of Molecular Catalysis A*, 1997, **123**, 141

133. D. Bhattacharya, S. Sharma, A.P. Singh, *Applied Catalysis A*, 1997, **150**, 53

134. G. Harvey, G. Maeder, *Collection Czechoslovak Chemical Communications*, 1992, **37**, 862

135. H.K. Heinichen, W.F. Hoelderich, *Journal of Catalysis*, 1999, **185**, 108

136. M. Casagrande, et al., *Applied Catalysis A*, 2000, **201**, 263

137. E. Fromentin, J.M. Coustard, M. Guisnet, *Journal of Catalysis*, 2000, **190**, 433

138. E. Fromentin, J.M. Coustard, M. Guisnet, *Journal of Molecular Catalysis A*, 2000, **159**, 337

139. A. Berreghis, et al., *Catalysis Letters*, 2000, **68**, 123

140. P. Andy, et al., *Journal of Catalysis*, 2000, **192**, 215

141. P. Botella, A. Corma, G. Sastre, *Journal of Catalysis*, 2001, **197**, 81

142. F. Richard, H. Carreyre, G. Perot, *Journal of Molecular Catalysis A*, 1995, **101**, L167

143. F. Richard, H. Carreyre, G. Perot, *Journal of Molecular Catalysis A*, 1995, **103**, 51

144. P. Amonzegh, et al., *Catalysis Letters*, 1995, **34**, 389

145. Yu. Isaev, J.J. Fripiat, *Journal of Catalysis*, 1999, **182**, 257

146. F. Richard, H. Carreyre, G. Perot, *Journal of Catalysis*, 1996, **159**, 427

147. L. Gilbert, M. Spagnol, *Patent PCT, Int. Appl. WO 9717324*, 1997

148. G. Harvey, et al., *Proceedings 9th International Zeolite Conference, Montreal*, 1992, p. 363

149. U. Freese, F. Heinrich, F. Roessner, *Catalysis Today*, 1999, **49**, 237

150. D. Rohan, et al., *Journal of Catalysis*, 1998, **177**, 296

151. A. Corma, et al., *Applied Catalysis*, 1989, **49**, 109

152. K. Gaare, D. Akporiaye, *Journal of Molecular Catalysis A*, 1996, **109**, 177

153. Spagnol, L. Gilbert, D. Alby, *Industrial Chemistry Library*, 1996, **8**, 29

154. E.G. Derouane, et al., *Journal of Catalysis*, 1999, **187**, 209

155. E.G. Derouane, et al., *Journal of Catalysis*, 2000, **194**, 410

156. K. Smith, Z. Zhenhua, P.K.G. Hodgson, *Journal of Molecular Catalysis*, 1999, **134**, 121

157. E.G. Boreskova, V.I. Lugin, K.V. Topchieva, *Kinetics and Catalysis*, 1964, **5**, 991

158. A.P. Singh, D. Bhattacharya, S. Sharma, *Journal of Molecular Catalysis A*, 1995, 102, 139

159. A.P. Singh, D. Bhattacharya, *Catalysis Letters*, 1995, **32**, 327

160. A. Chatterjee, et al., *Journal of Catalysis*, 1999, **185**, 23

161. A.K. Pandey, A.P. Singh, *Catalysis Letters*, 1997, **44**, 129

162. S.D. Kim, et al., *Journal of Molecular Catalysis A*, 2000, **152**, 33

163. V. Bosacek, E.A. Gunnewegh, H. van Bekkum, *Catalysis Letters*, 1996, **39**, 57

164. B. Chevrier, R. Weiss, *Angewandte Chemie International Edition*, 1974, **13**, 1

165. O. Kresnawahjuesa, R.J. Gorte, D. White, *Journal of Molecular Catalysis A*, 2004, **208**, 175

166. Y. Ma, et al., *Applied Catalysis A*, 1997, **165**, 199

167. H.W. Kouwenhoven, H. van Bekkum, in *Handbook of Heterogeneous Catalysis, vol. 5*, G. Ertl, H. Knozinger, J. Weitkamp (Eds.), Wiley-VCH, Weinheim, 1997, p. 2358

168. M. Haouas, A. Kogelbauer, R. Prins, *Catalysis Letters*, 2000, **70**, 61

169. E. Bourgeat-Lami, et al., *Applied Catalysis*, 1991, **72**, 139

170. G.H. Kuehl, H.K.C. Timken, *Microporous Mesoporous Materials*, 2000, **124**, 217

171. G.S. Paine, *PhD Thesis*, Nottingham Trent University, October 2002

2 Experimental Techniques

2.1 Heterophase ion exchange

2.1.1 Theory

This method is used to introduce cations into the zeolite. As mentioned in the previous chapter, the presence of $(AlO_2)^-$ units in the zeolite requires the presence of charge-compensating cations in the structure.

Heterophase ion exchange involves suspending a powdered zeolite in a solvent (usually water, but other solvents can be used, e.g. methanol) in which the exchange salt is dissolved. The suspension is then stirred for a certain time, after which it is filtered, washed and dried. The above procedure can be repeated several times.

2.1.2 Zeolite BEA

Zeolite BEA (NH_4-BEA) was provided in powder form by CATAL International Ltd. (product code CT121) with a quoted Si/Al ratio of 12.5. Two different batches were used, namely lot 15/701 and lot 35/1102, the two batches showed identical XRD powder patterns. The batch named lot 15/701 was used for the experiments presented in Chapters 3 to 5 while lot 35/1102 was used for the experiments reported in Chapter 6.

2.1.3 Preparation of Na-exchanged BEA

Na-BEA zeolite was prepared by aqueous exchange starting from the parent material. 5 g of zeolite were transferred in 250 ml of a 10^{-2} M solution of $NaNO_3$ (AnalaR, 98.5+%). The mixture was left stirring at room temperature for 24 hours, then filtered in a Buchner funnel, washed three times with 100 ml distilled water each time, and left drying in a vacuum oven. The above procedure was repeated for a total of three exchanges.

2.1.4 Preparation of transition metal-exchanged BEA

Transition metal-exchanged-BEA zeolites were prepared by aqueous exchange starting from the parent material. 5 g of parent zeolite were transferred in 250 ml of a 10^{-2} M solution of, for example, iron (III) nitrate (Fisher, 99.18%) in distilled water. The mixture was left stirring at room temperature for 24 hours, then filtered in a Buchner funnel, washed three times with 100 ml distilled water each time, and left drying in a vacuum oven. The above procedure was repeated for a total of three exchanges. The same method was also used to prepare Co-, Ni- and Cu-exchanged BEA using cobalt (II) nitrate hexahydrate (Aldrich, 98%), nickel (II) nitrate hexahydrate (Acros, 99%) and copper (II) nitrate (Fisher, 99.5+%), respectively. Additionally, two other Fe-BEA zeolites were prepared with the same procedure but using 1 M and 0.1 M iron (III) nitrate solutions respectively.

2.1.5 Preparation of Cu-exchanged BEA with copper acetate

Cu-BEA zeolite was prepared by aqueous exchange starting from the parent material. 5 g of parent zeolite where activated in air at 475 °C for 1 hour, then were transferred in 250 ml of a 10^{-2} M solution of copper (II) acetate (AnalaR, 99+%). The mixture was left stirring at room temperature for 24 hours, then filtered in a Buchner funnel, washed three times with 100 ml distilled water each time, and left drying for 24 hours in an oven at 383 K. The above procedure was repeated for a total of three exchanges.

2.2 Passivation of the external surface acidity of BEA.

2.2.1 Theory

The zeolite surface accessible to reactants comprises a large internal surface (the micropore system) and a smaller external surface (i.e. outside the micropores). This external surface can be active (and in some cases selective) and may also promote the formation of undesirable coke-like products which can cause deactivation by inhibiting access to the micropores [1].

In order to passivate (i.e. deactivate) the external-surface acidity of BEA it is possible to use tetraethyl orthosilicate (TEOS, see Figure 2.2.1) to deposit a thin external layer of

silica [2]. TEOS is a bulky molecule with a cross-sectional area of ca. 9.5 Å and thus does not diffuse into the pore system of BEA and when dissolved in a suitable solvent provides the desired silica layer on the external surface of the zeolite.

2.2.2 Experimental procedure

About 1.2 g of activated zeolite BEA were added to about 25 ml of hexane (Aldrich, 95+%) to which about 0.24 g of TEOS (Aldrich, 98%) were added, the solution was left stirring for 3 hours at room temperature. It was then filtered and washed with hexane. Subsequently, it was calcined in air for 3 hours.
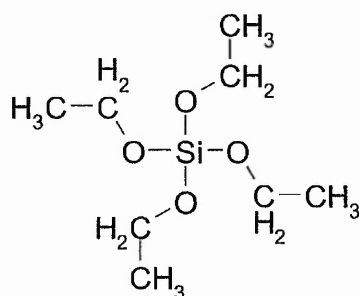
Figure 2.2.1 – The tetraethyl orthosilicate molecule, $Si(OCH_2CH_3)_4$

2.3 Adsorption of 2,6-dimethylpyridine on BEA

2.3.1 Theory

2,6-Dimethylpyridine (DMP, also called lutidine, see Figure 2.3.1) is a bulky organic base that readily deactivates Brønsted acid sites but is believed to have little effect on Lewis acid sites because of the blocking of the two methyl groups [3]. It can thus be used to study the involvement of Brønsted and Lewis acid sites in the acylation reaction by first adsorbing DMP on a BEA sample and then studying the sample in the catalytic reactor.

2.3.2 Experimental procedure

The zeolite sample was activated in vacuum at 5 °C min^{-1} up to 475 C and then left at 475 °C for 1 hour. Then the sample, still in vacuum, was cooled down to 150 °C and

subsequently exposed to about 4 mbar of DMP (Aldrich, 99%) for about 25 minutes. After this the sample was left outgassing in vacuum at 150 C for about 1 hour.
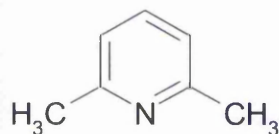
Figure 2.3.1 - 2,6-Dimethylpyridine molecule

2.4 X-Ray Diffraction (XRD)

2.4.1 Theory

X-ray diffraction is a technique used to identify the crystalline phases present in materials and to determine the structure of these phases. Figure 2.4.1 illustrates a typical XRD experiment.
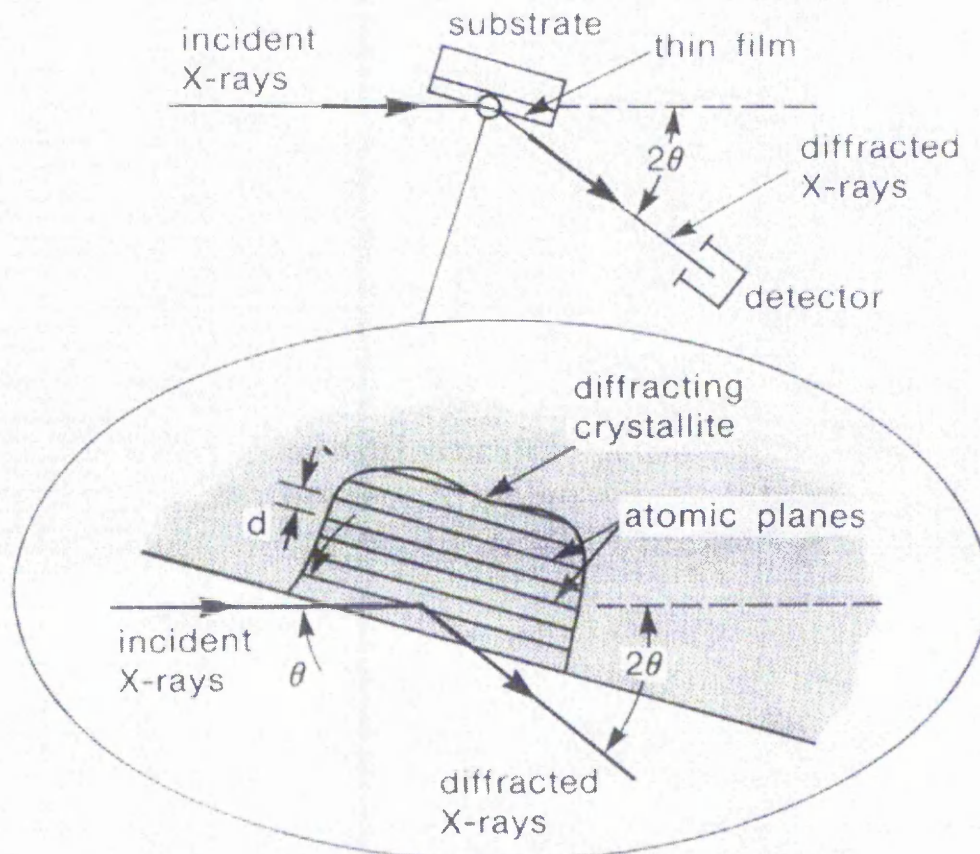
Figure 2.4.1 – Basic features of a typical XRD experiment [4]

XRD is based on the principle that when a monochromatic beam of x-rays is incident on a crystalline solid, diffraction occurs when the angle of incidence on planes of atoms in the structure satisfies the Bragg equation:

$$n\lambda = 2d \cdot \sin\theta$$

Where n is a small integer, λ is the wavelength of the x-ray beam (1.542 Å for x-rays generated from a copper target), d is the separation between planes in the crystal, and θ is the angle of incidence of the x-rays. For a single crystal the Bragg equation will be valid only for certain angles of incidence. For a finely ground crystalline powder containing many randomly orientated crystallites, there will be always some crystallites that satisfy the Bragg equation at any angle of incidence. Furthermore, the scattering power of an atom for x-rays depends on the number of electrons it possesses. Thus the position of the diffraction beams from the crystal depend only on the size and shape of the repetitive unit of a crystal and the wavelength of the incident beam, whereas the intensities of the diffracted beam depends on the type of atoms in the crystal and the location of the atoms in the fundamental repetitive unit, the unit cell. No two different substances, therefore, have absolutely identical diffraction partterns when the direction and intensity of all the diffracted beams are considered. By using the Bragg equation, it also possible to derive lattice spacings. By measuring the angles, 2θ, under which constructively interfering x-rays leave the crystal, the Bragg equation gives the corresponding lattice spacings, which are characteristics for a certain compound.

2.4.2 Experimental apparatus

Diffraction experiments were carried out on a Hiltonbrooks modified Philips 1050 powder diffractometer, using $CuK\alpha$ radiation, operating the generator at 42.5 kV and 18 mA. The scan range used was 5-35° 2θ with a step size of 0.02° and a step time of 6 seconds. The experiments presented in Chapter 6 were carried out on a PANalytical X'Pert PRO MPD x-ray diffraction system, which uses an incident beam monochromator that provides pure $CuK\alpha_1$ radiation and a linear detector (X'Celerator). The generator was operated at 40.0 kV and 40.0 mA, and the scan range used was 5-60° 2θ with a step size of ca 0.05° and a step time of ca 50 seconds.

2.5 Temperature Programmed Desorption – Mass Spectrometry (TPD-MS)

2.5.1 Theory – Temperature Programmed Desorption

TPD is a powerful technique to study adsorption and surface reactions, and also to study desorption rates. The general procedure is to expose a clean surface (adsorbent or substrate) to a low pressure of gas (adsorbate). Then, by gradually heating up the sample the adsorbed gas will desorb from the surface and can be analysed via a mass spectrometer to determine the desorption profile expressed in terms of intensity versus temperature.

Desorption is always activated because the particles have to be lifted from the foot of a potential well. Assuming the temperature dependence of the rate of desorption to be Arrhenius–like and applying the Langmuir model of adsorption, it can be shown that the activation energy of desorption is related to the temperature of maximum desorption rate for the adsorbate [5].

2.5.2 Theory – Mass Spectrometry

Mass spectrometry differs from traditional spectroscopic methods in that it does not involve the interaction of radiation with matter. Mass spectrometry requires that the molecule of interest is charged, this then allows the instrument to separate the different ions due to their mass to charge ratio (m/e). There are a number of different methods of separating charged ions, one of these relies on a magnetic field to deflect the charged particle. Ions are accelerated by a fixed voltage and subjected to a magnetic field that curves their trajectories differently according to their mass and charge. Thus, by varying this magnetic field it is possible to select which ions undergo sufficient curvature of their path so that they reach a detector. The spectrum produced by a mass spectrometer is, therefore, a plot of the number of ions detected (intensity) versus their mass to charge ratio.

Another method of separating ions is the so called time-of-flight. In this case all the molecules are provided with a certain amount of energy and then allowed to drift

towards the detector. The time they take to reach the detector will vary depending on the mass of the ions.

The instrument used in this study is called a quadrupole mass analyser and is based on alternating electric fields applied across four poles (see Figure 2.5.1).
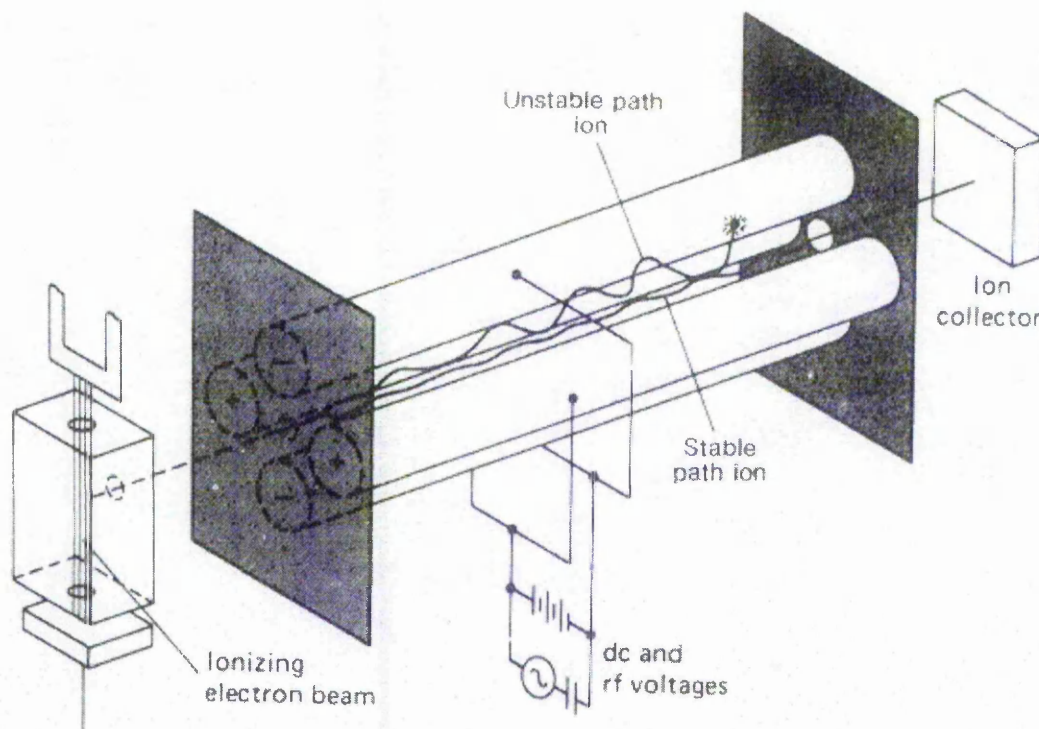
Figure 2.5.1 – Schematic diagram of a quadrupole mass analyser [3]

By applying AC and DC potentials to a set of four rods, ions are separated by mass as they pass through the quadrupole. The voltages can be changed quickly, allowing relatively rapid scanning of the mass range, which is usually limited to a maximum of ca 200 amu.

2.5.3 Experimental apparatus and procedure

TPD measurements were made in a compact, purpose built, stainless steel apparatus equipped with a 60 l s^{-1} ion pump. The desorption cell was connected through a leak valve to an independently pumped, multiplexed Pfeiffer Prisma quadrupole mass spectrometer operating under computer control (see Figure 2.5.2).

ITEM	DESCRIPTION	ITEM	DESCRIPTION
1	LECTURE BOTTLE (GAS)	11	ROTARY PUMP
2	LEAK VALVE	12	CAPACITANCE DIAPHRAGM (PRESSURE GAUGE)
3	AIR INLET VALVE	13	PIRANI GAUGE (PRESSURE GAUGE)
4	FLEXIBLE SS TUBING	14	SAMPLE HOLDER
5	VALVE	15	FURNACE
6	TEE PIECE	16	GAS DOSING VALVE
7	MOLECULAR SIEVE TRAP	17	ISOLATING VALVE
8	VALVE	18	TURBO MOLECULAR PUMP UNIT
9	THERMOCOUPLE	19	COLD CATHODE (PRESSURE GAUGE)
10	TEMPERATURE PROGRAMMER & CONTROLLER (COMPUTER INPUT/OUTPUT)	20	MASS SPECTROMETER (OUTPUT TO COMPUTER)

Figure 2.5.2 - Diagram showing the TPD–MS apparatus [7]

The zeolite (ca 50 mg) was introduced into the desorption cell, evacuated, heated to ca 750 K at 5 K per minute, kept at 750 K for 1 h and subsequently cooled to room temperature. After this, the base pressure in the apparatus was typically 5×10^{-8} mbar. Acetic anhydride (Aldrich, 99+% purity) was further purified by freeze/thaw pumping cycles and exposed to the zeolite sample at room temperature and ca 1 mbar pressure. Ammonia (Argo, 99%) was exposed to the sample at ca 5 mbar pressure, and at 423 K to avoid physisorption of ammonia [8].

After pumping back to the base pressure, the sample was heated to 875 K at 10 K per minute and the desorption spectra recorded.

2.5.4 Analysis of TPD–MS data

The desorption profile for ammonia was determined by analysis of the peak m/e = 16. The parent peak for ammonia at m/e = 17 was not analysed because it can receive a significant contribution from water in form of OH$^-$.

In the case of acetic anhydride, preliminary analysis of desorption results showed there are a wide range of significant reaction products desorbing, principally acetic acid, carbon monoxide, carbon dioxide, water, hydrogen and ketene. Ketene, $CH_2=C=O$, was

identified from the cracking pattern published by Cornu and Massot [9], which shows that the parent $m/e = 42$ is the second largest feature, but that the strongest contribution is at $m/e = 14$, from the CH_2 fragment. We have used $m/e = 14$ in our analysis, although we have also shown that essentially the same results are obtained if $m/e = 42$ is considered instead. $m/e = 14$ also has the advantage that it receives only relatively small contributions from acetic acid and acetic anhydride.

Cracking patterns in the mass spectrometer were determined *in situ* for acetic anhydride, water and acetic acid. To quantify the relative amounts of the anhydride and the acid desorbing, the mass spectrum was measured of the vapour above a mixture of acetic anhydride and acetic acid, prepared such that their partial pressures at room temperature were equal.

The cracking patterns are shown in Figure 2.5.3 & 2.5.4. They justify the following assumptions, which greatly facilitate the quantitative analysis of the desorption spectra.

1. The peak at $m/e = 60$ arises only from acetic acid.

2. The peak at $m/e = 43$ receives contributions from acetic acid and acetic anhydride, but not from ketene. Since acetic acid can be quantified from $m/e = 60$, its contribution to $m/e = 43$ can be calculated from its cracking pattern, and the amount of acetic anhydride desorbed determined by difference.

3. The peak at $m/e = 14$ receives contributions from ketene, acetic acid and acetic anhydride. Since the acid and the anhydride have already been quantified from the $m/e = 60$ and 43 peaks and their cracking patterns are known, the contribution of ketene to the $m/e = 42$ peak can be determined by subtraction.

4. The $m/e = 18$ peak arises only from the desorption of water. CO_2 was determined from the $m/e = 44$ peak, CO from the $m/e = 28$ peak and hydrogen from the $m/e = 2$ peak.

5. Isotopes are ignored in these calculations. For example, ketene would have a small contribution at $m/e = 43$ due to, for example, $CHD=C=O$ and $^{13}CH_2=C=O$. However these are very small contributions compared to the peak at $m/e = 42$, so that they are not significant in relation to experimental errors.

Amounts desorbed in each experiment were normalised to take account of the mass of material under study.
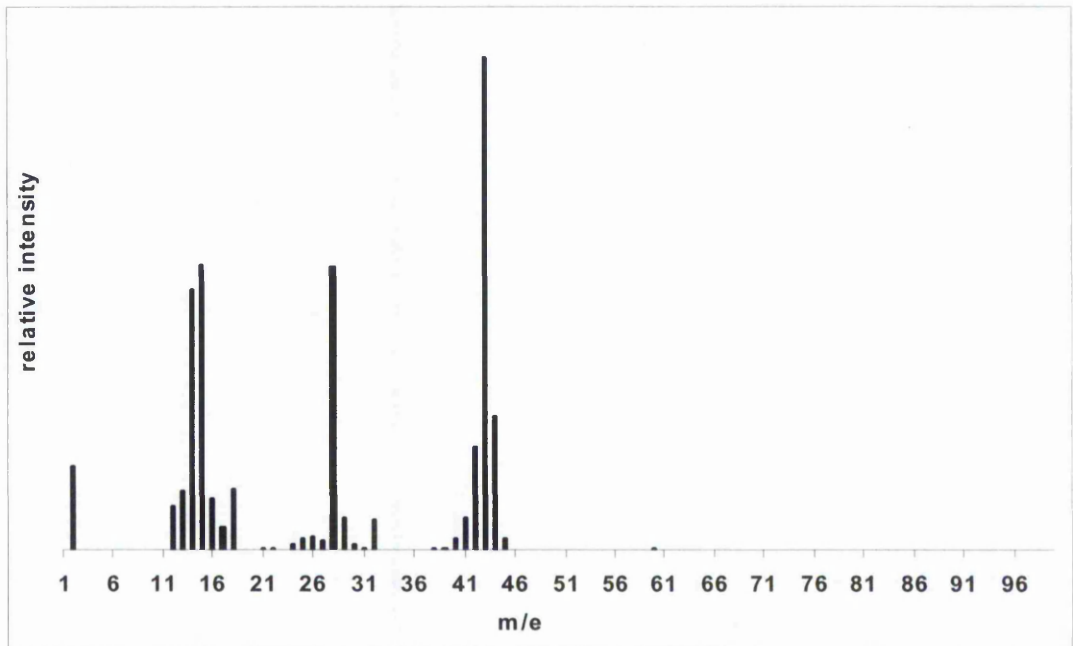
Figure 2.5.3 – The acetic anhydride fragmentation pattern
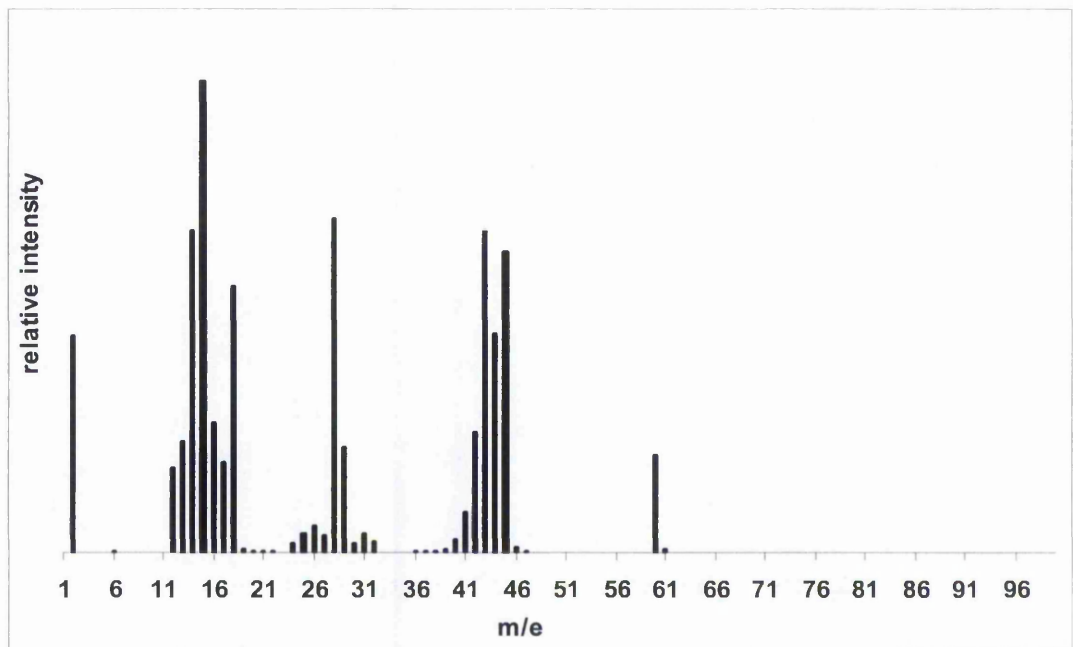
Figure 2.5.4 – The acetic acid fragmentation pattern

2.6 Fourier Transform Infra Red Spectroscopy (FTIR)

2.6.1 Theory:

Useful information on the adsorbed species present within a zeolite can be obtained by studying the adsorption of infrared radiation. IR spectroscopy, which is usually performed in the frequency range 4000 to 400 cm^{-1}, is based on the fact that interatomic bonds absorb radiation in the infrared region of the spectrum. Chemical bonds in different environments will absorb with varying intensities and at varying frequencies.

The basis of a typical IR experiment is to pass infrared radiation through a thin sample (wafer) of compound and measure which wavelengths of the applied infrared radiation are transmitted by the sample. The basic dispersive instrument uses a prism or a grating monochromator to scan trough the infrared region of radiation. However, Fourier transform instruments are now routinely used because they have better signal-to-noise ratio, better wavelength accuracy and smaller acquisition time than conventional dispersive instruments.
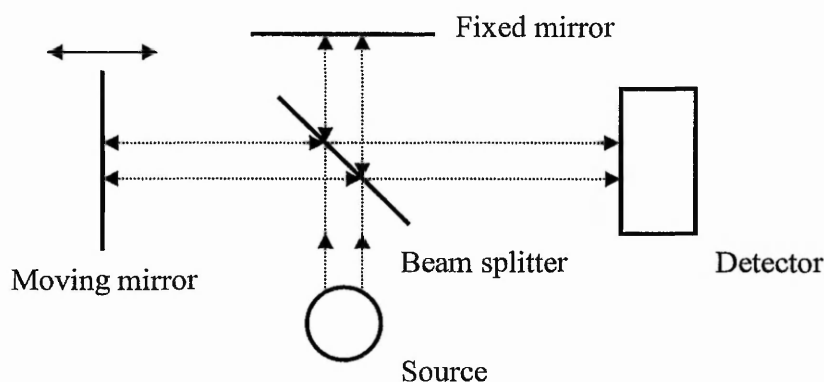
Figure 2.6.1 – Optical arrangement for a Fourier-Transform spectrometer

A Fourier transform instrument, depicted in Figure 2.6.1, contains no grating or prism, instead it relies on the technique of Michelson interferometry. A beam of radiation from the source is focused on a beam splitter constructed such that half the beam is reflected to a fixed mirror. The other half of the beam is transmitted to a moving mirror. Each component reflected by the two mirrors returns to the beam splitter. The moving mirror affects the relative path length of the two beams, thus introducing a phase difference. By

translation of the moving mirror, the spectral range is covered by the range of path difference reached. The amplitudes of the waves are combined to form an interferogram, and the resulting encoded beam passes on to the sample compartment and is detected by either a photon or thermal detector. Then, the interferogram is decoded by a mathematical operation (called Fourier transform) to give a spectrum of absorbance versus wavenumbers.

2.6.2 Experimental apparatus and procedure

IR experiments were carried out in a compact, purpose built, stainless steel apparatus, depicted in Figure 6, equipped with a 60 l s^{-1} ion pump. Measurements were performed using an ATI RS1 Fourier Transform Spectrometer equipped with an *in situ* stainless steel cell with calcium fluoride windows, the spectra were recorded in transmission mode.
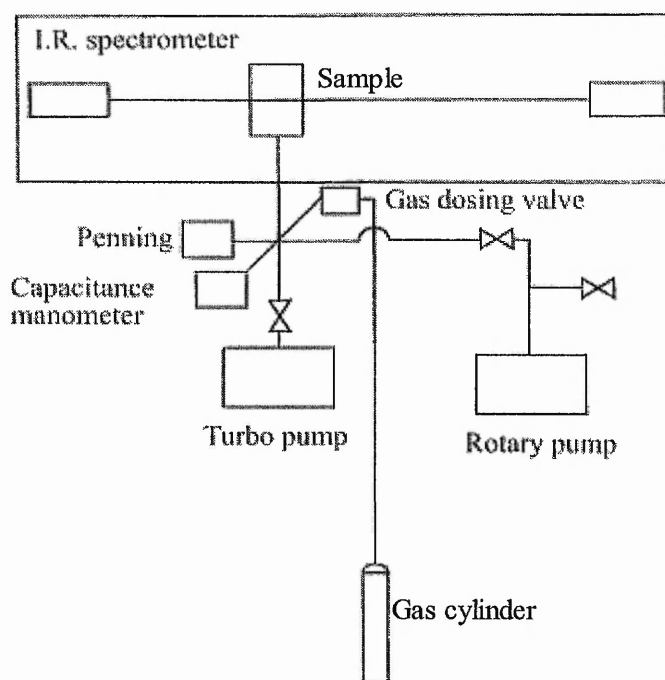
Figure 2.6.2 - *In situ* vacuum FTIR apparatus [10]

The zeolite wafer (ca 25 mg) was prepared by pressing the zeolite powder between two stainless steel tablets. It was then mounted in the *in situ* cell, evacuated, and heated to ca 750 K at 5 K per minute, kept at 750 K for 1 h and subsequently cooled to room temperature. After this, the base pressure in the apparatus was typically 5 x 10^{-8} mbar.

2.7 Catalytic Studies

2.7.1 Acylation of anisole with acetic anhydride

The acylation reaction was carried out in the liquid phase in a batch reactor consisting of a 100 ml round-bottomed flask connected to a reflux condenser, a thermometer and a stopper. Into this vessel, 0.2 mol of acetic anhydride (Aldrich, 99+%) and 0.4 mol of anisole (Aldrich, 99%) were added to the flask and mixed for 5 minutes using a magnetic stirrer. A small amount of sample was then extracted with a teat pipette and transferred into a sample bottle. Then a 0.2 µl sample was taken up in a 5 µl syringe and analysed by gas chromatography (GC). Subsequently, 300 mg of powdered activated catalyst was added to the reaction mixture and the system was heated to 333 K. Activation was achieved by heating the catalyst in flowing air up to a temperature of ca 748 K at a ramp rate of 5 K per minute, and then keeping it at 750 K for 1 h. The catalyst was at a temperature of ca 400 K when transferred to the flask, to minimise readsorption of water. After adding the catalyst, the mixture was stirred for 24 h, with samples taken after 5 min, after 30 min, and then at 30 min intervals for the first 5 h, and a final sampling after 24 h. N-decane (Aldrich, 99%) was used as internal standard to quantify the amount of components in the analysis.

2.7.2 Hydrolysis of acetic anhydride

The hydrolysis of acetic anhydride was carried out in the liquid phase at 298 K in a 100 ml round-bottomed flask connected to a reflux condenser. Into this vessel, 0.2 mol of acetic anhydride (Aldrich, 99+%) were added, plus 0.5 g of n-octane as internal standard (Lancaster, 99+%) and 300 mg of powdered activated catalyst. The mixture was then left stirring for 5 minutes at 298 K. After this, a sample was extracted and analysed by off-line gas chromatography (oven temperature of 343 K, no ramp rate). Then, 0.2 mol of either H_2O or D_2O (Aldrich, 99 atom % D) were added and the mixture was left stirring at 298 K for 2 hours, with samples extracted at regular intervals and analysed by off-line gas chromatography. The catalyst was then filtered off and the solution analysed by ^{1}H and ^{13}C NMR.

2.7.3 Micro-scale acylation with acetic anhydride-d$_6$

The acylation reaction was carried out in the liquid phase at 333 K in a 5 ml round-bottomed flask connected to a reflux condenser. Into this vessel 0.02 mol of anisole (Aldrich, 99%) was added, plus either 0.01 mol acetic anhydride (Aldrich, 99+%) or 0.01 mol acetic anhydride-d$_6$ (Aldrich, 99 atom % D), the resulting solution mixed at 333 K with a magnetic stirrer. Then 30 mg of powdered activated catalyst were added, and the reaction mixture was left stirring at 333 K for 24 hours. Then the catalyst was filtered off and the solution was analysed by ^{1}H and ^{13}C liquid NMR.

2.7.4 Micro-scale acylation with anisole-d$_8$

The same procedure as described in the previous paragraph was performed using 1 g of anisole-d$_8$ (0.0086 mol, Aldrich, 98 atom % D), 0.4392 g of acetic anhydride (0.0043 mol, Aldrich, 99+%) and 30 mg of powdered activated catalyst.

2.8 Gas Chromatographic Analysis (GC)

2.8.1 Theory

Chromatography is a method of separation in which two mutually immiscible phases are brought into contact, one phase is stationary and the other is mobile. In gas chromatography the mobile phase is a gas, the stationary phases can either be liquid (gas-liquid chromatography) or solid (gas-solid chromatography). The sample is introduced into the mobile phase and carried along through a column containing a distributed stationary phase (see Figure 1.7.1). When both phases are properly chosen, the sample components are gradually separated into bands in the mobile phase. At the end of the column, separated components emerge in order of increasing interaction with the stationary phase. The component that has least affinity for the stationary phase emerges first, the one that interacts more strongly elutes last.

Samples for gas chromatography must be volatile and thermally stable at the operating conditions, they are introduced into the gas flow via an injection port located at the top of the column. A continuous flow of carrier gas (helium) elutes the components from the column from where they pass trough a detector connected to a recording system.
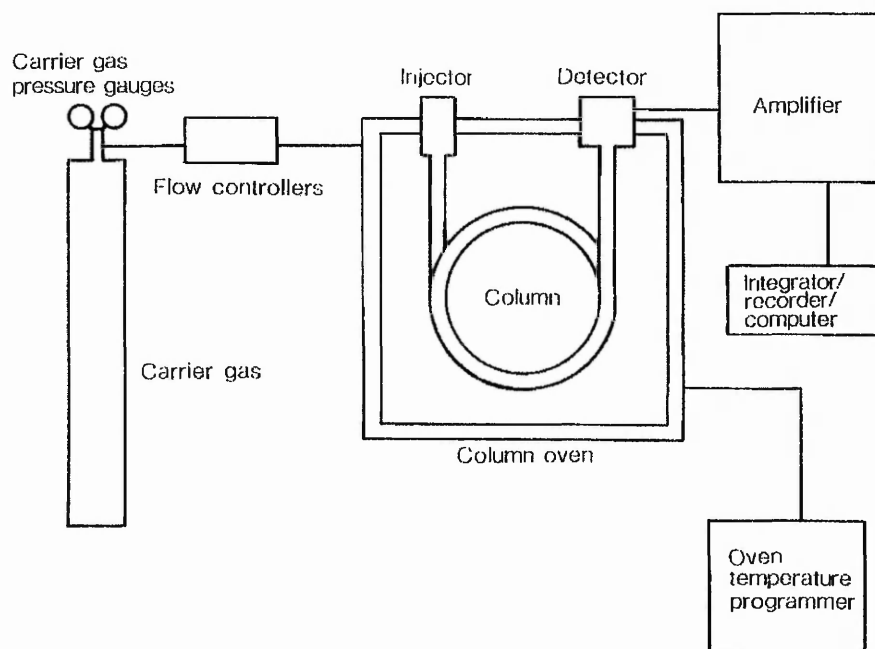
Figure 2.8.1 – Schematic diagram of a gas chromatograph [6]

The detector employed is a flame ionisation detector (FID). The FID responds to virtually all organic compounds except formic acid. Its response to air, inorganic gases, and water is low. It has a very high sensitivity to organic compounds and the widest linear range (10^7) of any detector in common use.

2.8.2 Experimental apparatus and procedure

GC measurements were performed with a Shimadzu GC-8A chromatograph equipped with a packed column containing an OV101 liquid phase (10% loading) on a chromosorb WHP support, and fitted with a flame ionisation detector (FID).

The gas chromatograph operating conditions employed were a column oven temperature programme from 353 to 473 K at 8 k min^{-1} and a detector temperature of 623 K. Small amounts of sample were extracted from the reaction mixture with a teat pipette and transferred into a sample bottle. Then a 0.2 µl sample was taken up in a 5 µl syringe and injected into the column through a self sealing silicone-rubber septum. This procedure was performed after 5 minutes, and then at 30 minute intervals for a period of 5 h, and in addition a 24 h sample was also extracted to determine the loss of activity of the catalyst with time.

2.8.3 Analysis of GC data

For any component a mixture, providing good resolution is achieved, the peak area is proportional to the amount of that component in the mixture. However, the response of the FID varies from one component to another. Thus a set of detector response factors needs to be determined for any particular analysis. The use of an internal standard allows for accurate quantification and eliminates the need for precisely measured injections, since a reference standard is included in each sample analysed. The internal standard used here, n-decane, was selected because it has a retention time such that it does not interfere with the other components present in the mixture. The procedure involves analysing a test sample containing known amounts of each component plus a known amount of internal standard. Since peak area is proportional to the amount of an eluted component and the detector response factor (DRF), then for an individual component a:

$$A_a = DRF_a \cdot C_a$$

For the internal standard:

$$A_{is} = DRF_{is} \cdot C_{is}$$

Where A is the peak area and C is the amount of component. The relative response factor of component a to the internal standard ($DRF_{a/is}$) is therefore:

$$DRF_{a/is} = (DRF_a/DRF_{is}) = (A_a/C_a)/(A_{is}/C_{is})$$

Rearranging:

$$C_a = (A_a/A_{is})/(C_{is}/DRF_{a/is})$$

The above equation allows the calculation of the concentration of each component in the mixture, from a knowledge of their peak area and their relative detector response factors.

2.9 Nuclear Magnetic Resonance (NMR)

2.9.1 Theory

A nucleus will possess a magnetic moment when its spin quantum number, I, in non-zero. In the absence of a magnetic field all of the magnetic states of that nucleus will be degenerate. However, when the nucleus is placed in an external magnetic field a number, $2I + 1$, of different orientations with different energies will arise. It is this splitting of the otherwise degenerate energy levels in a magnetic field that makes NMR spectroscopy possible.

The most widely studied nuclei, e.g. ^{1}H and ^{13}C, possess a spin quantum number of ½, and so when these nuclei are placed in a magnetic field two spin states arise. The difference in energy between these two states is proportional to the applied magnetic field and the frequency of radiation that corresponds to this energy is called the resonance frequency.

Even though a magnetic field, B_0, is applied to the sample, the effective magnetic field, B_{eff}, experienced by the nucleus will not necessarily be the same, since the motions of the electrons surrounding the nucleus will result in induced magnetic fields. Therefore the resonance frequency is characteristic of the chemical environment around the nucleus.

NMR data is generally presented using a dimensionless quantity called chemical shift, δ or ppm (parts per million). It is the difference between the resonance frequency in the unknown and the one in a reference compound, multiplied by a million, and then divided by the resonance frequency in the reference compound, this to give a dimensionless quantity independent of the applied magnetic field.

2.9.2 Experimental apparatus and procedure

^{1}H and ^{13}C NMR spectra were obtained on a JEOL JNM-EX270 FT-NMR instrument operating at a magnetic field strength of 6.34 Tesla and a frequency of 270 MHz for ^{1}H and at 67.8 MHz for ^{13}C, and measured in ppm downfield from TMS. $CDCl_3$ was used as solvent, unless otherwise stated.

2.9.3 Analysis of NMR data

Figure 2.9.1 presents the molecules of interest and their chemical shifts (^{1}H in blue and ^{13}C in red), which were measured from the pure compounds dissolved in $CDCl_3$.
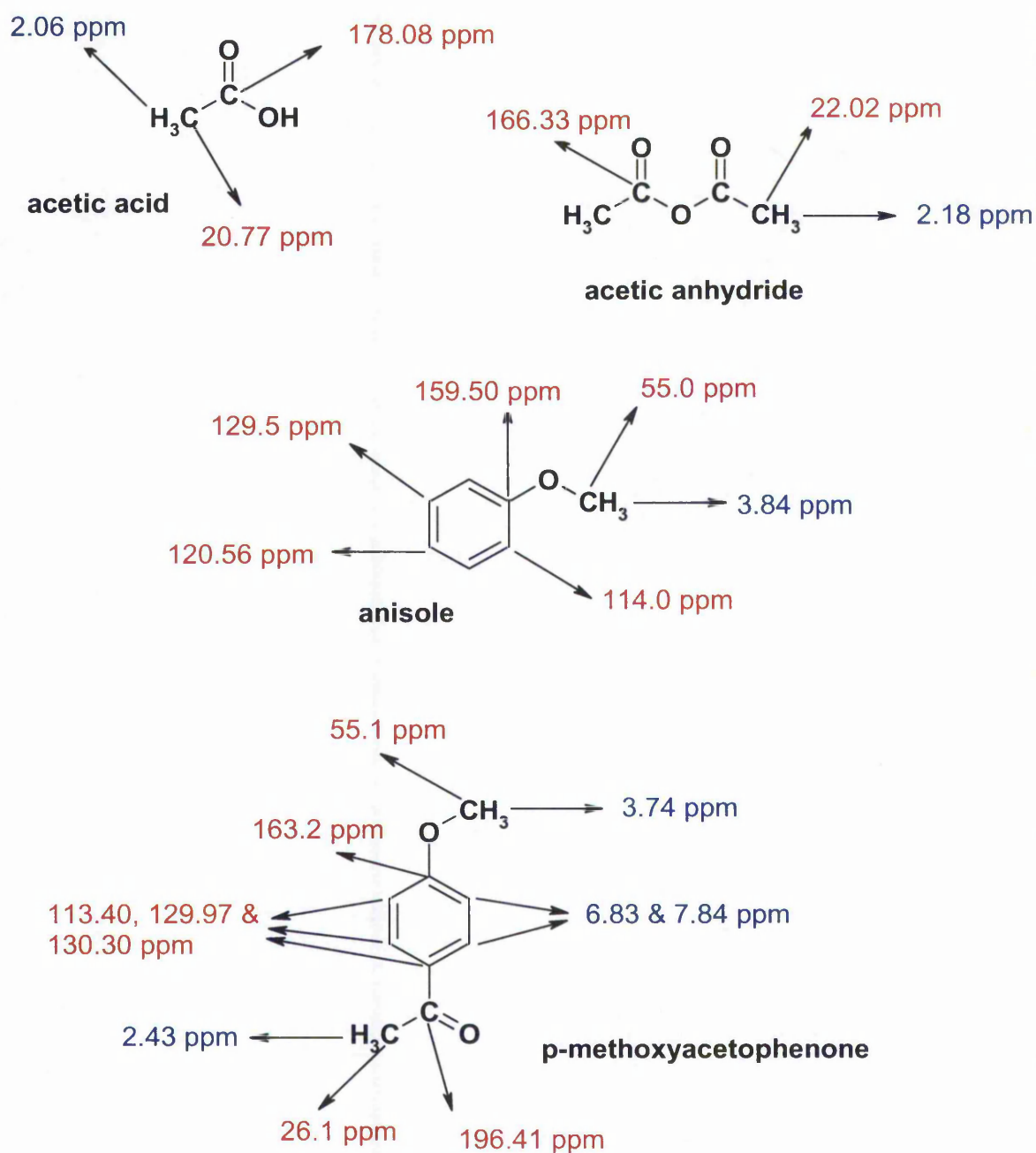
Figure 2.9.1 – NMR chemical shifts for pure substances dissolved in $CDCl_3$

The ^{1}H chemical shifts of the -O-CH$_3$ group on anisole and p-MAP can be used to analyse the results of the isotopic experiments. These two peaks are separated, thus providing a means to measure the percentage yield of the acylation reaction via the following equation:

$$\%yield_{p\text{-}MAP} = \frac{integral\ methoxy_{p\text{-}MAP}}{integral\ methoxy_{p\text{-}MAP} + integral\ methoxy_{anisole}} \cdot 100$$

It should be noted that the chemical shifts in Figure 2.9.1 refer to the pure substances while in the case of a solution of acetic anhydride, anisole and p-MAP the ^{1}H chemical shifts of the two -O-CH$_3$ groups switch positions. The methoxy group chemical shift for pure anisole is 3.84 ppm and for pure p-MAP is 3.74 ppm. However, in the case of the aforementioned solution, the shift for anisole is 3.78 ppm and for p-MAP is 3.83 ppm. This phenomenon will be discussed in more detail in Chapter 5.

2.10 Nitrogen adsorption

2.10.1 Theory

Nitrogen adsorption at 77 K is a commonly applied technique to determine various characteristics of porous materials such as surface area and pore volume. The pores that are present in a catalyst can be classified in different classes depending on their size:

1. Micropores (size < 2nm),
2. Mesopores (2nm < size < 50 nm)
3. Macropores (size > 50 nm)

The equilibrium amount of adsorbed nitrogen is measured as a function of the applied vapour pressure, giving rise to the adsorption isotherm. The adsorption isotherm is thus the relationship between the equilibrium amount adsorbed and the equilibrium pressure at a known temperature. This adsorbed amount can be given by the number of moles or by the corresponding volume at STP conditions. As the temperature of adsorption is generally lower than the critical temperatures of the adsorptive, the adsorbed amount is usually given as a function of the relative pressure p/p_0, where p_0 is the saturation

vapour pressure of the adsorptive. After the adsorption has been determined at pressures up to ca $p/p_0 = 0.95$, the desorption isotherm is often measured by the decreasing the pressure of the adsorbate gas. The desorption isotherm usually follows the adsorption curve, except where evaporation from pores takes place at a pressure lower than that of capillary condensation, giving rise to a hysteresis loop. The adsorption isotherm depends on the solid porous texture and according to the IUPAC classification [11] six types can be distinguished (see Figure 2.10.1).
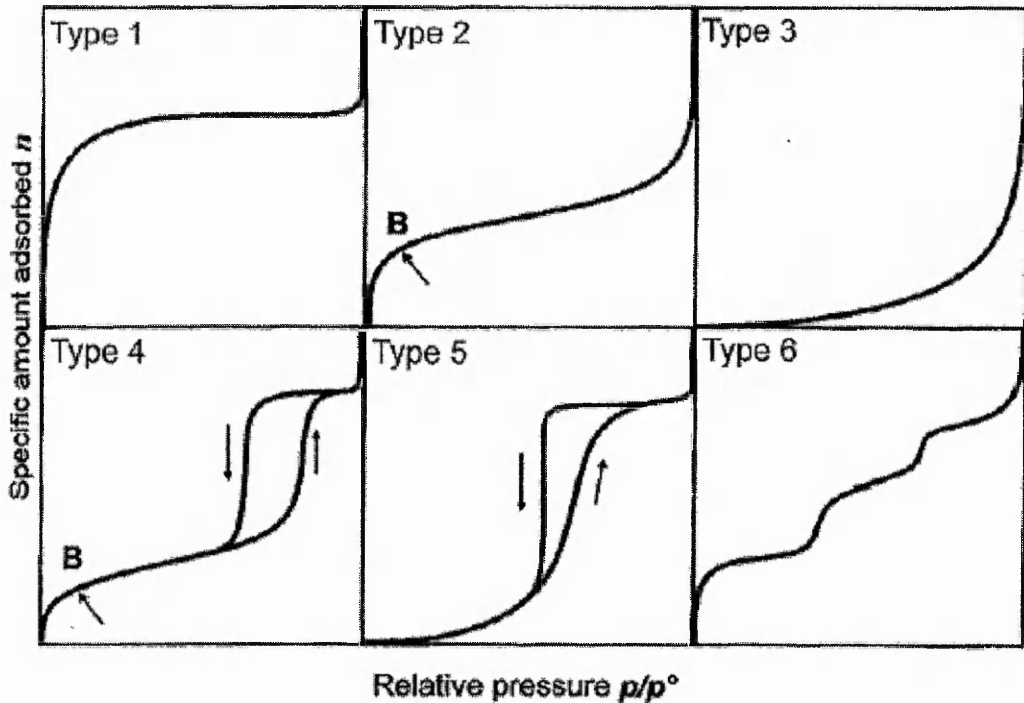
Figure 2.10.1 - Adsorption isotherms classified according to IUPAC [12]

Type 1 is characteristic for adsorbents with micropores. The adsorption takes place at very low pressure because of strong interaction between adsorbate and pore walls. Pore filling takes place without capillary condensation in the low relative pressure region ($p/p_0 < 0.3$). Once the micropores are filled, the adsorption continues on the external surface. Types 2 and 4 are indicative of either nonporous adsorbents or adsorbents having relatively large pores. At low relative pressure, the formation of a monolayer of adsorbed molecules is the dominant process. On the other hand, at high relative pressure multilayer adsorption and condensation in pores takes place. Type 4 isotherms are also typical of zeolites such as BEA, and it is due to the presence of a secondary pore system consisting of mesopores. Thus capillary condensation within the secondary pore structure can occur, leading to a hysteresis loop in the capillary condensation range of

the nitrogen isotherm. Types 3 and 5 arise under conditions were the adsorbent-adsorbate interactions are weak; such isotherms are relatively rare. The type 6 isotherm is indicative of a uniform ultramicroporous solid or of a nonporous solid with a uniform surface.

As already mentioned, the data from nitrogen adsoprtion isotherms can be used to determine the surface area and the pore volume of a sample. For example, in the case of meso and macroporous materials the BET method can be applied [13] to calculate the surface area. However this method can not be applied to microporous materials such as zeolites because the size of the molecules adsorbed and of the pores probed are in the same range. In microporous materials the adsorbed molecules fill the pores completely and, because of the limited space multilayer adsorption is suppressed. While fundamentally meaningless, the BET surface area is still frequently reported for zeolites (and other microporous materials) and can be used as a purely empirical value to compare the quality and porosity of materials of the same kind. In this thesis micropore volumes were calculated using the Quantachrome NovaWin2 software and applying the Dubinin-Radushkevitch plot [12].

2.10.2 Experimental apparatus

Nitrogen adsorption isotherms were obtained on a Quantachrome Nova 3200e surface area and pore size analyser equipped with an Edwards 3 rotary pump. 0.1 g of sample were left outgassing at 373 K for 1 h and then the adsorption of nitrogen was started.

2.11 References

1. T. Hibino, M. Niwa, Y. Murakami, *Zeolites*, 1993, **13**, 518

2. P.J. Kunkeler, D. Moeskops, H. van Bekkum, *Microporous Materials*, 1997, **11**, 313

3. A. Corma, C. Rodellas, A. Chiorino and F. Boccuzzi, *Journal of Catalysis*, 1987, **88**, 374 & H. Wang and Y. Zou, *Catalysis Letters*, 2003, **86**, 163

4. C.R. Brundle, C.A. Evans Jr., S. Wilson (Eds.), *Encyclopedia of Materials Characterization*, Butterworth-Heinemann, Boston, 1992

5. J.C. Riviere, *Surface Analytical Techniques*, Oxford University Press, Oxford, 1990

6. F.W. Fifield, D. Kealy, *Principles and Practice of Analytical Chemistry, 3rd ed.*, Blackie, Glasgow, 1990

7. J. Dixon, *PhD Thesis*, Nottingham Trent University, June 2004

8. A.M. Camiloti, et al., *Applied Catalysis A*, 1999, **182**, 107

9. A. Cornu, R. Massot, *Compilation of Mass Spectral Data, vol. 1, 2nd ed.*, Heyden, London, 1975

10. G.S. Paine, *PhD Thesis*, Nottingham Trent University, October 2002

11. P. A. Webb and C. Orr, *Analytical methods in fine particle technology*, Micromeretics, 1997

12. F. Rouquerol, J. Rouquerol and K. Sing, *Adsorption by powders and porous solids*, Academic Press, San Diego, 1999

13. S. Brunauer, P.H. Emmet and E. Teller, *Journal of the American Chemical Society*, 1938, **60**, 1553

3 Characterisation and Catalysis

3.1 Introduction

This Chapter will investigate the properties and catalytic activities of zeolite BEA and a series of ion-exchanged BEA zeolites. Zeolite BEA was modified by ion exchange to produce Na-, Fe-, Co-, Ni- and Cu-exchanged BEA samples. These samples together with the parent material were characterised by x-ray powder diffraction, inductively coupled plasma spectroscopy, temperature programmed desorption and Fourier transform infrared spectroscopy. In addition, each sample was tested for its catalytic activity in the acylation of anisole with acetic anhydride.

Each of the different techniques provides different and complementary information about the structure or the chemistry of the samples under study. X-ray powder diffraction (XRD) is a technique mainly used to identify crystallographic phases in the material. In this Chapter XRD will be used to investigate the effect of the ion exchange on the framework structure of zeolite BEA. Inductively coupled plasma (ICP) spectroscopy will be used to measure the bulk silicon to aluminium ratio and the degree of exchange of selected metal-exchanged BEA zeolites. The temperature programmed desorption apparatus coupled with a mass spectrometer (TPD-MS) allows the determination of the amount of a particular fragment (atom, ion or molecule) desorbing from the zeolite as a function of temperature. This technique will be used to investigate the activation of a series of zeolite BEA samples and to measure acidity of H-BEA by its interaction with ammonia. Information on the type and quantity of hydroxyl groups present in a series of zeolite BEA samples has been gathered by Fourier transform infrared spectroscopy (FTIR). In addition, this technique is better suited to determine the acidity of zeolites by adsorption of ammonia, since it can discriminate between Brønsted and Lewis acid sites. The catalytic activity of H-BEA and ion-exchanged BEAs will be reported and correlated with the chemical/physical properties of each respective sample.

Any relevant limitation in any of the techniques mentioned will be discussed together with the experimental results.

56

3.2 XRD results

The XRD patterns of known structure types of zeolites and other microporous molecular sieves are compiled in the "Collection of Simulated XRD Patterns for Zeolites" [1] as well as in the online data basis of the IZA [2].

The framework structure of zeolite BEA is made up of an intergrowth of tetragonal polymorph A and monoclinic polymorph B. As a consequence, the XRD powder pattern of zeolite BEA is a combination of sharp and broad reflections [3].

The XRD powder pattern of zeolite H-BEA is presented in Figures 3.2.1. Figure 3.2.2 presents the patterns of the metal-exchanged zeolite BEA samples. Figure 3.2.3 shows all the XRD patterns, concentrating on the region between 22 and 23 degrees 2θ. Comparison between Figures 3.2.1 and 3.2.2 shows that the ion-exchange procedure does not introduce extra phases into the sample.
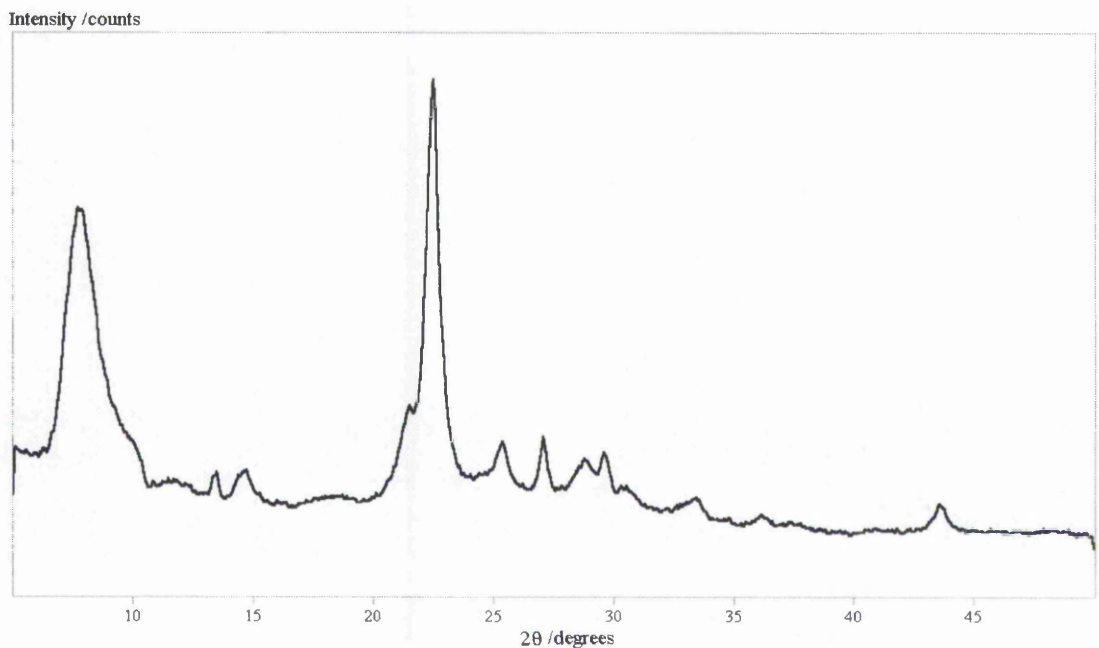
Figure 3.2.1 – XRD powder pattern of H-BEA
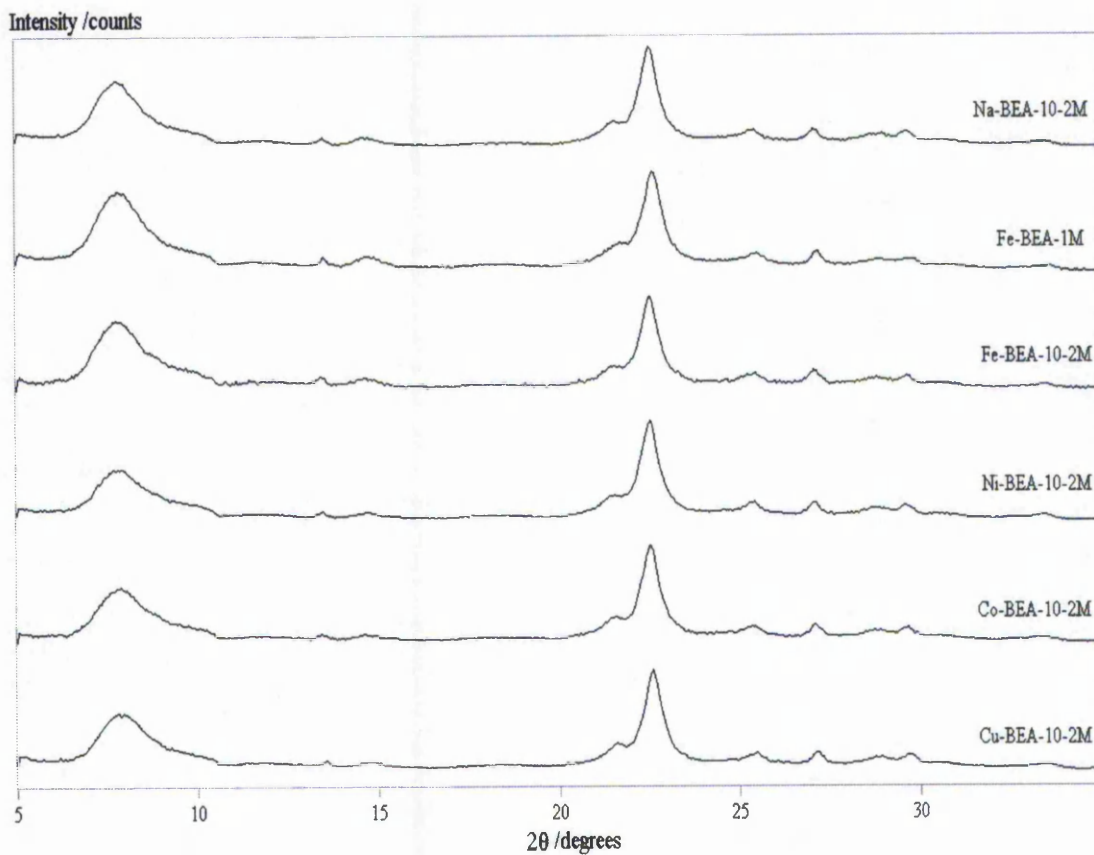
Figure 3.2.2 – XRD powder patterns of metal-exchanged BEA samples
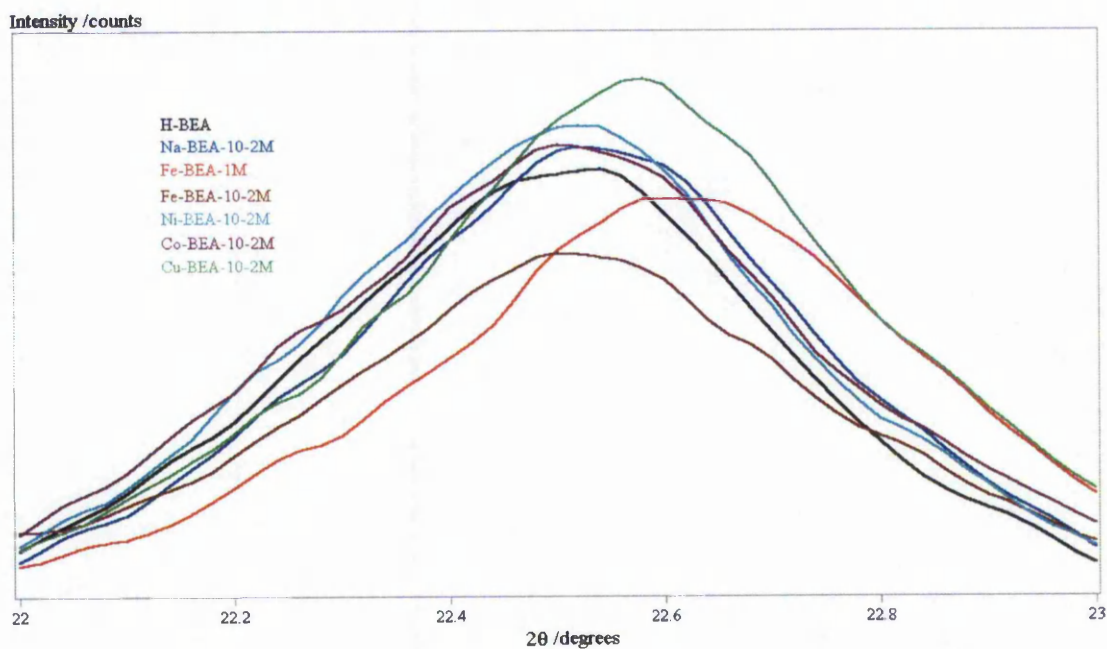
Figure 3.2.3 – XRD powder patterns of H-BEA and metal-exchanged BEA samples

All the samples in Figure 3.2.3 exhibit similar peak positions with the exception of Cu-BEA-10^{-2}M and Fe-BEA-1M, whose peaks are shifted to higher 2θ values.

XRD utilises the periodicity of the crystal lattice and, thus, can be used to deduce information about crystal structure, crystallite size, location and concentration of exchanged cations and crystallinity of a zeolite sample. However, it is not possible to obtain information on non-periodic properties of the crystals such as lattice defects, stacking faults and hydroxyl groups resulting from an incomplete condensation of Si-O-Si linkages during the synthesis. In addition, crystalline phases in concentrations below $\sim 5\%$ and amorphous phases cannot be detected [4].

3.3 ICP results

Inductively coupled plasma spectrometry is a useful method to quantify the elemental composition of a sample. It can be used to measure the bulk Si to Al ratio and to calculate the degree of exchange of a metal. The experiments were done once, and the results were collected as weight percentages of elements analysed, which can then be divided by the respective atomic masses to give atomic percentages. Thus, Si/Al ratio can be calculated. Then, after correction for ion charge, the degree of exchange for each metal counter-cation can be calculated as a percentage of the amount of aluminium in the sample. The results of these calculations are summarised in Table 3.3.1. The Si/Al ratio reported by the manufacturer is 12.5.

Table 3.3.1 – Metal content of selected zeolite BEA samples.

Sample	Si/Al	Degree of exchange /%
Na-BEA-10^{-2}M	12.5	30.4
Fe-BEA-1M	51.7	172
Fe-BEA-10^{-2}M	22.3	368
Co-BEA-10^{-2}M	12.5	44.0
Ni-BEA-10^{-2}M	12.5	25.8
Cu-BEA-10^{-2}M	12.5	32.9

The Si/Al ratio of all the 10^{-2}M-exchanged samples except Fe-BEA-10^{-2}M is constant and equal to the value of 12.5 quoted by the manufacturer. The amount of aluminium in the sample Fe-BEA-10^{-2}M decreases, and this dealumination process is even more extensive in the sample Fe-BEA-1M.

The degree of exchange of iron in Fe-BEA-10^{-2}M is ca 2.1 times the amount of iron in Fe-BEA-1M although the amount of iron in the exchange solution for Fe-BEA-1M was 100 times the amount for Fe-BEA-10^{-2}M.

3.4 TPD-MS Studies

3.4.1 Activation of H-BEA

The term "activation" refers to any thermal procedure that eliminates both water and ammonia that are present in the zeolite. Activation utilising thermal treatment can also be seen as the final step in producing the zeolite acid catalyst from the ammonium form. Heating decomposes the ammonium cation, releasing ammonia gas and leaving protons as the counter-cations [5].

The activation was performed as follows: NH_4-BEA was heated to 748 K at 5 K min^{-1} (Figure 3.4.1) and then left at 748 K for 1 hour. Subsequently the sample was cooled down to room temperature, and finally heated again up to 873 K (Figure 3.5.2). This final step was performed to study the effect of the activation process on H-BEA.
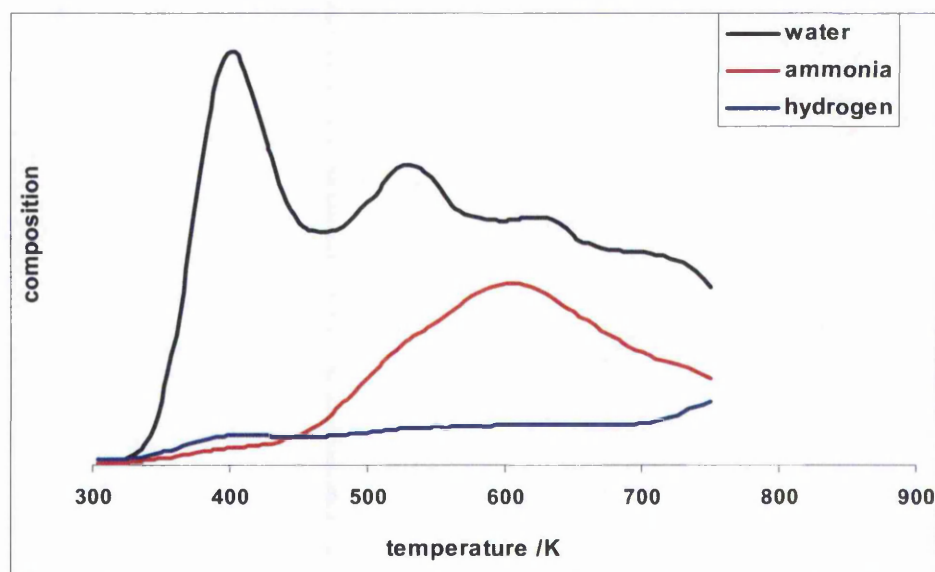
Figure 3.4.1 - H-BEA heated up to 748 K

In Figure 3.4.1, the desorption profile of water (m/e $= 18$) presents three peaks at 400, 530 and 630 K. Hydrogen (m/e $= 2$) desorbs with a peak at 410 K, and a very broad peak centred around 600 K. The desorption of ammonia (m/e $= 16$) is characterised by a single peak at 610 K. Other fragments desorbing in significant amounts are m/e $= 17$, which arises from both ammonia and water, and 28, 32 and 44, which arise respectively from CO (and N_2), O_2 and CO_2. No fragments with m/e higher than 44 have been detected indicating that no organic material is present in the starting zeolite BEA.
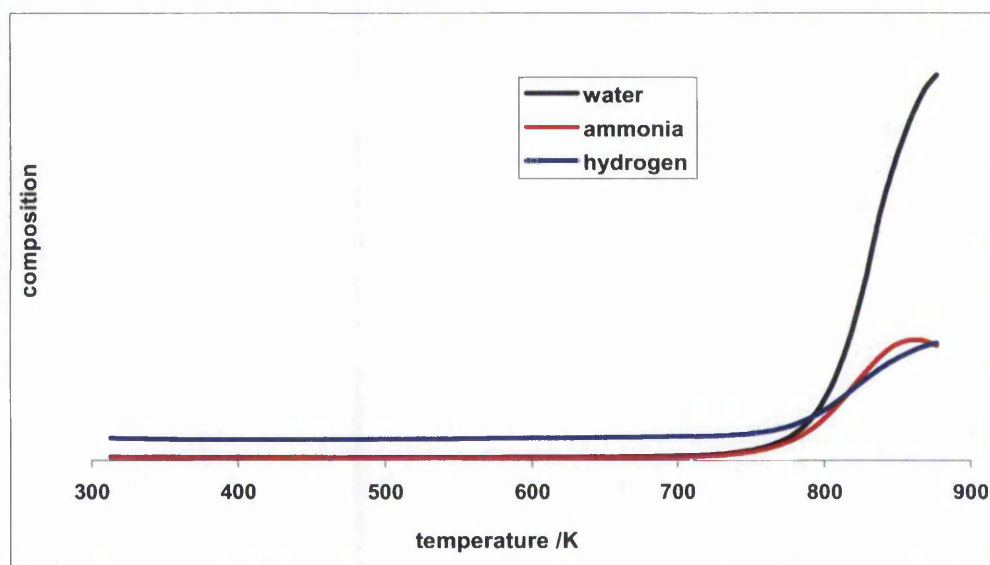
Figure 3.4.2 - H-BEA heated a second time to 873 K

During the second temperature ramp (Figure 3.4.2), there was no detectable desorption of either water, ammonia or hydrogen until about 750 K. This is an indication that the activation procedure is indeed successful in eliminating all the water and ammonia present in the starting zeolite BEA. After 750 K, both water, ammonia and hydrogen start to desorb rapidly from H-BEA. This sudden desorption of water is not due to any residual water left in the zeolite. Instead, it is probably a consequence of the dehydroxylation of the framework [6]. Dehydroxylation being a process that involves the elimination of water from two hydroxyl groups in the zeolite framework.

3.4.2 Activation of metal-exchanged BEA zeolites

The activation procedure was monitored in the TPD-MS for a series of metal-exchanged zeolite BEA samples. All the samples were heated in vacuum to 748 K at 5 K min^{-1} and then left at 748 K for 1 hour to complete the activation process. Figure 3.4.3 illustrates the desorption profiles of water (m/e $= 18$) and Figure 3.4.4 show the desorption profile of ammonia (m/e $= 16$).
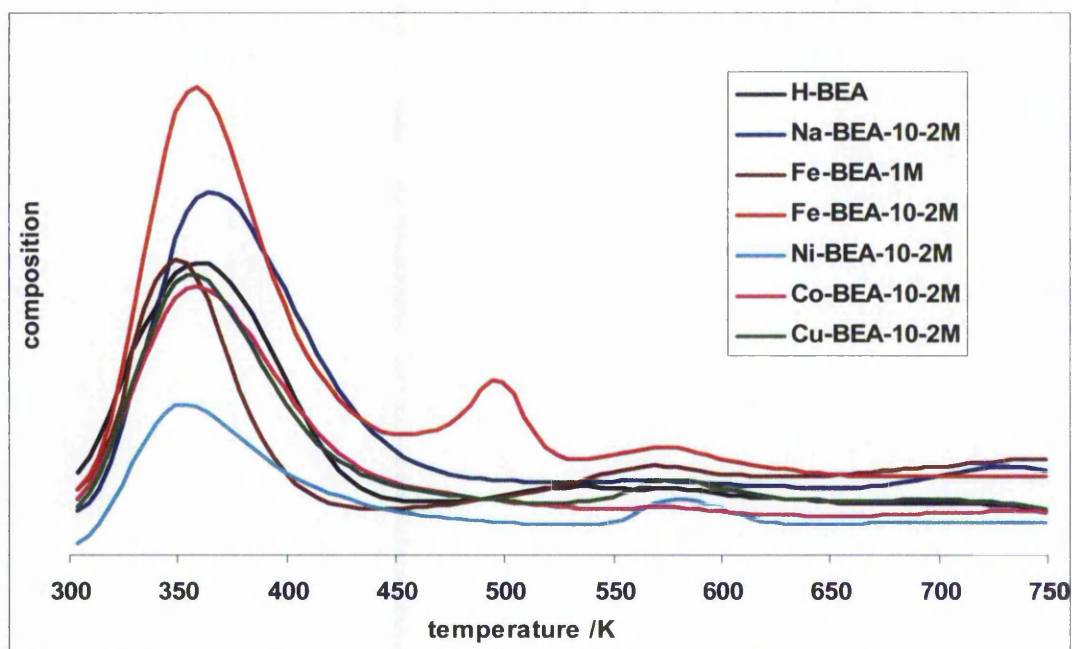
Figure 3.4.3 – Activation of zeolites: water desorption profiles

In all samples, except Fe-BEA-10^{-2}M, water desorbs in one major peak at ca 370 K and a much smaller one at ca 580 K. In the case of Fe-BEA-10^{-2}M, an additional peak of medium intensity is observed at ca 500 K.

Ammonia desorbs first in a small peak around 370 K, which is probably associated with the major water peak in Figure 3.4.3. The highest intensity peak for ammonia is located at at ca 600 K. The highest amount of ammonia desorbs from H-BEA, then Na-BEA-10^{-2}M and the other samples.
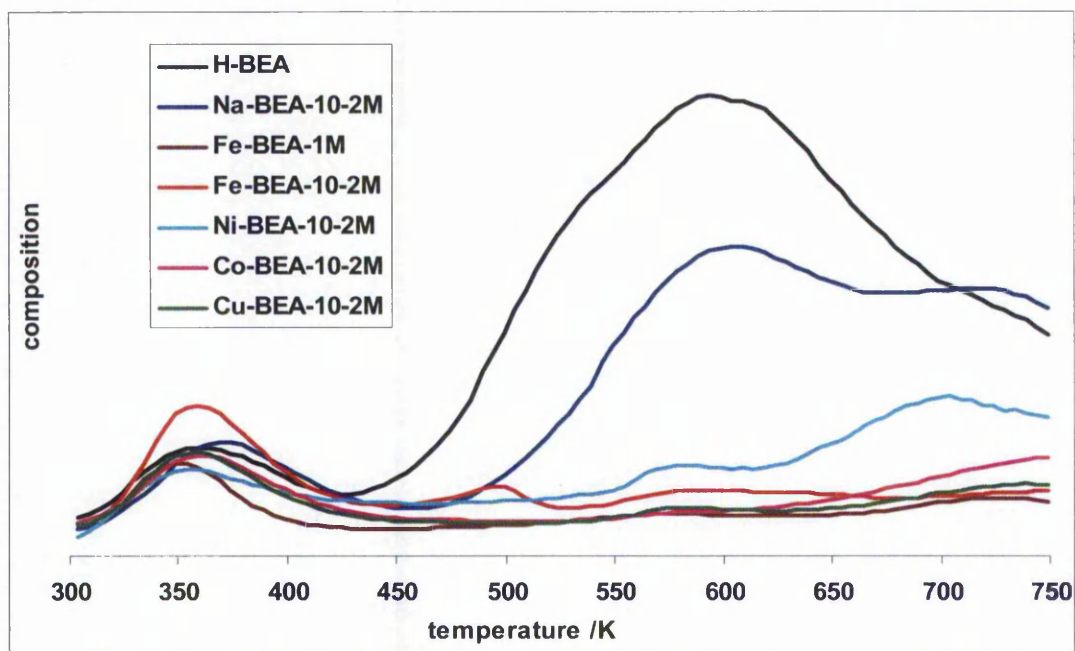
Figure 3.4.4 – Activation of zeolites: ammonia desorption profiles

The water and the ammonia-TPD curves were then integrated between 303 and 748 K and the results are summarised in Table 3.4.1.

Table 3.4.1 – Integrals calculated on normalised curves between 303 and 748 K

sample	Integral of water signal /arbitrary units	Integral of ammonia signal /arbitrary units
H-BEA	55.8	11.6
Na-BEA-10^{-2}M	71.0	8.25
Fe-BEA-1M	56.3	2.18
Fe-BEA-10^{-2}M	87.7	3.37
Co-BEA-10^{-2}M	49.0	4.16
Ni-BEA-10^{-2}M	30.3	2.80
Cu-BEA-10^{-2}M	53.1	2.57

The amount of ammonia desorbing can be taken as a measure of the degree of exchange attained in a particular sample. Since NH_4^+ is the counter-cation in the parent material, then the higher the degree of exchange of a particular sample the less the amount of ammonia that should be desorbing from it. In Figure 3.4.5 the degree of exchange of a series of BEA samples is plotted against the amount of ammonia desorbing during

activation. There is no clear correlation between the two quantities. However, there is some correlation between degree of exchange and ammonia in the case of the BEA samples with a Si/Al ratio of ca 12.5 (see Figure 3.4.6).
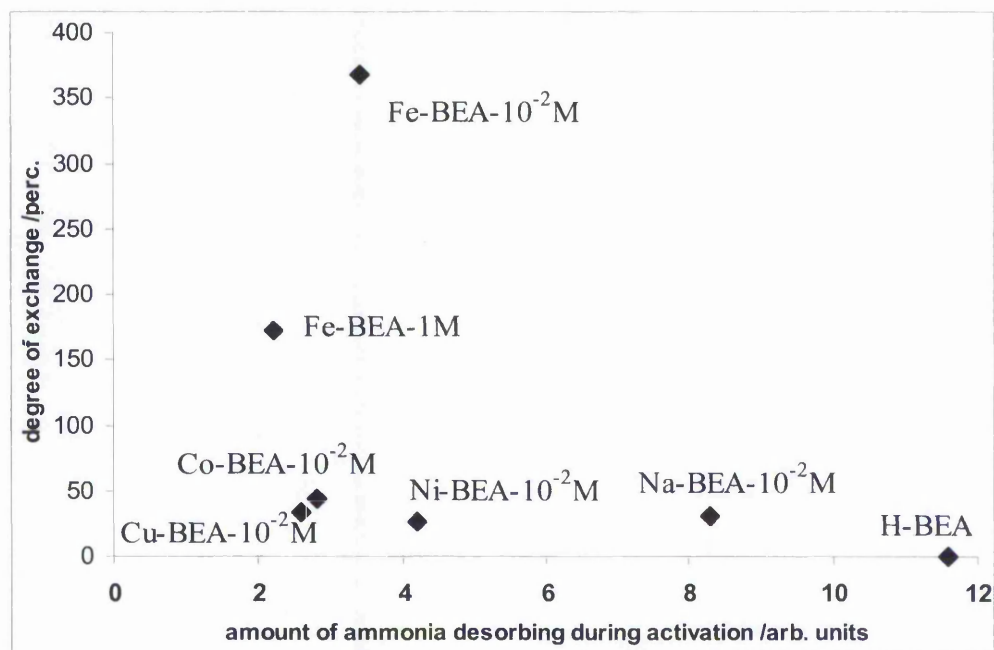
Figure 3.4.5 – Degree of exchange plotted versus amount of ammonia desorbing during activation.
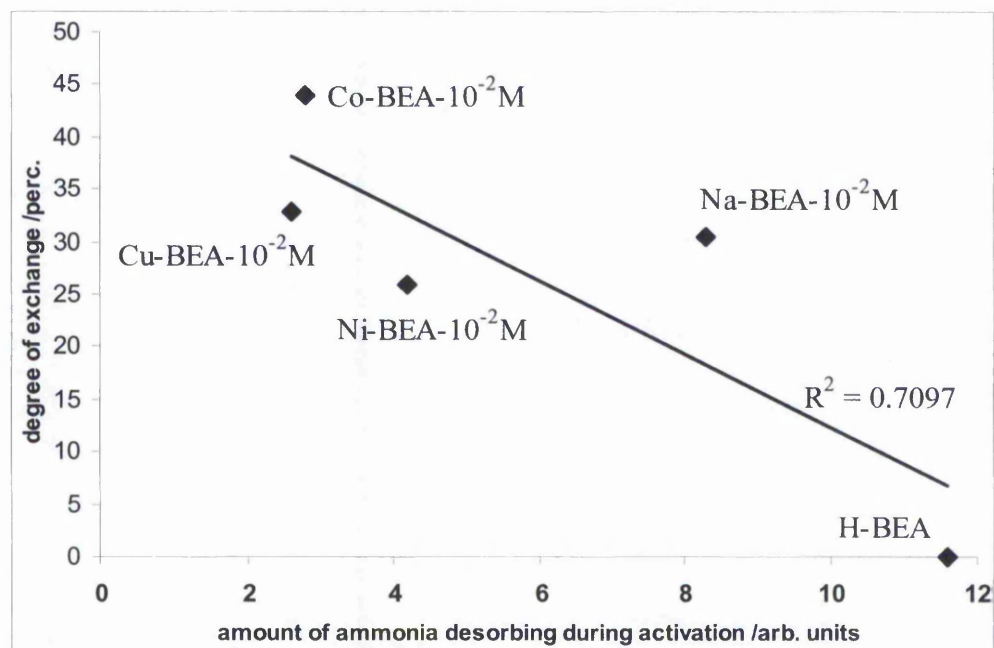
Figure 3.4.6 – Degree of exchange plotted versus amount of ammonia desorbing during activation for a series of selected BEA samples with Si/Al = 12.5.

3.4.3 Adsorption of ammonia on H-BEA

The adsorption of ammonia is a useful tool to study the acidity of materials such as zeolites. Ammonia is a hard base that adsorb on both Brønsted and Lewis acid sites and it is small in size so that it readily diffuses into the zeolite pores. In the TPD-MS experiment it is possible to study the amount of ammonia desorbing from the sample and the relative strength of interaction between ammonia and the substrate. The strength of interaction is proportional to the temperature for a particular adsorbate molecule and fixed heating rate. However it is not possible to distinguish between Lewis and Brønsted acid sites with this experimental apparatus and for some zeolites there is the possibility of diffusion limitation during the desorption of ammonia. This causes desorption at higher temperatures than those corresponding to the strength of interaction between the acid site and ammonia.

The desorption profiles in Figure 3.4.7 are for ammonia adsorbed at 333 and 363 K on H-BEA.
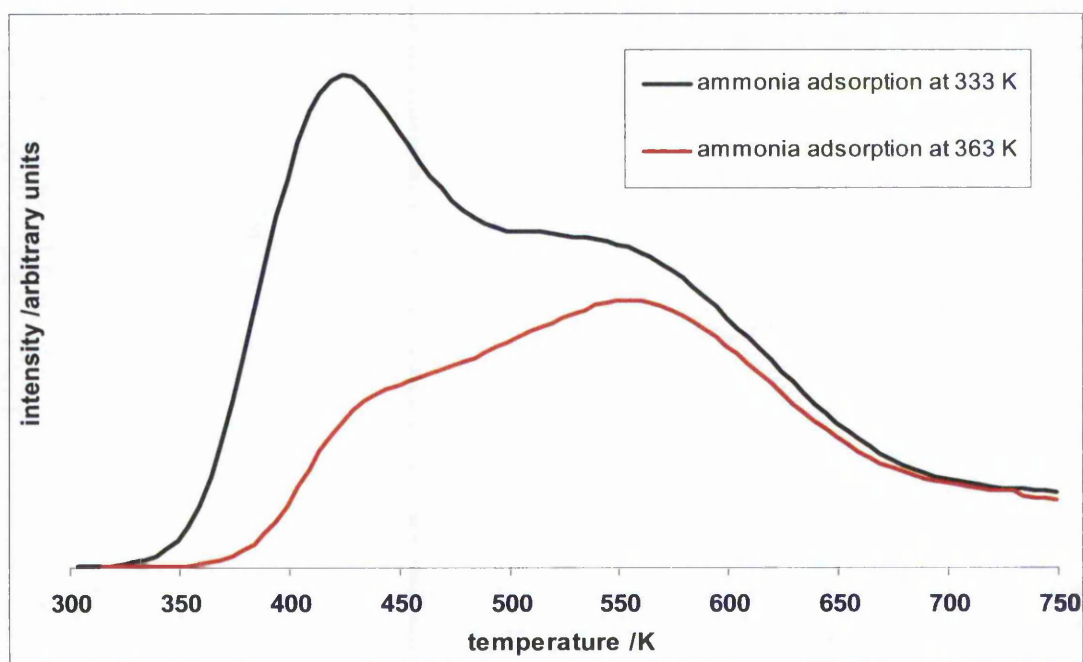
Figure 3.4.7 – Desorption profiles of ammonia after adsorption on H-BEA at different temperatures

In both cases there are two peaks at ca 425 K and at ca 550 K. The first peak is greatly reduced by increasing the adsorption temperature and it is attributed to weakly adsorbed ammonia. The second peak at ca 550 K is much less affected by an increase in adsorption temperature and it attributed to chemisorbed ammonia (i.e. ammonia interacting with either Brønsted or Lewis acid sites) [7]. The adsorption of ammonia was then carried out at 423 K and the desorption spectrum is shown in Figure 3.4.8. Only the peak at ca 550 K attributed to chemisorbed ammonia is present. There is no trace of any physisorbed ammonia when adsorption is carried out at 423 K.
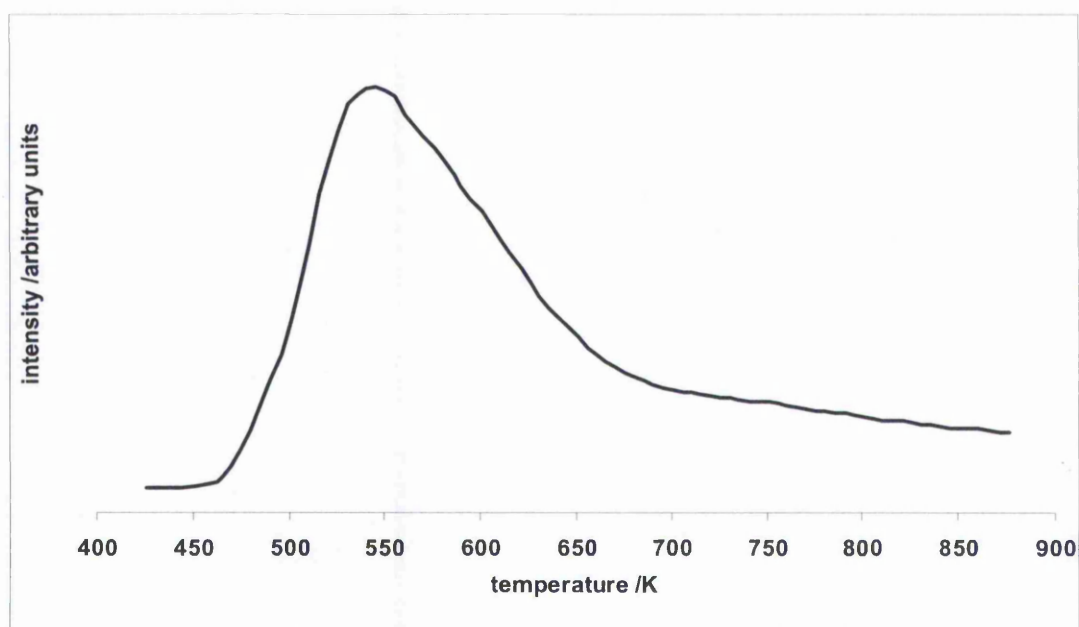
Figure 3.4.8 – Desorption profile of ammonia after adsorption on H-BEA at 423 K

3.5 FTIR results

3.5.1 The hydroxyl region of the infrared spectrum

The infrared spectrum of zeolites in the region between 3500 and 4000 cm^{-1} gives information on the type and quantity of the different hydroxyl species present in the sample. The non-acidic silanol groups (SiOH) [8] are present at the outer surface of the zeolite and at structural defects. Extraframework aluminium species with hydroxyl groups on their surface (AlOH) at 3663 cm^{-1} [9] may be present in the pores. This can be for one of two reasons: during the synthesis not all the aluminium atoms originally present in the synthesis gel are introduced into the zeolite lattice or, after dealumination, only some of the dealuminated aluminium atoms are completely extracted from the zeolite crystals [10]. The OH groups bridging between a silicon and an aluminium atom are acidic and are also referred to as Bronsted OH groups. Table 3.5.1 summarised the peaks present in the hydroxyl region of H-BEA and their identification according to Müller et al. [10]. In general, the weaker the O-H bond then the lower the stretching frequency and hence the higher the acid strength.

Table 3.5.1 – FTIR peaks in the hydroxyl region of the spectrum of activated H-BEA, identified after Müller et al. [10]

peak /cm^{-1}	Identification	Note
3780-3790	SiOH or AlOH	Absent
3733	SiOH	Highest intensity
3667	Extraframework AlOH	Absent
3613	Brønsted OH	Medium intensity

Figure 3.5.1 presents the spectra in the hydroxyl region of H-BEA and Na-BEA-10^{-2}M after activation, and Figures 3.5.2, 3.5.3 and 3.5.4 show the infrared spectra of transition metal exchanged BEA zeolites after activation. All the curves were normalised for varying sample thickness by integration of the bands in the region 1750-2095 cm^{-1}. These bands correspond to Si-O overtone vibrations in the zeolite lattice [11].
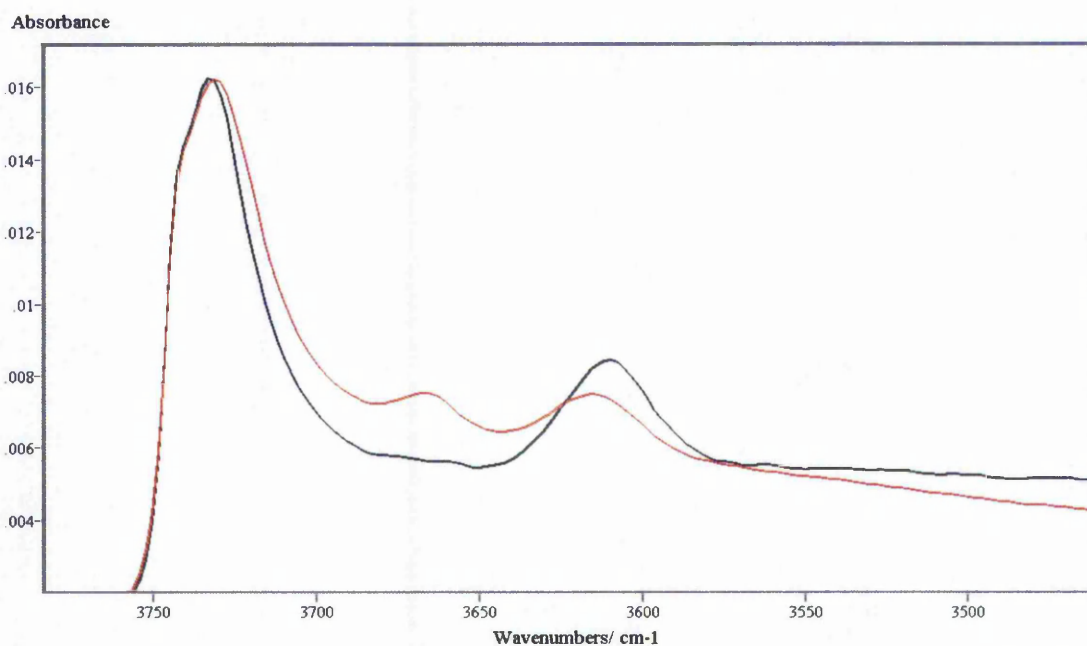
Figure 3.5.1 – FTIR spectra after activation of H-BEA (black line) and Na-BEA-10^{-2}M (red).
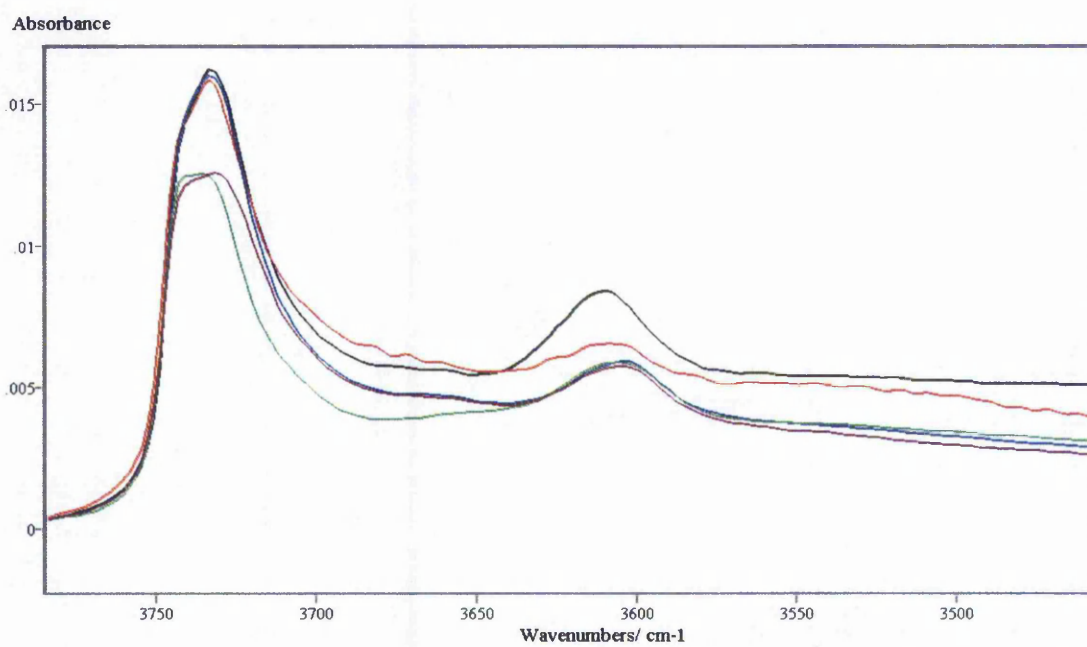
Figure 3.5.2 – FTIR spectra after activation of H-BEA (black line), Fe-BEA-10^{-2}M (red), Co-BEA-10^{-2}M (blue), Ni-BEA-10^{-2}M (purple) and Cu-BEA-10^{-2}M (green).
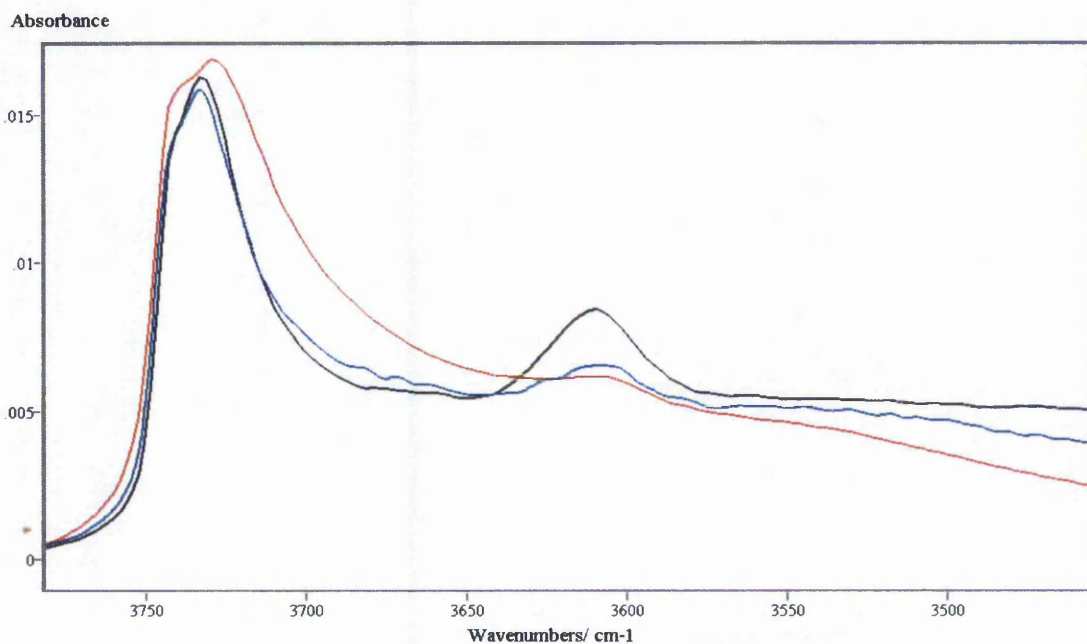
Figure 3.5.3 – FTIR spectra after activation of H-BEA (black line), Fe-BEA-1M (red) and Fe-BEA-10-2M (blue)
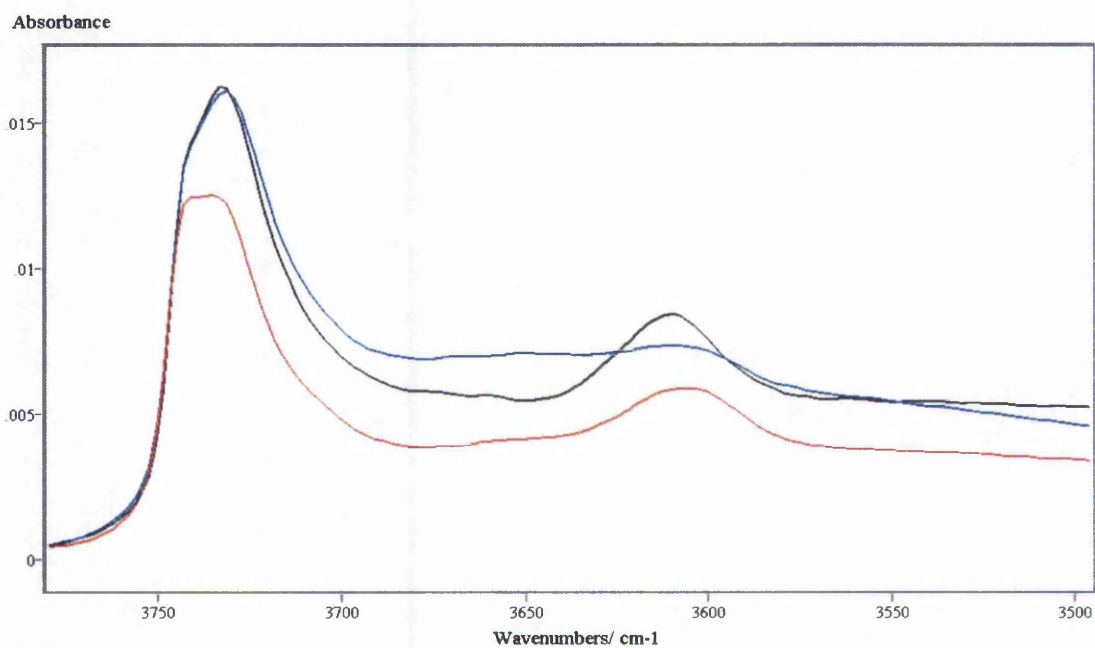
Figure 3.5.4 – FTIR spectra after activation of H-BEA (black line), Cu-BEA-10^{-2}M (red) and Cu-BEA-acetate-10^{-2}M (blue)

For all BEA samples (Figures 3.5.1-3.5.4) the SiOH peak is much larger than the Brønsted OH peak while this is not the case with other zeolites (e.g. ZSM-5 of similar Si/Al ratio) where the sizes of the two peaks are similar. There are two main reasons for this behaviour in BEA. The first one is that BEA is a material with many faults and faulting of the framework introduces SiOH groups. The second reason is because SiOH groups are mainly present in the external surface of zeolites and since BEA samples have generally much smaller particle sizes than other zeolites (e.g. ZSM-5) hence the higher number of SiOH groups in BEA.

The relative concentrations of SiOH groups, extralattice OH groups and Brønsted OH groups were calculated by integration of the peaks between 3750 and 3680 cm^{-1} for SiOH groups, between 3680 and 3645 cm^{-1} for extralattice OH groups, and between 3645 and 3570 cm^{-1} for Brønsted OH groups. These values were then normalised for varying sample thickness by integration of the lattice overtone vibration bands, and the results are summarised in Table 3.5.2. These results were shown to be reproducible.

Table 3.5.2 – Relative concentrations of hydroxyl groups of H-BEA and metal-exchanged BEA zeolites

Sample	Relative concentration /arbitrary units		
	SiOH groups (3750-3680 cm^{-1})	extralattice OH groups (3680-3645 cm^{-1})	Brønsted OH groups (3645-3570 cm^{-1})
H-BEA	35.2	0.176	9.36
Na-BEA-10^{-2}M	36.2	0.935	4.32
Fe-BEA-1M	38.1	0.000	1.52
Fe-BEA10^{-2}M	28.5	0.271	3.93
Co-BEA-10^{-2}M	34.5	0.120	5.35
Ni-BEA-10^{-2}M	27.2	0.077	5.50
Cu-BEA-10^{-2}M	24.0	0.070	6.39
Cu-BEA-acetate-10^{-2}M	34.5	0.132	3.26

3.5.2 Ammonia adsorption

The adsorption of ammonia was carried out in the FTIR apparatus to study the influence of the different exchanged metals on the Brønsted and Lewis acid sites of zeolite BEA. In contrast with the TPD-MS experiments, ammonia adsorbed on either Brønsted or Lewis acid sites gives rise to two different bands in the IR spectrum. One band at ca 1620 cm^{-1} is due to ammonia coordinated to aprotonic sites (i.e. Lewis acid sites) and the other band at ca 1450 cm^{-1} is due to protonated ammonia (i.e. adsorbed on a Brønsted acid site) [12, 13].

The adsorption of ammonia was carried out stepwise from 10^{-3} mbar to 2 mbar and at a temperature of 423 K, then the cell was evacuated at 423 K. The resulting spectra are presented in Figures 3.5.5 to 3.5.8. All the curves were normalised for varying sample thickness by integration of the bands in the region 1750-2095 cm^{-1}.
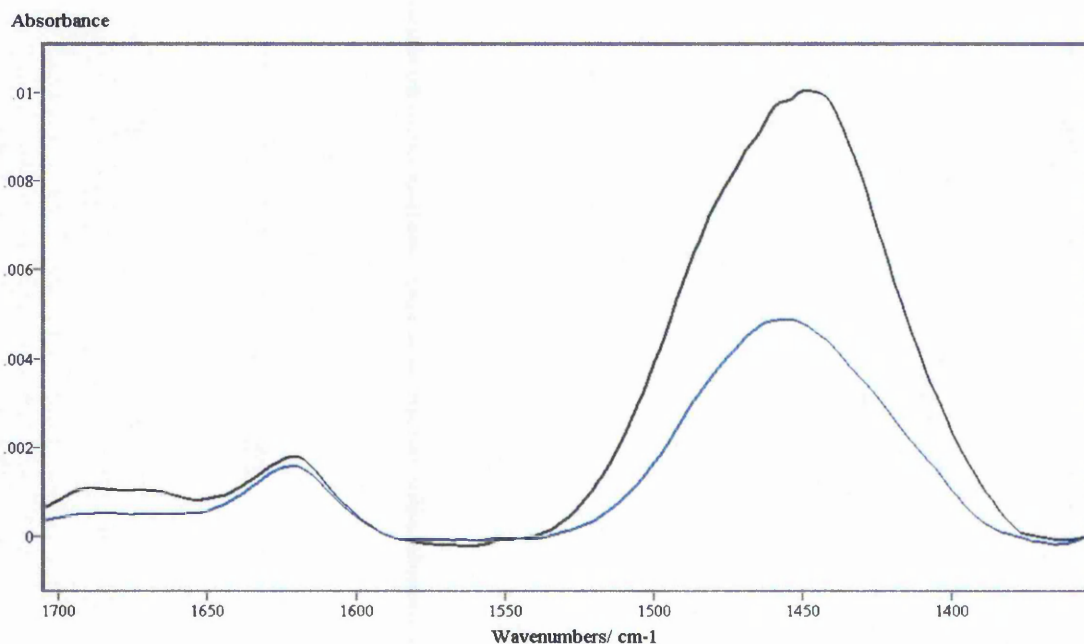
Figure 3.5.5 – FTIR spectra in the NH deformation region after adsorption of ammonia and subsequent evacuation of the cell. Samples are: H-BEA (black line) and Na-BEA-10^{-2}M (blue).
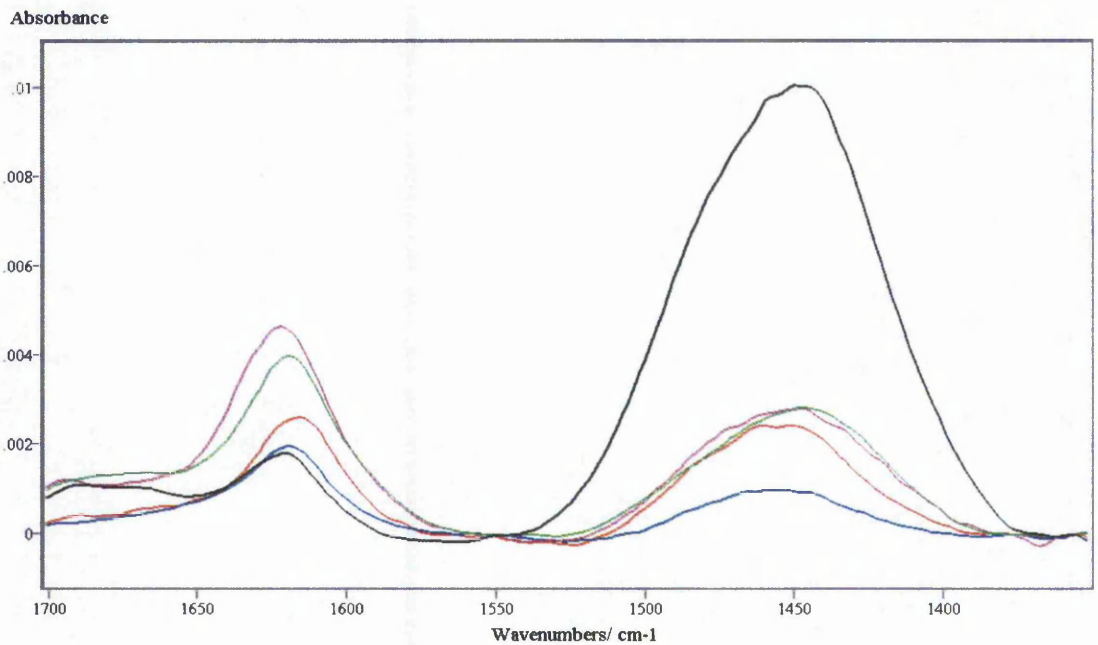
Figure 3.5.6 – FTIR spectra in the NH deformation region after adsorption of ammonia and subsequent evacuation of the cell. Samples are: H-BEA (black line), Fe-BEA-10^{-2}M (red), Co-BEA-10^{-2}M (blue), Ni-BEA-10^{-2}M (purple) and Cu-BEA-10^{-2}M (green).
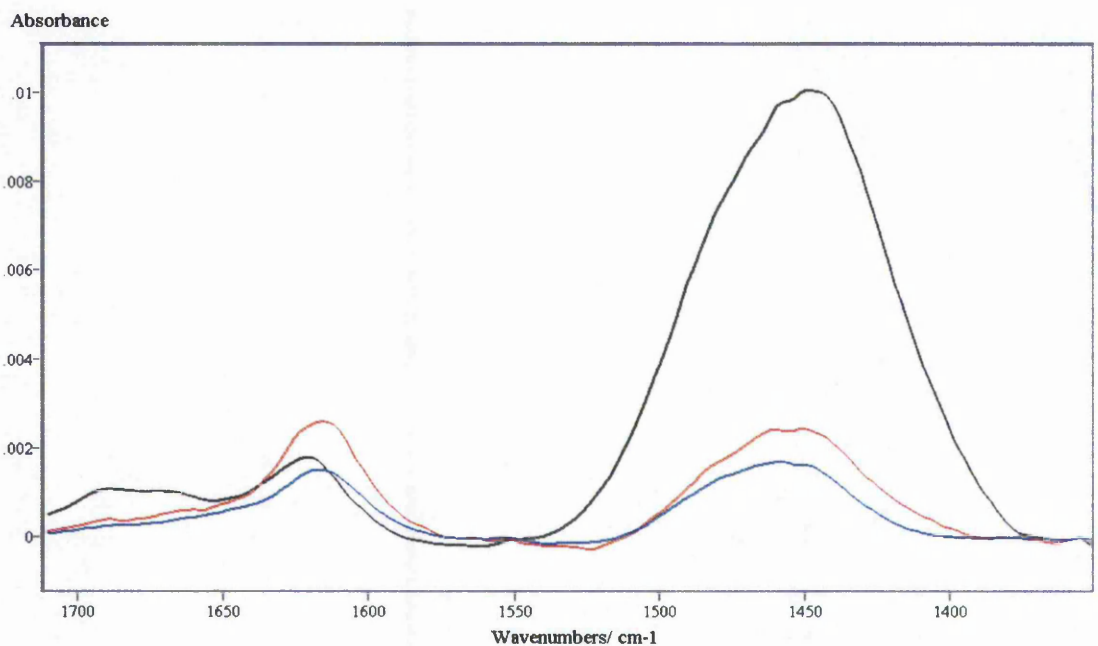
Figure 3.5.7 – FTIR spectra in the NH deformation region after adsorption of ammonia and subsequent evacuation of the cell. Samples are: H-BEA (black line), Fe-BEA-10^{-2}M (red) and Fe-BEA-1M (blue).
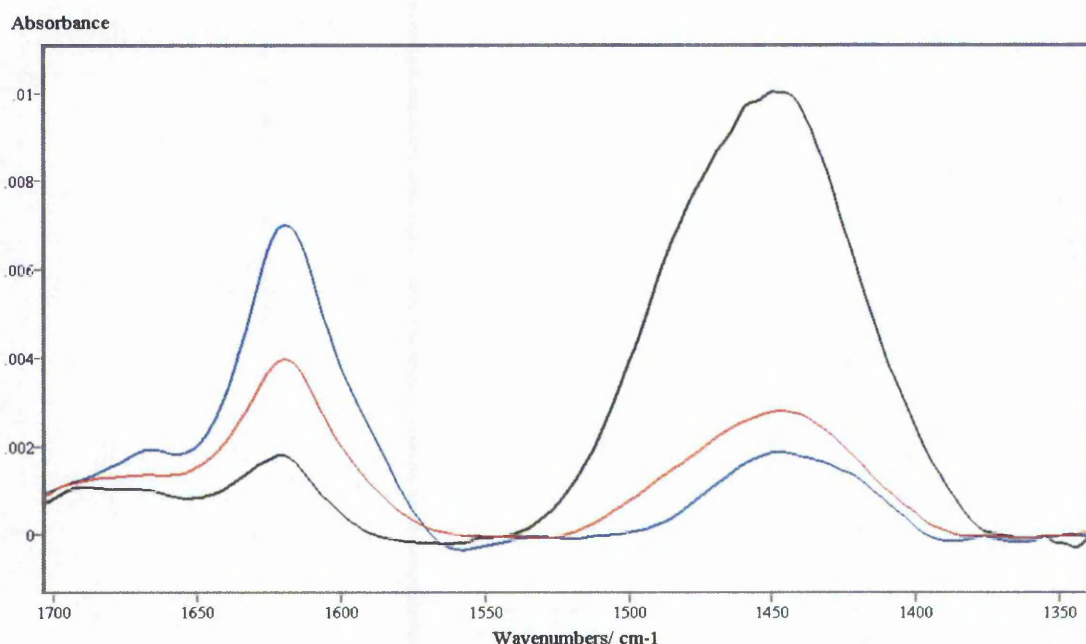
Figure 3.5.8 – FTIR spectra in the NH deformation region after adsorption of ammonia and subsequent evacuation of the cell. Samples are: H-BEA (black line), Cu-BEA-10^{-2}M (red) and Cu-BEA-acetate-10^{-2}M (blue)

The relative concentrations of Brønsted and Lewis acid sites were calculated by integration of the peaks between 1375 and 1545 cm^{-1} for Brønsted acid sites and between 1580 and 1655 cm^{-1} for Lewis acid sites. These values were then normalised for sample thickness as above, and the results are summarised in Table 3.5.2. These results were shown to be reproducible. Note that the values of the relative concentrations of Brønsted acid sites cannot be directly compared to the values of the relative concentrations of Lewis acid sites. To absolutely quantify the concentration of Brønsted and Lewis acid sites (e.g. mmol of ammonia per gram of zeolite) it is first necessary to know the molar extinction coefficient of the NH_4^+ and NH_3 bending modes (e.g. see reference 14).

Table 3.5.2 – The relative concentrations of Lewis and Brønsted acid sites for H-BEA and metal-exchanged BEA zeolites

Sample	Relative concentration /arbitrary units	
	Lewis acid sites (1580-1655 cm^{-1})	Brønsted acid sites (1375-1545 cm^{-1})
H-BEA	4.18	80.3
Na-BEA-10^{-2}M	4.07	38.2
Fe-BEA-1M	4.12	10.9
Fe-BEA-10^{-2}M	7.35	16.8
Co-BEA-10^{-2}M	4.95	6.40
Ni-BEA-10^{-2}M	12.8	21.6
Cu-BEA-10^{-2}M	10.2	20.5
Cu-BEA-acetate-10^{-2}M	19.5	12.8

3.6 Catalytic Results

The acylation reaction was carried out to evaluate the catalytic activity of H-BEA and ion-exchanged BEA zeolites. All samples were subject to the same reaction conditions as described in Chapter 2, i.e. 0.2 moles of acetic anhydride 0.4 moles of anisole and 300 mg of catalyst, with a reaction temperature of 333 K. The use of an excess of anisole has been shown to reduce catalyst deactivation [15]. Figure 3.6.1 illustrates the percentage yield of product (p-MAP) versus reaction time for H-BEA and a series of ion-exchanged BEA zeolites which have been prepared with a 0.01 molar solution of the corresponding metal nitrate. Figure 3.6.2 shows the catalytic results of Fe-BEA-1M and Cu-BEA-acetate-10^{-2}M compared with H-BEA, Fe-BEA-10^{-2}M and Cu-BEA-10^{-2}M. In all the catalytic experiments the selectivity to the *para*-product was more that 99%. Additionally, a blank experiment was carried out at the same conditions but with no catalyst, and it showed no formation of p-methoxyacetophenone. The initial rates of reaction were calculated by taking the percentage yield of p-MAP after 5 minutes and dividing this value by the time in seconds, the results were shown to be reproducible and are summarised in Table 3.6.1.
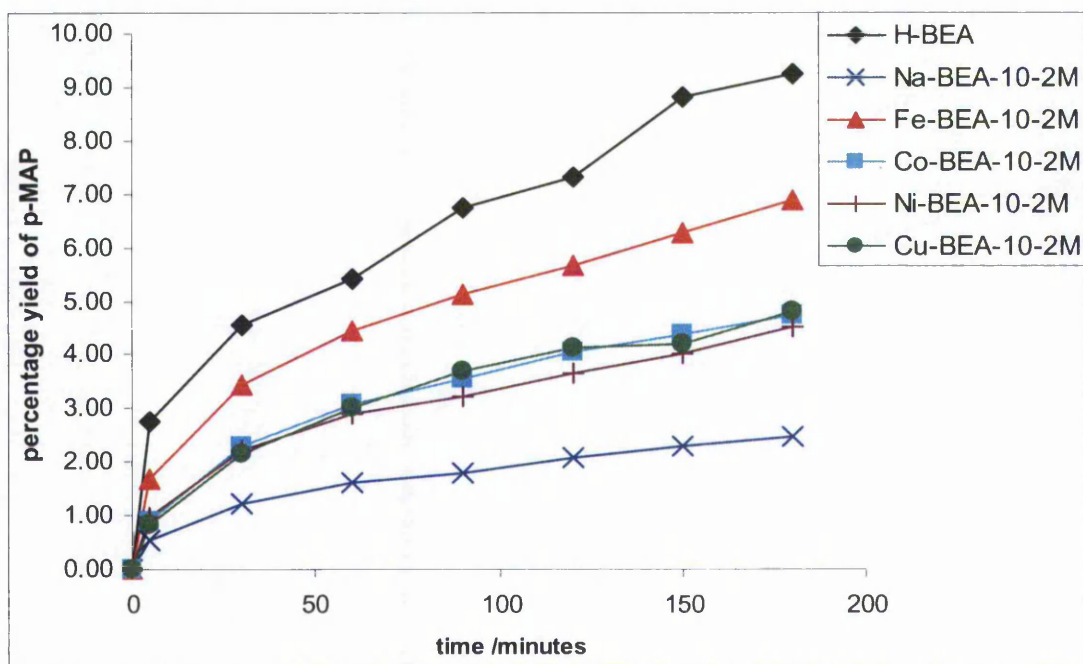
Figure 3.6.1 – Catalytic data for 10^{-2}M exchanged BEA samples
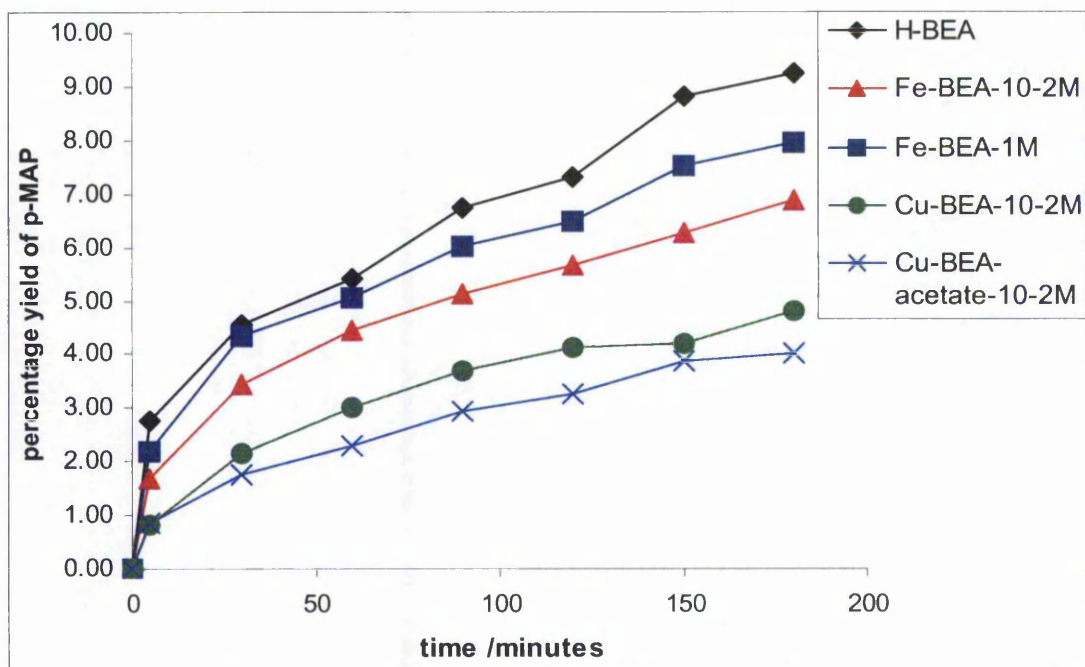
Figure 3.6.2 – Catalytic data

Table 3.6.1 - Initial rates of reaction

Sample	%yield p-map after 5 min	Initial rate /%yield p-map s^{-1}
H-BEA	2.74	9.15E-03
Na-BEA-10^{-2}M	0.52	1.74E-03
Fe-BEA-10^{-2}M	1.68	5.59E-03
Co-BEA-10^{-2}M	0.95	3.17E-03
Ni-BEA-10^{-2}M	0.97	3.24E-03
Cu-BEA-10^{-2}M	0.83	2.76E-03
Fe-BEA-1M	2.20	7.33E-03
Cu-BEA-acetate-10^{-2}M	0.86	2.88E-03

3.7 Relationships between catalytic activity and chemical properties

The graph in Figure 3.7.1 illustrates the relationship between the initial rates of reaction and the Brønsted acidity. Figure 3.7.2 is a plot of the initial rates of reaction versus the relative concentrations of Lewis acid sites.
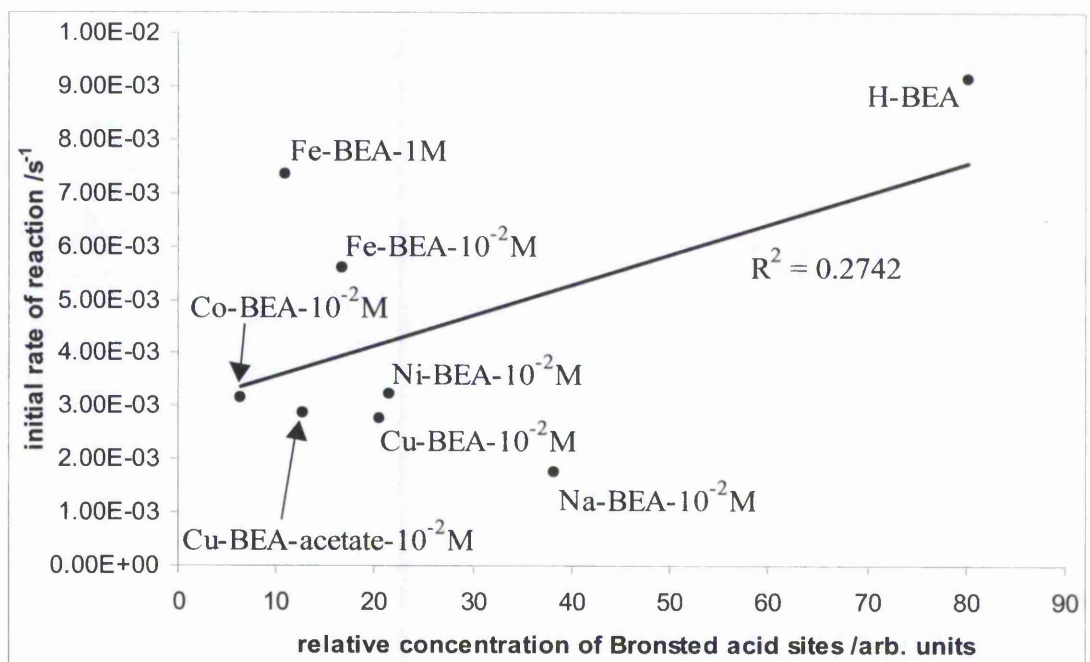
Figure 3.7.1 – Initial rates of reaction versus relative concentrations of Brønsted acid sites
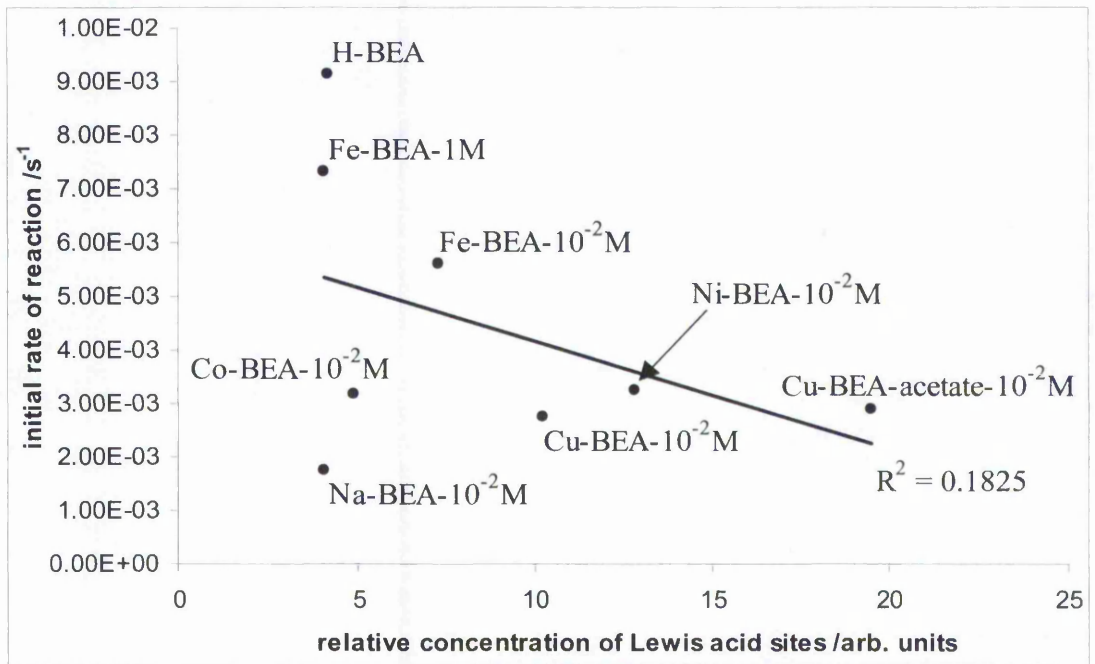
Figure 3.7.2 – Initial rates of reaction versus relative concentrations of Lewis acid sites

3.8 Conclusions

The results of the XRD experiments show that the ion-exchange procedure does not introduce any detectable extra phases. Enlargement of the portion of the spectrum between 22 and 23 degrees 2θ (see Figure 3.2.3) shows that all samples exhibit a similar peak position with the exception of Cu-BEA-10^{-2}M and Fe-BEA-1M. These peaks are shifted to higher 2θ values. This shifting of peaks in the XRD spectrum has been associated with changes in the amount of aluminium in the zeolite. Camblor et al. [16] reported an increased peak broadening and a shift to lower 2θ values as the aluminium content of their nanocrystalline BEA increased. These authors suggested that this phenomenon could be taken as an indication of the isomorphous substitution of Si by Al in the framework. A study by Trombetta et al. [17] found a similar phenomenon. Hence, a shift to higher 2θ values would indicate dealumination of the sample. Thus, from the XRD data alone, it can be concluded that the ion-exchange procedure does not modify the framework structure of zeolite BEA and does not produce dealumination of the zeolite framework except in the case of Cu-BEA-10^{-2}M and Fe-BEA-1M.

The ICP results show that the Si to Al ratio does not change after ion-exchange procedure for all samples except the iron-exchanged BEA samples. The Si/Al ratio for Fe-BEA-10^{-2}M is 22.3 and dealumination is even more extensive on Fe-BEA-1M with an Si/Al equal to 51.7. The results show that ion-exchange is indeed successful in all cases apart from the iron-exchanged ones. The highest degree of exchange is for Fe-BEA-10^{-2}M at 368% followed by Fe-BEA-1M at 172%. These results seem in contrast with the fact that the exchange solution in the case of Fe-BEA-1M was a hundred times more concentrated than in the case of Fe-BEA-10^{-2}M. The high degree of exchange suggests that iron may be present in the form of iron oxide species as well as counter-cations in the Fe-exchanged BEA zeolites. Joyner et al. [18] suggested that large iron oxide species can form in Fe-ZSM-5 zeolites and exhibit significant lower turnover numbers for the selective catalytic reduction of NO_x compared to iron nanoclusters and more isolated iron cations. However, the XRD powder patterns of Fe-BEA-10^{-2}M and Fe-BEA-1M do not show any peaks due to iron oxide species. In fact, they do not show any significant difference when compared with the parent material H-BEA. This would suggest that extended iron oxide species were not formed during the exchange process.

Analysis in the TPD apparatus of the activation procedure of H-BEA showed that after treatment at 748 K for 1 hour there was no detectable desorption of either water or

ammonia from the zeolite during a second temperature ramp up to 750 K. After this temperature the sudden desorption of water has been assigned to dehydroxylation of the zeolite framework [6]. Liu et al. [19] found that zeolite BEA is thermally stable up to 1033 K, after which temperature major destruction of the crystalline framework occurs. However, minor destruction of the framework was found for samples treated at a temperature as low as 673 K. Additionally, they report a $SiO_2/Al_2O_3 = 37.9$ (i.e.: Si/Al = 18.9), which is higher than 12.5 for the samples under current study. Bolton et al. [20] studied the thermal decomposition of ammonium-exchanged zeolite Y and found that the temperature required to dehydroxylate the zeolite increases with increasing SiO_2/Al_2O_3 molar ratio. In conclusion, the experimental results together with data from the literature corroborate the use of an activation temperature of 748 K for zeolite BEA. This activation procedure seems to remove all the ammonia and water present in the starting material avoiding at the same time any significant dehydroxylation of the framework.

The activation procedure was then monitored in the TPD-MS for a series of ion-exchanged BEA samples. Both the desorption profiles of water and ammonia resemble the ones in the case of H-BEA. A plot of the degree of exchange versus the amount of ammonia desorbing during activation for each sample does not show any linear correlation. However, the same graph with only samples with Si/Al equal to 12.5 shows some degree of correlation. Thus, in this case the amount of ammonia desorbing can be taken as an approximate indication of the degree of exchange attained in a particular sample. Since NH_4^+ is the counter-cation in the parent material, then the higher the degree of exchange of a particular sample the less the amount of ammonia that should be desorbing from it.

The adsorption of ammonia at different temperatures on H-BEA has then been monitored by TPD-MS. It shows that the adsorption must be performed at 423 K in order to avoid any physisorbed ammonia, in agreement with the findings of Forni et al. [7]. In the literature there has been some confusion over the experimental conditions for the determination of acidity of zeolites by temperature programmed desorption of different probe molecules. For example, Borade et al. [21] determined the acidity of zeolite BEA using the temperature programmed desorption of pyridine, with adsorption temperatures higher than 673 K which is too high for the determination of some Bronsted sites in zeolites [6]. Hedge et al. [22] established the strength of acid sites in zeolite BEA using the temperature programmed desorption of ammonia starting at room

temperature, which is too low for this adsorbate and results in large quantities of physisorbed molecules [7].

Analysis of the hydroxyl region of the infrared spectrum for H-BEA and ion-exchanged BEA zeolites after activation shows that the ion-exchange procedure reduces the amount of Brønsted OH groups. This indicates that the ion-exchange procedure was successful in exchanging cations for acidic protons in zeolite BEA. The amount of extraframework aluminium is higher for Na-BEA-10^{-2}M than H-BEA, for all other samples is either unchanged or has diminished. Studies have been made to investigate the nature of extraframework aluminium [23, 24]. In particular, Loefler et al. [25] proposed that the band at ca 3660 cm^{-1} corresponds to protons compensating negative charges of AlO$_4$ tetrahedra where the aluminium atom is connected with the zeolite framework only by one or two remaining chemical bonds.

The adsorption of ammonia on a series of BEA samples has been monitored by FTIR and shows that zeolite BEA possesses both Brønsted and Lewis acid sites. Lewis acidity in zeolite BEA has been associated with its high number of defect sites. These are generated when a tertiary building unit is rotated 90° around the c-direction with respect to TBUs in the same layer. The rotated TBU cannot connect properly with adjacent layers, resulting in partially coordinated T atoms which can create potential Lewis acid sites [26]. Kuehl et al. [27] observed octahedral aluminium species connected to the framework structure of zeolite BEA, and that these aluminium sites exhibit characteristics of Lewis acid sites. They suggested that such aluminium species are created by partial hydrolysis of framework Si-O-Al bonds. Similarly, Jia et al. [28] and Beck et al. [29] suggest that framework aluminium atoms in a non-tetrahedral coordination may exhibit Lewis acidic properties.

Upon sodium exchange the amount of Brønsted acid sites diminishes while the number of Lewis acid sites is unchanged. The copper-exchanged BEA samples exhibit much lower Brønsted acidity than H-BEA and a higher Lewis acidity. By comparing Cu-BEA-10^{-2}M and Cu-BEA-acetate-10^{-2}M it can be seen that to lower Brønsted acidity (and a lower number of Brønsted OH groups) corresponds higher Lewis acidity. This can be interpreted as the exchanged copper in zeolite BEA acting as a Lewis acid, as suggested in the case of ZSM-5 by Connerton et al. [30]. Interestingly, Dedecek et al. [31] studied the catalytic activity of Cu-BEA in NO decomposition, and concluded that Brønsted and Lewis acid sites do not contribute themselves to the catalytic activity of Cu-BEA zeolites in NO decomposition.

The adsorption of ammonia on Ni-BEA-10^{-2}M shows a decrease in Brønsted acidity and an increase in Lewis acidity with respect to H-BEA. In the case of Co-BEA-10^{-2}M, to a marked decrease in Brønsted acidity corresponds only a small increase in Lewis acidity. Fe-BEA-10^{-2}M sees a decrease in Brønsted acidity and an increase in Lewis acidity. In the case of Fe-BEA-1M the Brønsted acidity decreases while the Lewis acidity is unaffected.

The catalytic results show that H-BEA is the most active catalyst in the acylation of anisole with acetic anhydride. All the ion-exchanged samples exhibit some degree of catalytic activity. Fe-BEA-1M is the most active and Na-BEA-10^{-2}M is the least active. There is increasing interest in the application of transition metals as components of bifunctional catalysts in a series of reactions. For example, De Lucas et al. [32] studied the influence of the ion-exchanged metal (Cu, Co, Ni and Mn) on the selective catalytic reduction of NO_X over mordenite and ZSM-5. The most promising applications of Ni-exchanged zeolites are processes such as hydrogenation/dehydrogenation, hydrogenolysis [33], hydrodewaxing [34], hydrocracking and hydroisomerization [35, 36]. Tang et al. [37] found and that Co-exchanged faujasites could efficiently catalyse the epoxidation of styrene with O_2.

There is very low correlation between the initial rates of reaction and the relative concentrations of Brønsted acid sites, and an even lower correlation between initial rates and Lewis acidity. In the early days of research on catalysis by zeolites, Boreskova et al. [38] assumed that the acylation reaction took place on Lewis sites. Subsequently, Corma et al. [39] in 1989 suggested the intervention of Brønsted acidity on the basis of the activity of partially sodium-exchanged HY zeolites. Additional studies confirmed a Brønsted catalysed process in the acylation of aromatics [40 – 43]. However, Isaev et al. [44] studied the acylation of thiophene by butyryl chloride over ZSM-5, mordenite and Y, and determined the numbers of Brønsted and Lewis acid sites by FTIR of chemisorbed ammonia. They concluded that there is a correlation between the initial rates of reaction and the number of Lewis acid sites while there is no correlation between the initial rates and the number of Brønsted acid sites.

The experimental results presented in this Chapter provide some evidence on the existence of a Brønsted acid catalysed process in the acylation of aromatics over zeolites. Na-exchanged BEA has been shown to have lower catalytic activity and lower concentration of Brønsted acid sites than H-BEA while the two materials have about the same concentration of Lewis acid sites. This result would be an indication that the acylation of anisole with BEA catalysts is indeed a Brønsted catalysed process, as

already suggested in the literature. However, when taking into account the concentration of acid sites and catalytic activity of all the ion-exchanged samples, there is a very low degree of correlation between catalytic activity and Brønsted acidity. Also, there is even less correlation between Lewis acidity and catalytic activity. Thus, the results suggest that Brønsted acidity is more likely than Lewis acidity to play a role in the acylation reaction catalysed by BEA at least for some samples (i.e. H-BEA and Na-BEA-10^{-2}M). The studies presented in the next Chapter will investigate the catalytic mechanism from a different perspective, namely the interaction between acylating reagents or product and zeolite BEA.

3.9 References

1. M.M.J. Treacy, J.B. Higgins, *Collection of Simulated XRD Powder Patterns for Zeolites, 4th Ed.*, Elsevier, Amsterdam, 2001

2. http://www.iza-structure.org/databases/

3. J.M. Newsam, et al., *Proceedings of the Royal Society London A*, 1988, **420**, 375

4. J.W. Niemantsverdriet, *Spectroscopy in Catalysis*, Wiley-VCH, Weinheim, 1995

5. R. Szostak, *Molecular Sieves (Principles of Synthesis and Identification)*, Van Nostrand Reinhold, New York, 1989, p. 28

6. A.M. Camiloti, et al., *Applied Catalysis A - General*, 1999, **182**, 107

7. L. Forni, E. Magni, *Journal of Catalysis*, 1988, **112**, 444

8. I. Kiricsi, et al., *Journal of Physical Chemistry*, 1994, **98**, 4627

9. E. Bourgeat-Lami, et al., *Catalysis Letters*, 1990, **5**, 265

10. M. Müller, G. Harvey, R. Prins, *Microporous and Mesoporous Materials*, 2000, **34**, 281

11. H. van Bekkum, et al., *Introduction to Zeolite Science and Practice, 2nd Ed.*, Elsevier, Amsterdam, 2001

12. W.M. Zhang, et al., *Journal of Physical Chemistry B*, 2000, **104**, 4122

13. H. Knozinger, *Elementary Reaction Steps in Heterogeneous Catalysis*, R.W. Joyner, R.A. van Santen, Eds., Kluwer Academic Publishers, Dordrecht, 1993, p. 267

14. F. Yin, et al., *Journal of Physical Chemistry B*, 1997, **101**, 1824

15. D. Rohan, et al., *Journal of Catalysis*, 1998, **177**, 296

16. M.A. Camblor, A. Corma, S. Valencia, *Microporous and Mesoporous Materials*, 1998, **25**, 59

17. M. Trombetta, et al., *Physical Chemistry Chemical Physics*, 2000, **2**, 3529

18. R.W. Joyner, M. Stockenhuber, *Journal of Physical Chemistry B*, 1999, **103**, 5963

19. S.B. Liu, et al., *Journal of Catalysis*, 1991, **132**, 432

20. A.P. Bolton, M.A. Lanewala, *Journal of Catalysis*, 1970, **18**, 154

21. R.B. Borade, A. Clearfield, *Journal of Physical Chemistry*, 1992, **96**, 6729

22. S.G. Hedge, et al., *Zeolites*, 1989, **9**, 231

23. M. Anderson, J. Klinowski, *Journal of the Chemical Society Faraday Transactions I*, 1986, **82**, 3569

24. Q.L. Wang, *Journal of Catalysis*, 1991, **130**, 459

25. E. Loefler, et al., *Zeolites*, 1990, **10**, 266

26. J.C. Jansen, et al., *Catalysis Today*, 1997, **38**, 205

27. G.H. Kuehl, H.K.C. Timken, *Microporous and Mesoporous Materials*, 2000, **35-36**, 521

28. C. Jia, P. Massiani, D. Barthomeuf, *Journal of the Chemical Society Faraday Transactions I*, 1993, **89**, 3659

29. L. Beck, J.F. Haw, *Journal of Physical Chemistry*, 1995, **99**, 1076

30. J. Connerton, R.W. Joyner, M.B. Padley, *Journal of the Chemical Society Faraday Transactions*, 1995, **91**, 1841

31. J. Dedecek, et al., *Journal of Catalysis*, 2001, **200**, 160

32. A. De Lucas, et al., *Journal of Molecular Catalysis A*, 2005, **225**, 47

33. T. Inui, et al., *Industrial & Engineering Chemistry Research*, 1987, **26**, 647

34. J. Scherzer, A.J. Gruia, *Hydrocracking Science and Technology*, Marcel Dekker, New York, 1996, p. 223

35. A. Lugstein, A. Jentys, H. Vinek, *Journal of the Chemical Society Faraday Transactions*, 1997, **93**, 1837

36. A. Lugstein, A. Jentys, H. Vinek, *Applied Catalysis A*, 1999, **176**, 119

37. Q. Tang, et al., *Chemical Communications*, 2004, **4**, 440

38. E.G. Boreskova, V.I. Lugin, K.V. Topchieva, *Kinetics and Catalysis*, 1964, **5**, 991

39. A. Corma, et al., *Applied Catalysis*, 1989, **49**, 109

40. E.G. Derouane, et al., *Journal of Catalysis*, 1999, **187**, 209

41. A.P. Singh, D. Bhattacharya, Catalysis Letters, 1995, 32, 327

42. U. Freese, F. Heinrich, F. Roessner, *Catalysis Today*, 1999, **49**, 237

43. A.P. Singh, D. Bhattacharya, S. Sharma, *Journal of Molecular Catalysis A*, 1995, **102**, 139

44. Y. Isaev, J.J. Fripiat, *Journal of Catalysis*, 1999, **182**, 257

4 Adsorption Studies

4.1 Introduction

Despite great interest in the acylation of aromatics by carboxylic acid derivatives over zeolites, the adsorption, interaction and desorption of both reactants and products with the catalyst, in particular BEA, has not been thoroughly investigated. These are of considerable importance, since different authors have suggested that either adsorption phenomena [1] or product poisoning [2] may be rate determining.

Studies so far have only concentrated on the adsorption of the acylating agents on ZSM-5 and a few other zeolites, but not BEA. Bosacek et al. [3] used ^{13}C NMR spectroscopy to investigate the adsorption of the acylating agent acetyl chloride on metal-exchanged zeolites X, Y and ZSM-5. More recently, Kresnawahjuesa et al. [4] investigated the adsorption of acetic acid, acetic anhydride and acetyl chloride on ZSM-5.

The adsorption and desorption of acylation reagents and products over H-BEA and metal-exchanged BEA zeolites has thus been studied by *in situ* FTIR and TPD-MS experiments. The data from the TPD-MS experiments have been compared and correlated with the catalytic data presented in Chapter 3.

The results show that, upon adsorption on zeolite BEA, acetic anhydride undergoes decomposition into acetic acid and ketene. Additionally, the product of the reaction, *para*-methoxyacetophenone, when adsorbed on H-BEA decomposes into ketene and unidentified fragments.

The amount of ketene observed to desorb on heating is highest for Na-BEA-1M and lowest for H-BEA. This finding has similarities with earlier studies that have shown that ketene can be formed from the interaction of acetic acid with Na-ZSM-5 [5] but not with H-ZSM-5 [6].

There is an inverse correlation between the quantity of ketene desorbed and the activity of the catalysts for the acylation of anisole by acetic anhydride to yield p-methoxyacetophenone.

These results are interpreted to show the possible involvement of ketene in the acylation mechanism over zeolite BEA.

4.2 FTIR studies

4.2.1 Adsorption of acetic anhydride

Figure 4.2.1 shows infrared spectra of zeolite H-BEA at 333 K in contact with acetic anhydride at pressures ranging from 10^{-4} mbar to 10^{-1} mbar, together with a spectrum of gas phase acetic anhydride. At low pressures we observe C=O stretching vibrations at 1825 cm^{-1} and 1805 cm^{-1}, indicating the presence of adsorbed molecular acetic anhydride.
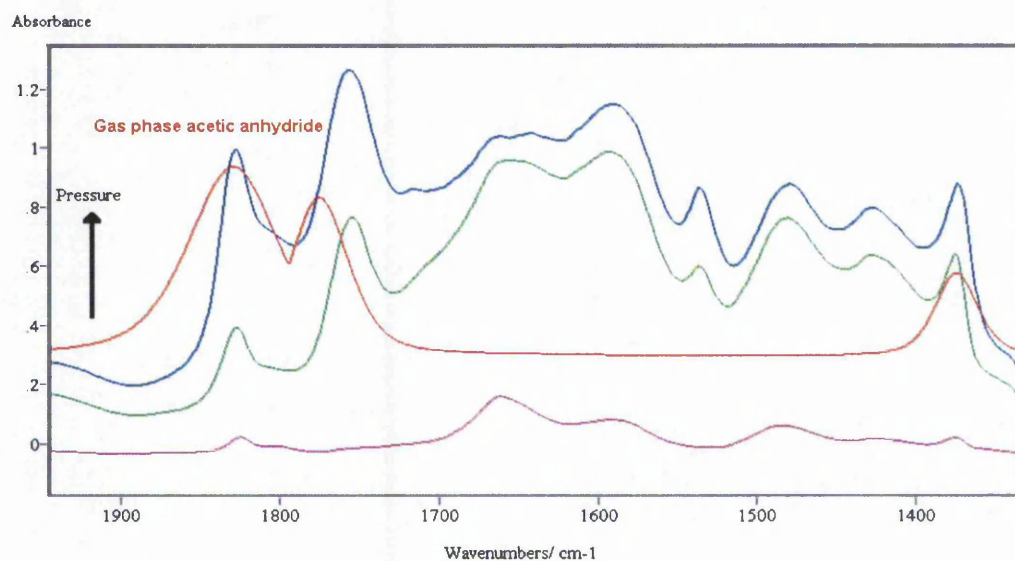
Figure 4.2.1 - Adsorption of acetic anhydride on H-BEA at 333 K and pressures from 10^{-3} mbar (purple line) to 10^{-2} mbar (green line) and 10^{-1} mbar (blue line). The red curve is the spectrum of acetic anhydride in the gas phase.

However, the more intense bands in the low pressure region are observed at 1670 cm^{-1} and 1595 cm^{-1} and at pressures below 10^{-2} mbar a band at 2375 cm^{-1} was found (see Figure 4.2.2). Increasing the pressure to 10^{-2} mbar leads to a growth of the bands at 1825 cm^{-1} and 1805 cm^{-1} and an intense band at 1755 cm^{-1} is observed as well. At pressures higher than 10^{-2} mbar (green curve), the bands at 1825 cm^{-1} and 1755 cm^{-1} increase and the band at 2375 cm^{-1} disappears, whereas the intensity of the other bands is roughly constant. Upon evacuation, the band at 1825 cm^{-1} almost completely disappears (Figure 4.2.3).
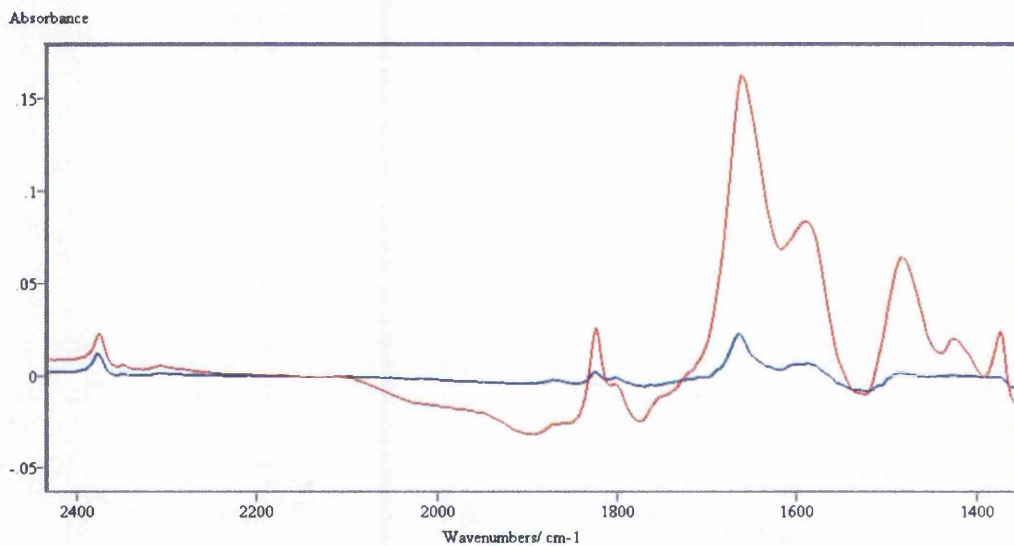
Figure 4.2.2 – Adsorption of acetic anhydride on H-BEA at 333 K and pressures from 10^{-4} mbar (blue line) to 10^{-3} mbar (red line).
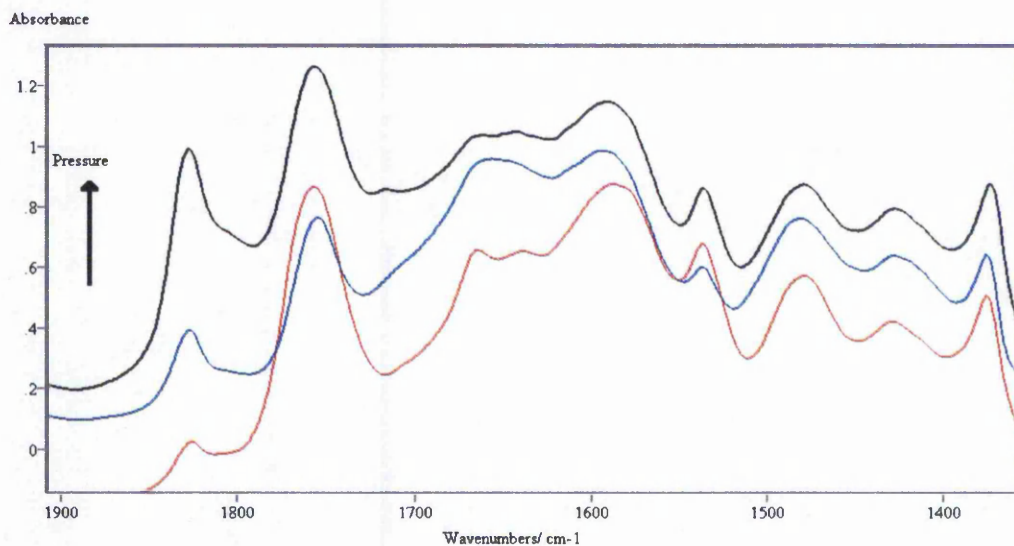
Figure 4.2.3 – Adsorption of acetic anhydride on H-BEA at 10^{-2} mbar (blue line) and at 10^{-1} mbar (black line), and spectrum after evacuation (red line).

A somewhat different picture emerges when acetic anhydride is adsorbed on Na-BEA-1M (Figure 4.2.4).
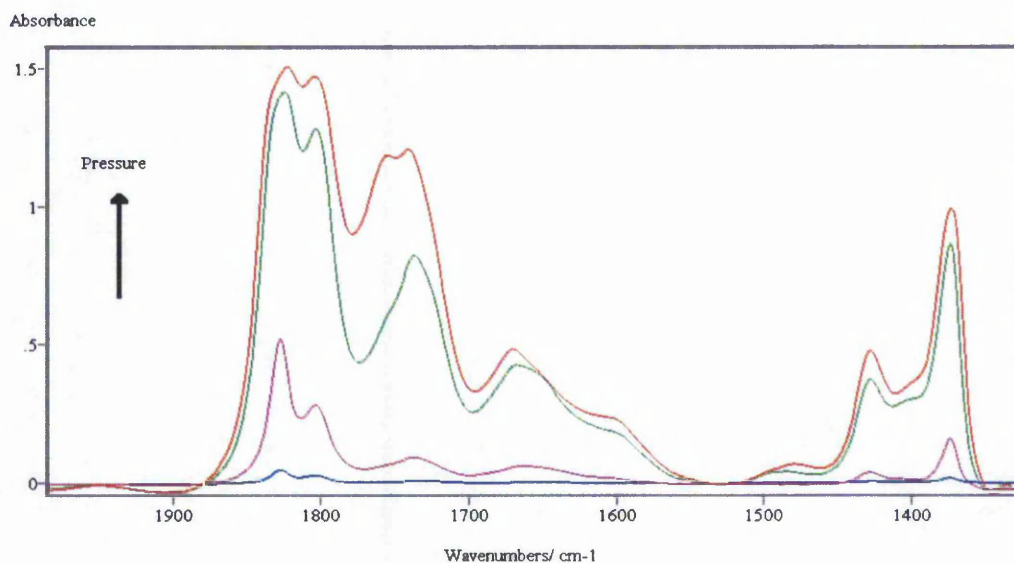
Figure 4.2.4 - Adsorption of acetic anhydride on Na-BEA-1M at 333 K and pressures from 10^{-3} mbar (blue line) to 1 mbar (red line).

At low pressures, two major bands are observed at 1805 cm^{-1} and 1825 cm^{-1}, together with a peak at 1370 cm^{-1} and a small band at 1426 cm^{-1}. Some minor contributions were found at 1660 cm^{-1} and 1755 cm^{-1}. At higher pressures, the band at 1755 cm^{-1} increases in intensity as do the two bands at 1825 cm^{-1} and 1805 cm^{-1}. At pressures below 10^{-2} mbar a very weak band at 2375 cm^{-1} was found as well (not shown).

The peaks and their assignments are summarised in Table 4.2.1.

Table 4.2.1 – Interpretation of selected peaks in the infrared spectra of acetic anhydride

Wavenumber/ cm^{-1}	Assignment	Notes
Acetic anhydride in the gas phase [7]		
1830	C=O symmetric stretch	Strong
1776	C=O antisymmetric stretch	Strong
1375	CH$_3$ symmetric bend	Medium
Adsorption of acetic anhydride on H-BEA at 10^{-3} mbar		
2375	C=C=O stretch	Adsorbed ketene
1825	C=O stretch	Weakly bound acetic anhydride
1805	C=O stretch	Weakly bound acetic anhydride
1670	C=O stretch	Adsorbed acetic acid
1595	C=O strecth	Adsorbed acetic acid
1485	COH in-plane bend	Adsorbed acetic acid
1370	CH$_3$ def	Adsorbed acetic acid
Adsorption of acetic anhydride on H-BEA at 10^{-2} mbar and 10^{-1} mbar		
1825	C=O stretch	Weakly bound acetic anhydride
1755	C=O stretch	Decomposition product of ketene
Adsorption of acetic anhydride on Na-BEA		
1825	C=O stretch	Weakly bound acetic anhydride
1805	C=O stretch	Weakly bound acetic anhydride
1755	C=O stretch	Strongly bound species
1660	C=O stretch	Strongly bound species
1370	CH$_3$ def	Strongly bound species

To assess the strength of the interaction of zeolite H-BEA with acetic anhydride, the zeolite with acetic anhydride adsorbed was heated under vacuum to 773 K and the intensity of the bands integrated. Since obviously there are at least two different adsorption modes, the band at 1755 cm^{-1} and bands in the range 1712 cm^{-1} and 1546 cm^{-1} were integrated (Figure 4.2.5).
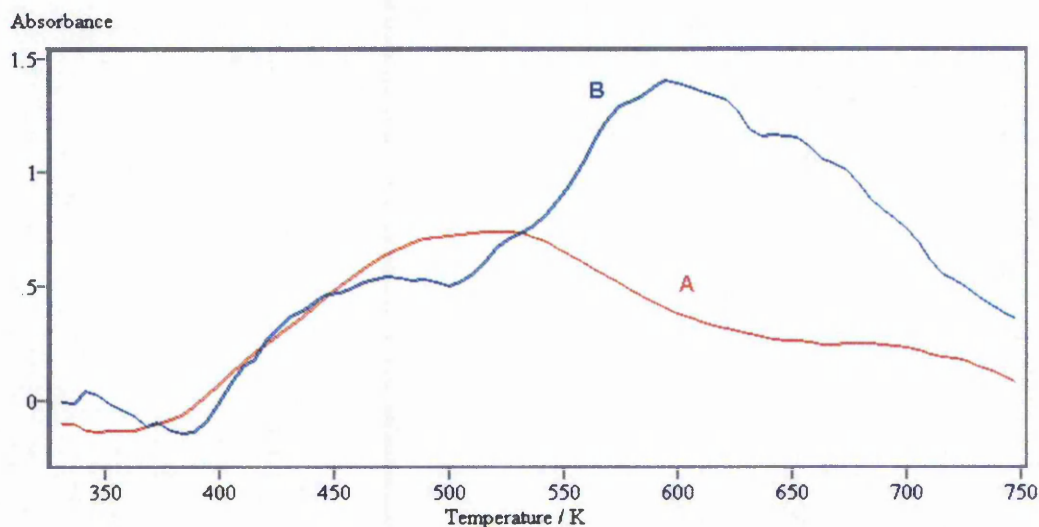
Figure 4.2.5 - Temperature programmed desorption of acetic anhydride from H-BEA. The curves represent integrals over the infrared bands at ca 1755 cm^{-1} (curve A) ^{and} the combined 1546-1712 cm^{-1} (curve B)

The intensity of the band versus temperature curves were then differentiated using Savitzky Golay differentiation [8] and multiplied by –1, so that they resemble familiar TPD curves. The results are shown in Figure 4.2.5. The curve corresponding to the band at 1755 cm^{-1} shows a desorption maximum at 509 K and a shoulder at 688 K. The TPD curve of the peaks between 1546 cm^{-1} and 1712 cm^{-1} shows maxima at 473 K and 594 K.

4.2.2 Adsorption of acetic acid

Infrared spectra resulting from the adsorption of acetic acid on H-BEA are shown in Figure 4.2.6. The main bands observed at pressures lower 10^{-2} mbar are at 1660 cm^{-1}, 1592 cm^{-1} and 1480 cm^{-1}. Increasing the pressure leads to an increase in the intensity of all the bands and a new band at 1413 cm^{-1}, as well as shoulders at 1708 cm^{-1} and 1754 cm^{-1} were observed.
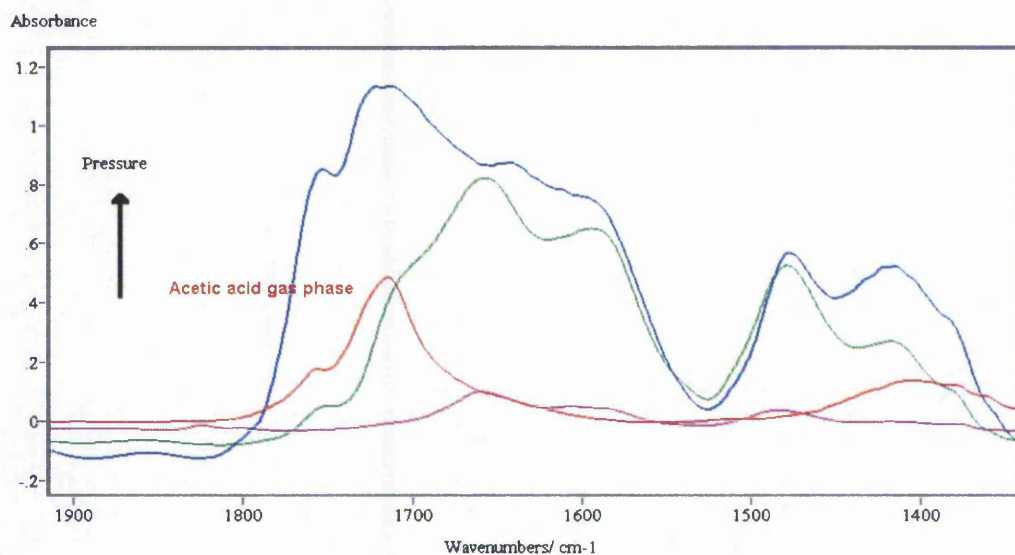
Figure 4.2.6 - Infrared spectra of the adsorption of acetic acid on H-BEA at 333 K and pressures from 10^{-3} mbar (purple line) to 1 mbar (blue line). The red curve is the spectrum of gas phase acetic acid.

For comparison, gas phase acetic acid is plotted in Figure 4.2.4 as well, and shows bands at 1410 cm^{-1}, 1715 cm^{-1} and a shoulder at 1757 cm^{-1}. The low-pressure spectra are very similar to the spectra obtained for acetic anhydride adsorption on zeolite H-BEA as shown in Figure 4.2.7.
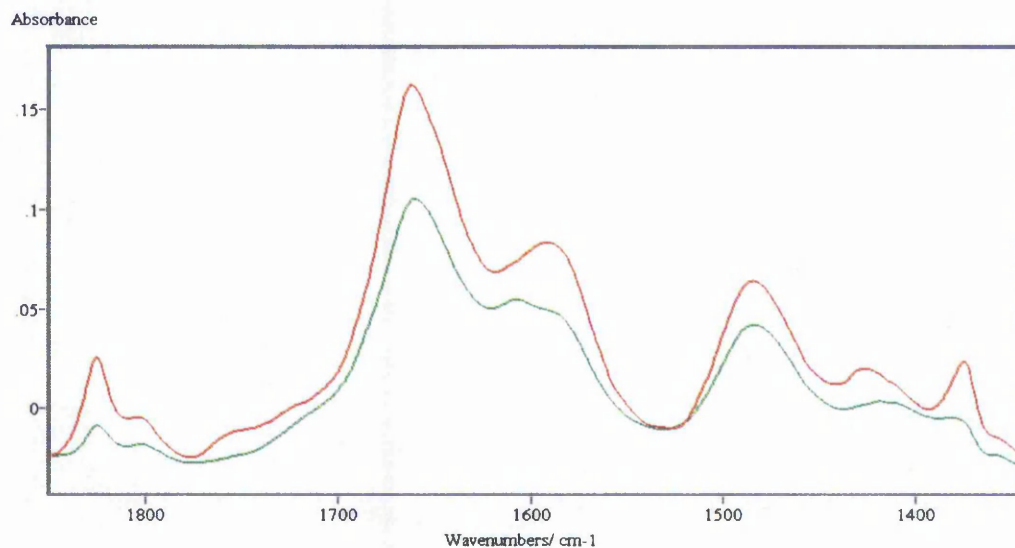
Figure 4.2.7 - Infrared spectra of the adsorption of acetic acid (green) and acetic anhydride (red) on H-BEA at 333 K and 10^{-3} mbar.

Table 4.2.2 – Interpretation of selected peaks in the infrared spectra of acetic acid

Wavenumber /cm^{-1}	Assignment	Notes
Gas phase acetic acid [9]		
1757	C=O stretch	Medium, acetic acid (monomer)
1715	C=O stretch	Strong, acetic acid (dimer)
1400	COH in-plane bend	Medium, very broad
Adsorption of acetic acid on H-BEA at 10^{-3} mbar		
1660	C=O stretch	Adsorbed acetic acid
1592	C=O stretch	Adsorbed acetic acid
1480	COH in-plane bend	Adsorbed acetic acid
Adsorption of acetic acid on H-BEA at 10^{-2} mbar and higher pressures		
1754	C=O stretch	Weakly bound acetic acid (monomer)
1708	C=O stretch	Weakly bound acetic acid (dimer)
1413	COH in-plane bend	Weakly bound acetic acid

For adsorption of acetic acid on H-BEA, the same manipulation was applied as for acetic anhydride and the TPD curves are shown in Figure 4.2.8. Again, the bands at 1754 cm^{-1} and 1708 cm^{-1} can be removed by evacuation at 333 K to a large extent. The TPD curve for the bands at 1660 cm^{-1}, 1592 cm^{-1} and 1480 cm^{-1} shows two desorption maxima at 503 K and 583 K. The small band at 1754 cm^{-1} disappeared completely at 557 K.
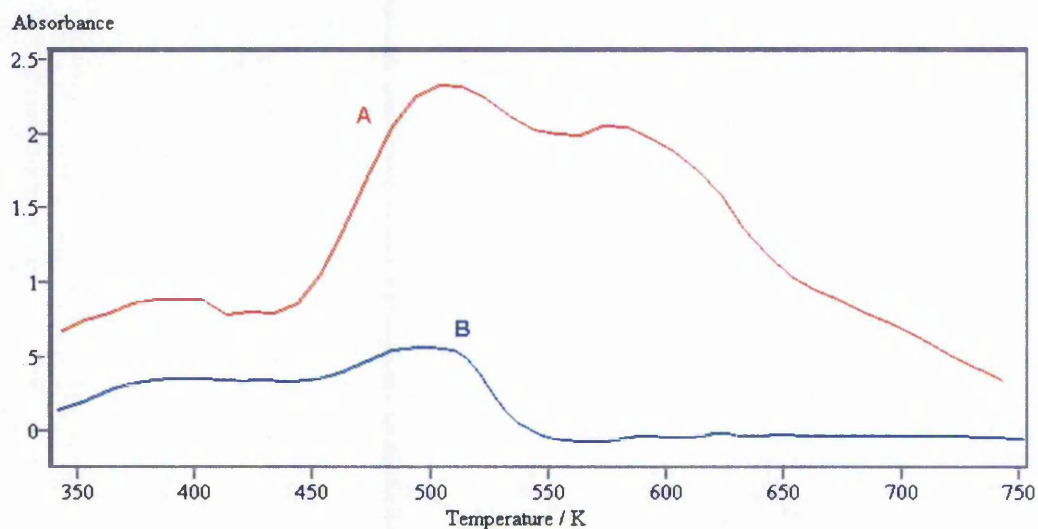
Figure 4.2.8 - Temperature programmed desorption of acetic acid from H-BEA. The curves represent integrals over the infrared bands at 1754 cm^{-1} (curve A) and the combined 1660 cm^{-1}, 1592 cm^{-1} and 1480 cm^{-1} (curve B)

4.2.3 Adsorption of *para*-methoxyacetophenone (p-MAP)

Figure 4.2.9 shows infrared spectra of *para*-methoxyacetophenone adsorbed on zeolite H-BEA, together with the spectrum of a KBr wafer containing p-MAP. At 10^{-2} mbar and 10^{-1} mbar p-MAP pressures, bands at 1677 cm^{-1} with a shoulder at 1640 cm^{-1} and 1370 cm^{-1} with a shoulder at 1418 cm^{-1} were observed. Increasing the pressure to 1 mbar slightly increases the intensity of these bands, and new bands at 1690 cm^{-1}, 1570 cm^{-1} and a shoulder at 1608 cm^{-1} and 1446 cm^{-1} appear. Evacuation at 333 K removes the band at 1690 cm^{-1} almost completely.

The remaining bands at 1690 cm^{-1}, 1570 cm^{-1} and 1608 cm^{-1} were integrated and converted into TPD curves as described previously. The only desorption peak observed was centred at 420 K (Figure 4.2.10).
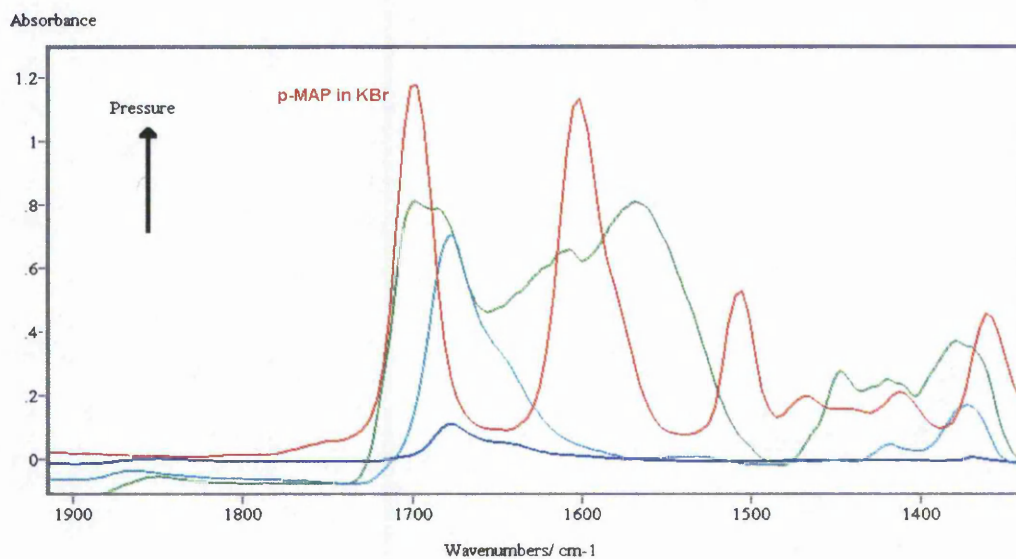
Figure 4.2.9 - Infrared spectra of the adsorption of p-MAP on H-BEA at 333 K and 10^{-2} mbar (blue line), 1 mbar (light blue line) and 10 mbar (green line).The red coloured curve is p-MAP in KBr.

Table 4.2.3 – Interpretation of selected peaks in the infrared spectra of p-MAP

Wavenumber /cm^{-1}	Assignment	Notes
p-methoxyacetophenone in KBr [9]		
1700	C=O stretch	Strong
1600	Ring vibration	Strong
1505	Ring vibration	Medium
1360	Carbonyl CH$_3$ def	Medium
Adsorption of p-MAP on HBEA at 10^{-2} mbar		
1677	C=O stretch	Decomposition product
1640	C=O stretch	Decomposition product
1418	COH in-plane bend	Shoulder
1370	CH$_3$ def	
Adsorption of p-MAP on HBEA above 10^{-2} mbar		
1690	C=O stretch	Weakly adsorbed p-MAP
1608	Ring vibration	Shoulder, weakly adsorbed p-MAP
1570	Ring vibration	Weakly adsorbed p-MAP
1446	Ring vibration	Shoulder, weakly adsorbed p-MAP
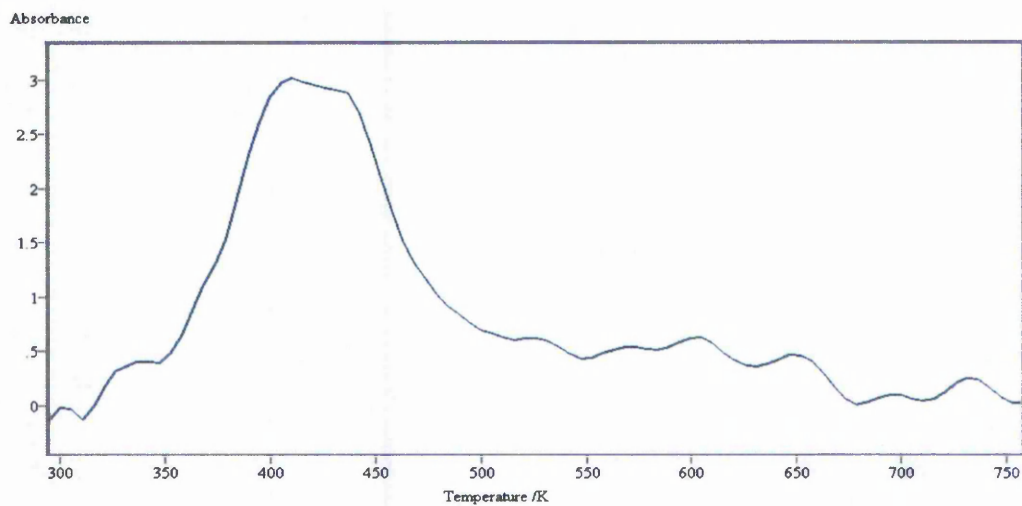
Figure 4.2.10 - Temperature programmed desorption of p-MAP from H-BEA. The curve represents integrals over the infrared bands between 1710 cm^{-1} and 1490 cm^{-1}

4.3 TPD-MS Studies

4.3.1 Adsorption of anisole and acetic anhydride on H-BEA

Figure 4.3.1 shows the desorption profiles of selected m/e peaks after adsorption of anisole on zeolite H-BEA. It is evident that anisole largely desorbs intact from the zeolite as the ratio between the molecular ion (m/e = 108) and any other major peak is essentially constant.
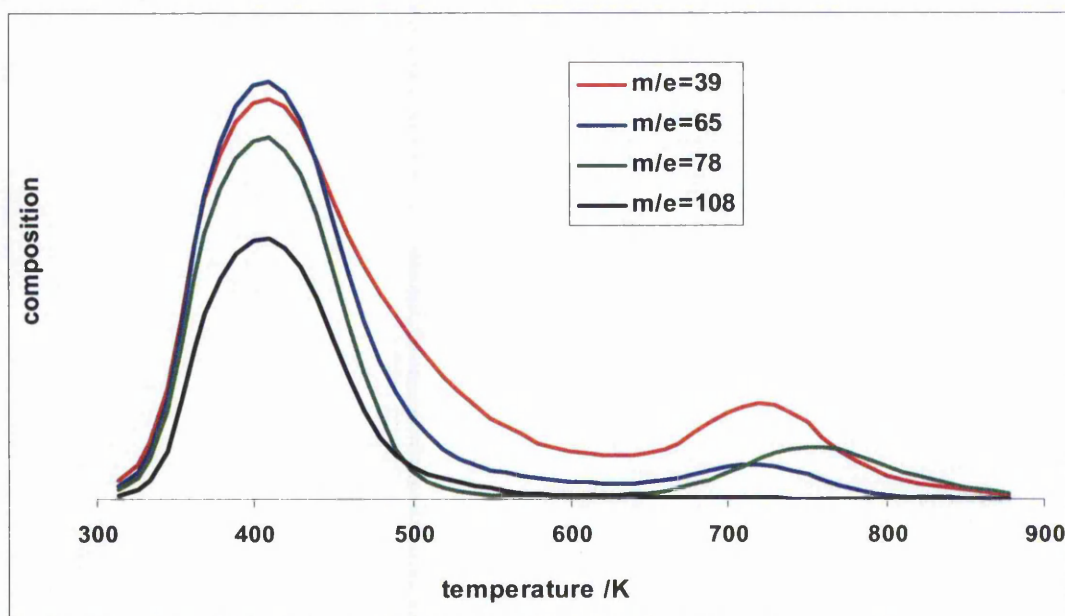
Figure 4.3.1 – Desorption profile of anisole from H-BEA

In the case of adsorption of acetic anhydride on H-BEA a number of different desorption products are detected. These products have been identified from the m/e peaks by using the method described in Chapter 2 Section 2.5.4. Figures 4.3.2 and 4.3.3 show desorption spectra from H-BEA, which follow a pattern that is typical of all of the materials studied, although the relative quantities of materials desorbed change markedly. As Figure 4.3.2 indicates, at around 370 K desorption of acetic anhydride is at its maximum. At a slightly higher temperature acetic acid desorption commences and dominates the desorption spectra in the range up to ca 550 K. Ketene desorption starts at a similar temperature to acetic acid but continues to occur up to the highest temperature studied, and there is a broad feature due to water desorption (see Figure 4.3.3). As noted in Chapter 3, there is no desorption of water in this region from the activated zeolite, so it is a decomposition product from acetic anhydride. Figure 4.3.3

shows the desorption results simultaneously obtained for water, carbon monoxide and carbon dioxide. Hydrogen desorption starts at ca 370 K and continues in a rather featureless way up to the highest temperatures studied. Small dips below the baseline in the desorption curves for acetic anhydride and ketene are thought to reflect small errors in the cracking patterns.
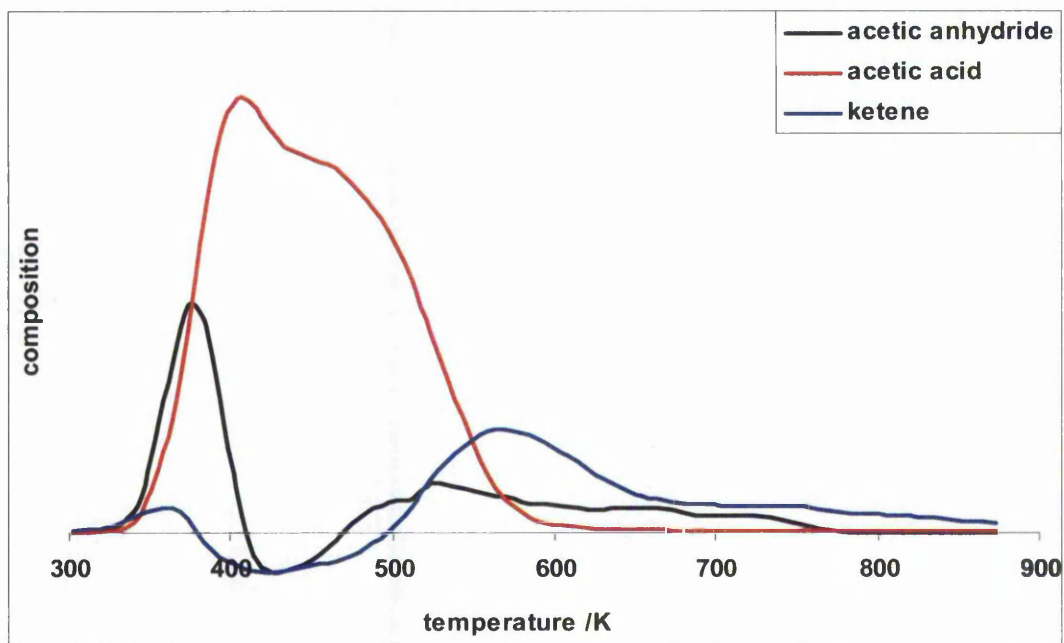
Figure 4.3.2 – Desorption profile after adsorption of acetic anhydride on H-BEA
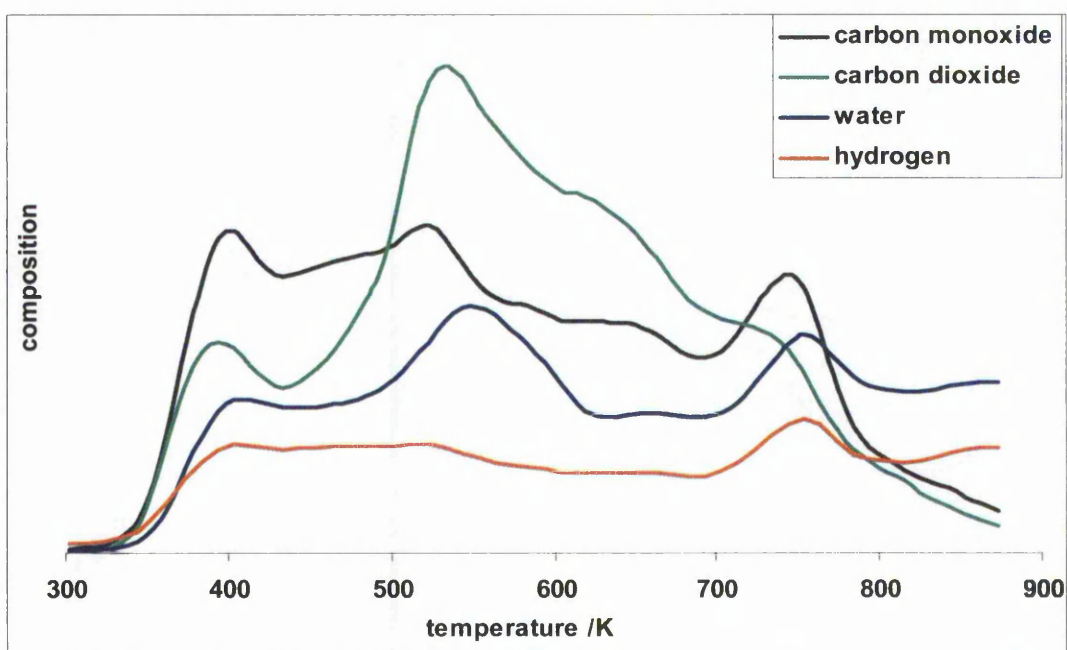
Figure 4.3.3 – Desorption profile after adsorption of acetic anhydride on H-BEA

Figure 4.3.4 shows the desorption profiles for acetic anhydride adsorbed on a zeolite BEA with a Si/Al = 150 (Zeolyst, CP811C-300). As in the case of H-BEA with Si/Al = 12.5, at around 370 K some desorption of acetic anhydride occurs. At a slightly higher temperature acetic acid desorption commences and dominates the desorption spectra in the range up to ca 550 K. The desorption of ketene starts at a similar temperature to acetic acid but continues to occur up to the highest temperature studied, with a maximum intensity peak at 700 K compared to about 570 K for H-BEA with Si/Al = 12.5.
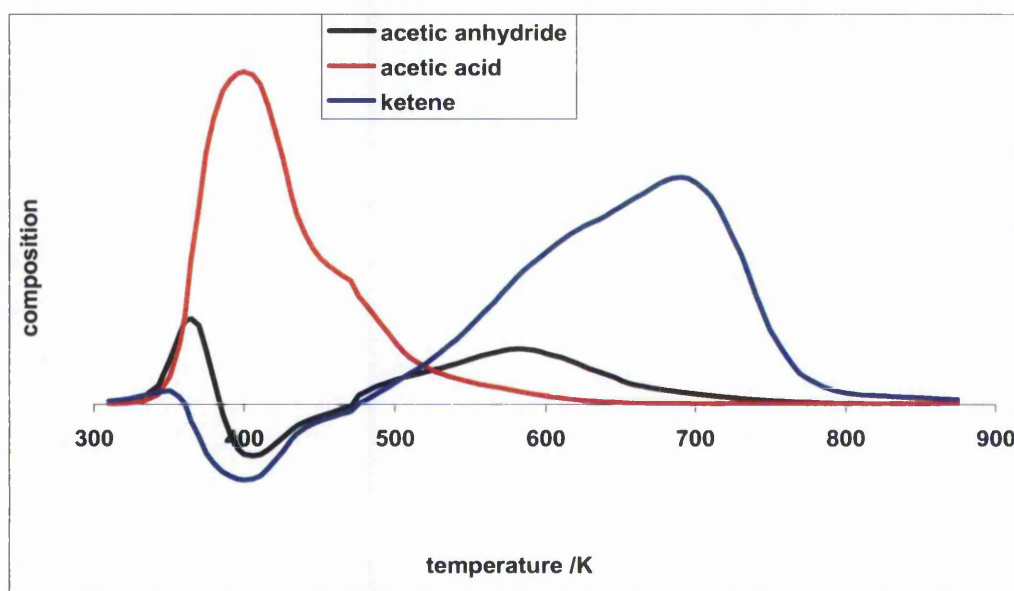
Figure 4.3.4 – Desorption profiles after adsorption of acetic anhydride
from H-BEA (Si/Al = 150)

Figure 4.3.5 compares the desorption of ketene from the two zeolite BEA samples and also from a purely siliceous mesoporous material (MCM-41). Data were normalised by weight of the sample. These results suggest that the less aluminium is present in the framework the higher the amount of ketene desorbing and the higher the temperature of desorption for the maximum intensity peak of ketene.
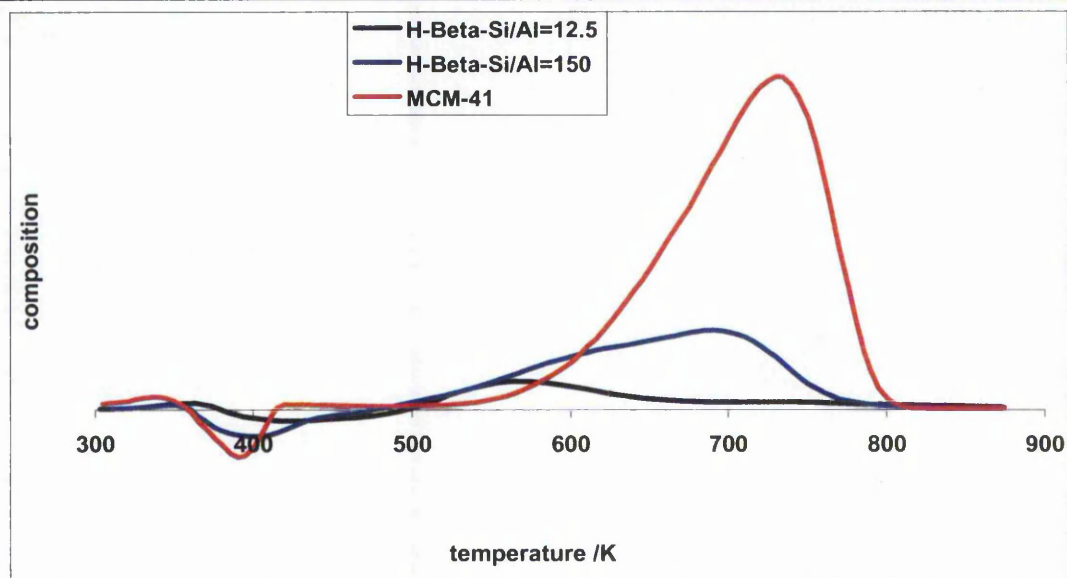
Figure 4.3.5 – Ketene desorbing from various samples

Figure 4.3.6 shows the desorption profiles for acetic anhydride adsorbed on NH_4-BEA. NH_4-BEA was prepared in the TPD-MS apparatus by first activating BEA, then adsorbing ammonia at 423 K, and subsequently outgassing the sample for 1 hour at 423K.
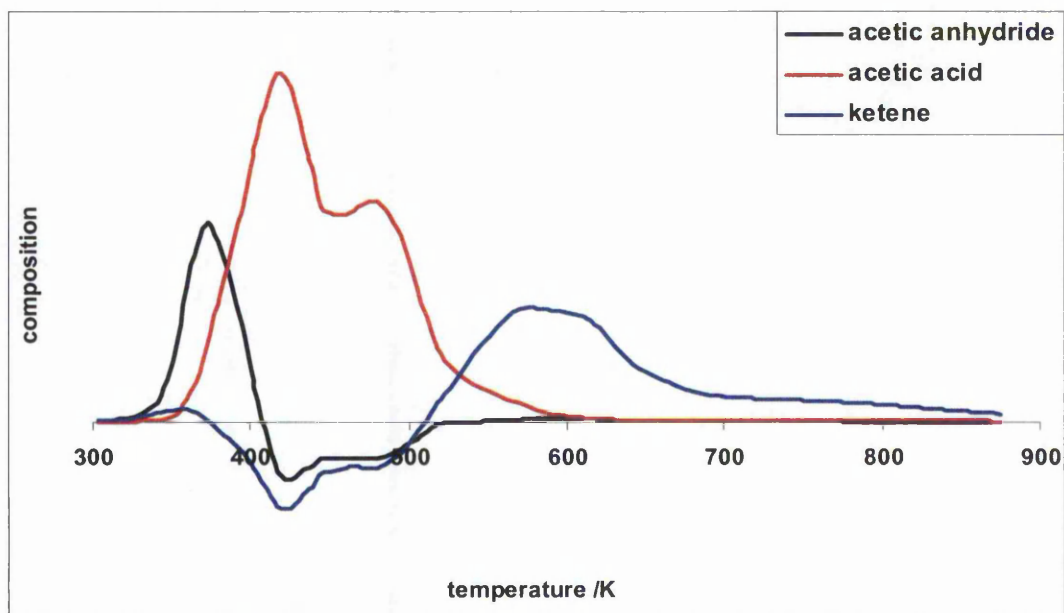
Figure 4.3.6 – Desorption profile after co-adsorption of ammonia and acetic anhydride

As in the case of H-BEA (Figure 3.3.2), acetic anhydride desorbs first followed by acetic acid and then ketene. The desorption profile of acetic acid shows a peak at 410 K and a second one at 480 K. The maximum intensity peak due to ketene is at 580 K.

4.3.2 Adsorption of acetic anhydride on metal-exchanged BEA samples

Figures 4.3.7 to 4.3.9 show the desorption results obtained respectively from Na-BEA-1M, Cu-BEA-1M and Fe-BEA-1M after acetic anhydride adsorption, concentrating on the intact organic species. Small dips below the baseline in the desorption curves for acetic anhydride and ketene are again believed to reflect small errors in the cracking patterns used in the equations applied to calculate concentrations. Note that the shape of the desorption patterns and their integral values were shown to be reproducible.
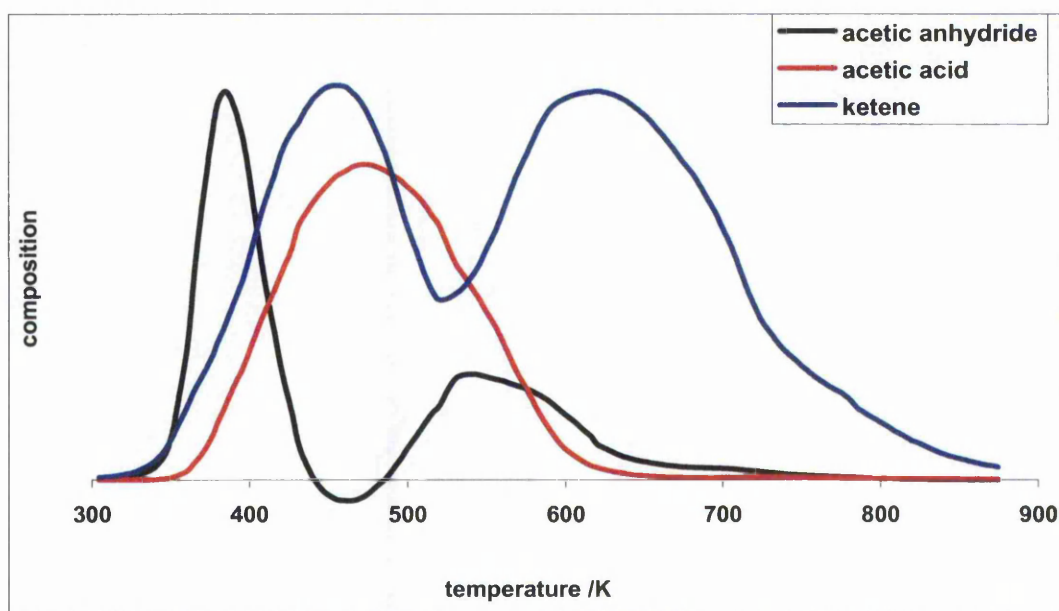
Figure 4.3.7 – Desorption profiles after adsorption of acetic anhydride on Na-BEA-1M
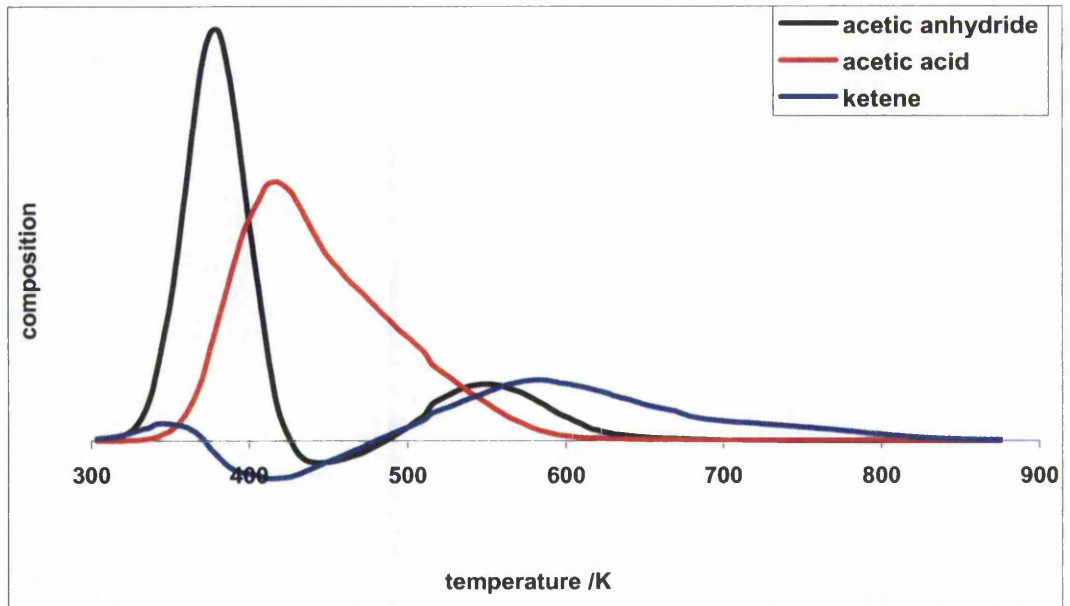
Figure 4.3.8 – Desorption profiles after adsorption of acetic anhydride on Cu-BEA-1M
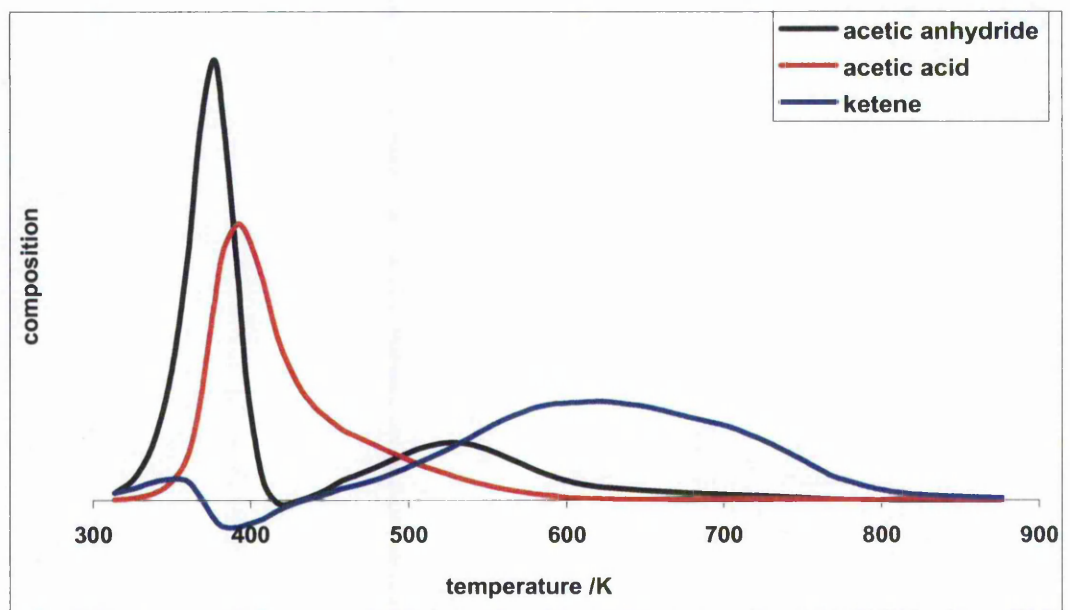
Figure 4.3.9 – Desorption profiles after adsorption of acetic anhydride on Fe-BEA-1M

Table 4.3.1 shows the relative amount of each components desorbing from each sample. These were calculated by integration of the desorption profiles up to 873 K.

Table 4.3.1 – Amounts desorbing from each sample

Sample	Acetic anhydride /arbitrary units	Acetic acid /arbitrary units	Ketene /arbitrary units
H-BEA	3.72	14.8	3.29
Na-BEA-1M	6.83	10.6	26.6
Cu-BEA-1M	17.0	20.4	5.88
Fe-BEA-1M	16.2	13.9	14.4

Figures 4.3.10 to 4.3.14 show the desorption results obtained respectively from Na-BEA-10^{-2}M, Fe-BEA-10^{-2}M, Co-BEA-10^{-2}M, Ni-BEA-10^{-2}M and Cu-BEA-10^{-2}M, concentrating on the intact organic species.
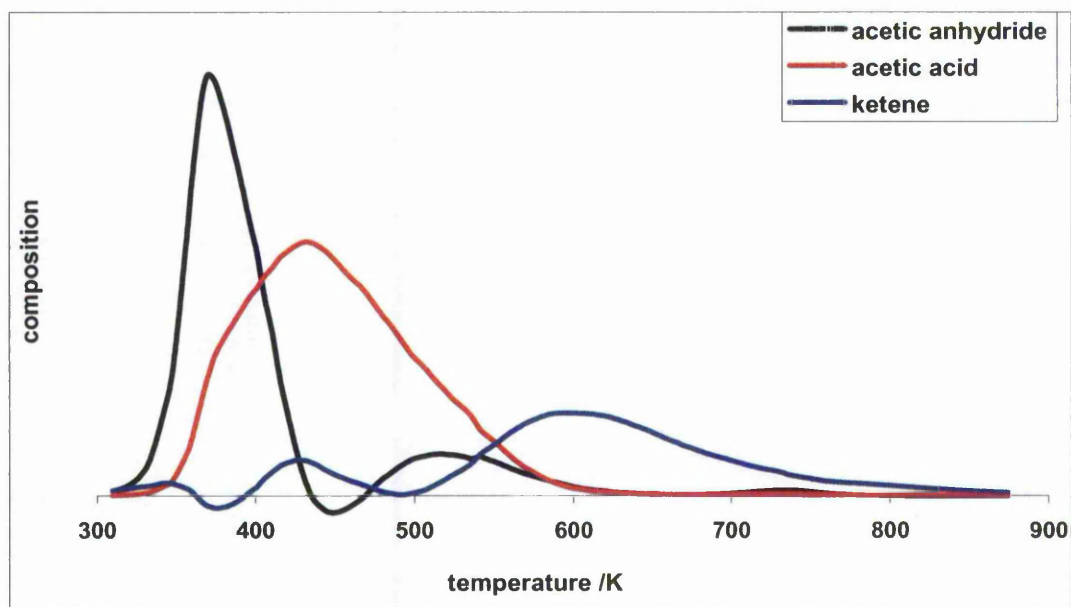
Figure 4.3.10 – Desorption profiles after adsorption of acetic anhydride on Na-BEA-10^{-2}M
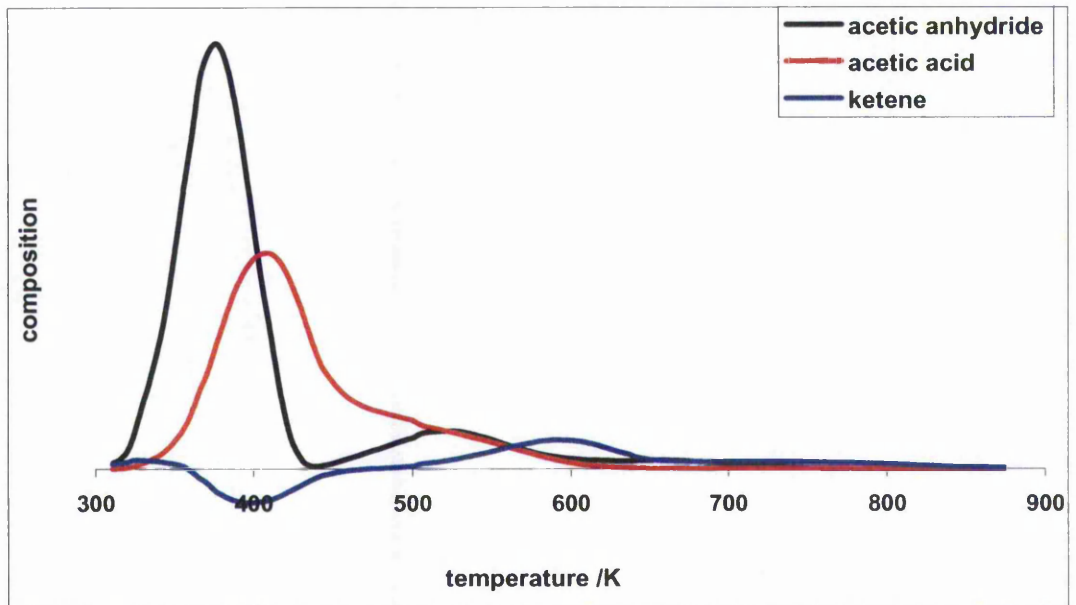
Figure 4.3.11 – Desorption profiles after adsorption of acetic anhydride on Fe-BEA-10^{-2}M
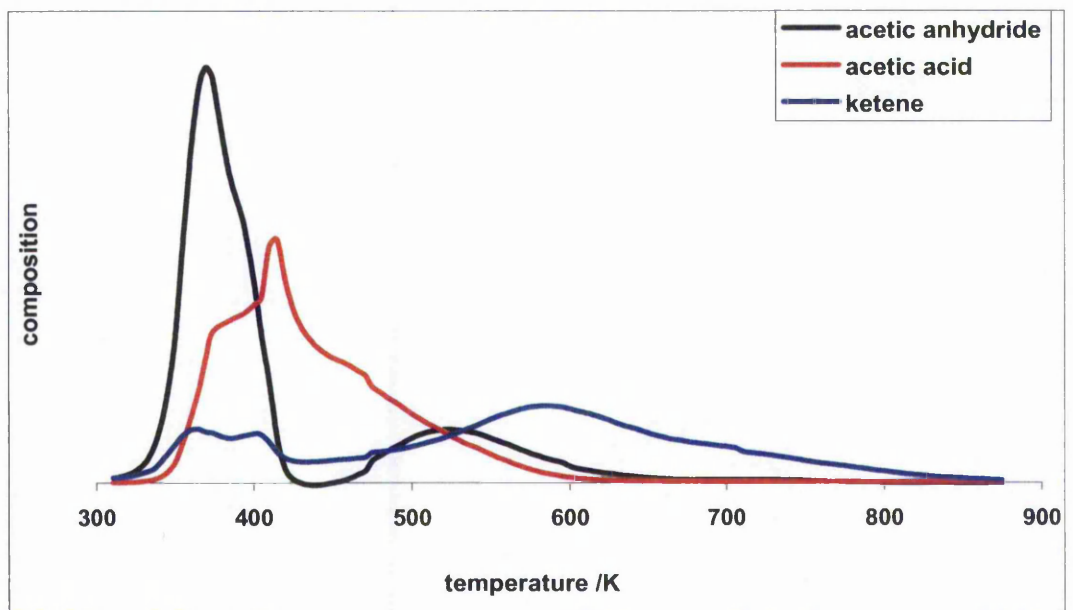
Figure 4.3.12 – Desorption profiles after adsorption of acetic anhydride on Co-BEA-10^{-2}M
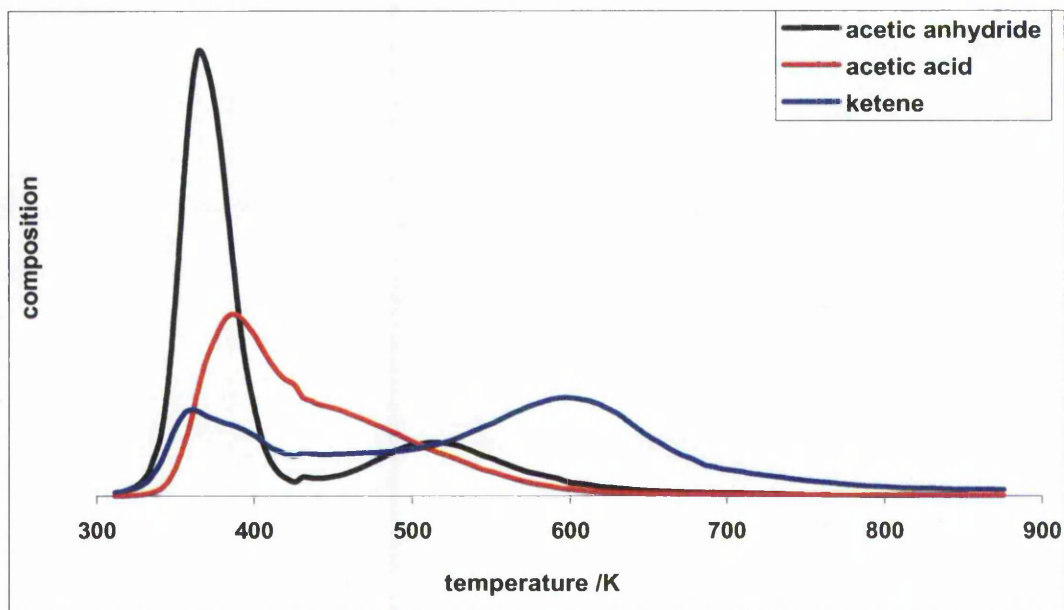
Figure 4.3.13 – Desorption profiles after adsorption of acetic anhydride on Ni-BEA-10^{-2}M
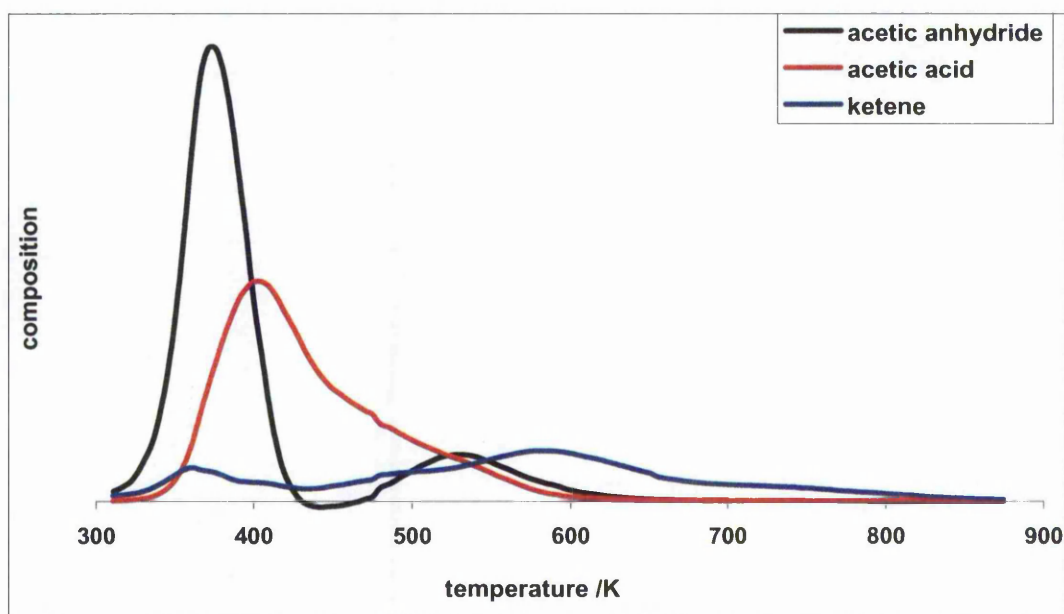
Figure 4.3.14 – Desorption profiles after adsorption of acetic anhydride on Cu-BEA-10^{-2}M

The amounts of components desorbing from each sample are summarised in Table 4.3.2.

Table 4.3.2 – Amounts desorbing from each sample

Sample	Acetic anhydride /arbitrary units	Acetic acid /arbitrary units	Ketene /arbitrary units
HBEA	3.72	14.8	3.29
Na-BEA-10^{-2}M	20.8	27.4	12.4
Fe-BEA-10^{-2}M	33.0	24.0	2.83
Co-BEA-10^{-2}M	12.9	12.2	10.2
Ni-BEA-10^{-2}M	13.0	10.3	13.2
Cu-BEA-10^{-2}M	17.5	15.2	8.31

4.4 Correlation between initial rate of reaction and TPD-MS results

This Section seeks to correlate the TPD-MS results and the catalytic rate measurements presented in Chapter 3. Perhaps surprisingly, there is an inverse correlation between the initial rate of acylation and the amount of ketene desorbed intact for a number of zeolites, as shown in Figure 4.4.1.
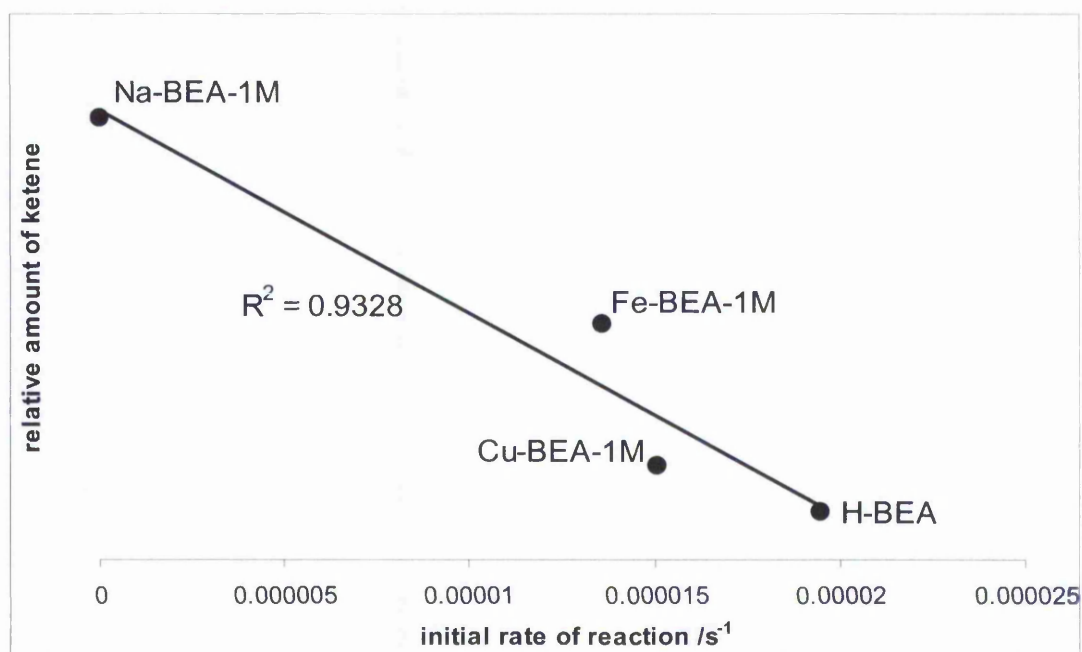
Figure 4.4.1 – Correlation between relative amount of ketene and initial rate of reaction

By contrast there is no simple correlation between catalytic performance and the quantities of either acetic acid (Figure 4.4.2) or acetic anhydride (Figure 4.4.3) desorbing from the zeolites.
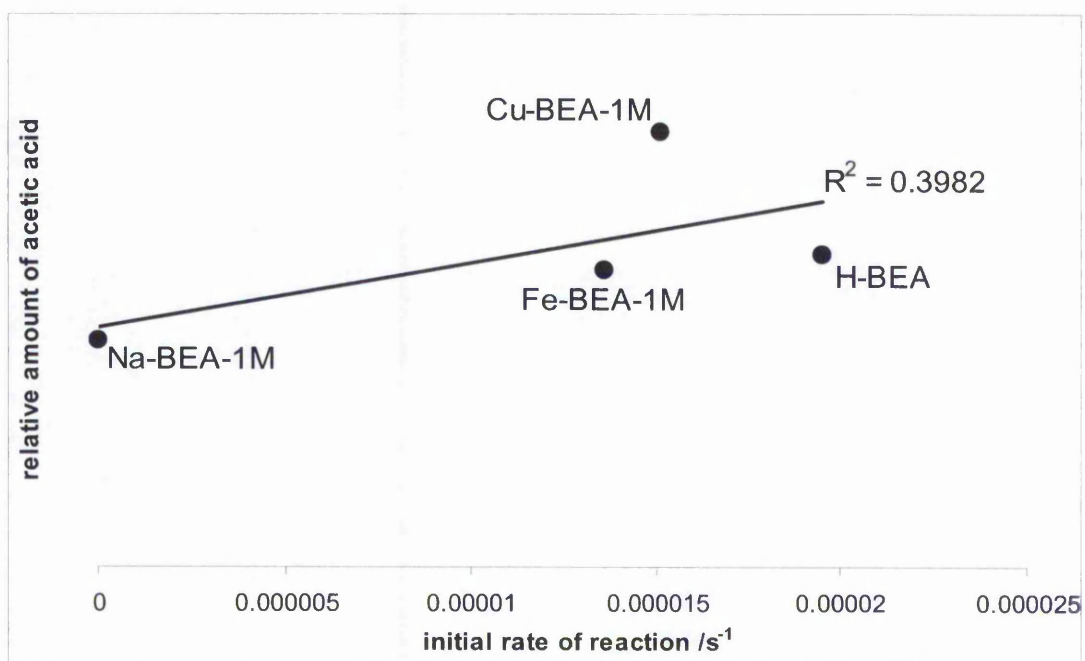
Figure 4.4.2 – Correlation between relative amount of acetic acid and initial rate of reaction
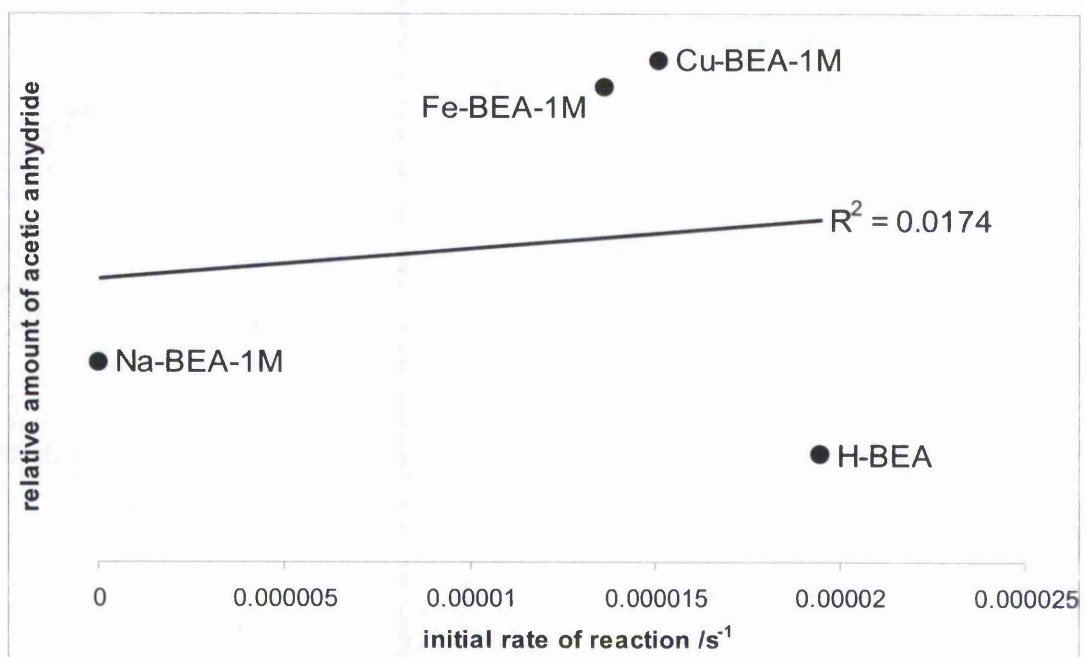
Figure 4.4.3–Correlation between relative amount of acetic anhydride and initial rate of reaction

To determine any correlation between the catalytic activity and the amount of components (nominally acetic acid, acetic anhydride and ketene) desorbing from each zeolite BEA-10^{-2}M sample, the amounts of components versus catalytic activity are plotted in Figures 4.4.4 to 4.4.7.
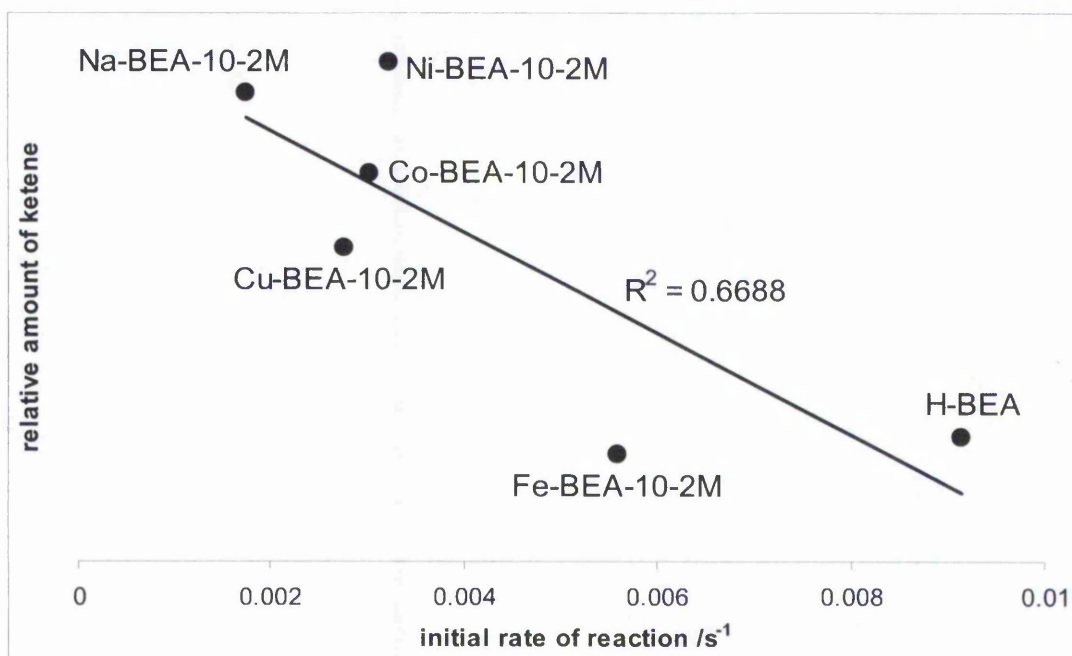
Figure 4.4.4 – Correlation between relative amount of ketene and initial rate of reaction
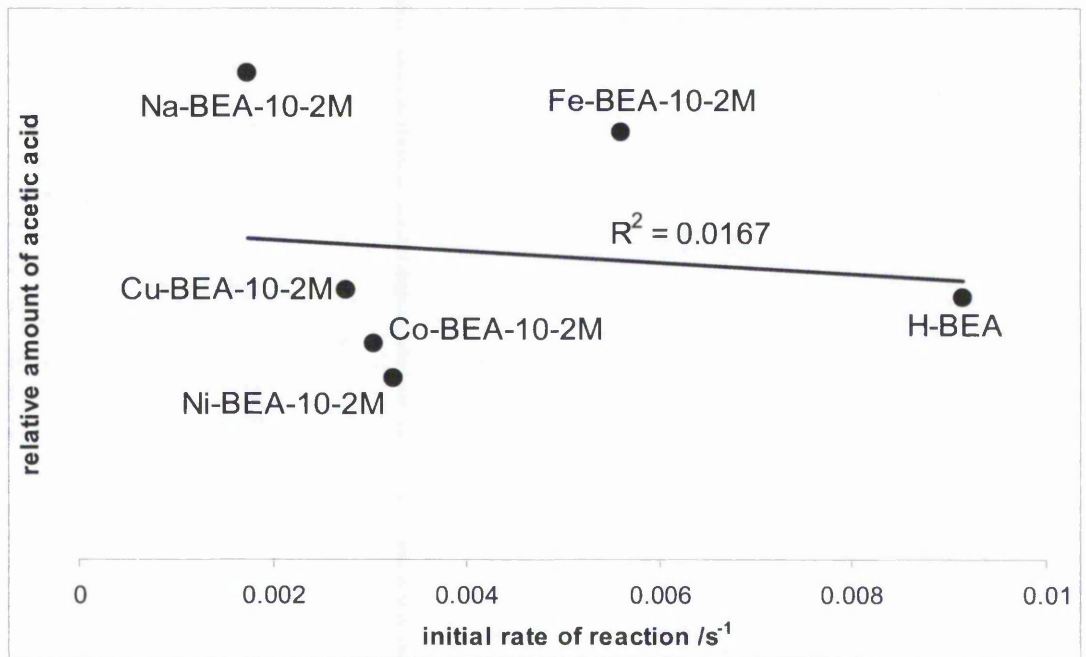
Figure 4.4.5 – Correlation between relative amount of acetic acid and initial rate of reaction
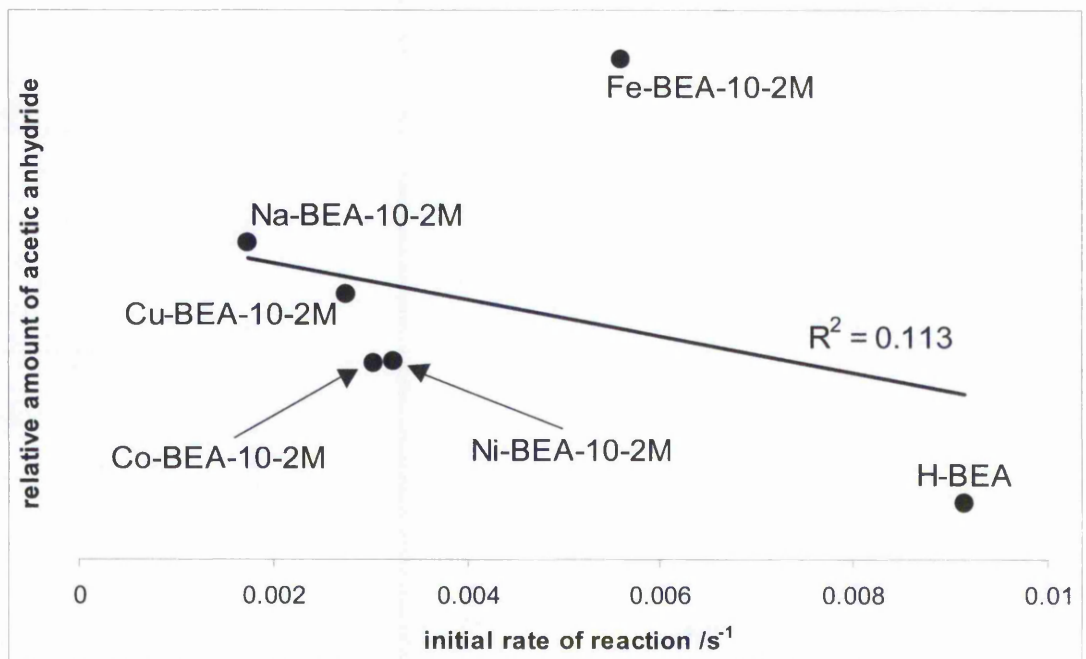
Figure 4.4.6–Correlation between relative amount of acetic anhydride and initial rate of reaction

4.5 Conclusions

The infrared spectra of acetic anhydride and acetic acid (Figures 4.2.1 and 4.2.6), both initially adsorbed on H-BEA, are significantly perturbed compared to the spectra of the respective free molecules.

On adsorption at 10^{-2} mbar, the spectrum of acetic acid shows features at 1660, 1592 and 1480 cm^{-1}, that are also observed when the anhydride is adsorbed (Figure 4.2.7). These bands are assigned to the adsorbed acid, interacting relatively strongly with the catalyst at room temperature since the TPD-MS results (Figure 4.3.2) show that much of the acetic acid desorbs with a maximum rate at 405 K. As the pressure is increased these features grow, and new features appear that are very similar to the spectrum of gas phase acetic acid. In agreement with the relatively small perturbation of the gas phase spectrum, the desorption results shown in Figure 4.2.8 confirm that this state interacts relatively weakly with the zeolite. At the highest pressures studied, (10^{-1} mbar, up to 10 mbar) the spectra appear to represent a linear combination of the strongly and more weakly bound states.

The infrared spectra together with the TPD-MS results suggest that the most complex interaction is that between acetic anhydride and H-BEA. In the FTIR, at the lowest pressures of adsorption, the only adsorbed species observed from acetic anhydride appears to be acetic acid, with the lowest pressure curves at 10^{-4} mbar and 10^{-3} mbar in Figure 4.2.1, closely resembling those taken at the same pressures with acetic acid (Figure 4.2.6). The two curves of H-BEA in contact with 10^{-3} mbar acetic acid and acetic anhydride dramatically show the close resemblance (Figure 4.2.7). Thus, it can be said that the chemical state of both substances is very similar when adsorbed at low pressures and that they adsorb in the form of the acid plus, in the case of the anhydride, another fragment. This fragment has been identified as ketene from a band at 2375 cm^{-1} (Figure 4.2.2). This band at 2375 cm^{-1} is found at higher frequency than gas phase ketene. However, this spectral region is typical of cumulated double bonds and electron rich substituents, e.g. nitrogen, shift the band to higher frequencies [9]. As the pressure of acetic anhydride is increased bands due to the anhydride can be observed, as well as a carbonyl band at ca 1755 cm^{-1} that is probably due to a decomposition product of ketene. This band increases in intensity when the ketene band at 2375 cm^{-1} disappears. The TPD results shown in Figure 3.2.3 are consistent with this assignment.

The IR spectra of acetic anhydride adsorbed on Na-BEA-1M (Figure 4.2.4) appear to be less perturbed than in the case of H-BEA. There are bands at 1825 and 1805 cm^{-1}, which are assigned to the symmetric and antisymmetric carbonyl stretches seen in the gas phase molecule at 1825 and 1760 cm^{-1} respectively; the CH$_3$ deformation mode is unmoved, at 1370 cm^{-1}. As the pressure is increased the spectra become more complex, and bands at frequencies close to the free molecule position become dominant. For reasons yet to be understood, those at 1825 and 1760 cm^{-1} are quite broad, and each appears to be split into a doublet. Even on this non-acidic material, there appears to be some decomposition of the anhydride into the acid, as indicated by the presence of the bands at 1660, 1592 and 1480 cm^{-1}. Only traces of bands due to ketene were observed here, so it either reacts or more likely, desorbs from the zeolite. In agreement with this, the TPD-MS results (Figure 4.3.7) show significant desorption of ketene from Na-BEA at 440 K.

The adsorption of p-MAP at low pressure (Figure 4.2.9) results in a species that has lost the aromatic deformation vibration (1600 cm^{-1}) and the aromatic CH stretching vibrations (not shown). Thus, at 1 mbar equilibrium pressure p-MAP decomposes over H-BEA, and the aromatic fragment desorbs, but a product containing a carbonyl group stays adsorbed (bands at 1677 cm^{-1} with a shoulder at 1640 cm^{-1}). A band at 2380 cm^{-1}, attributed to adsorbed ketene, is also present at this low pressure of adsorption. This is a highly interesting result, because it is evidence for the involvement of ketene in the reaction sequence. The concept of microscopic reversibility [10] can be applied, i.e., a site that can form the bond between the carbonyl group and the aromatic ring can also split the bond, and the product of the scission would be ketene.

At higher pressures of adsorption, some species with an intensive band at 1565 cm^{-1} are formed and upon evacuation at 333 K the adsorbate with bands attributed to the carbonyl group at 1677 cm^{-1} desorbs or reacts. The relatively low desorption temperatures for the product of 4-methoxyacetophenone (Figure 4.2.10) suggests that it interacts less strongly with the catalyst then either acetic anhydride (Figure 4.2.5) or acetic acid (Figure 4.2.8). The highest desorption temperature observed, 420 K, is however much higher than that used in the liquid phase acylation reaction, which is typically 333 K. It would therefore not be safe to rule out product desorption as being rate determining. However the relative desorption energies from infrared TPD experiments from acetic anhydride, acetic acid and anisole (not shown) favours adsorption of acetic anhydride/acetic acid as opposed to p-MAP. Researchers [11] have observed levelling off of the acylation reaction of anisole with acetic anhydride when

performed in a batch reactor. Adding p-methoxyacetophenone to the reaction mixture results in a decreased rate of reaction and thus suggests product poisoning. However, turnover numbers are in excess of one hundred turnovers per site and the results presented here suggest stronger bonding of acetic acid/acetic anhydride than the product, p-MAP. As already suggested by some authors [12, 13], multiply acylated products may well be poisoning the sites and the highly reactive ketene could contribute to their formation.

The TPD-MS results show that only a small fraction of any acetic anhydride adsorbed desorbs intact, with the smallest amount observed from H-BEA. Even on Na-BEA-1M, which might be expected to be comparatively unreactive, much more acetic acid desorption is observed. Only from a siliceous MCM-41 (not shown) is acetic anhydride the dominant desorption product.

Upon adsorption of acetic anhydride, the majority of the acetic acid formed within the zeolite pores is quite rapidly desorbed but most of the ketene remains within the zeolite pores. However some acetic acid does stay adsorbed and some ketene starts to desorb. As the temperature is further increased, there is evidence for the decomposition of adsorbed acetic acid into ketene and water. But much of the ketene remains adsorbed until temperatures above ca 530 K, when it decomposes into fragments such as CO and hydrogen. Some carbon dioxide formation is also observed, which may result from the water gas shift reaction or through a bimolecular decomposition of ketene.

These results show that the primary decomposition mode of acetic anhydride adsorbed on BEA is:

$$\text{acetic anhydride}_{(ads)} \rightarrow \text{acetic acid}_{(ads)} + \text{ketene}_{(ads)}$$

As the temperature of the solid is increased, the following sequence occurs:

$$\text{acetic anhydride} \rightarrow \text{acetic acid}_{(ads)} + \text{ketene}_{(ads)} \rightarrow$$
$$\text{acetic acid}_{(g)} + \text{(more) ketene}_{(ads \text{ and } g)} \rightarrow CO_{2(g)} + H_{2(g)} + \text{coke}$$
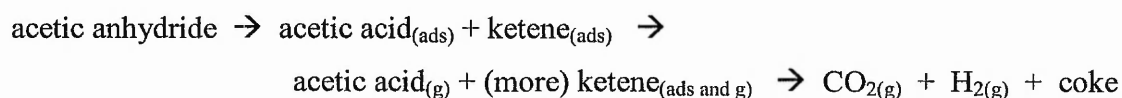
Both FTIR and TPD-MS data are consistent with the reaction sequence, and it is also significant that acetic anhydride is made industrially by the reverse reaction, of acetic acid with ketene [14].

Looking for correlations between the TPD-MS results and the catalytic rate measurements shows that there is an inverse correlation between the initial rate of

acylation and the amount of ketene desorbed intact for a number of catalysts. There is no simple correlation between catalytic performance and the quantities of either acetic acid or acetic anhydride desorbed.

This correlation can be seen as further evidence of the involvement of ketene in the acylation reaction, which is typically carried out at 330 - 400 K. There is a strong partial positive charge on the central carbon atom of the ketene molecule [15], which makes it an interesting possibility as an acylating agent through the mechanism shown in Figure 4.5.1. The inverse correlation suggests that the strength of bonding of ketene to the zeolite, and hence perhaps its degree of polarisation, determines the effectiveness in the acylation catalysis.
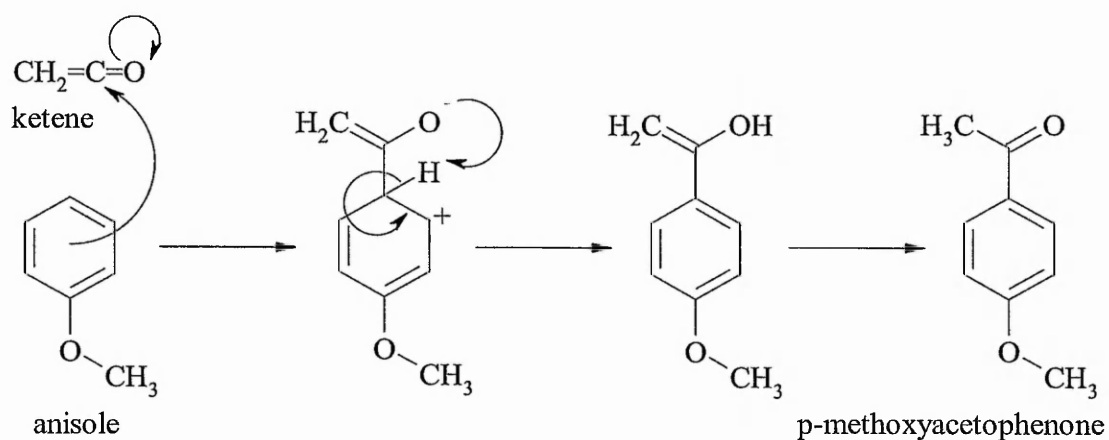
Figure 4.5.1 – Mechanism of acylation via ketene intermediate

4.6 References

1. E. Derouane, et al., *Journal of Catalysis,* 2000, **194**, 410

2. D. Rohan, et al., *Journal of Catalysis*, 1998, **177**, 296

3. V. Bosacek, E.A. Gunnewegh, H. van Bekkum, *Catalysis Letters*, 1996, **39**, 57

4. O. Kresnawahjuesa, R.J. Gorte, D. White, *Journal of Molecular Catalysis A*, 2004, **208**, 175

5. L.M. Parker, D.M. Bibby, I.J. Miller, *Journal of Catalysis*, 1991, **129**, 438

6. C.D. Chang, A.J. Silvestri, *Journal of Catalysis*, 1977, **47**, 249 & Y. Servotte, J. Jacobs, P.A. Jacobs, *Acta. Phys. Chem.*, 1985, **31**, 609

7. W. Guang, et al., *Journal of Physical Chemistry A*, 2000, **104**, 1576

8. B. Azambre, et al., *Talanta*, 1999, **50**, 359

9. D. Lin-Vien, et al., *Infrared and Raman characteristic frequencies of organic molecules*, Academic Press, San Diego, 1991

10. J. March, *Advanced Organic Chemistry*, 4th Ed., Wiley, New York, 1992, p. 215

11. E. G. Derouane, et al., J. Catal., 1999, 187(1), 209

12. D. Rohan, et al., *Journal of Molecular Catalysis A,* 1998, **129**, 69

13. C. Guignard, et al., *Applied Catalysis A*, 2002, **234**, 79

14. S.L. Cook, in *Acetic acid and its derivatives,* V.H. Agreda, J.R Zoeller (Eds.), Marcel Dekker, New York, 1995, p. 145

15. S. Warren, *Organic Synthesis: the Disconnection Approach*, Wiley, Chichester, 1982, p. 274

5 Isotopic Studies

5.1 Introduction

In Chapter 4 it was suggested that ketene may be formed within the pores of the zeolite by the interaction of acetic anhydride with zeolite BEA, and that this ketene may be the attacking species in the acylation of anisole over zeolite BEA. However, previous research [1] has favoured a different mechanism mediated by Brønsted acidity. Further investigation was thus needed in order to probe the hypothesis that ketene might be the acylating agent.

Ketene is a very reactive molecule and it is difficult to isolate it [2]. As a consequence it was necessary to find an indirect method able to detect the role of ketene in the reaction. Thus, to test the ketene hypothesis it was decided to study the acylation reaction using deuterium-exchanged reagents. This reaction was carried out using either acetic anhydride-d_6 with anisole or acetic anhydride with anisole-d_8. Then the reaction mixture was analysed by both ^{1}H and ^{13}C NMR. The zeolite samples under investigation were H-BEA and Cu-BEA-acetate-10^{-2}M, which has been shown to be active (albeit less than H-BEA) in the acylation reaction.

The idea is that the two proposed mechanisms, Brønsted acidity and ketene, will result in products having different number of deuterium atoms. It will then be possible be possible to gain further information on the actual mechanism of the acylation by analysing the product by NMR.

Figure 5.1.1 shows what is believed to be [3] the mechanism of acylation over zeolite BEA, if catalysed by Brønsted acidity. The mechanism shown in Figure 5.2.2 is the one the author has proposed and that involves the formation of ketene and its interaction with anisole. Please note that acetic anhydride-d_6 is used in Figures 5.2.1 and 5.2.2, however the same logic applies when using anisole-d_8.
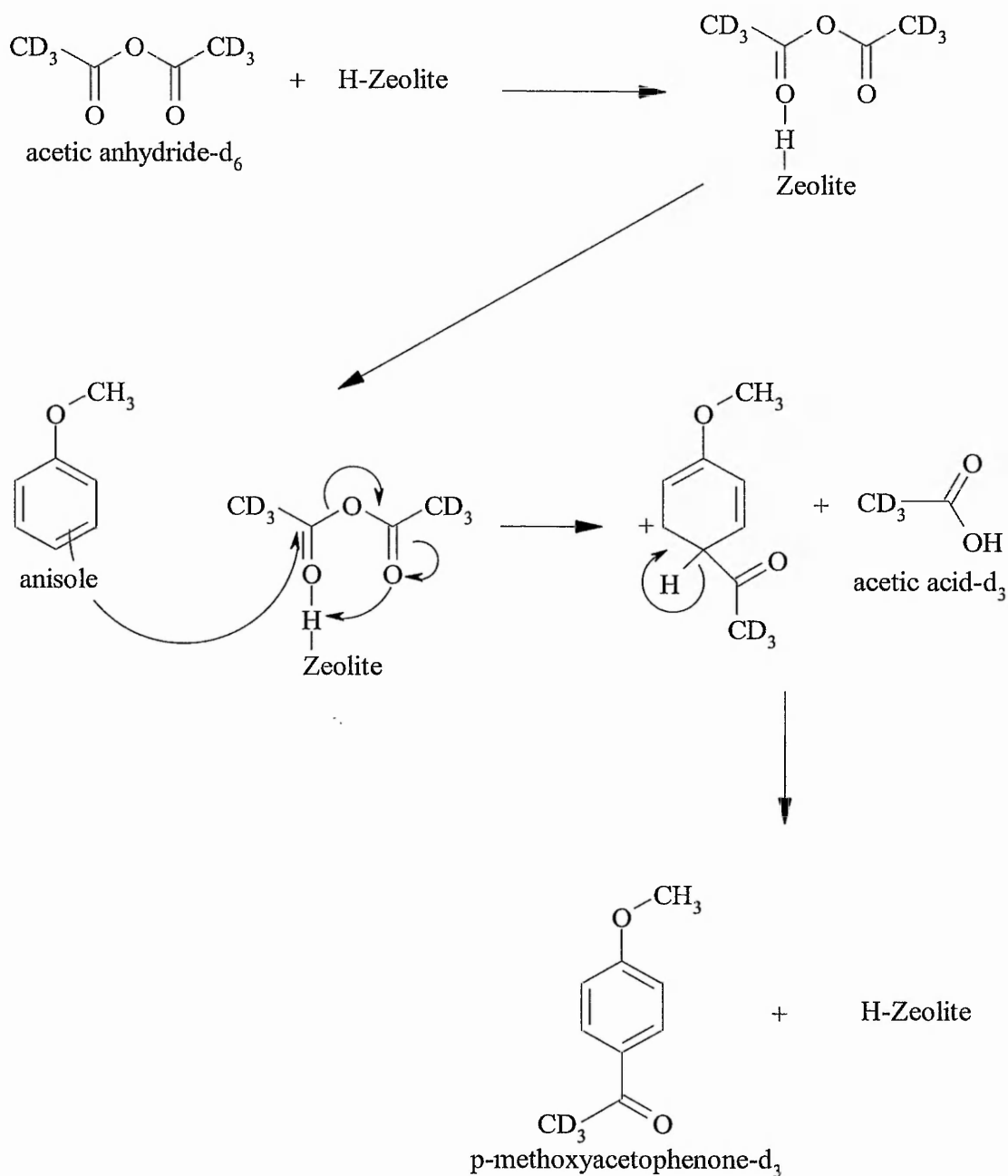
Figure 5.1.1 – The mechanism of acylation via Brønsted acid catalysis

acetic anhydride-d$_6$

zeolite BEA

acetic acid + CD$_2$=C=O
ketene-d$_2$

anisole

CD$_2$=C=O

p-methoxyacetophenone-d$_2$
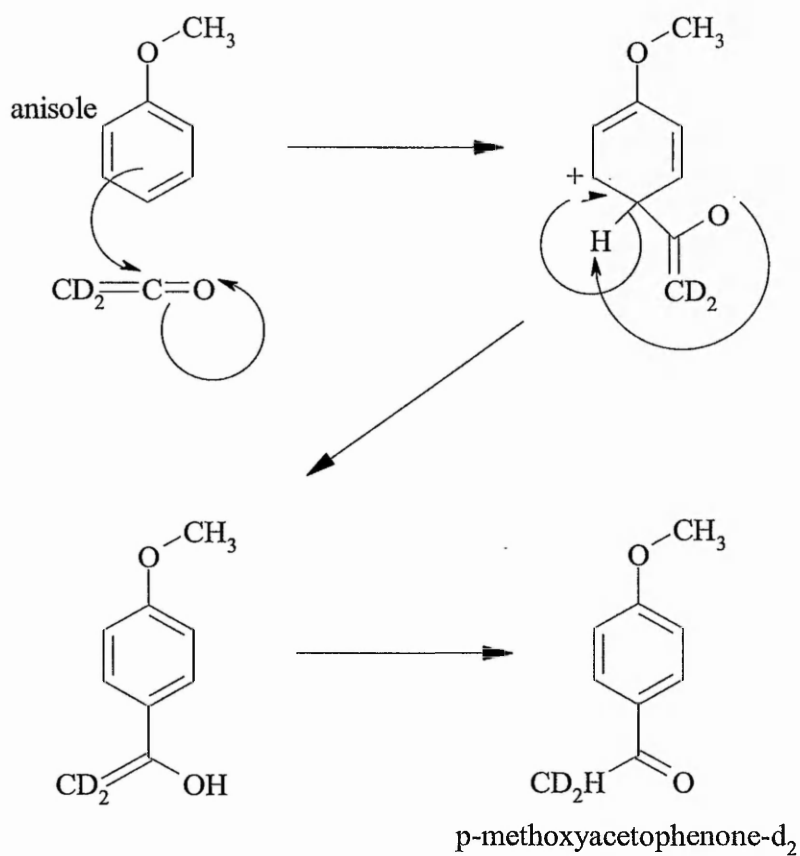
Figure 5.1.2 – The mechanism of acylation via ketene intermediate

Thus, if the acylation reaction proceeds via the Brønsted-acidity route then the product (p-MAP) would contain three deuterium atoms on the acyl group while in the case of ketene there would be only two deuterium atoms. Also, if an acylium ion were the intermediate species then the product would contain three deuteriums on the acyl group. Thus, by analysing the reaction mixture by both ^{1}H and ^{13}C NMR it should be possible to distinguish between the two mechanisms.

The same logic applies if one uses anisole-d_8 and acetic anhydride. In this case the Brønsted route would result in an acyl group on p-MAP having three hydrogens, while the ketene route would result in two hydrogens and one deuterium on the same group.

However, before starting the experiments with the isotopic reagents, it is necessary to ensure that there is no exchange of deuteriums and hydrogens upon interaction of acetic anhydride-d_6 with zeolite BEA (e.g. H-BEA). This can be achieved by studying the hydrolysis of acetic anhydride-d_6 with H_2O over H-BEA and analysing the product by NMR. The same question can also be studied by using acetic anhydride and D_2O, since H-BEA has been shown to readily exchange its hydrogens for deuteriums [4]. The results are presented in Section 5.2.

As mentioned in Chapter 2, the chemical shifts of the methoxy groups, $-O-CH_3$, in anisole and p-MAP switch positions on going from pure substance to reaction mixture. The methoxy group chemical shift observed for pure anisole is 3.84 ppm and for pure p-MAP is 3.74 ppm. However, in the case of a solution of acetic anhydride, anisole and p-MAP, the chemical shift for anisole is 3.78 ppm and for p-MAP is 3.83 ppm. This phenomenon has been studied and will be discussed in more detail in Section 5.5, below.

5.2 Hydrolysis of acetic anhydride

Before studying the hydrolysis of acetic anhydride with D_2O over H-BEA, a series of experiments were performed to prove that H-BEA indeed catalyses the hydrolysis of acetic anhydride with H_2O to give acetic acid. These hydrolysis experiments were performed at 298 K, since at 333 K (i.e. the same temperature as the acylation reaction) the reaction quickly develops heat and vapour thus breaking the reaction vessel. Two experiments were performed either with H-BEA or without catalyst, see Figure 5.2.1. In the case of H-BEA, the hydrolysis reaches completion within 5 minutes. In the case of the hydrolysis without catalyst, the curve shows an induction period up to 30 minutes, then the rate of reaction increases and the reaction reaches completion at ca 60 minutes. The induction effect is probably related to the formation of acetic acid [5]. As the hydrolysis takes place, the acetic acid tends to act as a co-solvent, which allows more anhydride to dissolve. The effect of increased solubility, rising temperature, and perhaps the catalytic effect of the forming acid combine to cause an exponential increase in the reaction rate.
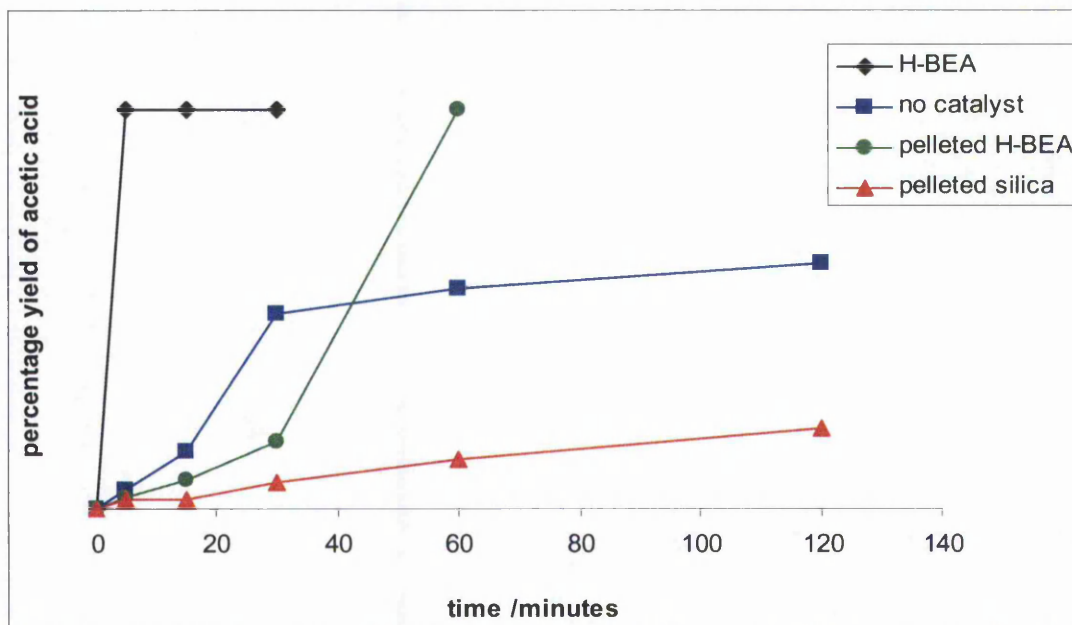
Figure 5.2.1 – Hydrolysis of acetic anhydride with H_2O at 298 K

Two additional experiments were performed using either H-BEA particles pelleted to 500-600 microns size or inert fumed silica with the same particle size range. This to elucidate if simple mechanical action of the dissolved particles could account for any

120

increase in activity of H-BEA in the hydrolysis of acetic anhydride. The results (see Figure 5.2.1) show that the hydrolysis with both samples does not reach completion within 2 hours. The higher activity of pelleted H-BEA in contrast with pelleted silica shows that the increase in activity is not simply due to mechanical action.

These results show that the hydrolysis with H-BEA of acetic anhydride is indeed catalysed by H-BEA. Figure 5.2.1 also shows that neither acetic anhydride nor acetic acid poison H-BEA (in its powder form), since the reaction reaches completion.

Once proven that H-BEA indeed catalyses the hydrolysis of acetic anhydride, an experiment was run by using acetic anhydride and D_2O over H-BEA. The resulting mixture was then analysed by ^1H and ^{13}C NMR to detect any possible exchange of deuteriums between D_2O and acetic anhydride or acetic acid. The resulting ^1H NMR spectrum is shown in Figure 5.2.2 and the ^{13}C NMR spectrum in Figure 5.2.3.
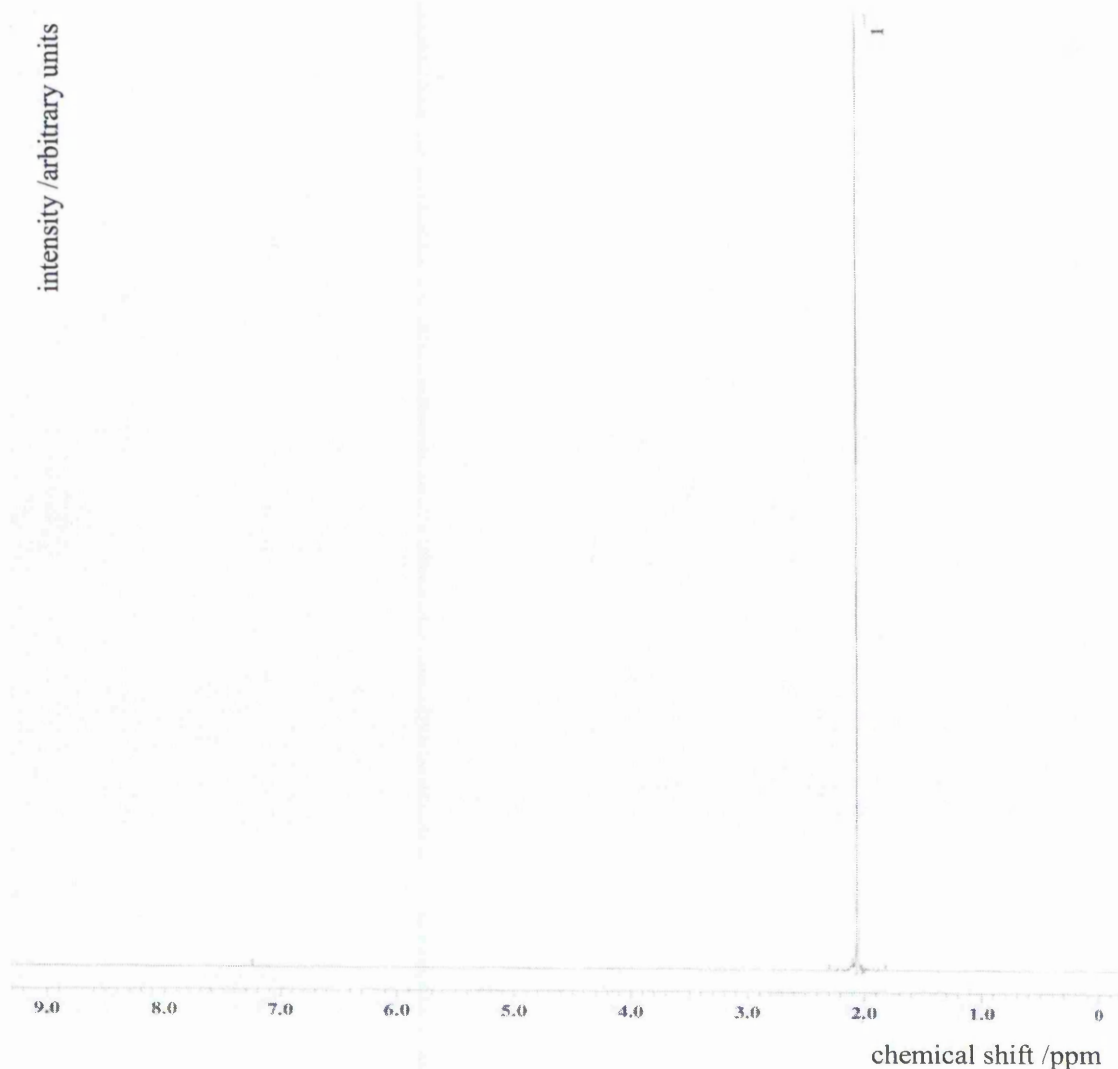
Figure 5.2.2 – The ^1H NMR spectrum of the products of hydrolysis of acetic anhydride with D_2O catalysed by H-BEA at 298 K

The proton NMR spectrum shows a single peak at ca 2.05 ppm, which is due to the methyl group of acetic acid. If any acetic anhydride were present, its methyl group would be expected to give a signal at ca 2.2 ppm. Note that all the NMR assignments in this Chapter were made from measurements performed on the pure compounds (see Chapter 2 Section 2.9.3). This result confirms the observation that the reaction has reached 100% yield, i.e. all of the acetic anhydride has been converted into acetic acid.

200.0 190.0 180.0 170.0 160.0 150.0 140.0 130.0 120.0 110.0 100.0 90.0 80.0 70.0 60.0 50.0 40.0 30.0 20.0 10.0 0

chemical shift /ppm
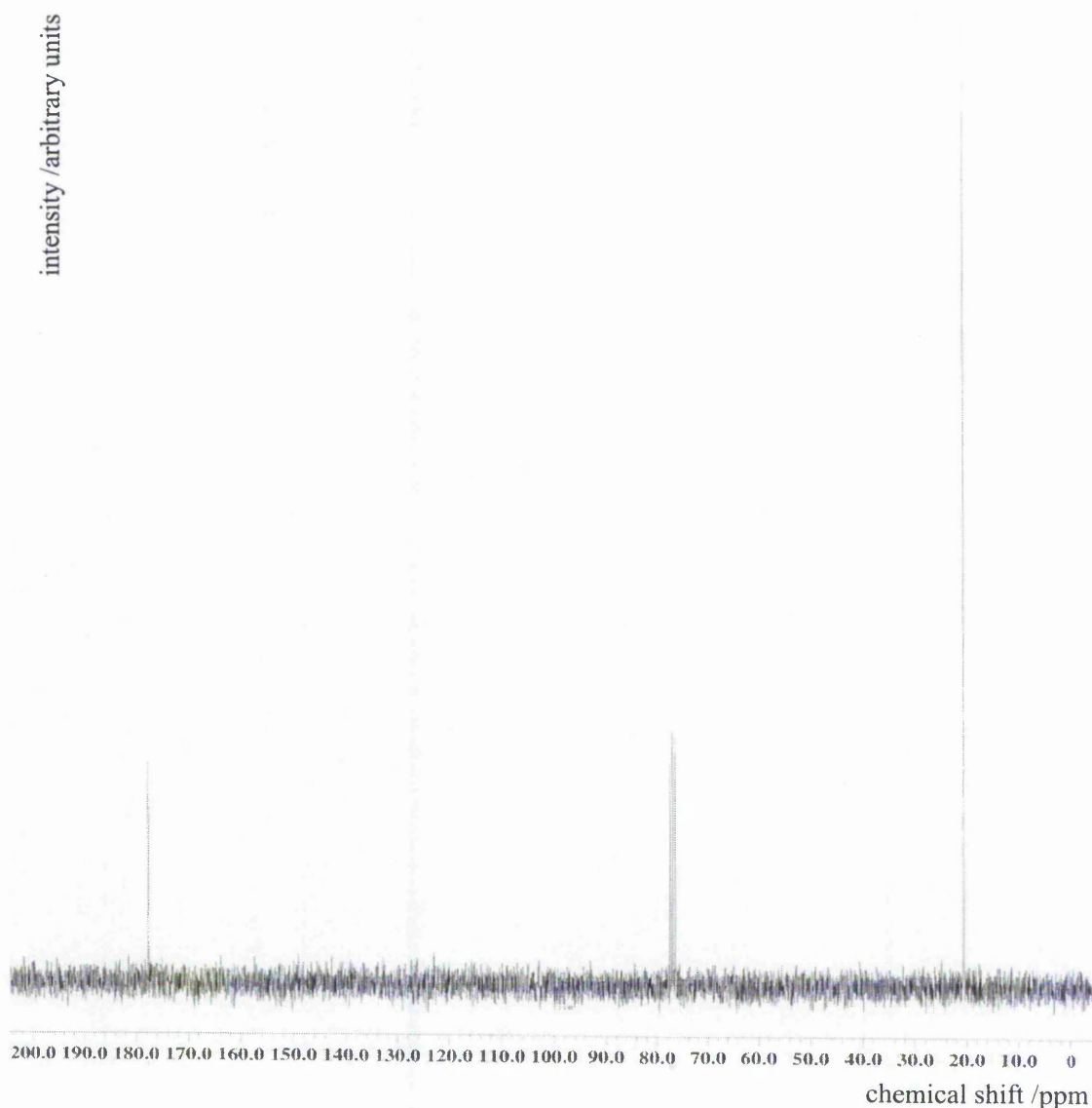
Figure 5.2.3 – The ^{13}C NMR spectrum of the products of hydrolysis of acetic anhydride with D$_2$O catalysed by H-BEA at 298 K

The ^{13}C NMR spectrum presents three signals at ca 21 ppm, 77 ppm, and 178 ppm. The signal at 77 ppm is due to the solvent, $CDCl_3$. Detailed examination of this peak at 77 ppm shows that it is split into a triplet, with three peaks of equal integrated intensity. This splitting of the NMR signal is due to the deuterium atom coupling with the carbon [6]. Coupling is an effect due to nearby nuclei with non-zero spin (e.g. deuterium) affecting the magnetic environment of the nucleus under observation (e.g. carbon). Deuterium has a spin I = 1, which means that there are three possible energy levels for a deuterium atom placed in a magnetic field. The carbon atom therefore experiences three slightly different magnetic fields depending upon the spin state of the deuterium nucleus to which it is attached. Since the difference in energy between the three states is very small, there is an essentially equal probability that a carbon atom will be bonded to a deuterium in any one of the three states. The result is that the carbon nucleus comes into resonance at three frequencies with equal probability (i.e. intensity), as in the case of $CDCl_3$. The peak at 21 ppm is the signal due to the carbon in the methyl group of acetic acid, and the signal at 178 ppm is due to the carbonyl carbon of acetic acid.

The absence of any peak due to acetic anhydride, expected at 22 ppm and 166 ppm, again confirms that the hydrolysis reaction reached 100% conversion.

The fact that the peak at 21 ppm is not split shows that the methyl group has no deuterium on it. This result means that there is no significant exchange of hydrogen and deuterium atoms between D_2O (and zeolite BEA) and the methyl groups on either acetic anhydride or acetic acid. Thus, it can be inferred that this would be the case also when ketene is formed by the interaction of acetic anhydride with zeolite BEA. However, it should be noted that, because of aforementioned safety reasons, the hydrolysis was carried out at 298 K while the acylation reaction is carried out at 333 K.

5.3 Acylation with isotopic reagents

The acylation reaction was first carried out with acetic anhydride and anisole over H-BEA. This reaction and the subsequent ones were run for 24 hours, after which the reaction mixture was analysed by NMR. Figure 5.3.1 shows the ^{1}H NMR spectrum and Figure 5.3.2 shows the ^{13}C NMR spectrum of the resulting mixture.
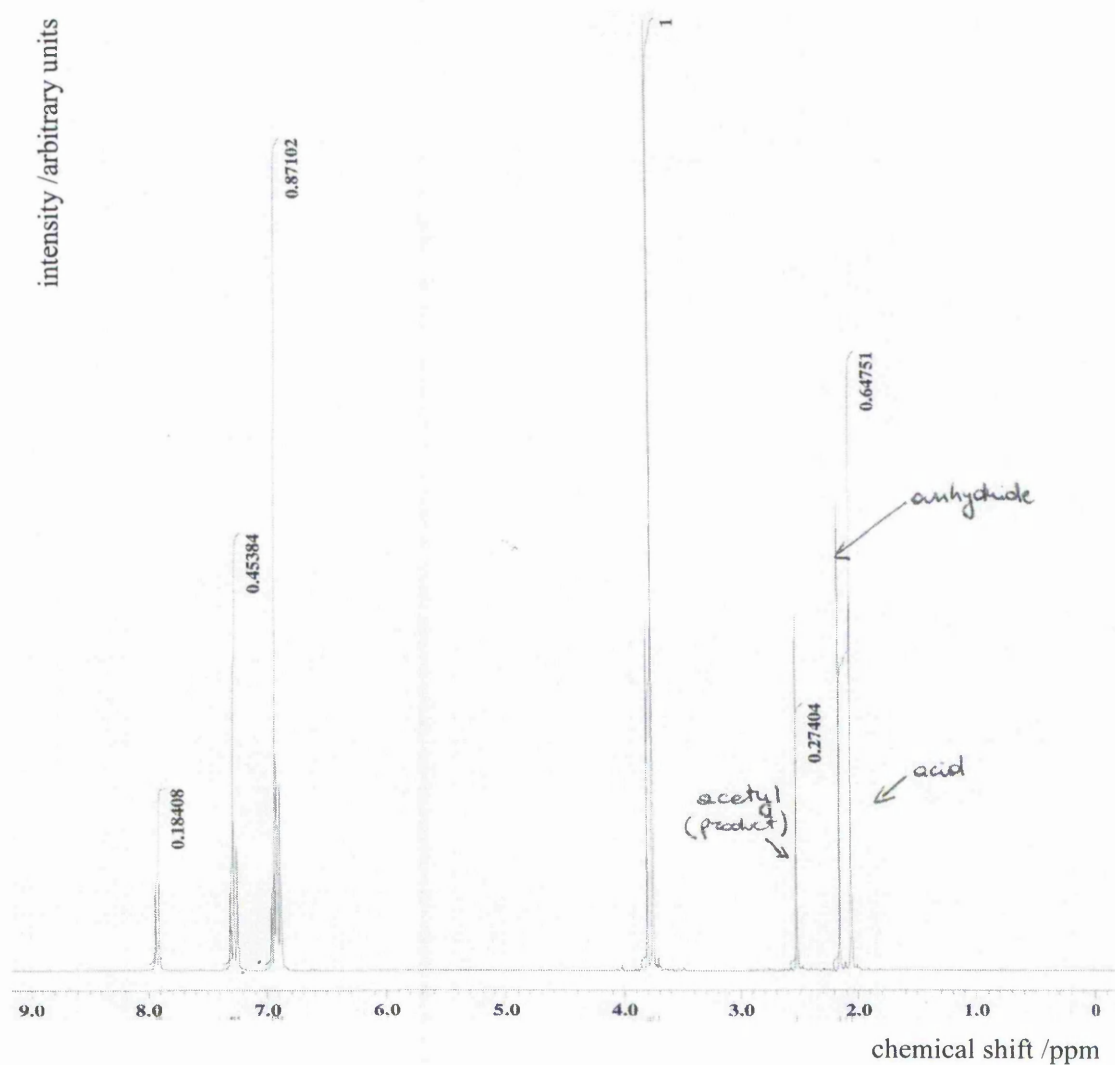
Figure 5.3.1 – The ^{1}H NMR spectrum of the products of acylation without deuterium-exchanged reagents over H-BEA

In the ^{1}H spectrum, the peak at 2.06 ppm is due to the methyl group of acetic acid, the one at 2.16 ppm is due to the two methyl groups of acetic anhydride, and the peak at 2.52 ppm is due to the acetyl group of p-MAP, the product of the reaction. Going

downfield, the next two peaks are due to the methoxy groups on anisole at 3.76 ppm and p-MAP at 3.80 ppm. Further downfield, the three peaks in the region 6 to 9 ppm are due to the hydrogen atoms present in the aromatic ring of both anisole and p-MAP. The peak at ca 6.9 ppm is due to both anisole and p-MAP, the one at ca 7.3 ppm is split into a triplet and is due to anisole, and the peak at ca 7.9 ppm is split into a doublet and is due to p-MAP.

In the ^{13}C NMR spectrum, the peaks at ca 20, 22 an 26 ppm are due, respectively, to the sp3 carbon atoms of acetic acid, acetic anhydride and the acetyl group of p-MAP. The two peaks at ca 55 ppm are due to the sp^3 carbon of the methoxy groups of both anisole and p-MAP, the smaller peak is probably due to p-MAP. The next peak at ca 77 ppm is due to CDCl$_3$ and is split into a triplet because of the already mentioned carbon-deuterium coupling. The peaks in the region 110 to 135 ppm are the signals from the sp^2 carbon atoms of the aromatic rings of both anisole and p-MAP. The peaks at 159 and 163 ppm are due to the carbons on the aromatic ring that bonds directly to the methoxy groups of anisole and p-MAP respectively. The peak at 166 ppm is due to the two sp^2 carbon of acetic anhydride. The peak at 177 ppm is the signal from the sp^2 carbon of acetic acid. The last peak at ca 197 ppm is the signal of the sp^2 carbon on the acetyl group of p-MAP.
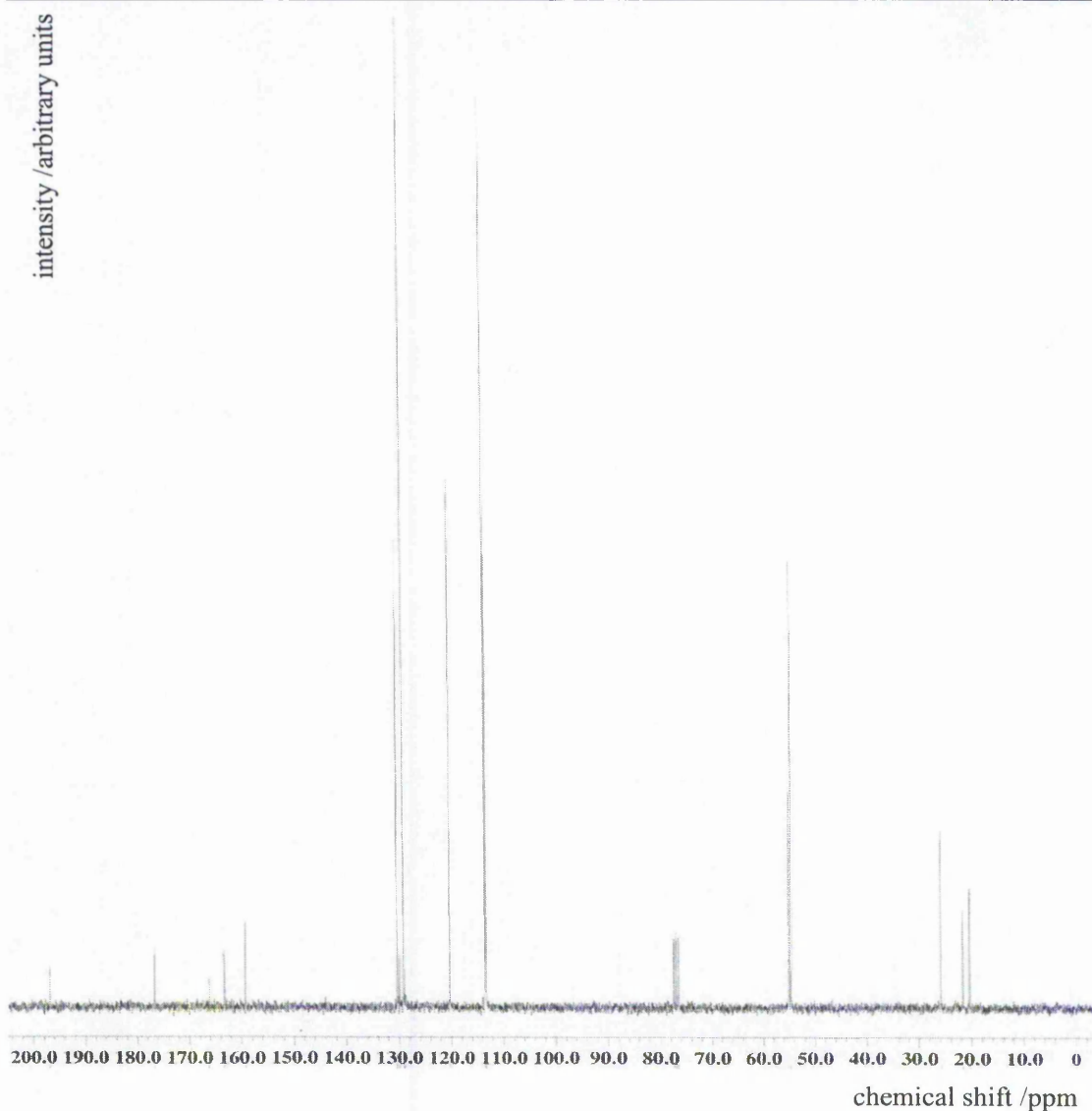
Figure 5.3.2 –The ^{13}C NMR spectrum of the products of acylation without deuterium-exchanged reagents over H-BEA

Figure 5.3.3 shows the proton NMR spectrum of the products of the reaction of acetic anhydride-d$_6$ with anisole over H-BEA. The peaks due to the methyl groups of acetic acid (2.06 ppm), acetic anhydride (2.18 ppm) and the acetyl group on p-MAP (2.52 ppm) are absent because these methyl groups are fully substituted with deuterium atoms. The peak due to the methoxy group of anisole is the largest of the spectrum at 3.80 ppm, while the peak due to the methoxy group on the product (p-MAP) is much smaller at 3.85 ppm. These results show that p-MAP is formed and all of the product acyl groups contain three deuterium atoms.
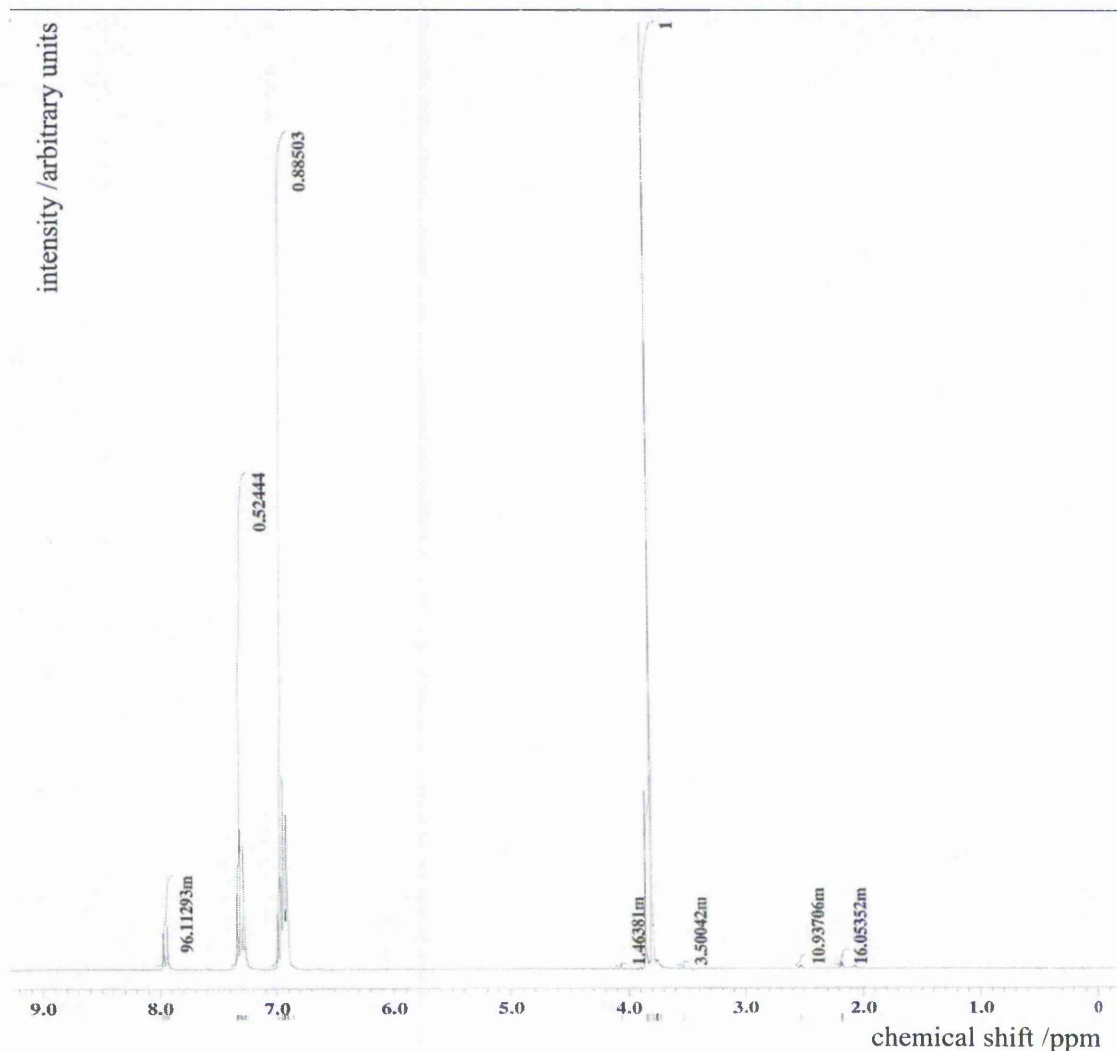
Figure 5.3.3 - ^{1}H spectrum of the products of acylation with acetic anhydride-d$_6$ over H-BEA

These observations seem to be confirmed by the ^{13}C NMR spectrum shown in Figure 5.3.4. The region between 0 and 50 ppm is devoid of any peak, probably because of multiple splitting of the signals due to the presence of deuterium atoms bonded to the carbon atoms of the methyl groups of acetic acid, acetic anhydride and p-MAP. When splitting a signal the intensity is divided among each peak thus decreasing the height of each resulting line. Since coupling to three deuteriums would split a carbon signal into seven lines and the signals in question are quite weak as compared to others further downfield (see Figure 5.3.2), it is possible that these signals had decreased so much in intensity as to be indistinguishable from the baseline noise. Thus, the absence of the three signals could be an indication that the carbon atoms of the methyl groups of acetic acid, acetic anhydride and p-MAP are each bonded to three deuteriums.
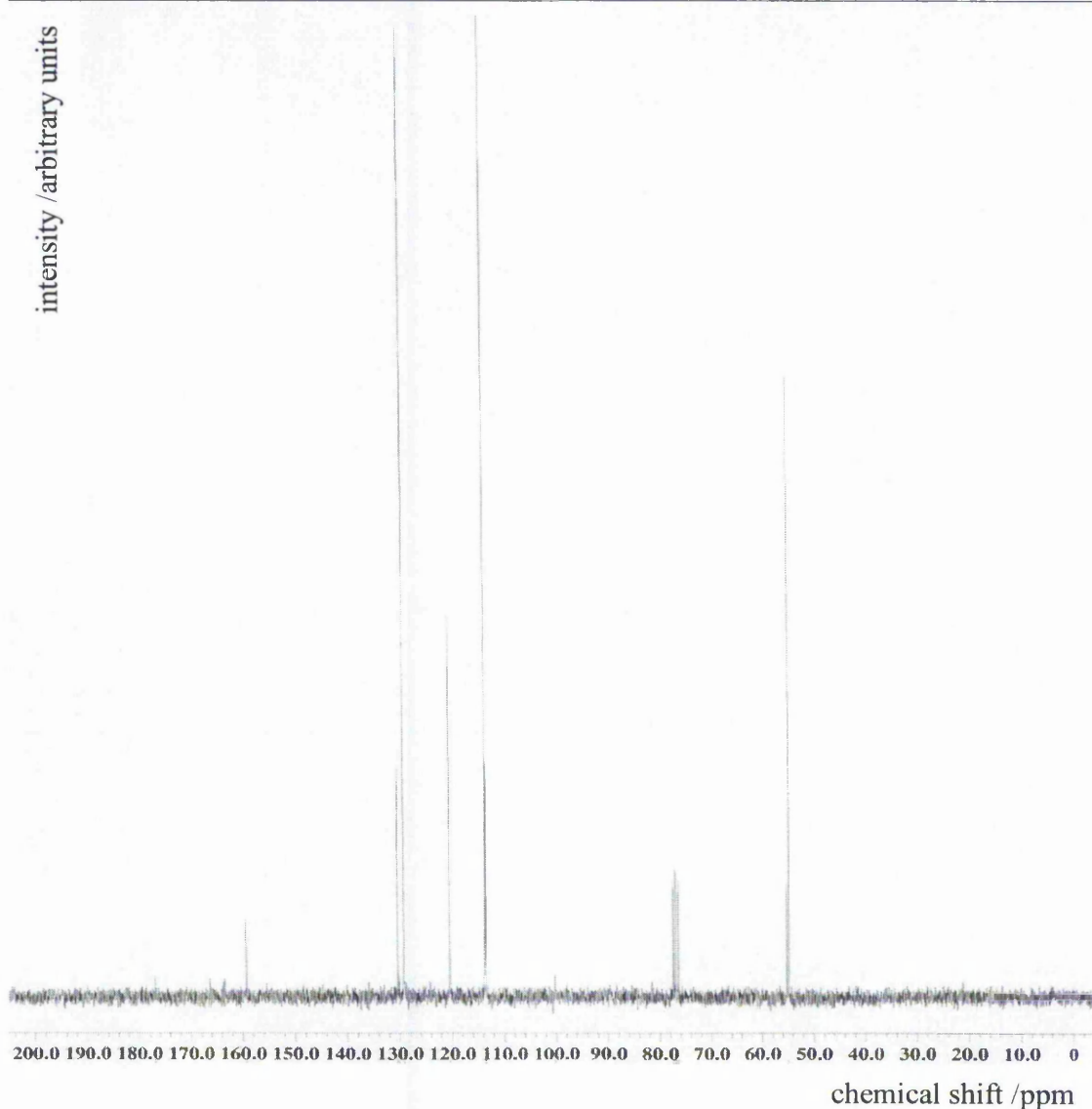
Figure 5.3.4 - ^{13}C spectrum of the products of acylation with acetic anhydride-d$_6$ over H-BEA

The ^{1}H and ^{13}C NMR spectra shown in Figure 5.3.5 and 5.3.6 respectively, are the results of the acylation of anisole-d$_8$ with acetic anhydride over H-BEA. In the proton spectrum, there is a peak at 2.03 ppm due to the methyl group of acetic acid, one at 2.13 ppm due to acetic anhydride and another one at 2.50 ppm due to the product, p-MAP. Further downfield there are no peaks present, as both the methoxy group and the aromatic ring on both anisole and p-MAP are fully substituted with deuterium atoms.
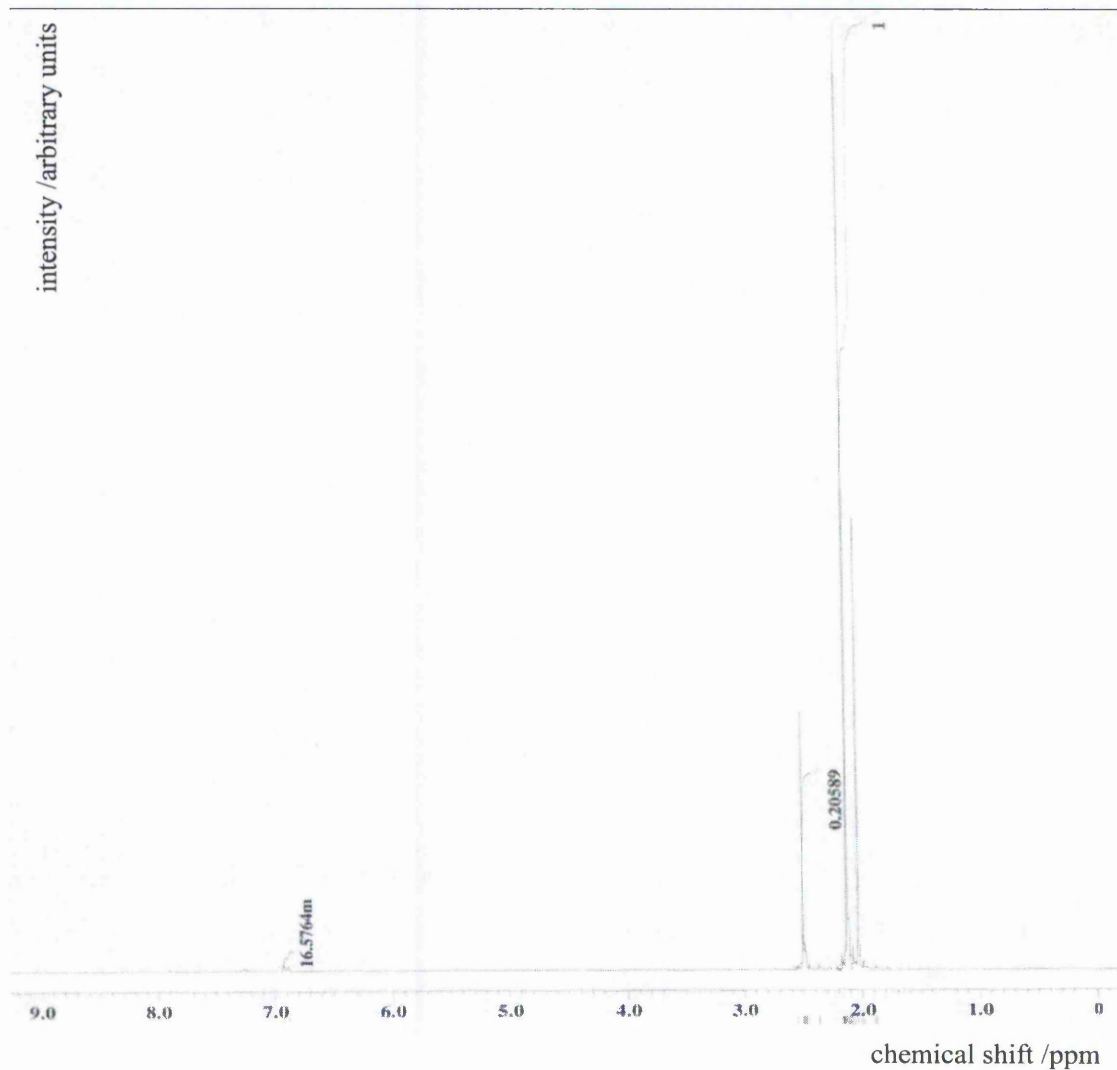
Figure 5.3.5 - ^{1}H spectrum of the products of acylation with anisole-d_8 over H-BEA

The ^{13}C NMR spectrum shown in Figure 5.3.6 confirms the results for the ^{1}H NMR spectrum. All the three peaks in the region 20 to 30 ppm are singlets, indicating that neither acetic acid nor acetic anhydride nor the acyl group on p-MAP have deuterium atoms present. The peak due to the methoxy group on both anisole and p-MAP is split into seven lines due to coupling with three deuterium atoms.
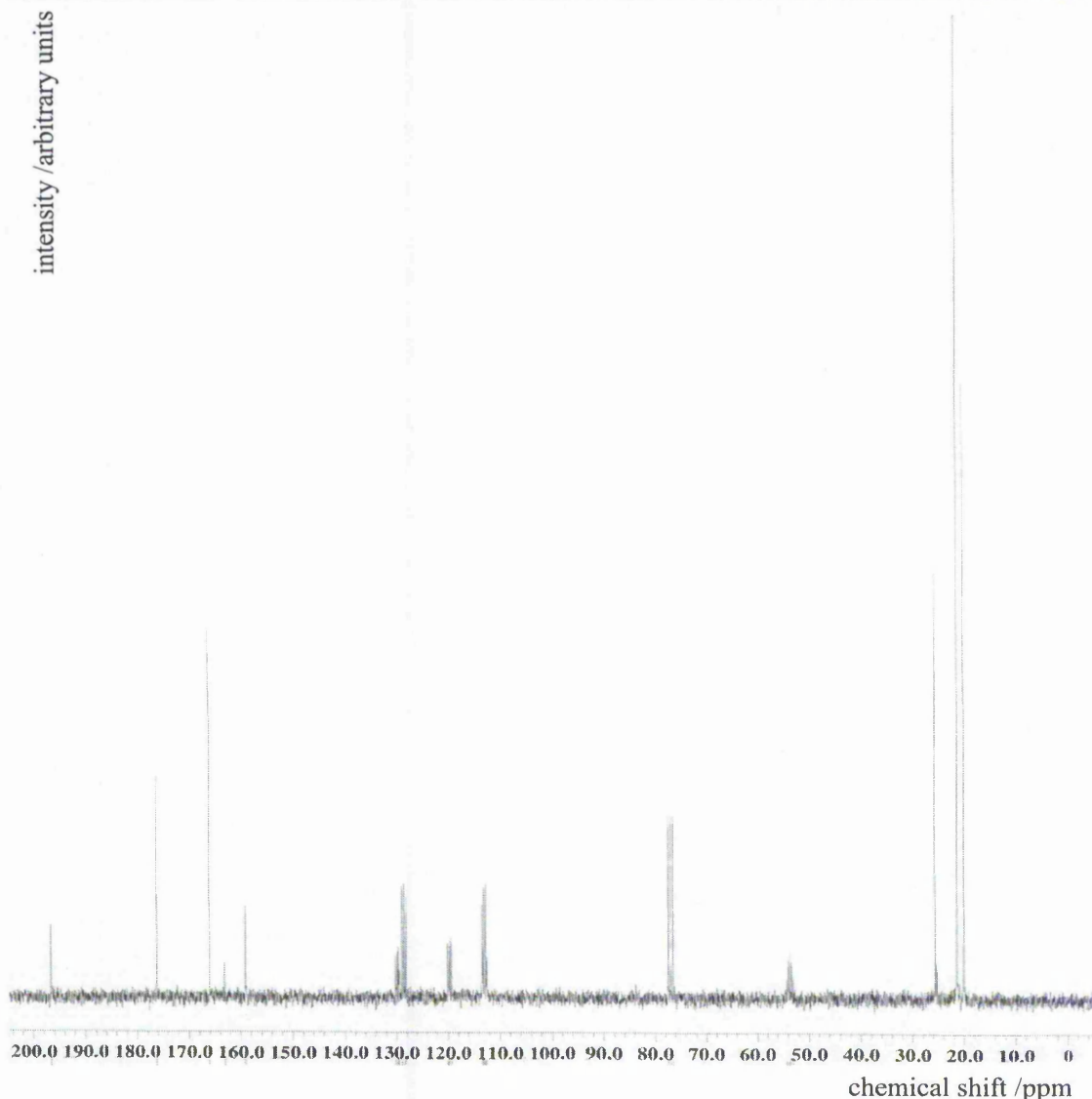
Figure 5.3.6 - ^{13}C spectrum of the products of acylation with anisole-d$_8$ over H-BEA

Up to this point, experiments in this Section have focused on the acylation as catalysed by H-BEA. However, transition metal exchanged BEA zeolites (e.g. Cu-BEA) have been shown to be active in the acylation of anisole. And comparison of the results for H-BEA with a transition metal exchanged BEA zeolite could provide additional information on the mechanism of acylation. Thus, a further reaction was carried out with acetic anhydride-d$_6$ and anisole over Cu-BEA-acetate-10^{-2}M. The spectra are shown in Figure 5.3.7 and 5.3.8 for ^1H NMR and ^{13}C NMR respectively. The ^1H spectrum resembles the one in Figure 5.3.3. It shows that p-MAP is formed (peak at 3.83 ppm) and that the acyl group on p-MAP is fully substituted with deuterium atoms. Again, the ^{13}C spectrum closely resembles the one in Figure 5.4.4. It shows that the

region between 0 and 50 ppm is devoid of any peak, probably because of multiple splitting of the signals due to the presence on deuterium atoms on those carbon atoms.
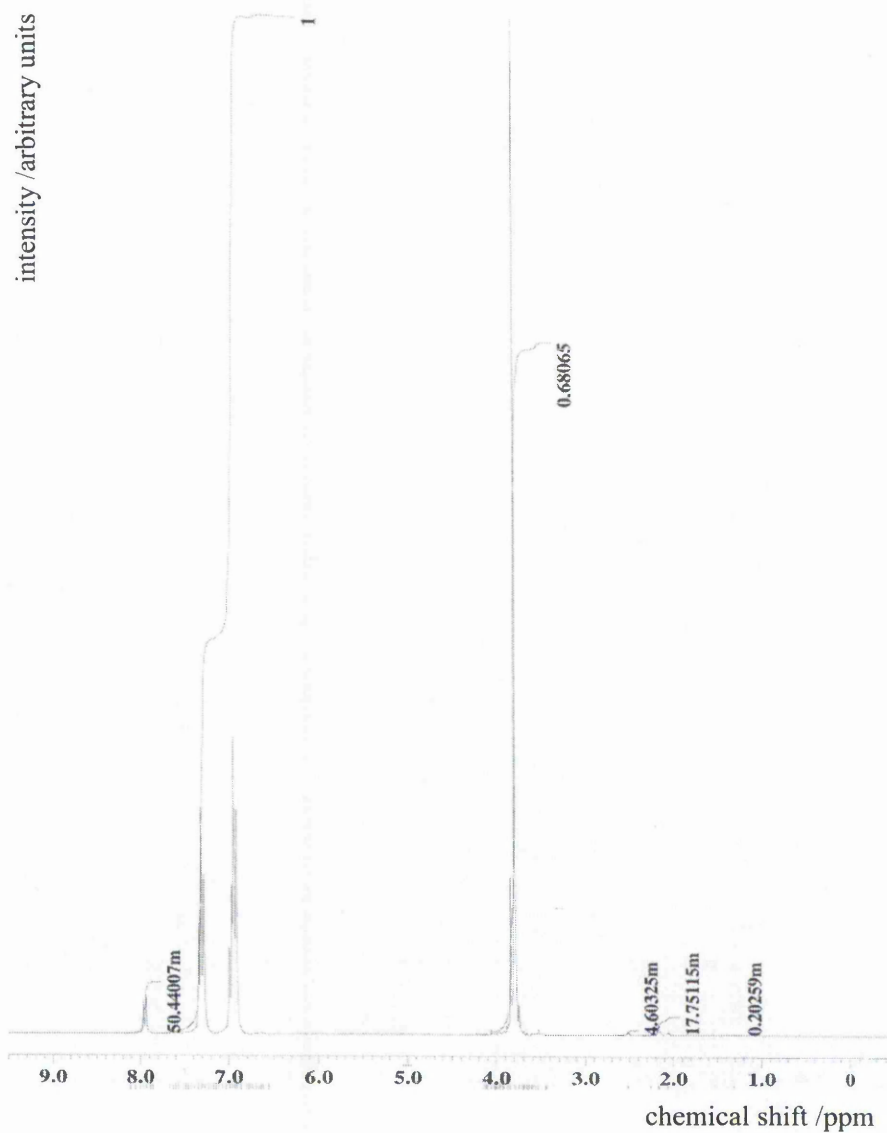
Figure 5.3.7 – ^{1}H spectrum of the products of acylation with acetic anhydride-d$_6$ over Cu-BEA- acetate-10^{-2}M
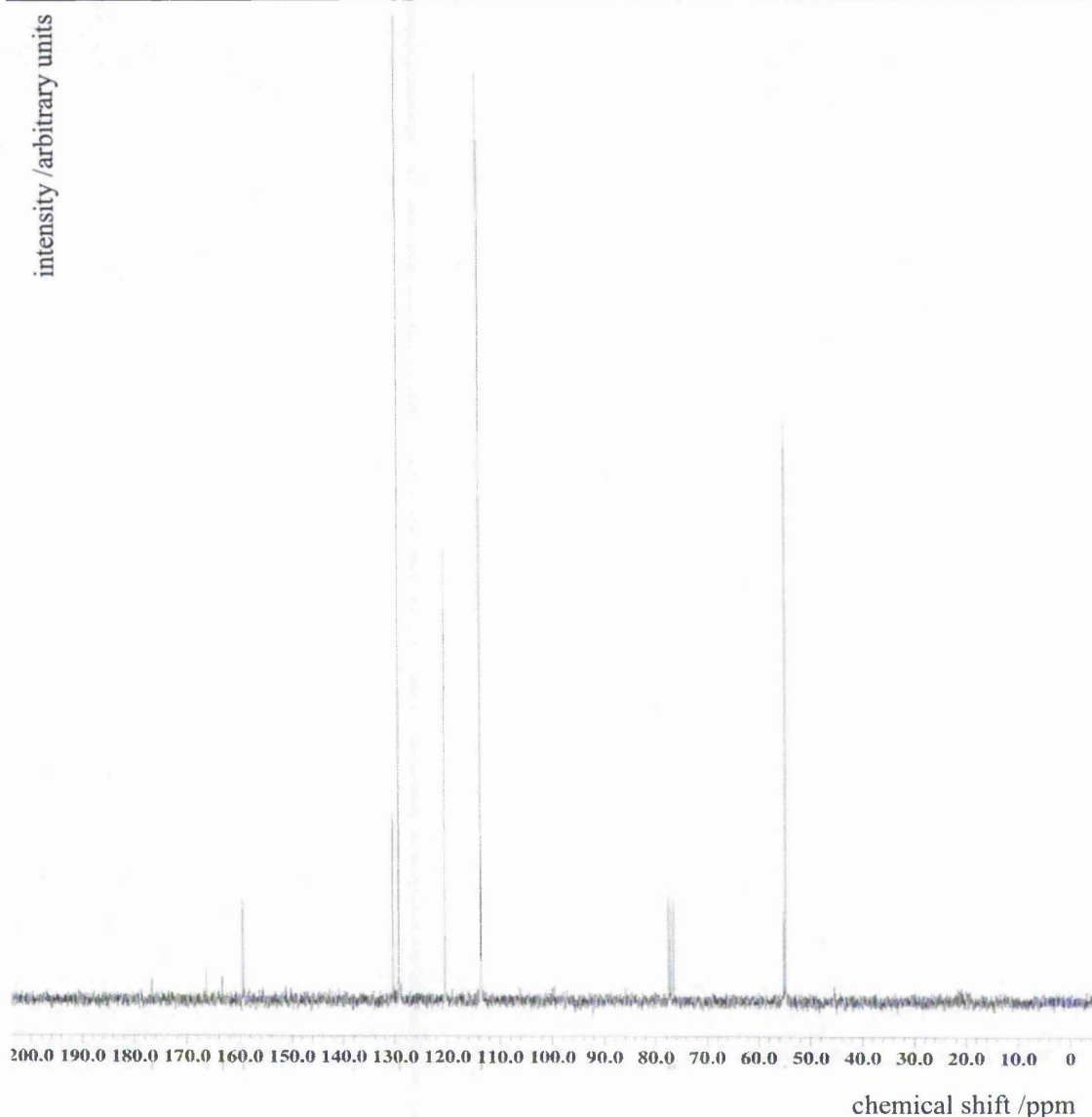
Figure 5.3.8 – ^{13}C spectrum of the products of acylation with acetic anhydride-d_6
over Cu-BEA- acetate-$10^{-2}M$

Since the ^1H NMR spectra are quantitative, it is possible to gain information on the yield of the various reactions after 24 hours. The percentage yield of the acylation reaction based on the conversion of anisole is calculated from the ^1H NMR spectrum by integrating the signals of the methoxy groups of anisole and p-MAP and using the following equation:

$$\%yield_{p-MAP} = \frac{integral\ methoxy_{p-MAP}}{integral\ methoxy_{p-MAP} + integral\ methoxy_{anisole}} \cdot 100 \qquad (5.3.1)$$

Equation 5.3.1 is based on the assumption that all of the anisole present in the starting mixture has either reacted to form p-MAP or has remained intact.

In the case of the reaction with anisole-d_8, the signals from the methoxy groups are absent because of coupling with deuteriums. Instead, it is possible to use the values of the integral of the signal of the two methyl peaks of acetic anhydride (divided by 2) and the integral of the signal of the acetyl group of p-MAP and then apply the following equation:

$$\%\text{yield}_{\text{p-MAP}} = \frac{\text{integral acetyl}_{\text{p-MAP}}}{\text{integral acetyl}_{\text{p-MAP}} + (\text{integral methyl}_{\text{anisole}} / 2)} \cdot 100/2 \qquad (5.3.2)$$

In Equation 5.3.2 it is assumed that all of the initial acetic anhydride has either reacted to give p-MAP or remained intact in solution. The resulting percentage yield value is based on the conversion of acetic anhydride and it is then divided by two to give the percentage yield based on the conversion of anisole, since the number of moles of acetic anhydride in the starting mixture is half the moles of anisole. The results are summarised in Table 5.3.1. Note that the experiments were only done once.

Table 5.3.1

Reaction	Percentage yield of reaction after 24 hours	
	methoxy	acetyl
Acetic anhydride and anisole over H-BEA	26.7	30.0
Acetic anhydride-d_6 and anisole over H-BEA	15.8	N/A
Anisole-d_8 and acetic anhydride over H-BEA	N/A	17.4
Acetic anhydride-d_6 and anisole over Cu-BEA- acetate-10^{-2}M	13.0	N/A

The results in Table 5.3.1 show that the acylation of anisole with acetic anhydride over H-BEA gives higher yield then the same reaction using acetic anhydride-d_6. In turn, the acylation of anisole with acetic anhydride-d_6 over H-BEA gives higher yield than the same reaction over Cu-BEA-acetate-10^{-2}M. In the case of the reaction without isotopic

exchanged reagents, the percentage yield calculated integrating the peaks of the methoxy groups of anisole and p-MAP is lower than the percentage yield calculated using the acetyl and methyl peaks of p-MAP and acetic anhydride respectively.

5.4 Conclusions

The results in Section 5.2 show that H-BEA catalyses the hydrolysis of acetic anhydride with H_2O. The reaction reaches completion (see Figure 5.2.1) and this is an indication that neither acetic anhydride nor acetic acid poison the catalyst. Then the hydrolysis was carried out with acetic anhydride and D_2O over H-BEA. The ^1H NMR spectrum in Figure 5.2.2 confirms that all acetic anhydride has been converted into acetic acid. The ^{13}C NMR spectrum in Figure 5.2.3 again confirms that only acetic acid is present. The signal of the methyl carbon of acetic acid at 21 ppm is not split. This shows that there is no exchange of deuterium atoms into the methyl group of acetic acid. From this, it is deduced that when acetic anhydride interacts with deuterated H-BEA it produces ketene. Conversely, when acetic anhydride-d_6 interacts with H-BEA it produces ketene-d_2.

The results for the acylation reaction over H-BEA without isotopic regents (Figure 5.3.1) show that the product, p-MAP, is formed (e.g. acetyl peak at 2.52 ppm) together with acetic acid (methyl peak at 2.06 ppm). The ratio between the integrals of the signals at 2.06 ppm and 2.52 ppm is about 1.06. This indicates that for each mole of product about one mole of acetic acid is produced, as expected from the reaction stoichiometry. However, the ratio between acetic anhydride and anisole is about 0.25. The ^{13}C NMR spectrum in Figure 5.3.2 again shows that p-MAP and acetic acid are produced in the reaction.

The ^1H NMR spectrum for the acylation with acetic anhydride-d_6 over H-BEA is shown in Figure 5.3.3. In this case the region 1 to 3 ppm is devoid of any significant peak because of deuterium exchange. However the signals due to the methoxy groups of anisole (3.80 ppm) and p-MAP (3.85 ppm) are present and show that again p-MAP is produced in the reaction. In the ^{13}C NMR spectrum (Figure 5.3.4) the region between 0 and 50 ppm is devoid of any peak. This is probably due to deuterium atoms splitting the signals of the sp^3 carbons of acetic anhydride, acetic acid and p-MAP.

Figure 5.3.5 shows the ^1H NMR spectrum of the acylation with anisole-d_8 over H-BEA. The peak at 2.50 ppm is the acetyl group of p-MAP and shows that a product is formed. The ^{13}C NMR spectrum (Figure 5.3.6) shows multiple splitting in the region 50 to 140 ppm of the carbon signals coupled with deuteriums. Comparison with Figure 5.3.2 shows how multiple splitting of a signal markedly reduces the height of the resulting

lines. This seems to confirm the observations regarding the ^{13}C NMR spectrum in Figure 5.3.4.

The proton and carbon NMR spectra for the acylation with acetic anhydride-d$_6$ over Cu-BEA-acetate-10^{-2}M are shown in Figures 5.4.7 and 5.4.8, respectively. These spectra have features identical to the ones in Figures 5.3.3 and 5.3.4 and show that p-MAP again is formed and it has three deuterium atoms on its acetyl group.

The results of the acylation reaction using isotopic-exchanged reagents show that the product formed p-MAP is not the result of a reaction between ketene and anisole. In the acylation over both H-BEA and Cu-BEA-acetate-10^{-2}M, the species attaching to the aromatic ring of anisole contains a methyl group. This species containing a methyl group could be an acyl ion such as in the classical Friedel Crafts acylation with AlCl$_3$ [7].

There are two possible explanations to interpret the results presented in this Chapter. One is that ketene is indeed formed during the acylation reaction over H-BEA but it is merely a by-product of the decomposition of acetic anhydride and does not take part in the reaction (i.e. it is a spectator species). The second explanation is that ketene is not formed at all during the acylation reaction. However this explanation would seem in contrast with the results of the adsorption experiments presented in Chapter 4. The reason for this is that the acylation reaction is carried out in the liquid phase while the adsorption experiments were performed in the gas phase with adsorption pressures of only a few millibars. Thus, the conditions that were favourable for the formation of ketene in the adsorption experiments are not the same conditions that are present during the acylation reaction. Hence ketene is formed in the adsorption experiments but not in the acylation of anisole with acetic anhydride over zeolite BEA. In this case the active species could be acylium-like.

5.5 Appendix: the chemical shifts of anisole and p-MAP

Analysis of ^{1}H NMR spectra for both pure substances and mixtures has shown that the peaks due to -O-CH$_3$ in anisole and p-MAP switch positions in going from pure substance to reaction mixture. The methoxy group chemical shift observed for pure anisole is 3.84 ppm and for pure p-MAP is 3.74 ppm. However, in the case of a solution of acetic anhydride, anisole and p-MAP (such as in the case of the acylation reaction mixture), the chemical shift for anisole is 3.78 ppm and for p-MAP is 3.83 ppm. To further investigate this phenomenon and any significance it could have on the analysis of the acylation data, a series of mixtures with known amounts of anisole, p-MAP and acetic anhydride were prepared and analysed by NMR.

Figure 5.5.1 illustrates the values of the proton NMR chemical shifts of the methoxy group of anisole and p-MAP at different concentrations. Figure 5.5.2 illustrates the results for a series of mixtures of acetic anhydride, anisole and p-MAP.

Comparison between the integral value of the acetyl peak due to p-MAP at ca 2.5 ppm and the integrals of the two peaks at about 3.7 to 3.9 ppm allows to distinguish between the signal due to the methoxy group of anisole and the one due to p-MAP.
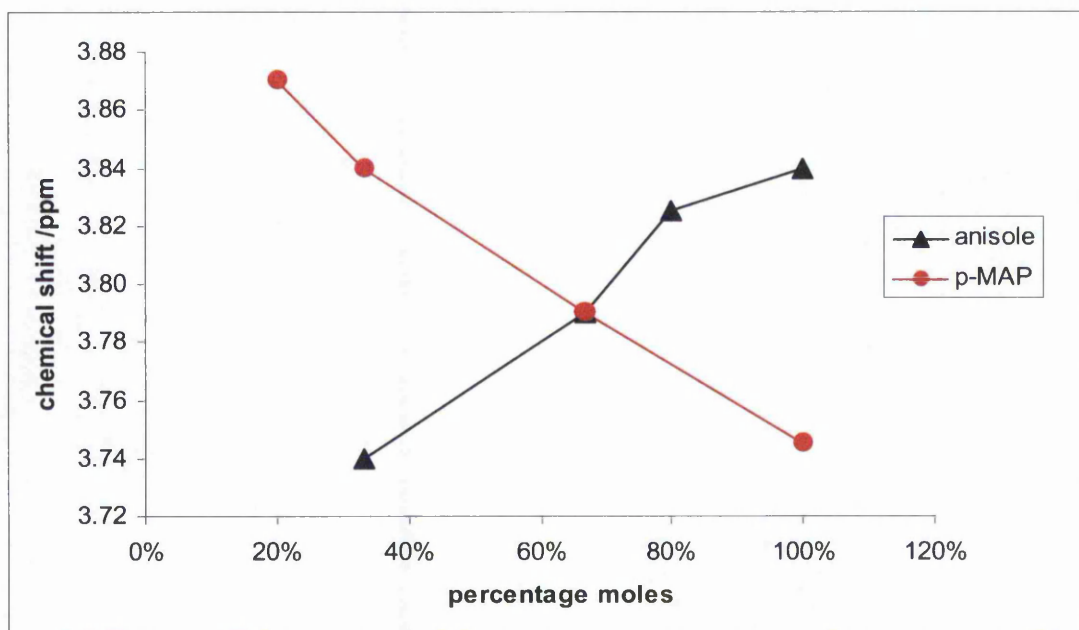
Figure 5.5.1 – Binary mixture, anisole and p-MAP
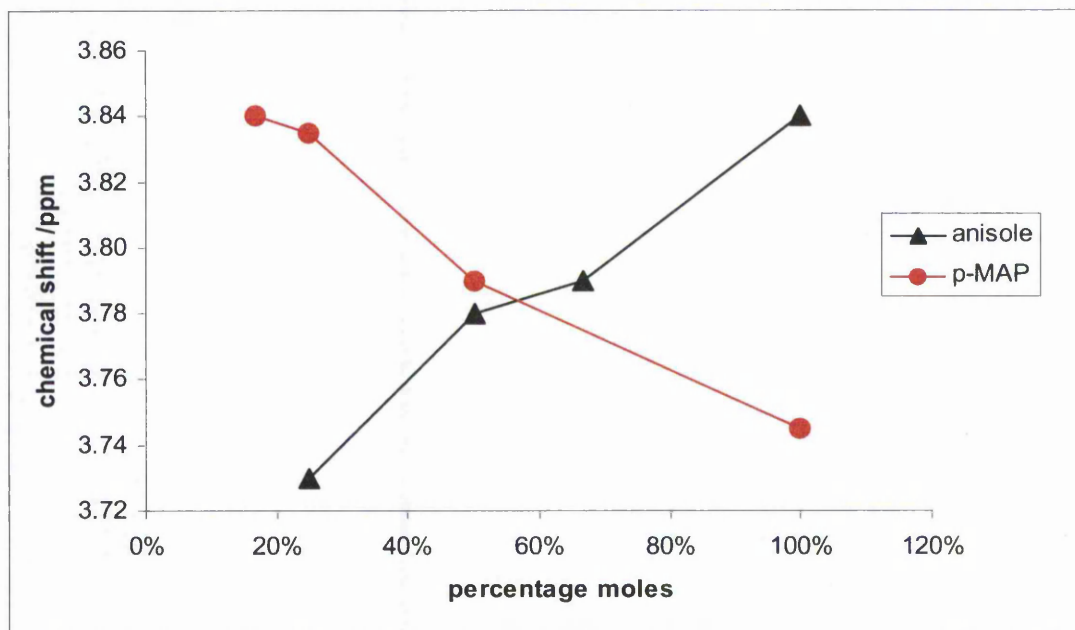
Figure 5.5.2 – Ternary mixture, acetic anhydride, anisole, p-MAP

To understand the reasons behind this phenomenon, experiments were carried out in which the pure substance (either anisole or p-MAP) was diluted with a series of different solvents prior to analysis. The results are summarised in Table 5.5.1 together with the electric dipole moments [8] for each solvent. It should be noted that the electric dipole-moment values that are reported were obtained in the gas phase.

Table 5.5.1

solvent	dipole moment /Debye	p-MAP shift /ppm	anisole shift /ppm
benzene-d$_6$	0.00	3.217	3.306
CCl$_4$	0.00	3.841	3.755
CDCl$_3$	1.04	3.745	3.843
acetone-d$_6$	2.88	3.882	3.764
DMSO-d$_6$	3.96	3.761	3.731
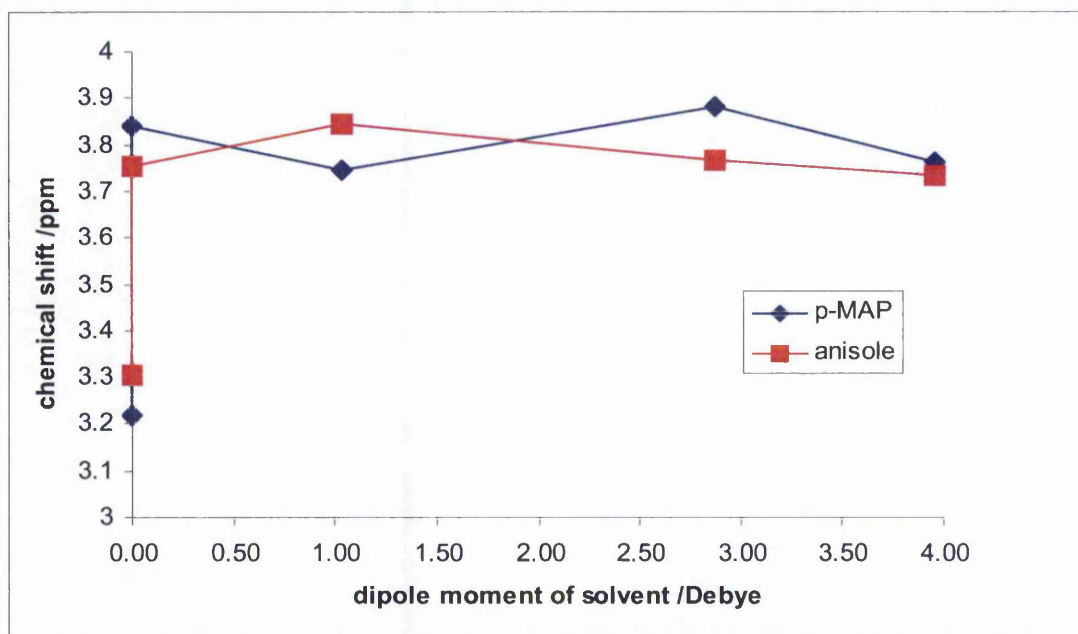
Figure 5.5.3 – ^{1}H chemical shifts versus dipole moment of different solvents

Figure 5.5.3 is a graphical representation of the results in Table 5.5.1. It shows that there is no clear relation between dipole moments and chemical shifts for either p-MAP or anisole.

5.6 References

1. A. Corma, et al., *Applied Catalysis*, 1989, 49, 109

2. S.L. Cook, in *Acetic acid and its derivatives,* V.H. Agreda and J.R Zoeller Eds., Pub. Marcel Dekker, New York, 1995, pg. 145

3. see Chapter 1 Section 1.12 and references therein

4. G. S. Paine, *unpublished data*

5. S.L. Cook, in *Acetic acid and its derivatives,* V.H. Agreda and J.R Zoeller Eds., Pub. Marcel Dekker, New York, 1995, pg. 145

6. D.H. Williams, I. Fleming, *Spectroscopic methods in organic chemistry, 4th Ed.,* McGraw-Hill, London, 1989, p. 63- and C.N. Banwell, E.M. McCash, *Fundamentals of molecular spectroscopy, 4th Ed.*, McGraw-Hill, London, 1994, p. 220-228

7. G.A. Olah, *Friedel-Crafts Chemistry*, Wiley, London, 1973

8. David R. Lide, Ed., *CRC Handbook of Chemistry and Physics, 81st Ed.*, 2000, CRC Press, Boca Raton

6 Site Location and Type

6.1 Introduction

Chapters 4 and 5 have been concerned with understanding the mechanism of acylation of anisole with acetic anhydride over H-BEA. This Chapter will be devoted to the investigation of the role of the external surface and the acidity of zeolite BEA in the acylation of anisole with acetic anhydride.

The zeolite surface accessible to reactants can be divided into a large internal surface (the micropore system) and a smaller external surface (i.e. outside the micropores). This external surface can be active (and in some cases selective) and may also promote the formation of undesirable coke-like products which can cause deactivation by inhibiting access to the micropores [1]. Thus, selective deactivation of either the internal or the external surface can be used to investigate if the active sites are located either in the internal surface or the external or both. In order to passivate (i.e. deactivate) the external-surface activity of BEA it is possible to use tetraethyl orthosilicate (TEOS) to deposit a thin external layer of silica [2, 3]. TEOS is a bulky molecule with a cross-sectional area of ca. 9.5 Å [2] and thus does not diffuse into the pore system of BEA and when deposited from a suitable solvent provides the desired silica layer on the external surface of the zeolite. This process is an example of chemical liquid deposition, and the experimental procedure is described in detail in Chapter 2.

Andy et al. [3] studied the liquid phase acylation of 2-methoxynaphthalene with acetic anhydride in the presence of zeolite BEA modified with TEOS. They concluded that the formation of the product 1-acetyl-2-methoxynaphthalene (1,2-AMN) occurs at the external surface of the zeolite while the desired product 2-acetyl-6-methoxynaphthalene (2,6-AMN) forms within the zeolite pores. For the acylation of isobutylbenzene with acetic anhydride and zeolite BEA, they found that the external surface contributes significantly to the formation of the product 4-isobutylacetophenone [3].

The mechanism proposed for the acylation reactions in Chapter 1 involves the protonic, Brønsted acid sites in the zeolite. It is therefore worthwhile investigating whether catalytic activity can be suppressed by deactivating these sites, or whether Lewis acidity, which is always present to some degree in zeolites, can also catalyse these

reactions. The bulky organic base 2,6-dimethylpyridine (DMP) has been shown to deactivate Brønsted acid sites readily, but it is believed to have little effect on Lewis acid sites because of the blocking of the two methyl groups [4, 5]. It can thus be used to investigate the role of Brønsted and Lewis acid sites in the acylation reaction by first adsorbing DMP on a zeolite BEA sample and then studying the sample in the catalytic reactor. The method for the preparation of the samples poisoned with DMP is described in Chapter 2.

Wang et al. [5] studied the gas-phase Fries rearrangement of phenyl acetate over H-BEA. DMP was carried into the reactor by N_2 and adsorbed onto H-BEA. After the treatment, the conversion of the reaction decreased thus indicating that the effective catalytic centres for this reaction are the Brønsted acid sites.

H-BEA was modified by either deposition of TEOS or by poisoning with DMP. Additionally, Cu-BEA-acetate-10^{-2}M was also poisoned with DMP. This copper-exchanged BEA sample has been shown to be catalytically active and has already been used for the experiments presented in Chapter 5. All the modified samples and the parent materials were characterised by powder XRD and N_2 adsorption isotherms to study the effect of the modifications on the structure of the catalyst and the pore volume. Ammonia adsorption was carried out on all samples and monitored by FTIR to investigate the effect of the modifications on their acidity. Also, the interaction between DMP and H-BEA and ammonia was studied by TPD-MS. Catalytic testing was carried out on all the samples at the same conditions as outlined in Chapter 2 to determine the effect of modifications on catalytic activity.

6.2 Characterisation by XRD and nitrogen adsorption isotherm.

Powder x-ray diffraction experiments were carried out on both the modified and the starting zeolite BEA samples to assess any influence that modification with either TEOS or DMP might have on the structure of zeolite BEA.

Comparison of the XRD patterns of H-BEA and H-BEA after deposition of TEOS (sample named H-BEA+TEOS) is shown in Figure 6.2.1. In this Figure the two XRD patterns have been offset by 200 counts, the same applies for Figures 6.2.2 and 6.2.3.
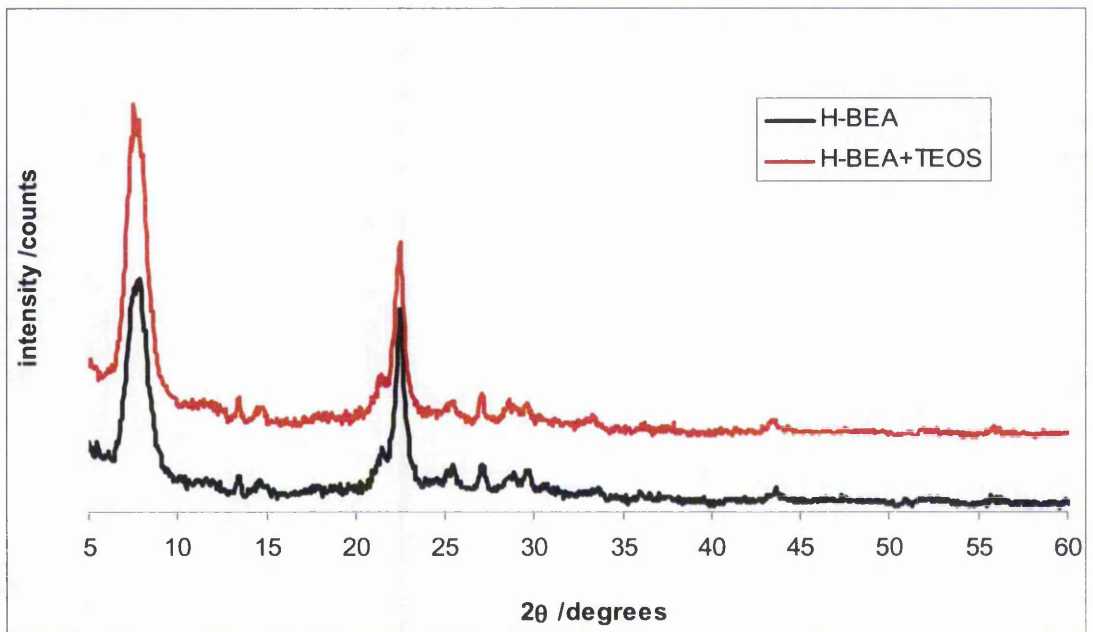
Figure 6.2.1 – XRD patterns of H-BEA and H-BEA+TEOS

All the peaks in the XRD pattern of H-BEA+TEOS match to the pattern of the parent H-BEA, showing that no extra phases are present after deposition of TEOS onto H-BEA. Comparison of the two XRD patterns shows that the peaks do not shift position (see also Figure 6.2.4), this indicates that no dealumination has taken place after treatment with TEOS [6, 7]. The width of the peak at ca 7.8° 2θ does not change thus indicating that the two samples have the same particle size (as derived from the Scherrer equation [8]).

The powder XRD patterns relating to the influence of DMP poisoning on the crystalline structure are presented in Figures 6.2.2 for H-BEA and H-BEA after adsorption of DMP

(H-BEA+DMP) and in Figure 6.2.3 for Cu-BEA-acetate-10^{-2}M and Cu-BEA-acetate-10^{-2}M after adsorption of DMP (Cu-BEA-acetate-10^{-2}M+DMP).
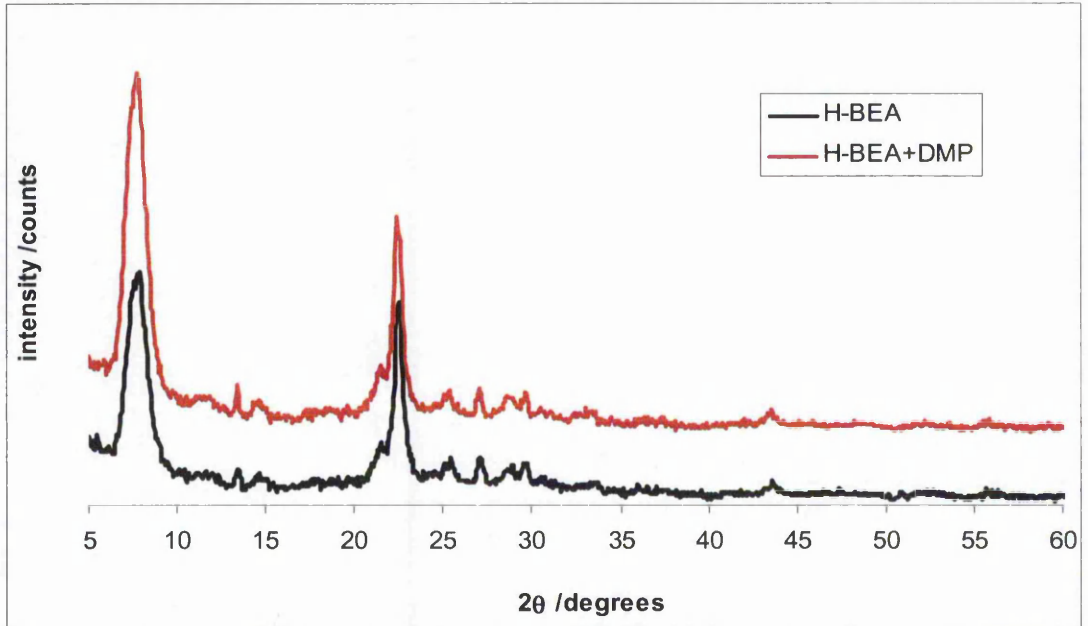
Figure 6.2.2 – XRD patterns of H-BEA and H-BEA+DMP
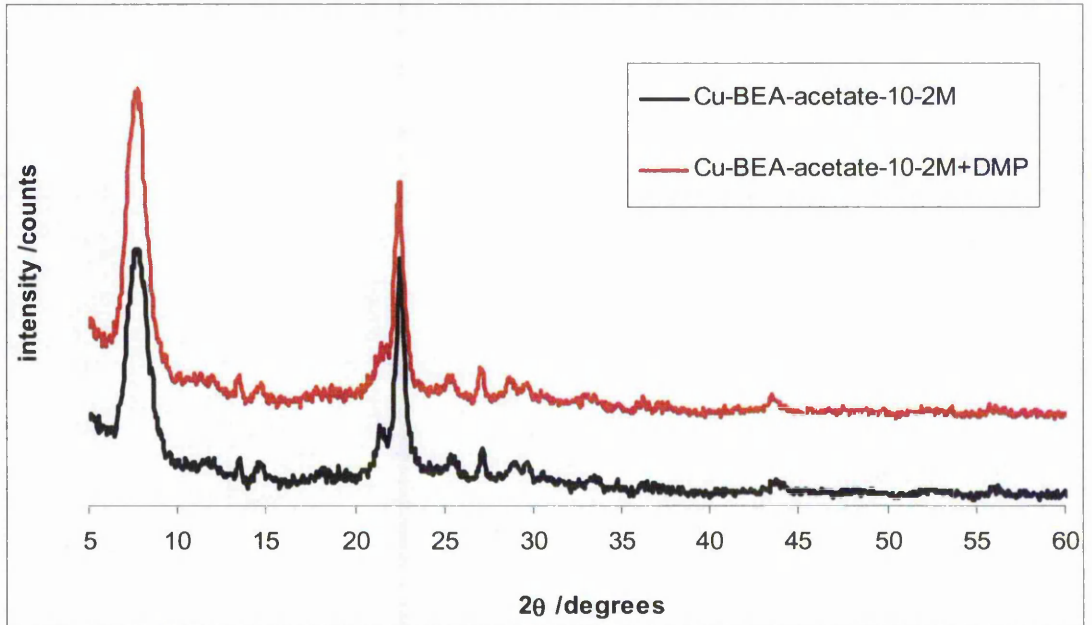
Figure 6.2.3 – XRD patterns of Cu-BEA-acetate-10^{-2}M and Cu-BEA-acetate-10^{-2}M+DMP

Both Figures 6.2.2 and 6.2.3 show that the samples retain the zeolite BEA structure after poisoning with DMP and no extra phases are present. As in the case of H-BEA treated with TEOS, the peaks do not shift position (see also Figure 6.2.4).
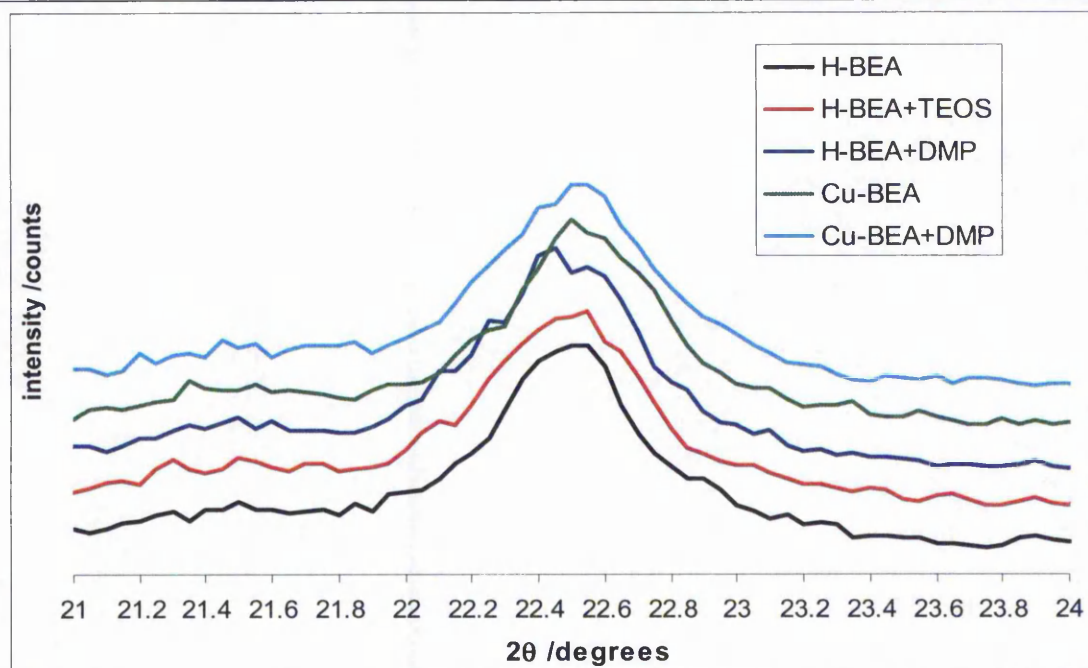
Figure 6.2.4 – Comparison of the peak positions for the XRD patterns of various samples

Nitrogen adsorption isotherms were measured to investigate the influence of the modification with either TEOS or DMP on the micropore volumes of both parent and modified zeolite BEA samples. Microporore volumes for each sample were calculated using the N_2 adsorption data and applying the Dubinin-Radushkevitch plot [9] on all the points in the adsorption isotherm. The results are presented in Table 6.2.1.

Table 6.2.1

Sample	Micropore volume /$cm^3 g^{-1}$
H-BEA	0.34
H-BEA+TEOS_uncalcined	0.24
HBEA+TEOS	0.31
H-BEA+DMP	0.32
Cu-BEA-acetate-10^{-2}M	0.30
Cu-BEA-acetate-10^{-2}M+DMP	0.14

The results show that the chemical liquid deposition of TEOS but without further calcination reduces the pore volume of H-BEA (sample called H-BEA+TEOS_uncalcined). However if the treatment with TEOS is followed by calcination (HBEA+TEOS, the method for its preparation is described in Chapter 2) the pore volume increases to a value similar to the starting material.

The adsorption of DMP decreases the micropore volume of H-BEA from a value of 0.34 cm^3 g^{-1} to 0.32 cm^3 g^{-1} for H-BEA+DMP. However, when Cu-BEA-acetate-10^{-2}M is poisoned with DMP at the same experimental conditions, its micropore volume decreases dramatically from 0.30 cm^3 g^{-1} to 0.14 cm^3 g^{-1}.

6.3 TPD-MS studies of H-BEA with DMP and NH$_3$

The strength of interaction between H-BEA and DMP, and the influence of the adsorption of DMP on the total acidity of H-BEA were studied by TPD-MS.

Figure 6.3.1 illustrates the desorption profiles of DMP after adsorption on H-BEA at 423 K. The peak with m/e = 107 is the molecular ion, the peak with m/e = 92 is the peak resulting from DMP losing a methyl group (CH$_3$), and the peak with m/e = 16 is due to NH$_2$, which is another fragmentation product of DMP. The curves indicate the DMP starts to desorb very slowly at ca 450 K, with the rate of desorption increasing at ca 730 K and continuing to increase up to 873 K, at which point the experiment ended. This indicates that the activation energy of desorption (i.e. the strength of interaction) for DMP is much higher than in the case of ammonia being adsorbed on H-BEA.
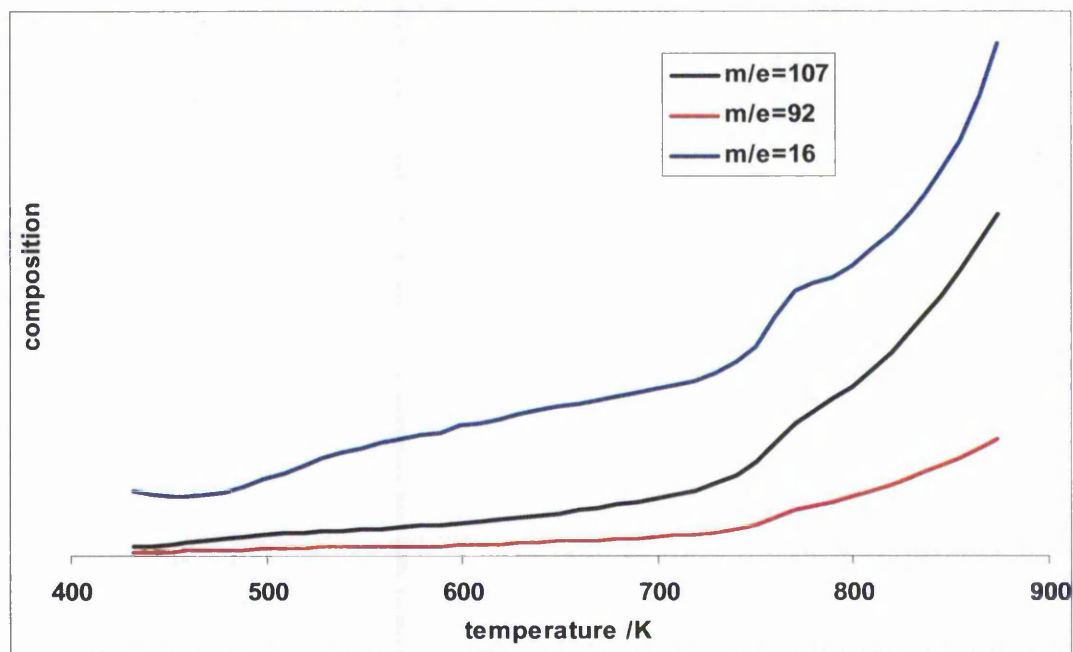
Figure 6.3.1 – TPD of DMP desorbing from H-BEA after adsorption at 423 K

An additional experiment was carried out in which DMP was first adsorbed at 423 K, then the sample cell evacuated, and subsequently ammonia was adsorbed on the sample at 423 K. This was done to assess the influence of the adsorption of DMP on the total acidity of H-BEA. Figure 6.3.2 illustrates the results. DMP (m/e = 107) is still desorbing with a similar profile as in Figure 6.3.1, and ammonia (m/e = 16) is desorbing with a peak at ca 550 K.
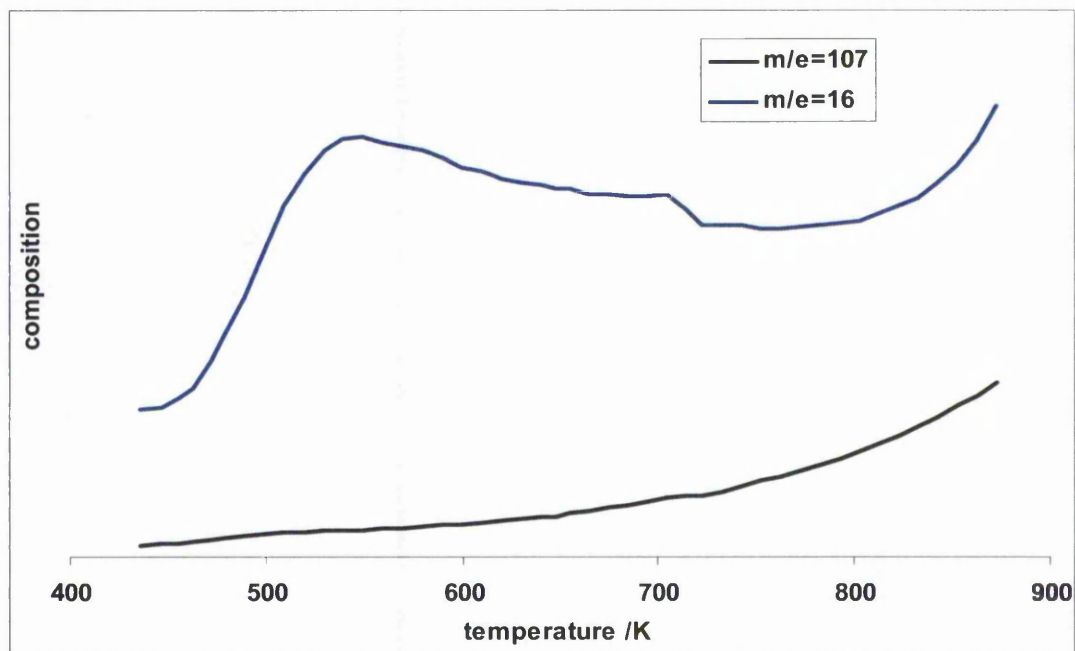
Figure 6.3.2 – TPD after coadsorption of DMP and ammonia on H-BEA at 423 K

However, visual inspection of the curve attributed to ammonia (m/e = 16) shows the influence of DMP on the signal. Thus, a similar method to the one used for the analysis of the desorption profiles of acetic anhydride (see Chapter 4) was used in this case to subtract from the signal at m/e = 16 the component due to the presence of DMP. The results are shown in Figure 6.3.3.
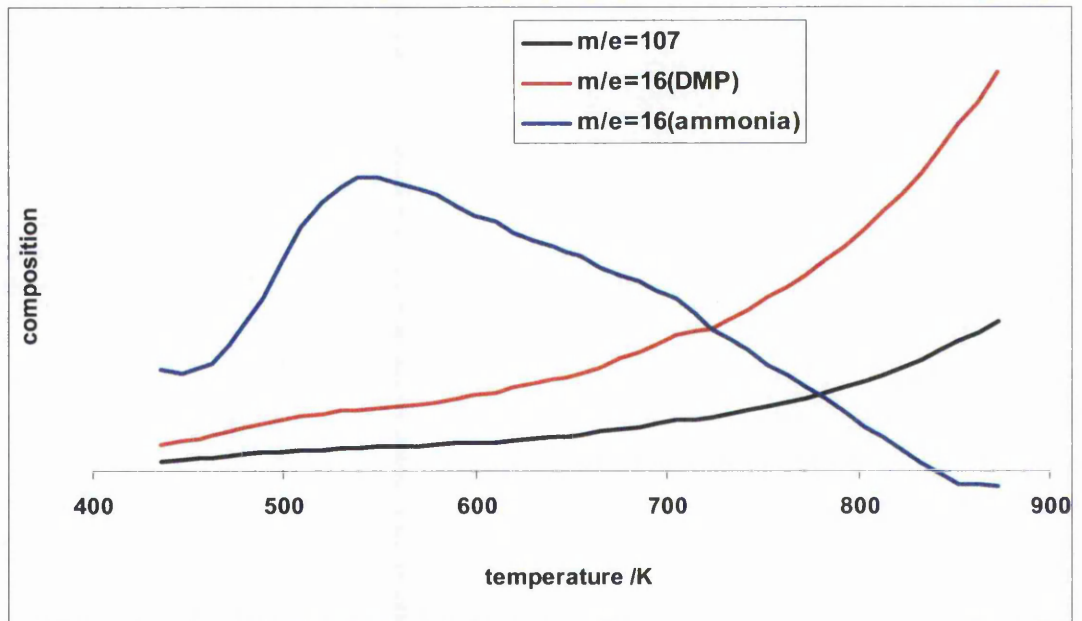
Figure 6.3.3 – Co-adsorption corrected

Figure 6.3.4 shows a comparison between the desorption profiles of ammonia adsorbed on H-BEA and ammonia adsorbed on H-BEA poisoned with DMP. Both curves were normalised to the weight of substrate.
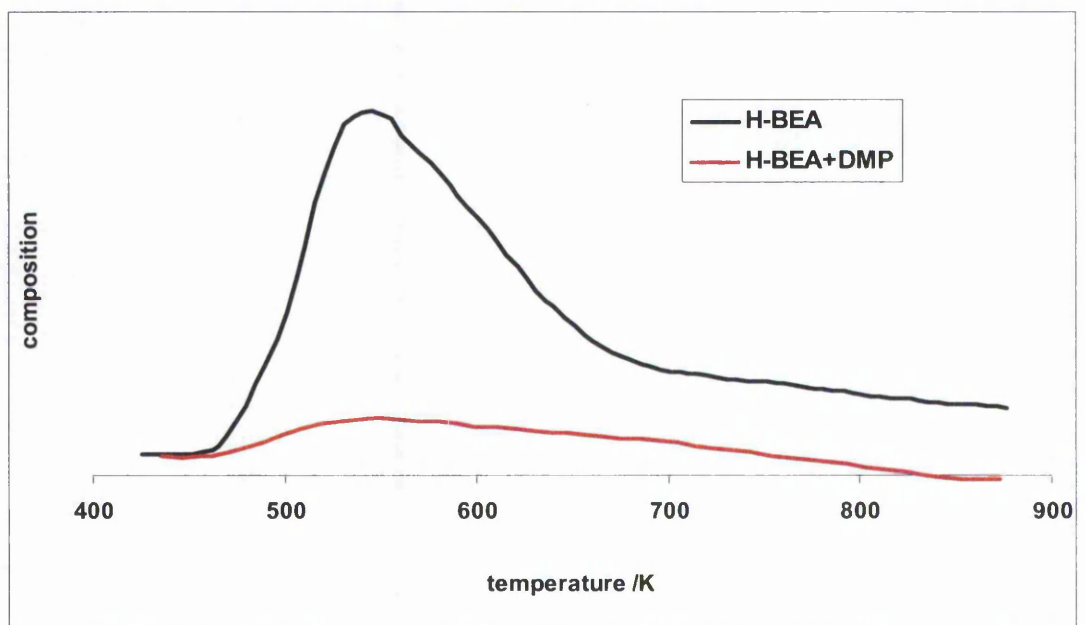
Figure 6.3.4 – Desorption profiles of ammonia adsorbed on H-BEA (black line) and ammonia adsorbed on H-BEA poisoned with DMP (red)

Figure 6.3.4 shows that ammonia desorbs in both cases with a maximum intensity peak at ca 550 K. Integration and comparison of the two curves indicates that the quantity of ammonia desorbing from the sample poisoned with DMP is ca 10 times less than in the case of H-BEA. Thus, it can be said that poisoning H-BEA with DMP reduces the total acidity by about ten times.

6.4 FTIR studies

The adsorption of ammonia was carried out in the FTIR apparatus to study the influence of either TEOS or DMP on the Brønsted and Lewis acid sites of H-BEA and Cu-BEA-acetate-10^{-2}M. The results are presented in Figure 6.4.1 for H-BEA modified with TEOS and in Figure 6.5.1 for samples poisoned with DMP. All the curves were normalised for varying sample thickness by integration of the bands in the region 1750-2095 cm^{-1}. These bands correspond to Si-O overtone vibrations in the zeolite lattice [10]. Both Figures present a peak at ca 1620 cm^{-1} due to NH_3 coordinated at Lewis acid sites, and another peak at ca 1450 cm^{-1} due to protonated ammonia, NH_4^+(i.e. adsorbed on a Brønsted acid site) [11, 12].

In contrast to the experiments carried out in the TPD-MS apparatus, poisoning with DMP was not carried out in situ in the FTIR cell. This is because strong bases such as pyridine and derivatives are not allowed in significant quantities in the FTIR apparatus.
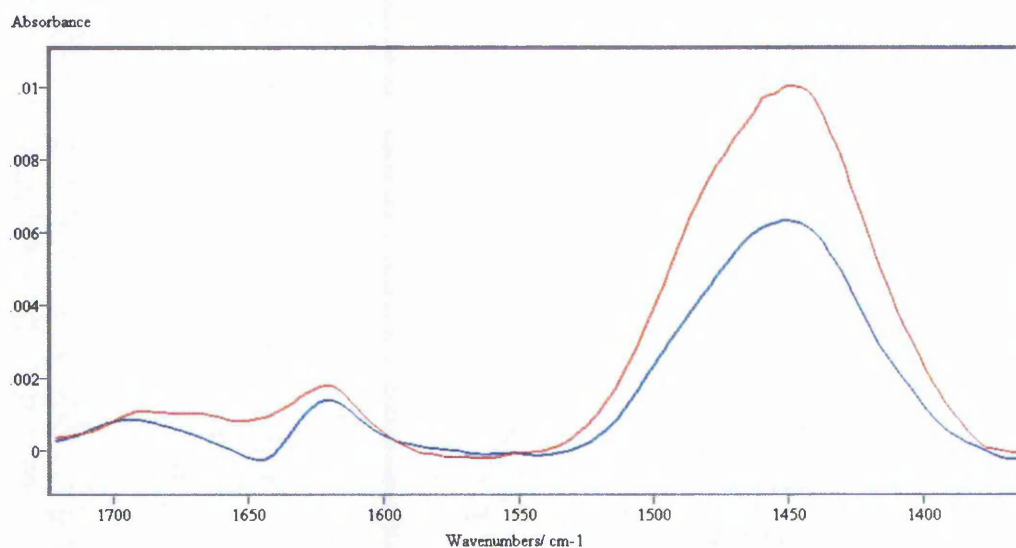
Figure 6.4.1 – Adsorption of ammonia on H-BEA (red) and H-BEA+TEOS (blue)
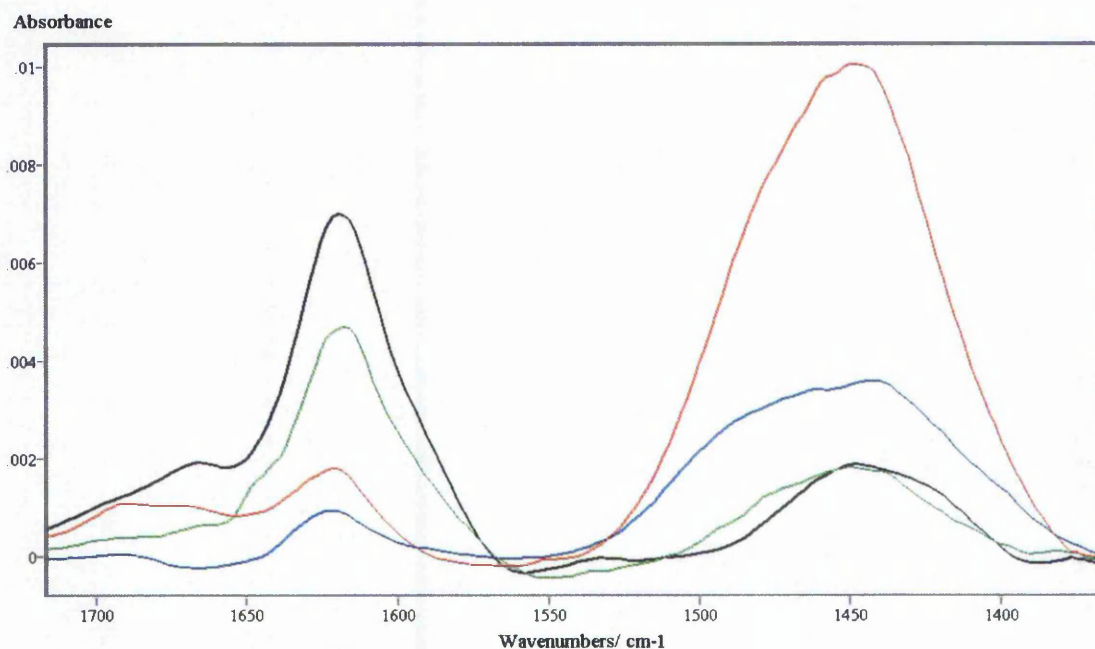
Figure 6.4.2 – Adsorption of ammonia on H-BEA (red), HBEA+DMP (blue), Cu-BEA (black) and Cu-BEA+DMP (green)

The relative concentrations of Brønsted and Lewis acid sites were calculated by integration of the bands at 1375-1545 cm^{-1} and at 1580-1655 cm^{-1} respectively and then normalised to the lattice overtone bands. The results are presented in Table 6.4.1.

Table 6.4.1

Sample	Brønsted acid sites conc. /arbitrary units	Lewis acid sites conc. /arbitrary units
H-BEA	80.3	4.18
H-BEA+TEOS	50.0	4.11
H-BEA+DMP	32.3	3.25
Cu-BEA-acetate-10^{-2}M	12.8	19.5
Cu-BEA-acetate-10^{-2}M+DMP	13.9	13.9

Treatment with TEOS is shown to significantly reduce the Brønsted acidity of H-BEA while having little effect on the amount of Lewis acid sites. Treatment with of H-BEA with DMP reduces Brønsted acidity to 40% with respect to H-BEA, while Lewis acidity is 76% of the parent material. When Cu-BEA-acetate-10^{-2}M is poisoned with DMP there is a slight increase in Brønsted acidity while Lewis acid site concentrations are reduced to 71% of the parent material.

150

6.5 Catalytic data

The zeolite BEA samples modified with TEOS and DMP were then used as catalysts in the acylation of anisole with acetic anhydride. The reaction conditions and sampling procedure were the same used throughout this Thesis and outlined in Chapter 2. The curves in Figure 6.5.1 refer to the reactivity of the parent material (H-BEA), the material modified with TEOS (H-BEA+TEOS) and a sample that has been subject to the same thermal treatment as in the deposition with TEOS (see Chapter 2) but without actually performing the deposition step (sample named H-BEA+TEOS_test).
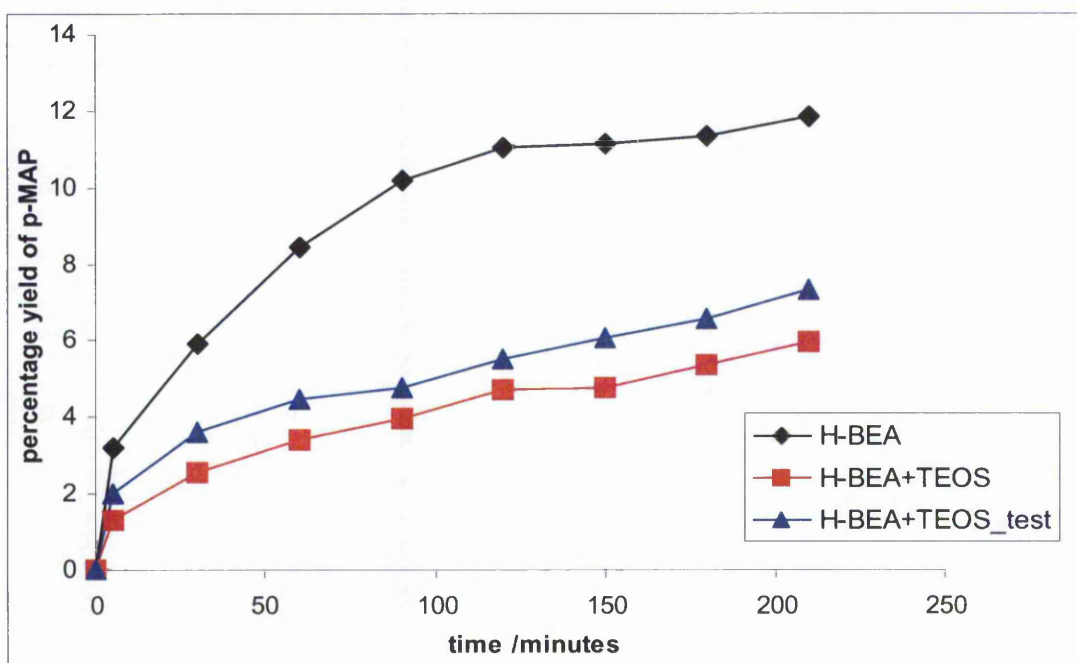
Figure 6.5.1 – Comparison of the catalytic activities of H-BEA, H-BEA+TEOS and a test H-BEA samples.

H-BEA has the highest activity and H-BEA+TEOS the lowest. H-BEA+TEOS_test has only a slightly higher activity than H-BEA+TEOS, thus showing how the simple thermal treatment that leads to the H-BEA+TEOS sample can be accountable for most of the loss in activity.

In Figure 6.5.1 are presented the results for the acylation carried over the zeolite BEA samples modified with DMP, together with their respective parent materials.
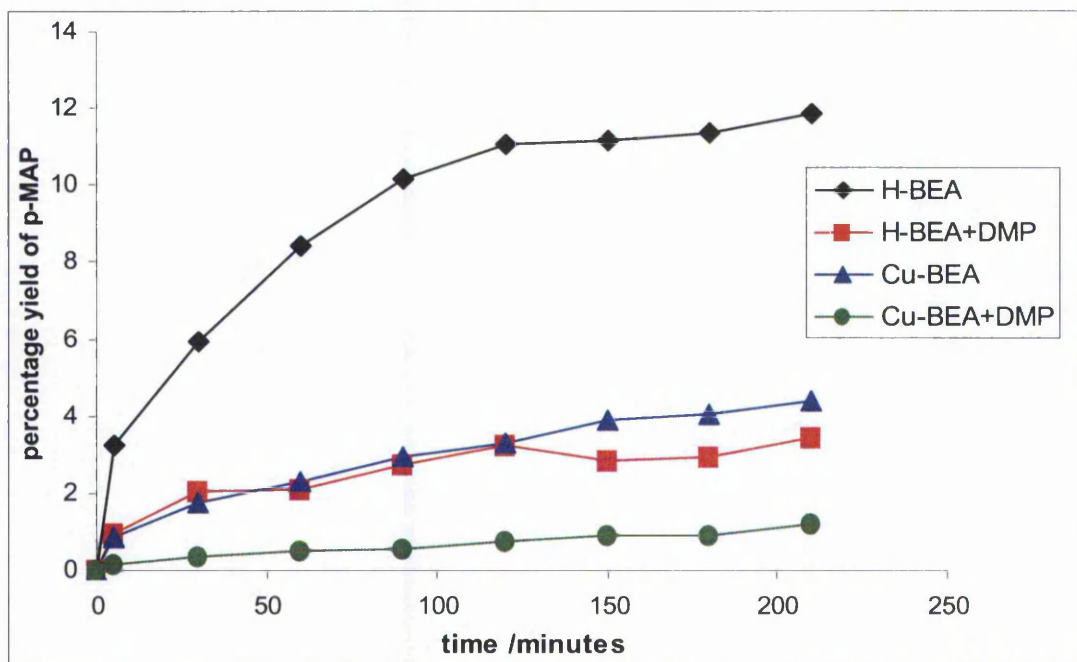
Figure 6.5.2 – Comparison of the catalytic activities of zeolite BEA samples poisoned with DMP and their respective parent materials.

The curves show that poisoning with DMP reduces the catalytic activity for both H-BEA and Cu-BEA-acetate-10^{-2}M.

Initial rates of reaction were calculated by taking the percentage yield value at 5 minutes and dividing by 300 seconds. The values are summarised in Table 6.5.1 below.

Table 6.5.1 – Initial rates of reaction for various samples

Sample	Initial rate of reaction /s^{-1}
H-BEA	1.07E-02
H-BEA+TEOS	4.39E-03
H-BEA+TEOS_test	6.62E-03
H-BEA+DMP	3.19E-03
Cu-BEA-acetate-10^{-2}M	2.88E-03
Cu-BEA-acetate-10^{-2}M+DMP	4.53E-04

6.6 Conclusions

Both H-BEA modified with TEOS and H-BEA and Cu-BEA-acetate-10^{-2}M poisoned with DMP have been shown to be less active in the acylation reaction than their respective parent materials.

The chemical liquid deposition of tetraethyl orthosilicate (TEOS) leaves the zeolite BEA framework intact and does not create any new phases, as shown by the XRD patterns. Calculations on the nitrogen adsorption isotherm data show that the micropore volume of H-BEA+TEOS is only slightly smaller than the one of the parent material (0.31 vs. 0.34 cc g^{-1}). Ammonia adsorption monitored by FTIR indicates that modification of H-BEA with TEOS diminishes the relative concentration of Brønsted acid sites but has little effect on the Lewis acid sites. The ratio between the relative concentrations of Brønsted acid sites in H-BEA and H-BEA+TEOS is about 1.6 while for Lewis acid sites this ratio is ca 1.0. This seems to indicate that Brønsted acid sites are present in both the external and the internal surface of the zeolite while the Lewis acid sites are present only within the micropores (i.e. the volume corresponding to the internal surface of the zeolite), as already suggested by Jansen et al. [13]. The activity of H-BEA+TEOS in the acylation of anisole with acetic anhydride is lower than the activity of H-BEA and the ratio between the initial rates of reaction of H-BEA and H-BEA+TEOS is ca 2.4. This indicates that both the surface and the Brønsted acid sites may be responsible for the catalytic activity of H-BEA in the acylation of anisole with acetic anhydride. However, a test sample (H-BEA+TEOS_test) was found to be only slightly more catalytically active than H-BEA+TEOS. This sample was prepared by subjecting H-BEA to the same thermal treatment as in the preparation of H-BEA+TEOS but without actually using TEOS. This finding suggests that the use of TEOS is not the only factor affecting the catalytic performance of H-BEA. Thus, to further investigate the extent by which TEOS deposition deactivates any acidic sites present on the external surface of zeolite BEA one would need to study by FTIR the adsorption of a bulky pyridine based molecule such as 2,6-di-tert-butyl-pyridine [14].

XRD experiments show that the poisoning of both H-BEA and Cu-BEA-acetate-10^{-2}M with 2,6-dimethylpyridine (DMP) does not affect the structure of the zeolite. The micropore volume in the case of H-BEA diminishes from 0.34 cm^3 g^{-1} to 0.32 cm^3 g^{-1} with adsorbed DMP. However, in the case of Cu-BEA-acetate-10^{-2}M the micropore volume markedly decreases from 0.30 cm^3 g^{-1} in the parent material to 0.14 cm^3 g^{-1} after

poisoning with DMP. TPD-MS experiments performed on H-BEA suggest that DMP bonds strongly with the substrate and also reduces the total acidity of H-BEA by ca 10 times. Contrary to what claimed in the literature [4, 5], the FTIR experiments show that DMP poisons both Brønsted and Lewis acid sites. The ratio between the relative concentrations of Brønsted acid sites in H-BEA and H-BEA+DMP is 2.5, and in the case of Lewis acid sites this ratio is 1.3. This would indicate that DMP indeed poisons the Brønsted acid sites, and has also a minor effect on Lewis acid sites. A somewhat different situation is found in the case of Cu-BEA-acetate-10^{-2}M where the ratio for Brønsted acid sites is 0.92 and the ratio for Lewis acid sites is 1.4. This indicates that Lewis acid sites in Cu-BEA-acetate-10^{-2}M are partly introduced by copper ion substituting hydrogen counter-cations. And these copper ions would be more readily accessible to DMP than the Lewis acid sites present in H-BEA. The fact that Brønsted acid sites are essentially unaffected would indicate that some of the acidic protons are less accessible to DMP than others.

For both H-BEA and Cu-BEA-acetate-10^{-2}M the catalytic activity diminishes when poisoned with DMP. The ratio between the initial rate of reaction of H-BEA and H-BEA+DMP is ca 3.4 and the same ratio for Cu-BEA-acetate-10^{-2}M and Cu-BEA-acetate-10^{-2}M+DMP is ca 6.4. In the case of H-BEA this indicates that the reaction is acid catalysed and that the sites responsible for most of the activity are probably Brønsted acid sites. This is in agreement with the findings for H-BEA+TEOS. In the case of Cu-BEA-acetate-10^{-2}M+DMP the loss of activity may be due both a loss in acidity (mainly Lewis acidity) and a much diminished micropore volume.

In conclusion, the results indicate that the acylation reaction is catalysed at least in part by the external surface of zeolite H-BEA and there is confirmation that the reaction is acid catalysed. In particular, poisoning experiments with DMP suggest that Brønsted acid sites participate in the catalysis in the case of H-BEA. However, experiments with Cu-BEA-acetate-10^{-2}M poisoned with DMP seem to indicate a role for Lewis acid sites in the catalysis. It is important to stress that in the case of Cu-BEA-acetate-10^{-2}M Lewis acid sites are also introduced by the copper counter-cations. This would suggest that copper acting as a Lewis acid can substitute for proton acidity in the catalysis of the acylation reaction.

Further investigations would be needed to better assess the validity and feasibility of modifications of zeolite BEA with TEOS and DMP and the impact on its properties.

6.7 References

1.   T. Hibino, M. Niwa, Y. Murakami, *Zeolites*, 1993, **13**, 518

2.   P.J. Kunkeler, D. Moeskops, H. van Bekkum, *Microporous Materials*, 1997, **11**, 313

3.   P. Andy, et al., *Journal of Catalysis*, 2000, **192**, 215

4.   A. Corma, et al., *Journal of Catalysis*, 1987, **88**, 374

5.   H. Wang and Y. Zou, *Catalysis Letters*, 2003, **86(4)**, 163

6.   M.A. Camblor, A. Corma, S. Valencia, *Microporous and Mesoporous Materials*, 1998, **25**, 59

7.   M. Trombetta, et al., *Physical Chemistry Chemical Physics*, 2000, **2**, 3529

8.   H. Lipson and H. Steeple, *Interpretation of x-ray powder diffraction patterns*, Macmillan, London, 1970

9.   S.J. Gregg, K.S.W. Sing, *Adsorption, Surface Area and Porosity, 2nd Ed.*, Academic Press, London, 1982

10. H. van Bekkum, et al., *Introduction to Zeolite Science and Practice, 2nd Ed.*, Elsevier, Amsterdam, 2001

11. W.M. Zhang, et al., *Journal of Physical Chemistry B*, 2000, **104**, 4122

12. H. Knozinger, *Elementary Reaction Steps in Heterogeneous Catalysis*, R.W. Joyner, R.A. van Santen, Eds., Kluwer Academic Publishers, Dordrecht, 1993, p. 267

13. J.C. Jansen, et al., *Catalysis Today*, 1997, **38**, 205

14. A. Corma, et al., *Journal of Catalysis*, 1998, **179**, 451

7 Overall Conclusions

As shown in Chapter 1, aromatic acylation reactions catalysed by zeolites have been the subject of a considerable research effort. In the case of the acylation of anisole, zeolite BEA was found to be the most active catalyst. However, questions regarding the mechanism of acylation remain open. Thus, the aims of this Thesis were the characterisation of a series of BEA samples and studies on the mechanism of acylation catalysed by BEA.

Chapter 3 investigates the effect of ion-exchange procedure on the chemical/morphological properties of BEA and the catalytic activity in the acylation of anisole of the various BEA samples. Ion-exchange procedures were shown to introduce counter-cations in zeolite BEA samples while retaining the framework structure and without dealumination, as determined by XRD and ICP respectively. Only in the case of Fe-BEA samples the degree of exchange is higher than 100% and this is accompanied by substantial dealumination. FTIR studies of the adsorption of ammonia have shown that the ion-exchange procedure modifies the acidic properties of BEA. For example, upon sodium exchange the amount of Brønsted acid sites diminishes while the number of Lewis acid sites is unchanged. The copper-exchanged BEA samples exhibit much lower Brønsted acidity than H-BEA and a higher Lewis acidity. This has been taken as an indication that the exchanged copper in zeolite BEA can act as a Lewis acid. Catalytic tests showed that H-BEA compared with ion-exchanged BEA samples is the most active catalyst in the acylation of anisole with acetic anhydride. Each of the ion-exchanged samples exhibited some degree of catalytic activity with Na-BEA-10^{-2}M being the least active. All the catalysts exhibit loss of activity with time. There is very low degree of correlation between the initial rates of reaction and the relative concentrations of Brønsted acid sites, and an even lower correlation between initial rates and Lewis acidity.

Chapter 4 investigates the adsorption of acylating reagents and product on H-BEA and on ion-exchanged BEA samples. TPD studies of the adsorption of acetic anhydride on BEA suggest that most of the acetic anhydride undergoes decomposition to acetic acid and ketene, and these results have been supported by similar experiments performed by FTIR. It is worth mentioning that acetic anhydride is produced industrially with acetic acid and ketene. Additionally, FTIR studies of the adsorption of p-MAP on BEA

suggest that p-MAP decomposes over H-BEA with the possible formation of ketene. Furthermore, adsorption and catalytic data shows that there is an inverse correlation between the initial rate of acylation and the amount of ketene desorbed intact for a number of catalysts. Together, these results have been interpreted as evidence of the involvement of ketene in the acylation reaction and a mechanism was proposed whereby ketene is formed from acetic anhydride interacting with BEA and then ketene attaches onto the aromatic ring of anisole to give p-MAP. The inverse correlation suggests that the strength of bonding of ketene to the zeolite, and hence perhaps its degree of polarisation, determines the effectiveness a particular catalyst in the acylation of anisole.

The adsorption studies also indicate stronger bonding of acetic acid/acetic anhydride than the product, p-MAP. Additionally, studies presented in Chapter 5 show that the hydrolysis of acetic anhydride catalysed by BEA reaches completion. This indicates that neither acetic anhydride nor acetic acid deactivates the catalyst. Thus, as already suggested in the literature, multiply acylated products may well be the species responsible for the deactivation.

Chapter 5 investigates the hypothesis that ketene is the species attaching onto anisole by using deuterium-exchanged reagents and then analysing the reaction products by NMR. The rationale is that deuterium-exchanged acetic anhydride interacting with H-BEA would produce deuterium-exchanged ketene that would then give a p-MAP molecule with only two deuterium atoms in its acyl group. However, the results showed that the product contained three deuteriums, and thus ketene can not be the attacking species. This result was confirmed by another experiment using deuterium-exchanged anisole and by using the same procedure with a copper-exchanged BEA sample. These findings could mean that ketene is merely a by-product of the decomposition of acetic anhydride and does not participate in the reaction. It is possible that ketene participates in the formation of the multiply acylated products that could be responsible for the deactivation of the catalyst. Another possibility is that ketene can be formed by the interaction of acetic anhydride and BEA in the gas phase (i.e. adsorption studies) but would not actually be produced in the liquid phase (i.e. during the acylation reaction).

Chapter 6 investigates the location and nature of the active sites in the acylation of anisole as catalysed by zeolite BEA. Samples were prepared by either tetraethyl orthosilicate (TEOS) deposition, which passivates the external surface acidity of the zeolite, or by adsorption of 2,6-dimethylpyridine (DMP), which poisons Brønsted acid sites but not Lewis acid sites. Experiments with TEOS have given mixed results and the

role of the external surface acidity in the acylation reaction remains an open question. Experiments with DMP and H-BEA showed that a lower Brønsted acidity corresponds to a lower catalytic activity. This finding is consistent with the results from Na-BEA presented in Chapter 3 and suggest that the acylation of anisole over H-BEA is a Brønsted catalysed reaction. However, experiments with a copper-exchanged BEA sample suggest that Lewis acid sites may play a role in the reaction over this catalyst, and these Lewis acid sites may likely be the copper ions introduced by ion-exchange. Additionally, the results with copper-exchanged BEA suggest that some Brønsted acid sites in BEA are neither accessible for copper exchange nor for interaction with DMP.

8 Appendix: Published Work

The following pages contain two papers based on part of the work presented in this Thesis. The first paper was published in: *Catalysis Today*, 2003, **81**, 553. The second paper was presented at the 14th International Zeolite Conference (Cape Town, SA) and then published in: *Studies in Surface Science and Catalysis*, 2004, **154C**, 2724.

Please note that the following pages are numbered accordingly with the original publication.

A temperature programmed desorption study of the interaction of acetic anhydride with zeolite beta (BEA)

Matteo L.M. Bonati, Richard W. Joyner*, Michael Stockenhuber*

The Catalysis Research Laboratory, Department of Chemistry and Physics, Nottingham Trent University, Clifton Lane, Nottingham NG11 8NS, UK

Abstract

The interaction of acetic anhydride with the Na- and H-forms of zeolite BETA, as well as with materials where copper or iron has been introduced into BEA by ion exchange, has been studied by temperature programmed desorption (TPD). In all cases acetic acid is a main desorption product in the temperature range 370–570 K. Ketene desorption is also significant, although it is argued that much of it is retained in the zeolite pores, where it undergoes further decomposition into carbon monoxide, hydrogen and water. There is an inverse correlation between the quantity of ketene desorbed and the activity of the catalysts in the catalytic acylation of anisole by acetic anhydride to yield p-methoxyacetophenone. The significance of this observation is discussed and an acylation mechanism involving ketene is proposed.
© 2003 Elsevier B.V. All rights reserved.

Keywords: Acetic anhydride; Acylation catalysis; Thermal desorption; Ketene; Zeolite beta

1. Introduction

Zeolite beta has been shown to be an effective catalyst for the acylation of anisole to give p-methoxyacetophenone {$CH_3–C(O)–C_6H_4–O–CH_3$} [1], with acetic anhydride as the preferred acylating agent. The reaction is catalysed by the acid form of the zeolite H-BEA, and has been assumed to occur by Brønsted acid catalysis [2]. However, one of us has recently shown that similar catalytic activity to that of the H-form is exhibited by Fe-BEA and Cu-BEA, where the transition metal is introduced by ion exchange and there is little residual Brønsted acidity [3].

* Corresponding authors. Tel.: +44-115-9486837;
fax: +44-115-9486838/8486694.
E-mail addresses: richard.joyner@ntu.ac.uk (R.W. Joyner),
michael.stockenhuber@atu.at.uk (M. Stockenhuber).

These results suggest that other catalytic mechanisms than Brønsted catalysis may be available, and the importance of a reversible transformation from tetrahedral aluminium to octahedral coordination as a result of adsorption of the anhydride has been postulated [3].

We are thus interested to understand the interaction of acetic anhydride with the different catalytically active forms of zeolite beta, and have studied this by a number of techniques. Of these temperature programmed desorption (TPD) has turned out to be the most informative, and the TPD results are presented here. We are particularly interested to look for the formation of ketene (CH_2=CO) since an earlier study has shown that it can be formed from the interaction of acetic acid with Na-ZSM-5 [4], but not with, e.g. H-ZSM-5 [5]. We will suggest that ketene formed in situ may be an effective acylating agent.

2. Experimental

H-BEA with a Si/Al ratio of 12.5/1 was obtained from Catal Ltd., Sheffield. Sodium, copper or iron were introduced by aqueous ion exchange. Approximately, 5 g of parent zeolite was added to 250 ml of a 1 M solution of the metal nitrate (Laboratory reagent grade) in distilled water. The solution was stirred at room temperature overnight. The catalyst was then separated by filtration, washed with distilled water and dried in air for 24 h at 298 K. This exchange procedure was then repeated twice. The iron and copper loadings in the zeolites were determined by dissolution of the zeolite in hydrofluoric acid, the resulting solution being analysed by atomic absorption spectroscopy.

TPD measurements were made in a compact, purpose built, stainless steel apparatus equipped with a $60 \, l \, s^{-1}$ turbo pump. The desorption cell was connected through a leak valve to an independently pumped, multiplexed Pfeiffer Prisma quadrupole mass spectrometer operating under computer control. The zeolite (ca. 50 mg) was introduced into the desorption cell, evacuated, heated to ca. 750 K at 5 K per minute and cooled to room temperature. After this, the base pressure in the apparatus was typically 5×10^{-6} Pa. Acetic anhydride (Aldrich, +99% purity) was further purified by freeze/thaw pumping cycles and exposed to the zeolite sample at room temperature and ca. 10^2 Pa pressure. After pumping back to the base pressure, the sample was heated to 875 K at 10 K per minute and the desorption spectra recorded.

Preliminary analysis of desorption results showed there are a wide range of significant reaction products from acetic anhydride, principally acetic acid, carbon monoxide, carbon dioxide, water, hydrogen and ketene. Ketene was identified from the cracking pattern published by Cornu and Massot [6], which shows that the parent m/e of 42 is the second largest feature, but that the strongest contribution is at $m/e = 14$, from the CH_2 fragment. We have used $m/e = 14$ in our analysis, although we have also shown that essentially the same results are obtained if $m/e = 42$ is considered instead. $m/e = 14$ also has the advantage that it receives only relatively small contributions from acetic acid and acetic anhydride.

Cracking patterns in the mass spectrometer were determined in situ for acetic anhydride, water and acetic acid. To quantify the relative amounts of the anhydride and the acid desorbing, the mass spectrum was measured of the vapour above a mixture of acetic anhydride and acetic acid, prepared such that their partial pressures at room temperature were equal.

The cracking patterns justify the following assumptions, which greatly facilitate the quantitative analysis of the desorption spectra:

1. The peak at $m/e = 60$ arises only from acetic acid.
2. The peak at $m/e = 43$ receives contributions from acetic acid and acetic anhydride, but not from ketene. Since acetic acid can be quantified from $m/e = 60$, its contribution to $m/e = 43$ can be calculated, and the amount of acetic anhydride desorbed determined by difference.
3. The peak at $m/e = 14$ receives contributions from ketene, acetic acid and acetic anhydride. Since the acid and the anhydride have already been quantified from the $m/e = 60$ and 43 peaks and their cracking patterns are known, the contribution of ketene to the $m/e = 42$ peak can be determined by subtraction.
4. The $m/e = 18$ peak arises only from the desorption of water. CO_2 was determined from the $m/e = 44$ peak, CO from the $m/e = 28$ peak and hydrogen from the $m/e = 2$ peak.

Amounts desorbed were normalised to take account of the mass of material under study. Two blank experiments were performed. Exposure of the empty TPD apparatus to acetic anhydride, followed by pumping and temperature ramping, showed that there was negligible adsorption on the apparatus walls. In a further experiment, H-BEA was heated to 750 K, cooled to room temperature, and temperature programmed again. There was no detectable desorption of water during this second heating, up to at least 750 K.

3. Results and discussion

Fig. 1 shows desorption spectra from H-BEA, which follow a pattern that is typical of all of the materials studied, although the relative quantities of different compounds desorbed change markedly. As Fig. 1a indicates, at around 370 K some desorption of acetic anhydride occurs. At a slightly higher temperature acetic acid desorption commences and dominates the desorption spectra in the range up to ca. 550 K. Ketene desorption starts at a similar temperature to
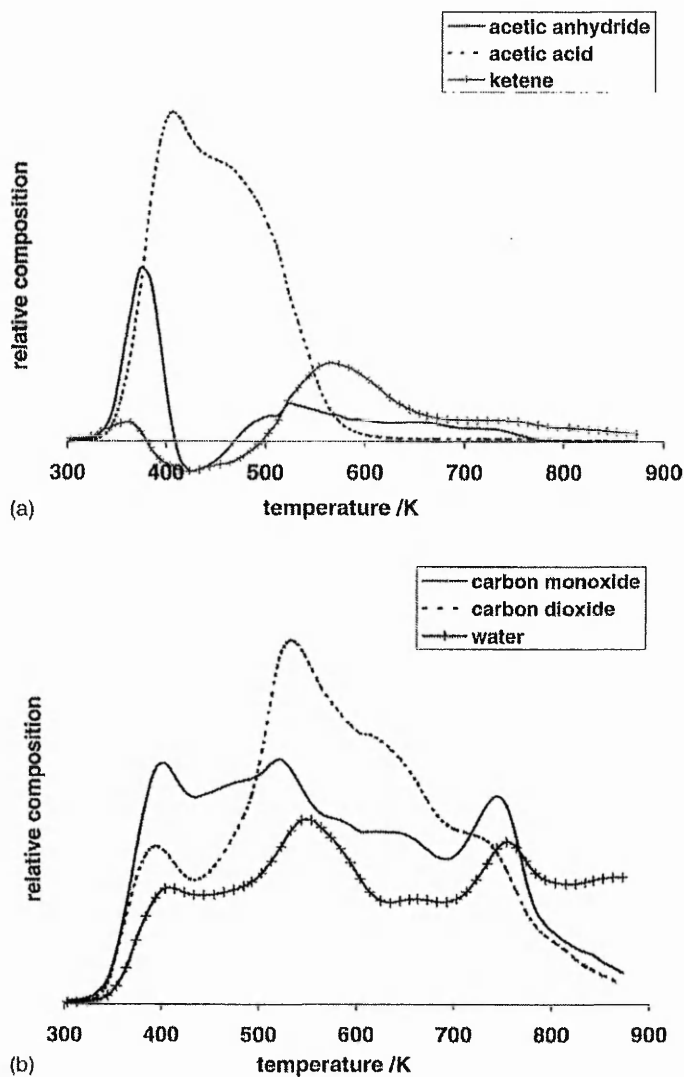
Fig. 1. Desorption results obtained after the adsorption of acetic anhydride at room temperature on H-BEA. (a) Curves for acetic anhydride, acetic acid and ketene; (b) curves for carbon monoxide, carbon dioxide and hydrogen.

acetic acid but continues to occur up to the highest temperature studied, and there is a broad feature due to water desorption (Fig. 1b). As noted already, there is no desorption of water in this region from the activated zeolite, so it must be a decomposition product from acetic anhydride. Fig. 1b shows the desorption results simultaneously obtained for water, carbon monoxide and carbon dioxide. Hydrogen desorption starts at ca. 370 K and continues in a rather featureless way up

to the highest temperatures studied. Fig. 2a–c show the desorption results obtained, respectively, from Na-BEA, Cu-BEA and Fe-BEA, concentrating on the organic species. Small dips below the baseline in the desorption curves for acetic anhydride and ketene are thought to reflect small errors in our cracking patterns.

The results show that on all the samples studied only a small fraction of any acetic anhydride adsorbed desorbs intact, with the smallest amount observed
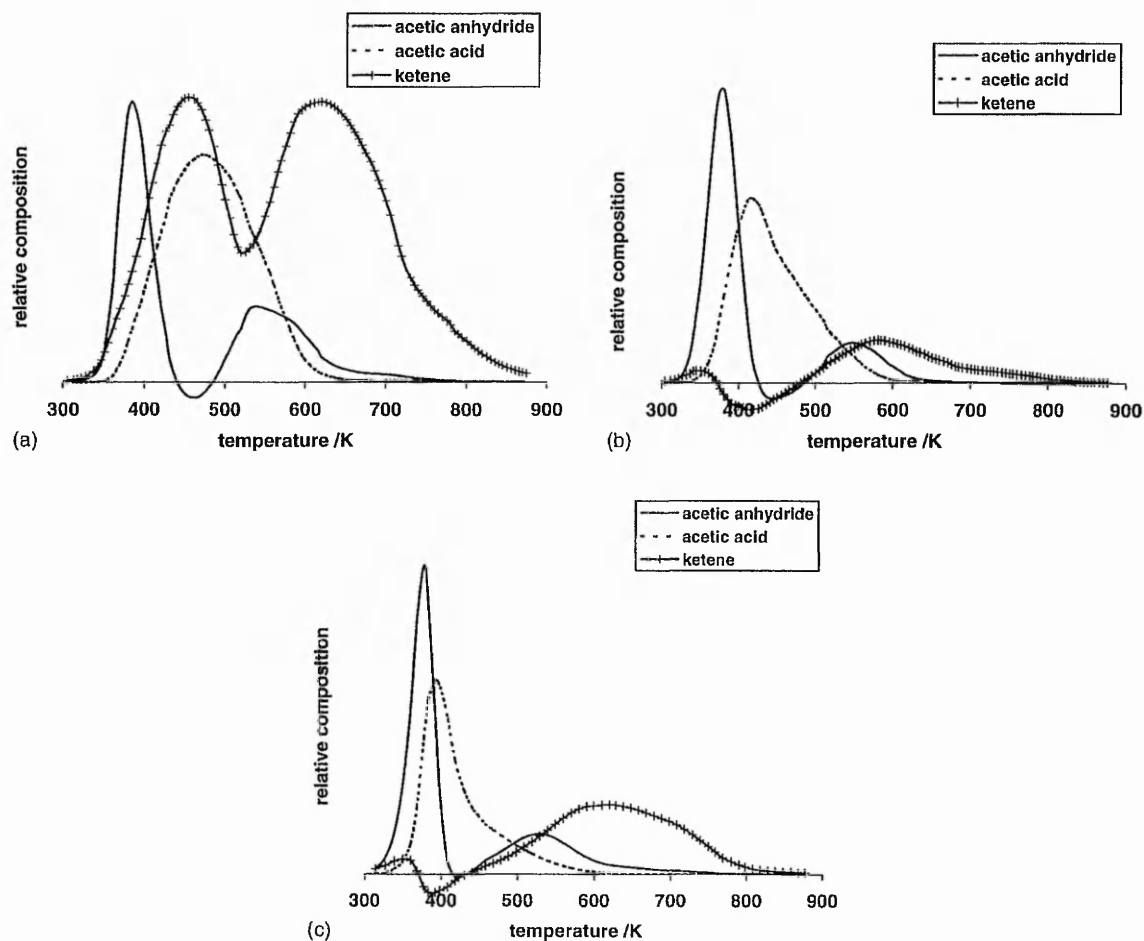
Fig. 2. Desorption results obtained after the adsorption of acetic anhydride at room temperature on (a) Na-BEA, (b) Cu-BEA and (c) Fe-BEA.

from H-BEA. Even on Na-BEA, which might be expected to be comparatively unreactive, much more acetic acid desorption is observed. Only from a purely siliceous MCM-41, which is not of direct relevance to the present study, have we found acetic anhydride to be the dominant desorption product.

Our results show that the primary decomposition mode of acetic anhydride is

Acetic anhydride (ads) → Acetic acid + Ketene (ads)
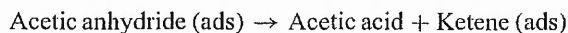
The desorption spectra are consistent with this, since acetic acid and ketene are both adsorbed at relatively low temperatures. We also consider it to be signifi-

cant that acetic anhydride is made industrially by the reverse reaction of acetic acid with ketene [7]. The majority of the acetic acid formed within the zeolite pores is quite rapidly desorbed but most of the ketene is retained. However, even at 500 K some acetic acid does stay adsorbed and some ketene starts to desorb, quite large amounts in the case of Na-BEA (Fig. 2a). As the temperature is further increased, there is evidence for the decomposition of adsorbed acetic acid into ketene and water. But much of the ketene remains adsorbed until temperatures above ca. 530 K, when it decomposes into fragments such as CO and hydrogen. Some carbon dioxide formation is also observed,
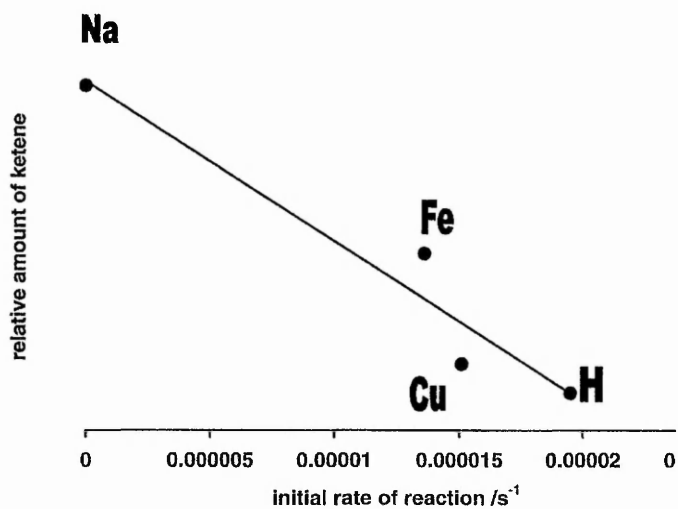
Fig. 3. The relation between the initial rate of acylation of anisole by acetic anhydride at 333 K (3), and the total amount of ketene desorbed from the catalyst.

which may result from the water gas shift reaction or through a bimolecular decomposition of ketene.

We have looked for correlations between our desorption results and the catalytic rate measurements of Apperley et al. [3]. Perhaps surprisingly, there is some inverse correlation between the initial rate of acylation and the amount of ketene desorbed intact for a number of catalysts, as shown in Fig. 3. There is no
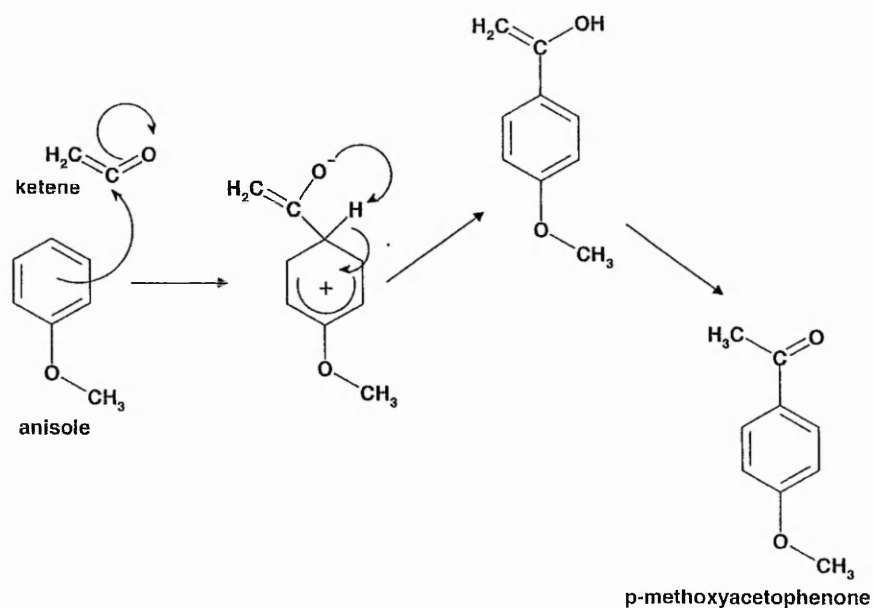
Scheme 1. A possible mechanism for the acylation of anisole by ketene.

simple correlation between catalytic performance and the quantities of either acetic acid or acetic anhydride desorbed from the different catalysts.

It is tempting to see this correlation as evidence of the involvement of ketene in the acylation reaction, which is typically carried out at 330–400 K. There is a strong partial positive charge on the central carbon atom of the ketene molecule [8], which makes it an interesting possibility as an acylating agent through the mechanism shown in Scheme 1. The inverse correlation suggests that the strength of bonding of ketene to the zeolite, and hence perhaps its degree of polarisation, determines its effectiveness in the acylation catalysis.

Acknowledgements

References

[1] M. Spagnol, M. Gilbert, E. Benazzi, C. Marcilly, WO9635655, 1996.
[2] A. Corma, M.J. Climent, H. Garcia, J. Primo, Appl. Catal. 49 (1989) 109.
[3] D.C. Apperley, G. Paine, M. Stockenhuber, J. Catal., submitted for publication.
[4] L.M. Parker, D.M. Bibby, I.J. Miller, J. Catal. 129 (1991) 438.
[5] C.D. Chang, A.J. Silvestri, J. Catal. 47 (1977) 249;
Y. Servotte, J. Jacobs, P.A. Jacobs, Acta Phys. Chem. 31 (1985) 609.
[6] A. Cornu, R. Massot, Compilation of Mass Spectral Data, vol. 1, 2nd ed., Heyden and Son, London, 1975.
[7] S.L. Cook, in: V.H. Agreda, J.R. Zoeller (Eds.), Acetic Acid and its Derivatives, Marcel Dekker, New York, 1995, p. 145.
[8] N. Isaacs, Physical Organic Chemistry, 2nd ed., Longmans, London, 1995.

ADSORPTION STUDIES OF ACYLATION REAGENTS AND PRODUCTS ON ZEOLITE BETA CATALYSTS

Bonati, M.L.M., Joyner, R.W., Paine, G.S. and Stockenhuber, M.

Catalysis Research Laboratory, School of Science, Nottingham Trent University, Clifton Lane, Nottingham NG11 8NS, UK.

ABSTRACT

We report in situ infrared spectroscopy of the adsorption of acetic anhydride, acetic acid and 4-methoxyacetophenone on H-BEA and Na-BEA. The results are intended to cast light on the mechanism of acylation by H-BEA and other materials, and are interpreted in the light of a temperature programmed desorption study that we have recently reported, [1]. On Na-BEA there is relatively little perturbation of the spectrum of adsorbed acetic anhydride, compared to that of the free molecule, although even here the presence of more strongly and weakly bound states can be differentiated. Even here, there is some indication that the adsorbed anhydride decomposes into adsorbed acetic acid. Much of the adsorption of acetic acid on H-BEA is molecular, but again the spectra and correlated temperature desorption results show the presence of both strongly and more weakly adsorbed states. The most complex spectra are observed for acetic anhydride adsorbed on H-BEA. The species observed initially is acetic acid rather than the anhydride, and complex spectra and desorption patterns result as the adsorption pressure is increased. 4-methoxyacetophenone is more weakly adsorbed than either the acid or the anhydride.

INTRODUCTION

Despite great interest in the acylation of aromatics by carboxylic acid derivatives over zeolites, the adsorption, interaction and desorption of reactants and products with the catalyst has not been thoroughly investigated. These are of considerable importance, since different authors have suggested that adsorption phenomena [2] or product poisoning [3] may be rate determining. We have started to investigate the reaction of anisole with acetic anhydride to give p-methoxyacetophenone over zeolite beta (BEA), and have recently reported a temperature programmed desorption study [1]. We showed that ketene is an important product in the desorption of acetic anhydride from a number of differently exchanged zeolite BEA catalysts, and that there is an inverse relationship between catalytic activity and the formation of ketene in the desorption.

EXPERIMENTAL

Zeolite Beta was supplied by Catal Ltd., Sheffield and analysis by combined ^{29}Si MAS NMR and ^{1}H MAS NMR ([4]) shows Si/Al = 19 ±1. Samples were modified in a number of different ways. H-BEA samples were prepared as follows; the parent material (NH$_4^+$-BEA) was activated under vacuum (10^{-5} - 10^{-6} mbar) at 773K for 1h. Na-BEA was prepared as follows. 5g of zeolite NH$_4$-BEA was added to 250 ml of a 1M solution of Na nitrate in distilled water. The solution was stirred at room temperature overnight. The catalyst was then separated by filtration, washed with distilled water and dried in air for 24h at 298 K. This exchange procedure was repeated twice, until the maximum level of exchange was achieved. For infrared spectroscopy, samples were pressed into thin self supporting wafers weighing ca 20 mg, and measurements were performed using an ATI RS1 Fourier transform spectrometer equipped with an in situ stainless steel cell with calcium fluoride windows, capable of a base pressure < 10^{-7} mbar.

Proceedings: 14th International Zeolite Conference
Editors: E. van Steen et al
ISBN: 0-958-46636-X

25 – 30 April 2004
Cape Town, South Africa
Produced by: Document Transformation Technologies

2724

RESULTS

Adsorption of acetic anhydride

Fig 1 shows infrared spectra of zeolite H-BEA at 333 K in contact with acetic anhydride at pressures ranging from 10^{-4} mbar to 10^{-1} mbar, together with a spectrum of gas phase acetic anhydride. At low pressures we observe C=O stretching vibrations at 1825 cm^{-1} and 1805 cm^{-1} for the adsorbed species.
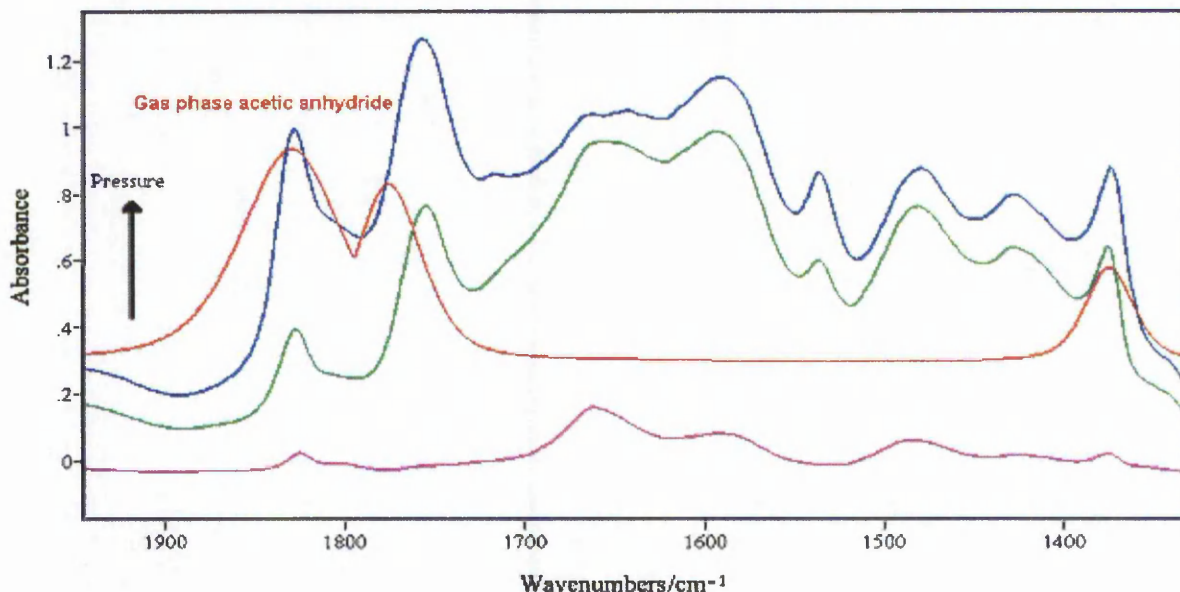
Figure 1. Adsorption of acetic anhydride on H-BEA at 333 K and pressures from 10^{-3} mbar (purple line) to 10^{-1} mbar (blue line). The red curve is the spectrum of acetic anhydride in the gas phase.

However, the major bands in the low pressure region are observed at 1670 cm^{-1} and 1595 cm^{-1}. Increasing the pressure to 10^{-2} mbar leads to a growth of the bands at 1825 cm^{-1} and 1805 cm^{-1} and an intense band at 1755 cm^{-1} is observed as well. At pressures higher than 10^{-2} mbar (green curve), the bands at 1825 cm^{-1} and 1755 cm-1 increase, whereas the intensity of the other bands is roughly constant. Upon evacuation, the band at 1825 cm^{-1} almost completely disappears.

A somewhat different picture emerges when acetic anhydride is adsorbed on Na-BEA (fig.2).
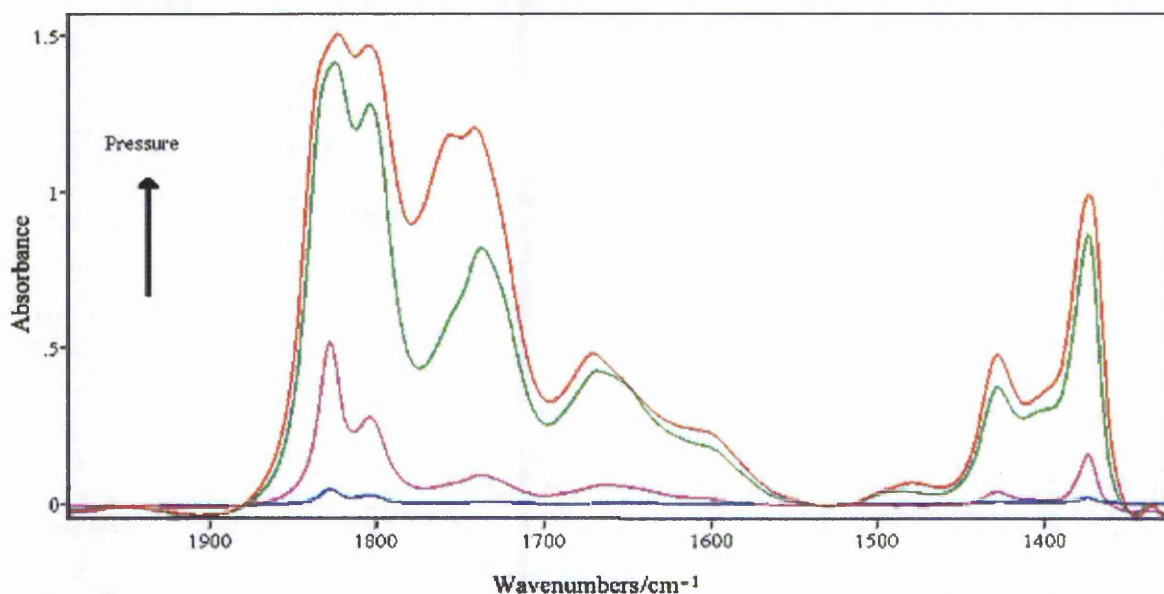
Figure 2. Adsorption of acetic anhydride on Na-BEA at 333 K and pressures from 10^{-3} mbar (blue line) to 1 mbar (red line).

At low pressures, two major bands are observed at 1805 cm⁻¹ and 1825 cm⁻¹, together with a peak at 1370 cm⁻¹ and a small band at 1426 cm⁻¹. Some minor contributions were found at 1660 cm⁻¹ and 1755 cm⁻¹. At higher pressures, the band at 1755 cm⁻¹ increases in intensity as do the two bands at 1825 cm⁻¹ and 1805 cm⁻¹. At pressures below 10^{-2} mbar a band at 2375 cm⁻¹ was found as well (not shown).

To assess the strength of the interaction of zeolite H-BEA with acetic anhydride, the zeolite with acetic anhydride adsorbed was heated under vacuum to 773 K, and the intensity of the bands integrated. Since obviously there are two different adsorption modes, the band at 1755 cm⁻¹ and bands in the range 1712 cm⁻¹ and 1546 cm⁻¹ were integrated.
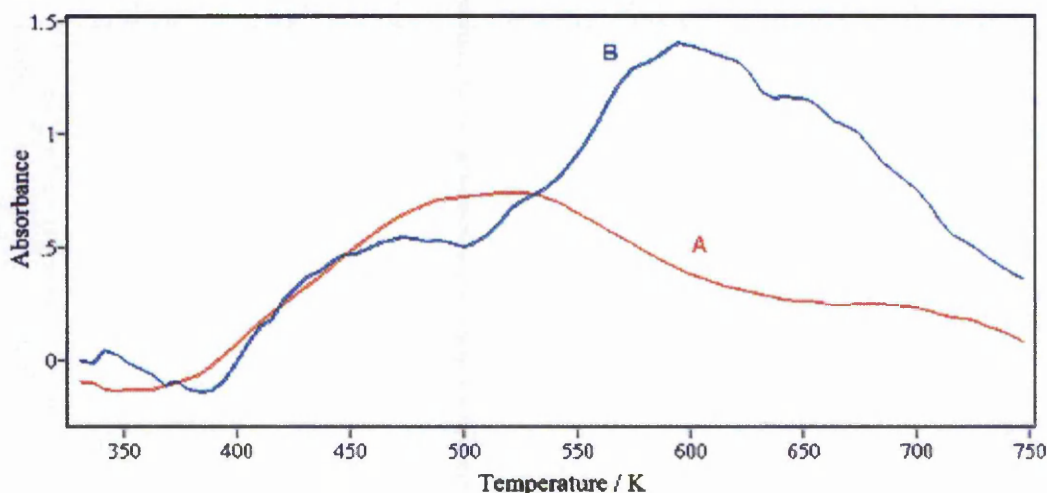
Figure 3. Temperature programmed desorption of acetic anhydride from H-BEA. The curves represent integrals over the infrared bands at ca 1755 cm⁻¹ (curve A) and the combined 1546-1712 cm⁻¹ (curve B).

The intensity of the band versus temperature curves where then differentiated using Savitzky Golay differentiation and multiplied by −1, so that they resemble familiar TPD curves. The results are shown in Figure 3.The curve corresponding to the band at 1755 cm⁻¹ shows two desorption maxima at 509 K and a shoulder at 688 K. The TPD curve of the peaks between 1546 cm⁻¹ and 1712 cm⁻¹ shows maxima at 473 K and 594 K.
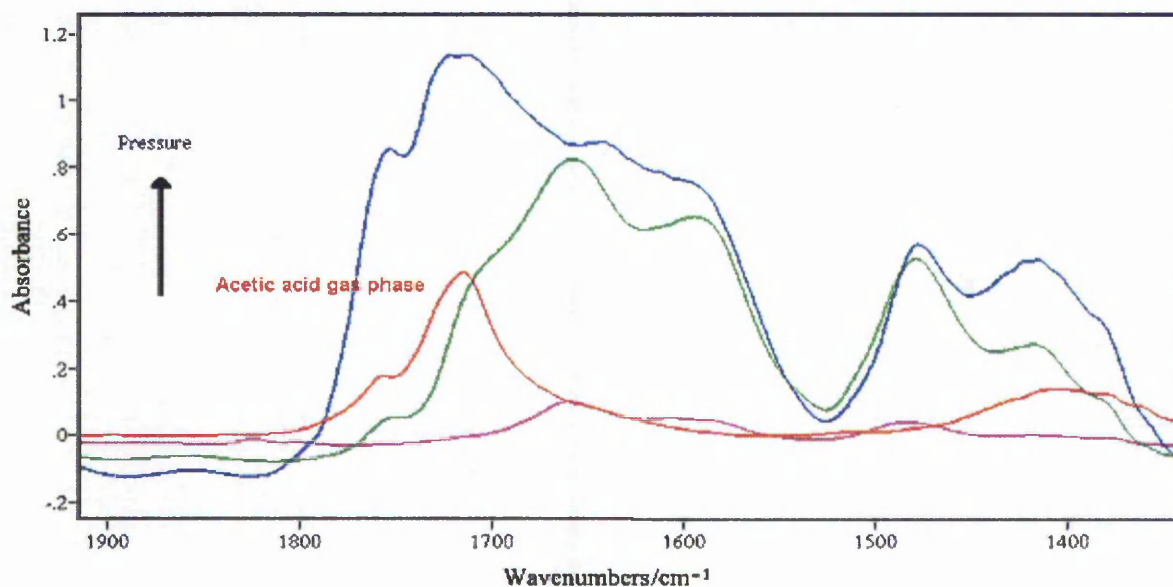
Figure 4. Infrared spectra of the adsorption of acetic acid on H-BEA at 333 K and pressures from 10^{-3} mbar (purple line) to 1 mbar (blue line). The red curve is the spectrum of gas phase acetic acid.

Adsorption of acetic acid

Infrared spectra resulting from the adsorption of acetic acid on H-BEA are shown in figure 4. The main bands observed at pressures lower 10^{-2} mbar are at 1660 cm^{-1}, 1592 cm^{-1} and 1480 cm^{-1}. Increasing the pressure leads to an increase in the intensity of all the bands and new bands at 1413 cm^{-1}, a shoulder at 1708 cm^{-1} and 1754 cm^{-1} were observed.

For comparison, gas phase acetic acid is plotted in fig 4 as well, and shows bands at 1410 cm^{-1}, 1715 cm^{-1} and a shoulder at 1757 cm^{-1}. The low pressure spectra are very similar to the spectra obtained for acetic anhydride adsorption on zeolite H-BEA (figure 5).
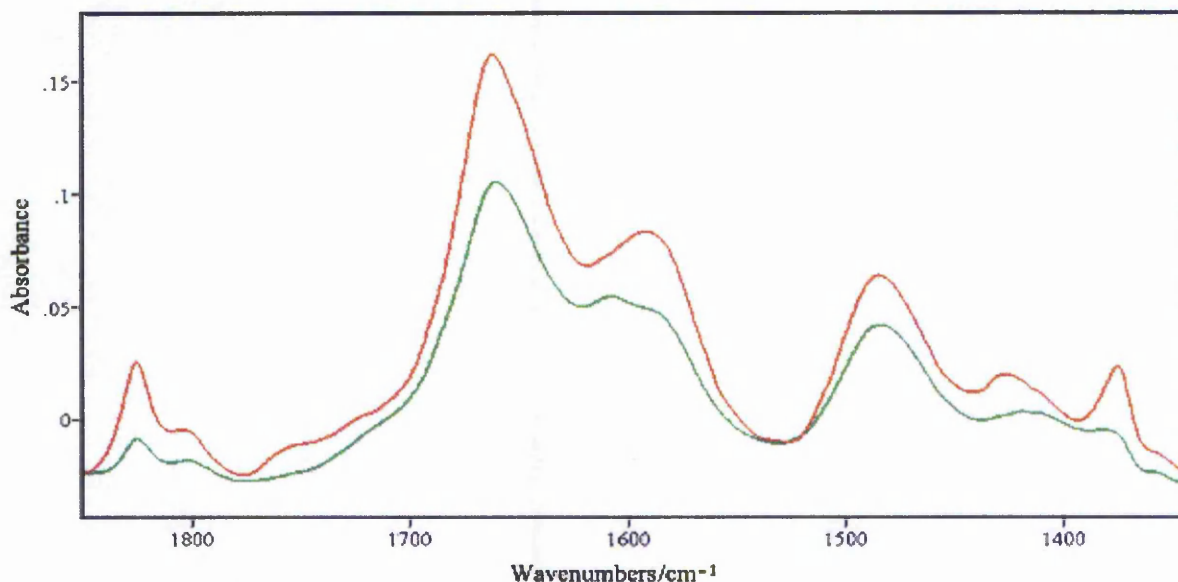
Figure 5. Infrared spectra of the adsorption of acetic acid (green) and acetic anhydride (red) on H-BEA at 333 K and 10^{-2} mbar.

For adsorption of acetic acid on H-BEA, the same manipulation was applied as for acetic anhydride and the TPD curves are shown in fig. 6. Again, the bands at 1754 cm^{-1} and 1708 cm-1 can be removed by evacuation at 333 K to a large extent. The TPD curve for the bands at 1660 cm^{-1}, 1592 cm-1 and 1480 cm^{-1} shows two desorption maxima at 503 K and 583 K. The TPD curve for the small band at 1754 cm^{-1} disappeared completely at 557 K.
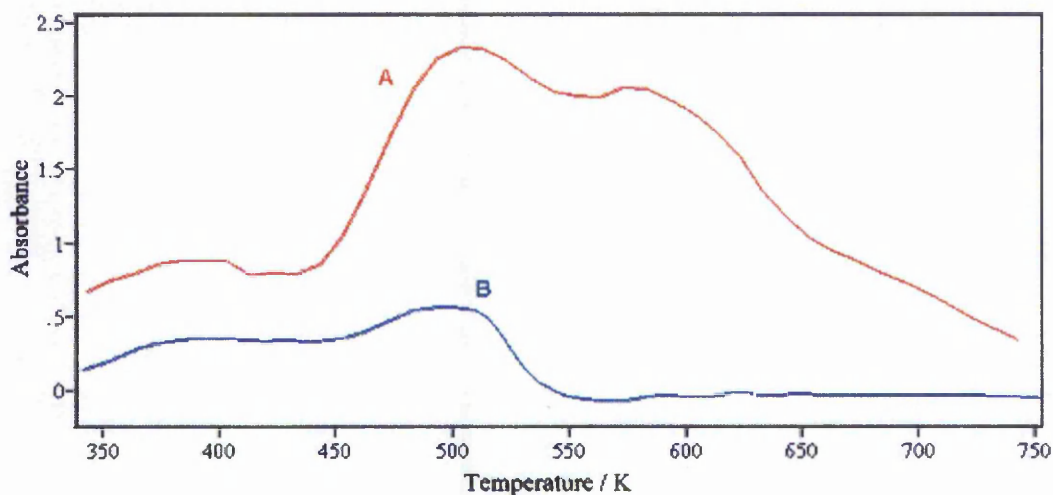
Figure 6. Temperature programmed desorption of acetic acid from H-BEA. The curves represent integrals over the infrared bands at 1754 cm^{-1} (curve A) and the combined 1660 cm^{-1}, 1592 cm-1 and 1480 cm^{-1} (curve B).

Adsorption of p-methoxyacetophenone (p-MAP)

Fig 7 shows infrared spectra of p-methoxyacetophenone adsorbed on zeolite H-BEA, together with the spectrum of a KBr wafer containing p-methoxyacetophenone and a spectrum of anisole adsorbed on H-BEA at 333K, 10^{-2} mbar. At 10^{-2} mbar and 10^{-1} mbar p-MAP pressures, bands at 1677 cm^{-1} with a shoulder at 1640 cm-1 and 1370 cm-1 with a shoulder at 1418 cm^{-1} were observed.
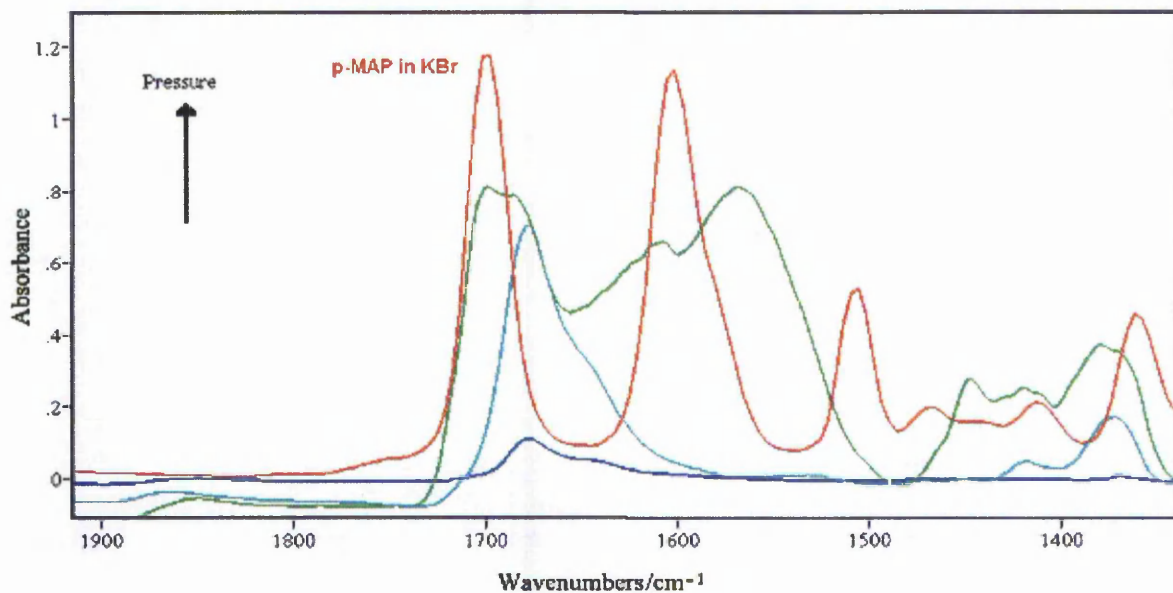
Figure 7. Infrared spectra of the adsorption of p-MAP on H-BEA at 333 K and 10^{-2} mbar (blue line), 1 mbar (light blue line) and 10 mbar (green line). The red coloured curve is p-MAP in KBr.

Increasing the pressure to 1 mbar slightly increases the intensity of these bands, and new bands at 1690 cm^{-1}, 1570 cm^{-1} and a shoulder at 1608 cm^{-1} and 1446 cm^{-1} appear. Evacuation at 333 K removes the band at 1690 cm^{-1} almost completely.
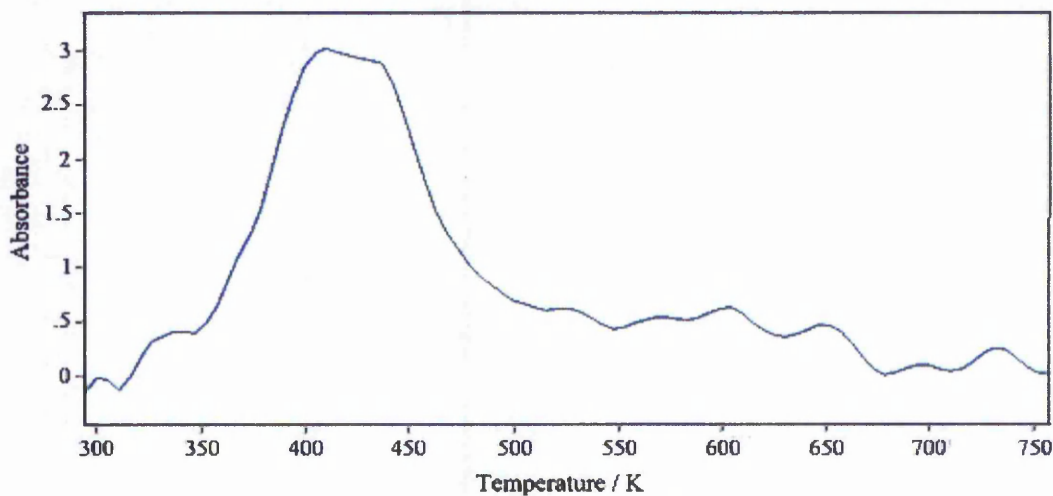
Figure 8. Temperature programmed desorption of p-MAP from H-BEA. The curve represents integrals over the infrared bands between 1710 cm^{-1} and 1490 cm^{-1}.

Thus, the remaining bands at 1690 cm^{-1}, 1570 cm^{-1} and 1608 cm^{-1} were integrated and converted into TPD curves. The only desorption peak observed was centred at 420 K (fig. 8).

DISCUSSION

Our temperature programmed desorption study [1] showed that both acetic anhydride and acetic acid undergo complex decomposition reactions in H-BEA and to a lesser extent Na-BEA. We concluded that the decomposition path is the reverse of a commercial synthetic route to acetic anhydride, namely the reaction of acetic acid with ketene [5]. As the temperature of the solid is increased, the following sequence occurred:

$$\text{Acetic anhydride} \rightarrow \text{acetic acid}_{(ads)} + \text{ketene}_{(ads)} \rightarrow$$

$$\text{acetic acid}_{(g)} + (\text{more}) \text{ketene}_{(ads\ and\ g)} \rightarrow CO_{2(g)} + H_{2(g)} + \text{coke}$$
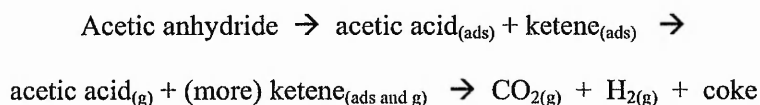
Figures 1 and 4 show that the spectra of acetic acid and acetic anhydride, both initially adsorbed on H-BEA, are significantly perturbed compared to the spectra of the respective free molecules. On adsorption at 10^{-2} mbar, the spectrum of acetic acid shows features at 1660, 1592 and 1480 cm^{-1}, that are also observed when the anhydride is adsorbed (Fig. 4). Since our TPD study showed that much of the adsorbed acetic acid desorbs intact with a maximum rate at 404 K, we assign these bands to the adsorbed acid, interacting relatively strongly with the catalyst at room temperature. As the pressure is increased these features grow, and new features appear that are very similar to the spectrum of the gas phase acid. In accord with the relatively small perturbation of the gas phase spectrum, the TPD results shown in Figure 3 confirm that this state interacts relatively weakly with the zeolite. At the highest pressures studied, (10^{-1} mbar, up to 10 mbar) the spectra appear to represent a linear combination of the strongly and more weakly bound states.

As might be expected, the spectrum of acetic anhydride adsorbed on Na-BEA appears to be least perturbed. There are bands at 1825 and 1805 cm^{-1}, which are probably the symmetric and antisymmetric carbonyl stretches seen in the gas phase molecule at 1825 and 1760 cm^{-1} respectively; the CH$_3$ deformation mode is unmoved, at 1370 cm^{-1}. As the pressure is increased the spectra become more complex, and bands at frequencies close to the free molecule position become dominant. For reasons that we do not understand, those at 1825 and 1760 cm^{-1} are quite broad, and each appears to be split into a doublet. Even on this non-acidic material, there appears to be some decomposition of the anhydride into the acid, as indicated by the presence of the bands at 1660, 1592 and 1480 cm^{-1}. Only traces of bands due to ketene were observed here, so it either reacts or more likely, desorbs from the zeolite. Indeed we observed significant desorption of ketene from Na-BEA at 430 K [1].

The infrared results confirm the TPD observations that the most complex interaction is that between acetic anhydride and H-BEA. At the lowest pressures studied, the only adsorbed species observed from acetic anhydride appears to be acetic acid, with the lowest pressure curve s at 10^{-4} mbar and 10^{-3} mbar in Figure 1, closely resembling those taken at the same pressures in Figure 3. The two curves of H-BEA in contact with 10^{-2} mbar acetic acid and acetic anhydride dramatically show the close resemblance. Thus, we can conclude that the chemical state of both substances is very similar when adsorbed at low pressures and that they adsorb in the form of the acid and another fragment, most likely ketene (a band at 2375 cm^{-1}). This band at 2375 cm^{-1} is found at higher frequency than gas phase ketene. However, this spectral region is typical of cumulated double bonds and electron rich substituents, e.g., nitrogen, shift the band to higher frequencies [6]. As the pressure is increased bands due to the anhydride can be observed, as well as a carbonyl band at ca 1755 cm^{-1} which we believe is due to a decomposition product of ketene. This band increases in intensity when the ketene band at 2375 cm^{-1} disappears.

The TPD results shown in Figure 4 are supportive of this assignment. As we have already observed [1] ketene decomposes and/or desorbs at relatively low temperatures, as is the case for this spectral band.

p-MAP adsorption at low pressure results in a species that has lost the aromatic deformation vibration (1600 cm^{-1}) and the aromatic CH stretching vibrations (not shown). Thus, at 1 mbar equilibrium pressure p-MAP decomposes over Zeolite H-BEA, and the aromatic fragment desorbs, but a product containing a carbonyl group stays adsorbed (bands at 1677 cm^{-1} with a shoulder at 1640 cm^{-1}). We also observe the band at 2380 cm^{-1}, attributed to adsorbed ketene. This is a highly interesting result, because it is evidence for the involvement of ketene in the reaction sequence. The concept of microscopic reversibility can be applied, i.e., a site that can form the bond between the carbonyl group and the aromatic ring can also split the bond. The product of the scission is ketene.

At higher pressures, some species with an intensive band at 1565 cm^{-1} are formed and upon evacuation at 333 K the adsorbate with bands attributed to the carbonyl group at 1677 cm^{-1} desorbs or reacts. The relatively low desorption temperatures for the product of 4-methoxyacetophenone suggests that it interacts

less strongly with the catalyst then either acetic acid or its anhydride. The highest desorption temperature observed, 420 K, is however much higher than that used in the liquid phase acylation reaction, which is typically 350 K. It would therefore not be safe to conclude that product desorption could not be rate determining. However the relative desorption energies from infrared TPD experiments from acetic anhydride, acetic acid and to a lesser extent anisole (not shown) favours adsorption of acetic anhydride/acetic acid as opposed to p-MAP. We and others [7] have observed levelling off of the acylation reaction of anisole with acetic anhydride when performed in a batch reactor. Adding p-methoxyacetophenone to the reaction mixture results in a decreased rate of reaction and thus suggests product poisoning. However, turnover numbers are in excess of one hundred turnovers per site and the results presented here suggest stronger bonding of acetic acid/acetic anhydride than the product, p-MAP. As suggested some time ago [8], multiply acylated products may well be poisoning the sites and the highly reactive ketene will contribute to their formation.

ACKNOWLEDGEMENTS

REFERENCES

1. Bonati, M. L. M.,Joyner, R. W.and Stockenhuber, M. Catal. Today, 81 (2003), 653.
2. Derouane, E. G.,Crehan, G.,Dillon, C. J.,Bethell, D.,He, H.and Derouane-Abd Hamid, S. B. J. Catal., 194 (2000) (2), 410.
3. Rohan, D.,Canaff, C.,Fromentin, E.and Guisnet, M. J. Catal., 177 (1998) (2), 296.
4. Muller, M.,Harvey, G.and Prins, R. Microporous Mesoporous Mat., 34 (2000) (3), 281.
5. Cook, S. L. "Acetic Acid and its Derivatives"; Marcel Dekker, New York:, 1995.
6. Lin-Vien, D.,Colthup, N. B.,William, G. F.and Grasselli, J. G. "Infrared and Raman characteristic frequencies of organic molecules"; Academic Press: San Diego, 1991.
7. Derouane, E. G.,Dillon, C. J.,Bethell, D.and Derouane-Abd Hamid, S. B. J. Catal., 187 (1999) (1), 209.
8. Rohan, D.,Canaff, C.,Magnoux, P.and Guisnet, M. J. Mol. Catal. A-Chem., 129 (1998) (1), 69.